

AD-A071 261

PURDUE UNIV LAFAYETTE IND RAY W HERRICK LABS  
ACOUSTIC INTERACTION WITH A TURBULENT PLANE JET. (U)  
AUG 77 F W CHAMBERS, F WILLIAMS  
HL-77-31

F/G 20/4

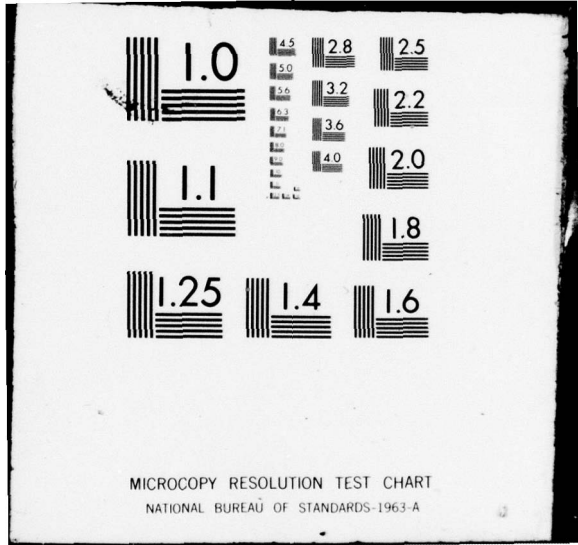
N00014-67-A-0226-0025  
NL

UNCLASSIFIED

1 of 5

AD  
A071261





AD A 071 261

DDC ACCESSION NUMBER



LEVEL

DATA SHEET

PHOTOGRAPH

THIS SHEET



INVENTORY

Rpt. # 7, HL 77-31

DOCUMENT IDENTIFICATION

DISTRIBUTION STATEMENT A

Approved for public release;  
Distribution Unlimited

DISTRIBUTION STATEMENT

Accession For	
NTIS GRA&I	<input checked="" type="checkbox"/>
DDC TAB	<input type="checkbox"/>
Unannounced	<input type="checkbox"/>
Justification	<input type="checkbox"/>
By _____	
Distribution/ _____	
Availability Codes	
Dist	Avail and/or special
A	

DISTRIBUTION STAMP

DDC	
RECEIVED	
JUL 17 1979	
D	

DATE ACCESSIONED

79 07 05 095

DATE RECEIVED IN DDC

PHOTOGRAPH THIS COPY

DDC FILE COPY

Research Contract No. ONR N00014-67-A-0226-0025

with

partial support from NSF GK 19317

ACOUSTIC INTERACTION WITH A  
TURBULENT PLANE JET

Sponsored by

OFFICE OF NAVAL RESEARCH

Report #7

HL 77-31

Submitted by:

F.W. Chambers, Graduate Research Assistant  
V.W. Goldschmidt, Principal Investigator

Approved by:

Raymond Cohen, Director  
Ray W. Herrick Laboratories

August 1977

*Approved for public release; distribution  
unlimited*

Note:

This report is part of a thesis submitted by Mr. Frank W. Chambers, in partial fulfillment of the requirements for the degree of Doctor of Philosophy. The research described was completed in July 1977. Professor Goldschmidt assisted in this work as thesis advisor and major professor.

## TABLE OF CONTENTS

LIST OF TABLES . . . . .	v
LIST OF FIGURES . . . . .	vii
NOMENCLATURE . . . . .	xiii
ABSTRACT . . . . .	xvii
CHAPTER I - INTRODUCTION TO THE PROBLEM . . . . .	1
CHAPTER II - BACKGROUND AND SURVEY OF THE LITERATURE . . . . .	7
A. Turbulent Plane Jets and Related Flows . . . . .	8
B. Instability of Jets and Mixing Layers . . . . .	28
C. Disturbed Plane Jets and Related Flows . . . . .	51
D. Large Scale Orderly Structures in Turbulent Flows . . . . .	68
CHAPTER III - EXPERIMENTAL APPARATUS AND TECHNIQUES . . . . .	85
A. Flow Field . . . . .	85
B. Acoustic System . . . . .	94
C. Pressure Profile Measurements . . . . .	99
D. Hot Wire Anemometer Measurements with Straight Wire Probes . . . . .	110
E. Hot Wire Anemometer Measurements with X-Wire Probes . . . . .	120
F. Energy Spectrum Measurements . . . . .	128
CHAPTER IV - EXPERIMENTAL RESULTS AND DISCUSSION . . . . .	133
A. Measurements of Frequency Dependence . . . . .	133
1. Pressure Profile Measurements . . . . .	134
2. Jet Widening Rate and Velocity Decay Rate Results . . . . .	136
B. Measurements of Changes in the Turbulent Structure . . . . .	160
1. Jet Half Width Results . . . . .	161
2. Turbulence Intensity Measurements along the Jet Centerline . . . . .	166
3. Turbulence Intensity Measurements Transverse to the Jet Centerline . . . . .	178

4. Reynolds Stress Measurements . . . . .	200
5. Turbulent Energy Spectrum Measurements . . . . .	227
C. Summary of Experimental Results . . . . .	249
CHAPTER V - DISCUSSION OF THE INTERACTION . . . . .	252
A. Comparison of Experimental Results to the Literature . . . . .	252
1. Frequency Dependence Comparison . . . . .	252
2. Comparison of Mean Flow Results with the Literature . . . . .	269
3. Comparison of Turbulent Characteristics with the Literature . . . . .	280
B. Analysis of the Behavior of the Flow Based upon Assumptions of Self-Similarity . . . . .	317
1. Existence Time . . . . .	319
2. Local Mass Flow Rate . . . . .	320
3. Entrainment . . . . .	321
4. Turbulent Energy Production . . . . .	324
C. Comments on Proposed Theories and Models Explaining the Acoustic Interaction with Free Shear Flows . . . . .	334
1. Simcox and Hoglund . . . . .	335
2. Morkovin and Paranjape . . . . .	336
3. Crow and Champagne . . . . .	336
4. Rockwell . . . . .	338
5. Winant and Browand . . . . .	339
6. Other Theories or Mechanisms . . . . .	339
D. Possible Mechanism of the Interaction . . . . .	342
CHAPTER VI - CONCLUSIONS AND RECOMMENDATIONS FOR FURTHER STUDY . . . . .	345
LIST OF REFERENCES . . . . .	347
APPENDICES	
APPENDIX A - BASIC MEAN FLOW PROPERTIES . . . . .	355
1. Vertical Uniformity of Centerline Mean Velocity . . . . .	355
2. Nozzle Boundary Layers . . . . .	357
3. Jet Initial Velocity Profiles . . . . .	360
APPENDIX B - SOUND FIELD MEASUREMENTS . . . . .	365
1. Frequency Dependence of Sound Pressure Levels Near the Nozzle Mouth . . . . .	365
2. 700 Hz and 1600 Hz Sound Field Measurements . . . . .	367
APPENDIX C - FLUCTUATION PHENOMENON STUDY . . . . .	372

APPENDIX D - X-WIRE MEASUREMENT DERIVATION, PROGRAM, AND DISCUSSION . . . . .	388
1. Sensitivity Relation Derivation . . . . .	388
2. Digital Processing Program . . . . .	395
3. X-Wire Measurement Accuracy . . . . .	397
APPENDIX E - DERIVATIONS BASED UPON ASSUMPTIONS OF SIMILARITY . . . . .	403
1. Reynolds Shear Stress . . . . .	403
2. Reynolds Shear Stress Turbulent Energy Production . . . . .	408
3. Existence Time . . . . .	411
4. Mass Flow and Entrainment Rates . . . . .	412
5. Requirements for Complete Self-Preservation	413
APPENDIX F - ENERGY SPECTRUM MEASUREMENT PROGRAM .	415
VITA . . . . .	417

## LIST OF TABLES

Table		Page
IV-1	Data Set D117 Results. . . . .	147
IV-2	Data Set D119 Results. . . . .	147
IV-3	Data Set D120 Results. . . . .	148
IV-4	Data Set D201 Results. . . . .	148
IV-5	Data Set D202 Results. . . . .	149
IV-6	Data Set D219 Results. . . . .	150
IV-7	Data Set D221 Results. . . . .	151
IV-8	Data Set D222 Results. . . . .	151
IV-9	Turbulence Intensities Along the Centerline, No Sound Case . . . . .	169
IV-10	Turbulence Intensities Along the Centerline, 700 Hz Case . . . . .	170
IV-11	Turbulence Intensities Along the Centerline, 1600 Hz Case. . . . .	171
IV-12	Longitudinal Turbulence Intensity Distributions at $X/D = 20$ . . . . .	186
IV-13	Longitudinal Turbulence Intensity Distributions at $X/D = 40$ . . . . .	186
IV-14	Longitudinal Turbulence Intensity Distributions at $X/D = 60$ . . . . .	186
IV-15	Reynolds Stress and Lateral Intensity Distri- butions, No Sound Case . . . . .	187
IV-16	Reynolds Stress and Lateral Intensity Distri- butions, 700 Hz Case . . . . .	187

Table		Page
IV-17	Reynolds Stress and Lateral Intensity Distributions, 1600 Hz Case. . . . .	188
IV-18	Summary of Frequency Dependent Changes in Mean Flow. . . . .	250
V-1	Natural Frequencies and Sensitive Frequencies Reported For Free Shear Flows . . . . .	256
V-2	Mean Flow Properties Reported For Turbulent Plane Jets . . . . .	270
V-3	Calculated Existence Time . . . . .	320

Appendix  
Table

A-1	Nozzle Boundary Layer Properties . . . . .	359
A-2	Shear Layer Momentum Thickness . . . . .	361

## LIST OF FIGURES

Figure		Page
II-1	Description of Plane Jet Terminology . . .	9
III-1	Schematic Diagram of Experimental Facility .	86
III-2	Experimental Flow Field . . . . .	92
III-3	Experimental Facility . . . . .	93
III-4	Schematic Diagram of Acoustical Instrumentation . . . . .	100
III-5	Schematic Diagram of Pressure Profile Instrumentation . . . . .	103
III-6	Typical Differential Pressure Transducer Calibration . . . . .	106
III-7	Typical Pressure Profiles With Measured Half Widths . . . . .	108
III-8	Typical Half Width and Velocity Decay Results . . . . .	109
III-9	Schematic of Longitudinal Turbulence Intensity Instrumentation. . . . .	113
III-10	Typical Straight Wire Probe Calibration . .	116
III-11	Typical Straight Wire Probe Linear Calibration . . . . .	119
III-12	Schematic Diagram of X-Wire Measurement Instrumentation . . . . .	126
III-13	Typical X-Wire Probe Linearized Calibration.	129
III-14	Typical X-Wire Probe Sensitivity Calibration	130
IV-1	Mean Velocity Profiles . . . . .	135

Figure	Page
IV-2	Strouhal Number Dependence of Widening Rate for all Data . . . . . 139
IV-3	Strouhal Number Dependence of Geometric Origin for all Data. . . . . 140
IV-4	Strouhal Number Dependence of Velocity Decay Rate for all Data . . . . . 141
IV-5	Strouhal Number Dependence of Velocity Origin for all Data . . . . . 142
IV-6	Strouhal Number Dependence of Widening Rate for Six Profile Data . . . . . 143
IV-7	Strouhal Number Dependence of Geometric Origin for Six Profile Data . . . . . 144
IV-8	Strouhal Number Dependence of Velocity Decay Rate for Six Profile Data . . . . . 145
IV-9	Strouhal Number Dependence of Velocity Origin for Six Profile Data . . . . . 146
IV-10	Jet Half Width Growth with and without Disturbance . . . . . 162
IV-11	Comparison of 700 Hz Case Half Widths Resulting from Different Acoustic Driver Location . . . . . 164
IV-12	Distribution of Longitudinal Turbulence Intensity along the Jet Centerline. . . . . 167
IV-13	Distribution of Lateral Turbulence Intensity along the Jet Centerline . . . . . 168
IV-14	Profiles of Undisturbed Case Longitudinal Turbulence Intensities . . . . . 180
IV-15	Profiles of Undisturbed Case Lateral Turbulence Intensities . . . . . 181
IV-16	Profiles of 700 Hz Case Longitudinal Turbulence Intensities . . . . . 182
IV-17	Profiles of 700 Hz Case Lateral Turbulence Intensities . . . . . 183

Figure		Page
IV-18	Profiles of 1600 Hz Case Longitudinal Turbulence Intensities . . . . .	184
IV-19	Profiles of 1600 Hz Case Lateral Turbulence Intensities . . . . .	185
IV-20	Profiles of Longitudinal Turbulence Intensities at $X/D = 20$ . . . . .	191
IV-21	Profiles of Lateral Turbulence Intensities at $X/D = 20$ . . . . .	192
IV-22	Profiles of Longitudinal Turbulence Intensities at $X/D = 40$ . . . . .	194
IV-23	Profiles of Lateral Turbulence Intensities at $X/D = 40$ . . . . .	195
IV-24	Profiles of Longitudinal Turbulence Intensities at $X/D = 60$ . . . . .	197
IV-25	Profiles of Lateral Turbulence Intensities at $X/D = 60$ . . . . .	198
IV-26	Profiles of Undisturbed Case Non-Dimensional Reynolds Stresses . . . . .	202
IV-27	Profiles of Undisturbed Case Reynolds Stress Correlations . . . . .	203
IV-28	Profiles of 700 Hz Case Non-Dimensional Reynolds Stresses . . . . .	206
IV-29	Profiles of 700 Hz Case Reynolds Stress Correlations . . . . .	207
IV-30	Profiles of 1600 Hz Case Non-Dimensional Reynolds Stress . . . . .	209
IV-31	Profiles of 1600 Hz Case Reynolds Stress Correlations . . . . .	210
IV-32	Profiles of Non-Dimensional Reynolds Stresses at $X/D = 20$ . . . . .	211
IV-33	Profiles of Reynolds Stress Correlations at $X/D = 20$ . . . . .	212
IV-34	Profiles of Non-Dimensional Reynolds Stresses at $X/D = 40$ . . . . .	215

Figure	Page
IV-35	Profiles of Reynolds Stress Correlations at $X/D = 40$ . . . . . 217
IV-36	Profiles of Non-Dimensional Reynolds Stresses at $X/D = 60$ . . . . . 218
IV-37	Profiles of Reynolds Stress Correlations at $X/D = 60$ . . . . . 219
IV-38	Calculated Reynolds Stresses at $X/D = 20$ . 222
IV-39	Calculated Reynolds Stresses at $X/D = 40$ . 223
IV-40	Calculated Reynolds Stresses at $X/D = 60$ . 224
IV-41	Reynolds Stresses Calculated with Graphical Mean Velocity Profile Slopes . . . . . 225
IV-42	Undisturbed Case Shear Layer Spectrum . . 229
IV-43	700 Hz Case Shear Layer Spectrum . . . . 230
IV-44	1600 Hz Case Shear Layer Spectrum . . . . 231
IV-45	Undisturbed Case Spectrum at $X/D = 1$ . . . 234
IV-46	700 Hz Case Spectrum at $X/D = 1$ . . . . 235
IV-47	1600 Hz Case Spectrum at $X/D = 1$ . . . . 236
IV-48	Undisturbed Case Spectrum at $X/D = 3$ . . . 238
IV-49	700 Hz Case Spectrum at $X/D = 3$ . . . . 239
IV-50	1600 Hz Case Spectrum at $X/D = 3$ . . . . 240
IV-51	Undisturbed Case Spectrum at $X/D = 5$ . . . 242
IV-52	700 Hz Case Spectrum at $X/D = 5$ . . . . 243
IV-53	1600 Hz Case Spectrum at $X/D = 5$ . . . . 244
IV-54	Spectra at $X/D = 9$ . . . . . 245
IV-55	Spectra at $X/D = 15$ . . . . . 246
IV-56	Spectra at $X/D = 30$ . . . . . 247
IV-57	Oscilloscope Traces of Anemometer Output with Probe Positioned on Jet Centerline . . . . 248

Figure		Page
V-1	Longitudinal Turbulent Intensities Along Jet Centerline . . . . .	282
V-2	Lateral Turbulent Intensities Along Jet Centerline . . . . .	287
V-3	Transverse Profiles of Undisturbed Case Longitudinal Turbulent Intensities . . . .	288
V-4	Undisturbed Transverse Profiles of Lateral Turbulent Intensities . . . . .	291
V-5	Transverse Profiles of Disturbed and Undis- turbed Longitudinal Turbulence Intensities .	294
V-6	Transverse Profiles of Disturbed and Undisturbed Lateral Turbulent Intensities .	297
V-7	Undisturbed Case Profiles of Non-Dimensional Reynolds Stress . . . . .	301
V-8	700 Hz Case Profiles of Non-Dimensional Reynolds Stress . . . . .	304
V-9	Transverse Profiles of Reynolds Stress Correlation . . . . .	307
V-10	Calculated Mass Flow Rate Behavior . . . .	322
V-11	Calculated Entrainment Rate Behavior . . . .	323
V-12	Reynolds Stress Profiles Fit to Data at X/D = 40 . . . . .	326
V-13	Reynolds Stress Profiles Fit to Data at X/D = 60 . . . . .	327
V-14	Calculated Turbulent Energy Production Profiles at X/D = 40 . . . . .	328
V-15	Calculated Turbulent Energy Production Profiles at X/D = 60 . . . . .	329
V-16	Calculated Turbulent Energy Production Rate Non-Dimensionalized by Mean Velocity at Mouth	331
V-17	Calculated Turbulent Energy Production Rate Non-Dimensionalized by Centerline Mean Velocity . . . . .	333

Appendix Figures	Page
A-1	Vertical Profiles of Mean Velocity . . . 356
A-2	Nozzle Boundary Layer Mean Velocity Profiles 358
A-3	Mean Velocity Profiles at Jet Mouth . . . 362
A-4	Comparison of Measured Mean Velocity Profile at Mouth to Hyperbolic Tangent Profile . . 363
B-1	Frequency Dependence of Sound Pressure Levels Measured Near Mouth of Jet . . . . 366
B-2	700 Hz Case Transverse Sound Pressure Level Profiles . . . . . 368
B-3	1600 Hz Case Transverse Sound Pressure Level Profiles . . . . . 369
B-4	Sound Pressure Levels at Various Vertical Positions along Jet Centerline . . . . . 370
C-1	Pressure Profiles Displaying Intermittent Fluctuations for an 1100 Hz Disturbance Frequency . . . . . 373
C-2	Recordings of the Intermittent Fluctuations. 376
C-3	Probability Density of Velocity on Jet Centerline at $X/D = 50$ for Unmodified Nozzle 380
C-4	Probability Density of Velocity on Jet Centerline at $X/D = 50$ for Nozzle with Screens at Mouth . . . . . 382
C-5	Probability Density of Velocity on Jet Centerline at $X/D = 50$ for Nozzle with Screen Upstream . . . . . 384
C-6	Probability Density of Velocity on Jet Centerline at $X/D = 50$ for Nozzle with Frame Upstream . . . . . 386
D-1	X-Wire Terminology . . . . . 388
D-2	Comparison of Longitudinal Intensities Measured with a Straight Wire Probe and an X-Wire Probe . . . . . 398

## NOMENCLATURE

A	Coefficient in mean velocity profile Equation V-2
$A_1$	Term in X-wire derivation defined in Equation D-8
$A_2$	Term in X-wire derivation defined in Equation D-9
$A_3$	Term in X-wire derivation Equation D-11
$A_4, A_5$	Terms in X-wire derivation Equation D-13
B	Jet velocity half width
$C_r$	Real component of complex wavespeed
$C_1$	Jet geometric origin
$C_2$	Jet velocity origin
D	Width of plane jet nozzle exit, diameter of round jet nozzle exit
$e_1, e_2$	Fluctuating voltage output of X-wire sensors 1 and 2
E	Hot wire anemometer dc bridge output voltage
f	Frequency
$f(\eta)$	$\bar{U}/U_m$
$F_{max}$	Maximum analysis frequency employed in Fourier analyzer
G	Coefficient in mean velocity profile Equation V-2
J	Mean velocity momentum flux per unit height of flow field in a given plane of constant X
$J_0$	Mean velocity momentum flux per unit height of flow field at $X = 0; U_0^2 D$
$K_1$	Jet widening rate

$K_2$	Jet centerline velocity decay rate
$L$	Arbitrary characteristic length
$N$	Amplitude of perturbation in instability analysis
$P$	Local shear stress turbulent energy production rate
$P_1, P_2$	Terms in total shear stress turbulent energy production defined by Equations E-23 and E-24
$Q$	Mass flux per unit height of flow field in a given plane of constant $X$
$Q_0$	Mass flux per unit height of flow field at $X = 0$ ; $\rho U_0 D$
$Re$	Reynolds number, $\frac{\rho \bar{U} L}{\mu}$
$Re_D$	Reynolds number, $\frac{\rho U_0 D}{\mu}$
$Re_\theta$	Reynolds number, $\frac{\rho U_0 \theta}{\mu}$
$St$	Strouhal number, $\frac{fL}{\bar{U}}$
$St_D$	Strouhal number, $\frac{fD}{U_0}$
$St_\theta$	Strouhal number, $\frac{f\theta}{U_0}$
$S_{u1}, S_{u2}$	Sensitivity of X-wire sensors 1 and 2 to X-direction velocity
$S_{v1}, S_{v2}$	Sensitivity of X-wire sensors 1 and 2 to Y-direction velocity
$t$	Time
$t_e$	Existence time, defined in Equation E-28
$T$	Sample length of Fourier analyzer
$u$	Instantaneous X-direction velocity fluctuation
$u'$	Rms of X-direction velocity fluctuation, $\sqrt{u'^2}$

U	Instantaneous X-direction velocity
$U_m$	X-direction mean velocity on jet centerline
$U_0$	X-direction mean velocity at jet mouth
$U_\infty$	Free stream mean velocity above a boundary layer
v	Instantaneous Y-direction velocity fluctuation
$v'$	Rms of Y-direction velocity fluctuation, $\sqrt{v'^2}$
V	Instantaneous Y-direction velocity
x	Axial direction coordinate in instability equations
X	Axial direction coordinate in jet flow field
y	Lateral direction coordinate in instability equation
$y'$	Lateral direction coordinate in shear layer
Y	Lateral direction coordinate in jet flow field
$Z_1, Z_2$	Coefficients in hot wire calibration Equation III-1
$\alpha$	Complex constant in instability equations
$\alpha_i$	Imaginary part of $\alpha$ ; spatial growth rate of disturbance in instability equations
$\alpha_r$	Real part of $\alpha$ ; wave number in instability equations
$\beta$	Complex constant in instability equations
$\beta_i$	Imaginary part of $\beta$ ; temporal growth rate of disturbance in instability equations
$\beta_r$	Real part of $\beta$ ; frequency in instability equations
$\delta$	Boundary layer thickness; distance from wall at which $\bar{U}/U_\infty = 0.99$
$\delta^*$	Boundary layer displacement thickness
$\eta$	Non-dimensional lateral coordinate, $Y/B$
$\eta_0$	Non-dimensional lateral coordinate, $\sigma Y/X$

$\eta_1, \eta_2$	Dummy variables in nested integrals substituting for $\eta$
$\theta$	Boundary layer momentum thickness, defined in Equation A-1
$\theta_+, \theta_-$	Shear layer momentum thickness on plus and minus Y sides of jet centerline
$\mu$	Dynamic viscosity
$\nu$	Kinematic viscosity
$\rho$	Fluid density
$\sigma$	Empirical coefficient of non-dimensional lateral coordinate in Equations II-4, II-5
$\psi$	Perturbation streamfunction of instability Equation II-7
$\Omega$	Lateral coordinate dependent amplitude function in instability Equation II-7

## ABSTRACT

Chambers, Frank William, Ph.D., Purdue University, August, 1977. Acoustic Interaction with a Turbulent Plane Jet. Major Professor: V. W. Goldschmidt.

Effects of a transverse acoustic field upon properties of a turbulent plane jet were investigated. The jet Reynolds number was 6000. Mean pressure profiles were measured to determine the jet widening rate, velocity decay rate, and virtual origins for applied pure tone acoustic frequencies of 200 Hz to 4200 Hz. Turbulent intensities, Reynolds shear stresses, and turbulent energy spectra were measured without an acoustic disturbance, and with disturbance frequencies of 700 Hz and 1600 Hz. Intensities were measured along the jet centerline from  $X/D = 0$  to  $X/D = 80$ . Spectra were measured in the jet shear layer and along the centerline from  $X/D = 0$  to  $X/D = 40$ . Intensities and shear stresses were measured at  $X/D = 20, 40,$  and  $60$  from  $Y/B = 0$  to  $Y/B = 2$ . Assumptions of self-similarity were employed in calculations of the mass flow rates, entrainment rates, Reynolds shear stresses, and shear stress turbulent energy production in the main region of the jet.

Acoustic fields of a wide frequency range were found to produce changes in the mean flow of the jet. Certain frequencies were found to increase the magnitude of turbulent intensities and Reynolds shear stresses in the main region without greatly affecting their transverse profiles. These increased magnitudes were observed to decrease with distance from the nozzle. The interaction of the acoustic field and the jet appears to originate in the shear layers in the initial region, and a description of the interaction mechanism was proposed.

## CHAPTER I INTRODUCTION TO THE PROBLEM

The influence of sound upon jets has been observed since at least 1858, when John Leconte (1858) noticed gas lamp flames pulsating in synchronization to music of Beethoven being performed on a violoncello. To Leconte, the phenomenon was purely an intellectual curiosity with no apparent practical application. The growth of technology since 1858 has made the phenomenon a subject of considerable practical interest, for now there are numerous applications of fluid jets.

A jet is a flow from a nozzle into a medium which may be moving or at rest. The jet may be laminar or turbulent, and as it moves away from the nozzle it slows, spreads, and mixes with fluid entrained from the surroundings. Jets are found in fluidic amplifiers and switches, jet pumps and ejectors, gas turbine combustors, turbine blade film coolers, aircraft and marine jet propulsion devices, aerosol generators, and many mixing processes. All of these applications of jets depend in some manner upon the spreading and mixing behavior.

This behavior has been found to be influenced by a number of factors, including the Reynolds number, the Mach

number, the conditions upstream of the nozzle, and the presence of a disturbing sound field. However, the knowledge of the effects of changes in these factors is entirely empirical. Given the values of these parameters, the spreading rate cannot be predicted. This lack of a theoretical solution is the major problem of turbulence, and is termed the closure problem. Basically, it is the result of having a larger number of unknowns than equations, and centers upon the turbulent shear stress. Various forms for the shear stress have been offered, the most well known being Prandtl's mixing length. These models do not model the shear stress sufficiently to accurately predict the structure of the turbulent flow, and hence reliance upon empiricism is necessary. One of the primary goals of this study was to obtain empirical information linking the applied sound field and the changes in the mean flow and the turbulent structure of the jet. This information was sought in an effort to improve the understanding of the mechanism of the interaction between the sound and the flow as well as to improve the basic understanding of the development process that occurs in a turbulent jet. A description of more detailed goals is presented following a short history of the studies of the effect of applied sound on jets.

Sound can produce changes in both laminar and turbulent jets. In his pioneering paper, Leconte (1858) noted

that the laminar jets he observed were operating at a pressure just below that which caused them to "flare" or become turbulent. He wrote that the flames pulsated in such perfect harmony with the music that, "A deaf man might have seen the harmony." He proved to his satisfaction that the phenomenon was not caused by mechanical vibrations, but by a direct influence of the music. Clapping and shouting did not affect the flame. Thus Leconte saw that appropriate sound could precipitate transition in a laminar jet.

For at least the next seventy years, studies of sound-influenced jets were concerned with this case of early transition. G. B. Brown (1932, 1935) reviews the early research on the phenomenon and mentions that John Tyndall studied it at the suggestion of Leconte. Tyndall found that unburned gas jets made visible by smoke were affected in the same manner as flames. In 1867 he explained the effect as an early transition to turbulence. Lord Rayleigh followed Tyndall's studies with his own studies of flames, smoke jets, and liquid jets disturbed by acoustic standing waves. He observed that "a serpentine motion of the jet" was produced before transition. In 1878, Rayleigh published, "On the Instability of Jets," a pioneering mathematical analysis of stability that is still of value.

G. B. Brown (1932, 1935) continued the study of acoustically produced transition in flames and smoke jets. He found that noise as well as pure tones could provoke the

onset of turbulence, and applied stroboscopic photography to the study of the induced vortex motion. He also found that sound increased the spreading of jets, and hypothesized that this was the result of oscillation of the outer edges of the jet. He applied sound selectively to different regions of the jet and discovered that the region nearest the jet mouth was most sensitive. His work may be considered the transition point between classical and modern studies of the phenomenon.

Modern studies of the phenomenon often have been motivated by practical considerations, such as the question of what effect sounds have on fluidic devices containing jets. These studies have been concerned with quantification as well as description of the effects. The most common concern has been the question of what frequencies produce the greatest effects upon a given jet. Few studies have concentrated upon detailed observations of the effects of sound upon the turbulent structure.

Goldschmidt and Kaiser (1971) did conduct a study of frequency dependence and structural changes in a turbulent plane jet, and their results provided a stimulus for the current study. Their measurements were concentrated in the far region of the jet, and were performed in an effort to either verify or contradict the analytical predictions of Simcox (1969). These predictions were based upon a model of a direct acoustic-turbulent interaction

throughout the jet. The comparison of measurements and predictions was inconclusive, and provided motivation for further study.

Goldschmidt and Kaiser's (1971) results did show changes in the turbulent structure of the flow in the far region, and one of the goals of the present study was to extend these measurements. It was believed that knowledge of the far region turbulence intensity and Reynolds shear stress distributions for disturbed and undisturbed flows would help to describe the characteristics of the interaction mechanism and allow evaluation of the predictions of Simcox (1969). For these reasons, such measurements were performed.

An interaction mechanism different than that proposed by Simcox was suggested by a survey of papers describing large scale structures in jets. These papers, described in the next chapter, raised the possibility that the interaction mechanism could involve effects of sound upon a large scale structure in the initial region of the jet. This structure in turn could produce changes in the downstream structure of the flow. In order to evaluate the possibility of such an interaction mechanism, measurements of turbulent energy spectra and intensities were performed in the initial region of the jet. The energy spectrum measurements were extended to the far region to determine the extent of changes in spectra.

These measurements were performed with the belief that knowledge of these characteristics of the effects of the disturbing sound field would help approach several goals. One goal was to obtain information that could be of benefit in practical applications of jets. Information on the frequency dependence of the effects upon the jet could be of use in determining how to make a fluidic amplifier insensitive to a noisy environment, for example. Alternatively, this information could be of use in acoustically augmenting a mixing process involving a jet. A second goal was to obtain confirmation or denial of the direct interaction model of the phenomenon, and provide information for a more extensive model. A final goal was to gain a better understanding of the development process of a turbulent plane jet and of the interrelations of the various factors governing this development. It was believed that greater knowledge of the acoustic-turbulent interaction mechanism would not only improve understanding of acoustic effects but would also clarify the basic structural development in the undisturbed jet.

## CHAPTER II BACKGROUND AND SURVEY OF THE LITERATURE

A background for an understanding of the problem of the interaction of sound with a turbulent plane jet is developed in this chapter. The classical studies reviewed in the last chapter reveal that the effects of applied sound are observable in several aspects of the behavior of a jet. Thus the range of the literature providing insights into the phenomenon is rather broad. For this reason, the literature survey presented in this chapter has been confined to a representative selection of the extensive number of papers available in the literature and should not be considered an exhaustive review. In addition, material is presented which provides an introductory background to the reviewed papers.

The chapter is grouped into four sections. The first section covers undisturbed plane jets and related free shear flows such as round jets, wakes, and mixing layers. The section presents information on mean flow characteristics and turbulent flow structures of such flows. Hydrodynamic stability is the topic of the second section, which provides information on vortex growth in shear flows. Disturbed shear flows are considered in the third section,

which is directly related to the topic of this study. The final section covers coherent structures in turbulent flows. This last topic has attracted much attention in recent years, as experimental studies using various techniques have revealed that some turbulent flows are overlaid upon orderly large scale flow structures.

#### A. Turbulent Plane Jets and Related Flows

Turbulent plane jets and related flows such as turbulent round jets, turbulent mixing layers, and turbulent wakes have basic similarities in structure. In addition to these similarities, the flows share similar descriptive terminology. The structure and terminology of a plane jet is illustrated in Figure II-1. The jet leaves the nozzle of width "D" with an initial centerline mean velocity " $U_0$ ." The initial mean velocity profile may be relatively uniform in the central region of the jet with relatively thin shear layers at the edges. Such a profile is called a "top hat" profile for its resemblance to the shape of a top hat. These profiles generally are produced by nozzles which have large contraction ratios (the ratio of inlet to outlet area of the nozzle). If the mouth of the jet is preceded by a long straight section, the initial velocity distribution can be fully developed as in pipe or duct flow. As the flow leaves the nozzle, shear or mixing layers are formed on the edges between the potential core of the jet and the surrounding fluid. The flow inside the

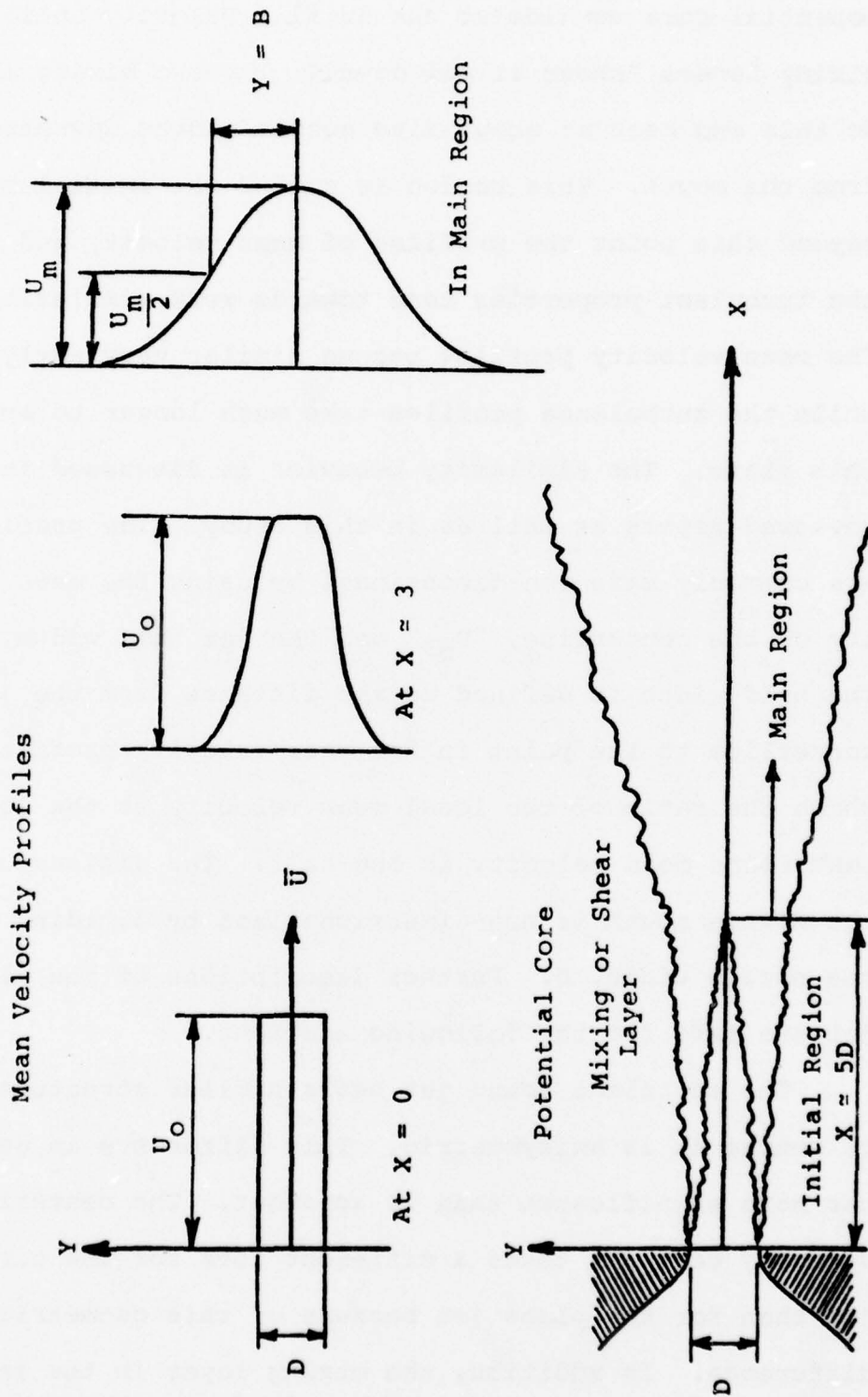


Figure II-1 Description of Plane Jet Terminology

potential core remains at the initial velocity until the mixing layers "shear it all down." The two mixing layers do this and meet at about five nozzle widths downstream from the mouth. This region is called the initial region. Beyond this point the profiles of mean velocity and of the turbulent properties tend towards self-similarity. The mean velocity profiles become similar very early, while the turbulence profiles take much longer to approach this state. The similarity behavior is discussed in the reviewed papers as well as in this study. The profiles are commonly made non-dimensional by using the mean velocity on the centerline, " $U_m$ ," and the jet half width, "B." The half width is defined as the distance from the jet centerline to the point in the mean velocity profile at which the ratio of the local mean velocity to the local centerline mean velocity is one-half. The distance from the nozzle mouth is non-dimensionalized by dividing by the nozzle width, D. Further descriptions of the plane jet are left for the following sections.

The turbulent round jet has a similar structure, but of course it is axisymmetric. This difference in geometry has more significance than is apparent. The centerline velocity decrease takes a different form for the circular jet than for the plane jet because of this geometrical difference. In addition, the mixing layer in the initial region of the circular jet is a single cylindrical layer,

while the plane jet initial region is bounded by two separate plane mixing layers. The importance of this difference will be discussed later.

The plane mixing layer is equivalent to one of the mixing layers bounding the initial region of the plane jet. A mixing layer is formed at the boundary of two flows with different velocities. The mixing layer is the most common flow used for experimental studies of instability phenomena, and the results which are obtained can be directly applied to the initial region of plane jets. The mixing layer differs from the plane jet in not having a characteristic velocity which changes with axial position.

A number of assumptions may be employed in order to obtain equations for the mean profile width and velocity distribution as functions of position in the plane jet. Smaller terms in the equations of motion can be neglected. The momentum of the jet remains constant, as it is free, with no external forces acting on it. The flow is also assumed to be self-preserving in the far region of the jet. A self-preserving flow is one in which all the non-dimensional parameters retain their similarity as the flow continues. These assumptions lead to the conclusion that for a plane turbulent jet, the growth of the half width is directly proportional to the increase in distance from the mouth. That is  $\frac{dB}{dX} = \text{constant}$ , the half width grows linearly with distance from the mouth. It is also found that

the inverse square of the ratio of the local centerline mean velocity to the mean velocity at the mouth is directly proportional to the distance from the mouth. That is,  $\left(\frac{U_m}{U_0}\right)^{-2} \propto X/D$ . Non-dimensionalizing those relations, the following equations are found which apply to the similar region of the plane jet flow field.

$$\frac{B}{D} = K_1 \left( \frac{X}{D} - C_1 \right) \quad (\text{II-1})$$

$$\left( \frac{U_m}{U_0} \right)^{-2} = K_2 \left( \frac{X}{D} - C_2 \right) \quad (\text{II-2})$$

The constant  $K_1$  is called the jet widening rate, and  $K_2$  is called the centerline velocity decay rate. The constant  $C_1$  is called the geometric virtual origin, and accounts for the fact that the linear widening does not extrapolate to zero width at the mouth of the jet. Similarly,  $C_2$  is called the velocity virtual origin. The two origins generally do not coincide.

Another assumption can be made about the form of the Reynolds turbulent shear stress in the similar region of the jet. When this assumption is combined with the previous assumptions, the non-dimensional mean velocity profile may be calculated. Schlichting (1968) states that W. Tollmien was the first to do this in 1926, using Prandtl's mixing length hypothesis for the shear stress. The resulting profile is of the form,

$$\frac{\bar{U}}{U_m} = f(Y/X) \quad (\text{II-3})$$

Reichardt (1942) and Görtler (1942) arrived at slightly different solutions by making different assumptions about the form of the shear stress. Reichardt's solution tends to fit experimental data better at the edges of the jet while Görtler's exhibits a better fit in the central region. Reichardt's solution is:

$$\frac{\bar{U}}{U_m} = e^{-(\eta_0^2/2)} \quad (\text{II-4})$$

$$\text{where } \eta_0 = \sigma \frac{Y}{X}$$

$\sigma$  is an empirical constant.

Görtler's solution is:

$$\frac{\bar{U}}{U_m} = \cosh^{-2} \eta_0 \quad (\text{II-5})$$

where  $\eta_0$  is defined in the same way as above.

Note that both of these equations assume that the geometric origin is located at the mouth. They may be modified to account for shifted geometric origins by using  $X - D(C_1)$  in place of  $X$ .  $B$  is directly proportional to this parameter, and the equations can be changed to a form in which  $Y/B$  is the independent variable.

Experimental values for these mean velocity profiles may be obtained most simply from measurements of the mean pressure profiles made with pitot tubes. Direct

experimental determination of values of the turbulent properties of the flow such as the turbulent intensity, the ratio of the rms turbulent velocity fluctuations to the mean velocity, requires more sophisticated instrumentation such as hot wire anemometers. The first plane jet measurements with hot wire anemometers appear to have been made by Miller and Comings (1957) and van der Hegge Zijnen (1958). They measured mean velocity profiles and longitudinal turbulent intensities at distances up to 40 nozzle widths from the nozzle. This distance is not now considered sufficient for the turbulent structure to have attained self-preservation. van der Hegge Zijnen's turbulent intensity measurement values are rather low, and their accuracy is somewhat suspect. One interesting result of his study concerns the effects of Reynolds number on jet development. He measured velocity profiles for two jets at the same Reynolds number, 13,300 based on nozzle width,  $D$ , and initial velocity,  $U_0$ . The jets had similar geometry but differed in size and flow speed. He found that the two jets had different widening rates. He speculated that the flow conditions in the nozzle might be responsible for this unexpected difference. He also compared the mean velocity and Reynolds stress profiles (calculated from the mean velocity profile) that he measured with the various theories, and found that Reichardt's mean velocity profile and Reynolds stress hypothesis

provided the best comparison.

Among the earliest direct hot wire measurements of Reynolds stresses performed in plane jets were those of Heskestad (1965) and Bradbury (1965). They both performed very thorough investigations of the turbulent structure of plane jets. Bradbury's measurements were performed in a jet that exhausted into surroundings that were moving at a lower velocity in the downstream direction. This parallel flow was added in order to reduce measurement errors at the edges of the jet caused by the large turbulent fluctuations and the low mean velocities. He measured the mean velocity profiles, static pressure profiles, intermittency factor (per cent of time flow is turbulent at a point), turbulent intensities, and shear stresses in the main region of the jet. In addition he calculated the turbulent energy balance and the turbulent microscales, and measured turbulent energy spectra and various properties of the irrotational flow bounding the turbulent regions of the jet. All measurements were at a Reynolds number of approximately  $3 \times 10^4$ . He concluded that the jet approached a self-preserving state beyond 30 nozzle widths from the mouth of the jet and that there were certain similarities in the turbulent structures of the self-preserving turbulent plane jet and the plane wake.

Heskestad's measurements were also performed primarily in the self-preserving region of a plane turbulent jet

which had a developed initial velocity profile. In the self-preserving region, the lateral profiles of mean velocity and the turbulent intensities, the intermittency, and the terms of the mean momentum and mean energy equations were measured. These measurements were performed at a Reynolds number of approximately  $3.4 \times 10^4$ . In addition, the Reynolds number dependence of the distribution of the longitudinal turbulent intensity along the jet centerline was studied for Reynolds numbers from  $4.7 \times 10^3$  to  $3.7 \times 10^4$ . Heskestad concluded that the jet widening, velocity decay, and turbulent intensity profiles reached an "approximately" self-preserving state at  $X/D = 65$ . He stated that some of the terms of the energy equation did not reach a self-preserving state until  $X/D$  of approximately 100. The changes in Reynolds number were found to have an effect; the turbulent intensities along the axis decreased as the Reynolds number was increased. A comparison was made with the previous measurements in plane jets. These works, including those of Miller and Comings (1957) and van der Hegge Zijnen (1958), had been done in the region inside  $X/D = 40$ . Heskestad observed that his velocity decay results appeared to contain a subrange of linear behavior from  $X/D = 10$  to 40 that exhibited a smaller slope than at larger distances downstream. He noticed subtle trends in the previous studies that also gave some indication of such a subrange. He compared the

widening rates found in these studies to those he found at larger  $X/D$ 's (his half width data goes down only to  $X/D = 47$ ) and, noting that his widening rate was larger, claimed further evidence of a subrange of mean flow behavior. The validity of this hypothesis based upon a comparison of widening rates is debatable. Recall that widening rates have been found to differ for different jets, even at the same Reynolds number with similar geometries as in the results of van der Hegge Zijnen (1958). However, most measurements have been performed within what Heskestad terms the subrange, and the possibility remains that widening rates of all jets approach a common asymptote at large distances downstream. Heskestad also observed that for self-preservation, the geometric and velocity origins must coincide. A proof of this requirement is presented in Appendix E.

The origins of plane jets were found not to coincide by Flora and Goldschmidt (1969). They found that the two origins did not coincide, and that their location depended very strongly upon the turbulent intensity of the flow upstream of the nozzle. The origins were also found to be essentially independent of the nozzle geometry for constant flow conditions upstream of the nozzle.

The mean flow behavior of jets of numerous investigators was reviewed by Young (1973), and the table he presents shows values for the widening rate varying between

0.085 to 0.130. An updated version of this table is presented in Chapter V as Table V-2. Young's table does not suggest any value for an asymptotic widening rate.

Mean flow characteristics of plane turbulent jets are also discussed by Gutmark and Wygnanski (1976). Their paper presents a thorough set of measurements of mean velocities, turbulent intensities, and third and fourth order terms needed in the turbulent energy balance and hot wire corrections for finite turbulence levels. Measurements of two-point correlations and the intermittency factor are also presented. The turbulence measurements were obtained as conventional averages and as conditioned turbulent zone averages. Except very near the centerline of a jet, the flow is not always turbulent. There is a distinct boundary between the turbulent and non-turbulent (irrotational) regions called the interface. This interface continuously moves, causing the intermittency (the part of the time the flow is turbulent) at points away from the centerline to be less than 1.0. The turbulent zone average is the average of the quantity measured only when within the interface averaged over the time the flow was turbulent.

Gutmark and Wygnanski's (1976) measurements were performed at a Reynolds number of approximately  $3 \times 10^4$  in a plane jet facility basically similar to that of other researchers. The two-dimensionality of the finite height jet

is maintained by planes bounding the top and bottom of the flow field. Without these planes, the flow would asymptotically approach an axisymmetric form. The facility differed from others in that it was surrounded by screens placed well outside the immediate vicinity of the jet. The screens were used to minimize the effects of drafts in the room on the entrained flow.

They found that their jet had a widening rate of approximately 0.1, and noted that this value is close to that obtained by other researchers. They speculated as to whether plane turbulent jets all approach an asymptotic widening rate in the self-preserving state and concluded that it was rather questionable. They noted further that the initial conditions of turbulent intensity appear to have an effect on the spreading, but that the magnitude of the effect appears small and there is not much supporting data. They found that the mean profile and turbulent intensities reached an approximately self-preserving state by  $X/D = 40$ . The lateral profile of the longitudinal turbulent intensity in a plane jet normally has a relative minimum at the centerline, reaching maxima on both sides. Gutmark and Wygnanski state that this saddle-shaped profile may be the result of the merging of the mixing layers at the end of the potential core, and that it (the saddle) disappears with increasing downstream distance. They compare their measurements of the shear stress correlation

with those of Heskestad (1965) and Bradbury (1965) and note that while these previous works show the correlation decreasing to small values near the edges of the jet, their measurements, both conventional and zone averaged, increase greatly in the same region. They offer no explanation, but it appears that one possibility is that the screens that surrounded their set up eliminated the effects of room drafts, and hence they measured a purer, more influenced by the jet, correlation at the jet edges. However, they also present a lateral correlation that shows a very large negative value with one of the points of the correlation very far from the centerline on the edge of the jet. Cervantes (1976) duplicated the correlation in a similar set up (without screens) at a lower Reynolds number and did not obtain such a large negative value. No explanation of these differences is available other than the effect of the screens or a measurement error. Otherwise, Gutmark and Wagnanski's results are similar to those of Bradbury and Heskestad. The difference may be attributed to the differences in the three set ups. Bradbury's jet exhausted into moving air, and Heskestad's nozzle had a relatively small contraction following a long narrow duct, resulting in a relatively non-uniform initial velocity profile. After comparing the various measurements, Gutmark and Wagnanski state in their concluding remarks that "a carefully controlled experiment

linking the initial conditions to the far-field flow certainly seems worthwhile at this stage."

The effect of initial conditions upon the spread of a heated plane jet has been studied by Jenkins and Goldschmidt (1973). They found that an increase in the initial temperature difference between the jet and the surroundings has significant effects upon the spreading rate and the geometric origin of the velocity and the temperature profiles. Little effect was found upon the origins or rates of the centerline velocity and temperature decay. Bashir and Uberoi (1975) also performed measurements in a heated two-dimensional jet. They found that their jet achieved complete self-similarity at and beyond  $X/D = 40$ .

Witze and Dwyer (1976) studied what they call the "turbulent radial jet," which can be called the axisymmetric counterpart of the plane jet. It is a jet issuing from a circumferential slot on a cylinder. They found a widening rate which is comparable to that of plane jets for the asymptotic case of very large slot radius. They note that the widening rate linearity is a much more sensitive indicator of flow self-similarity than the non-dimensionalized mean velocity profiles which are constrained to pass through two points; at the centerline and at the half width.

Another flow field geometry closely related to the plane jet is the plane mixing layer. Wagnanski and Fiedler

(1970) performed a thorough study of the mixing layer, measuring conventional mean properties, conditioned zone averages in the turbulent and non-turbulent regions, and conditioned ensemble averages. These ensemble averages were measured at fixed distances from the instantaneous location of the turbulent-non-turbulent interface. They observe that the high velocity side of the layer resembles a wake while the low velocity side behavior resembles that of a jet. They note that the conventional mean velocity profile is somewhat misleading. "The conventional mean velocity profile,  $\bar{U}$ , never exists in the flow, it is only the result of a long time averaging process over random excursions of the interface."

Champagne, Pao and Wagnanski (1976) provide further insight on the mixing layer. They note the very large dependence of the development of the mixing layer upon the initial conditions. They observe that two previous mixing layer studies revealed fundamentally different development of the flow, and that a third study was able to reproduce either set of results by either fully tripping the boundary layer on the splitter plate upstream of the mixing layer or partially (not to turbulent flow) tripping it. The authors speculate in accord with Bradshaw (1966) that the growth of the mixing layer and the magnitude of the peak in the turbulence intensity profile are proportional to the disturbance level in the splitter plate

boundary layer. They speculate further as to whether a single universal self-preserving form exists for the mixing layer. Two answers are offered. The first is that there is not a universal self-preserving state, for the boundary layer conditions have a very strong influence upon the initial shear layer behavior which in turn determines the self-preserving flow behavior. The second answer is that the initial conditions are not the determining factor, but that the boundary conditions of the flow in the self-preserving region play that role. They cite two cases in evidence; one which suggests that the width of the flow confining plates controls the behavior of the flow, and one suggesting that the flow is independent of this width. They draw no conclusion, and suggest the need for more research on the problem.

The round turbulent jet shares many characteristics with the plane turbulent jet. Wygnanski and Fiedler (1969) present measurements of mean velocities, turbulent intensities and stresses, intermittency factors, correlations, spectra, and convective velocity. The measurements were performed at a Reynolds number of  $10^5$  based on the nozzle diameter. They note that the jet widening rate is a more sensitive indicator of self-preservation than the mean velocity profile, and that the widening rate and geometric origin depend strongly upon how far down the jet the half widths are measured. The longitudinal turbulent intensities

were found to exhibit self-similarity at  $X/D = 40$ , while the radial and tangential turbulent intensities did not reach self-similarity until  $X/D = 70$ , at which point the jet was self-preserving. They speculate that this difference in the onset of self-similarity is caused by the different modes of energy transfer from the mean motion. A comparison of turbulent intensities with the results of earlier measurements reveals the importance of the very low frequency components. At  $X/D = 90$ , 27% of the energy in the longitudinal fluctuations is at frequencies of 2 Hz and below, and 50% is below 5 Hz. Wagnanski and Fiedler's study concentrated upon measurements in the self-preserving region of the jet. Other studies of round jets have concentrated upon measurements in the initial region, which is responsible for the noise production of round jets which are aircraft powerplant exhausts.

One such study was performed by Bradshaw, Ferris, and Johnson (1964). Measurements were performed in a round jet at a Reynolds number of approximately  $3.5 \times 10^5$  with a Mach number of 0.3. Thus the flow was near the point at which compressibility effects become important for the mean flow. The authors explain that the Mach number effects reported in some previous studies are likely effects of the changing nozzle boundary layer which was carefully measured and found to be laminar in their case. A detailed analysis of the turbulent intensities and Reynolds stresses across

the mixing layer is presented, with emphasis placed upon the influence of the irrotational fields of the intense eddies in the center of the layer. The spectra of the turbulent intensities are also analyzed at locations across the jet, and it is observed that the spectra exhibit peaks in the inner region which are not present in the outer region. These peaks are said to indicate "some sort of wave motion in a preferred frequency range." In an effort to learn more about the static pressure fluctuations within the jet, frequency spectra and correlations were studied in the inner region. It was concluded that the irrotational field associated with the pressure fluctuations was composed of a small range of frequencies corresponding to the peaks in the spectra of the radial and tangential intensities measured near the center of the mixing layer. The irrotational field also is said to appear to be responsible for the convective velocities associated with the radial and longitudinal velocity fluctuations. It is concluded that the initial region of the jet is dominated by a group of large eddies which act as a series of jets which erupt outwards mixing with the entrained flow. These large eddies are found to be responsible for nearly one-quarter of the shear stress in the mixing layer within approximately two  $X/D$  of the mouth. Similar behavior is described in references reviewed in Section D of this chapter.

Bradshaw et al. performed measurements aimed at gaining information about the pressure fluctuations inside the potential core of the jet. They stated that it was impossible to measure the pressure fluctuations directly. Ko and Davies (1971) also sought measurements of the pressure fluctuations within the core for purposes of understanding jet noise phenomena. Noting that the hot wire is a mass flux sensitive transducer, they claim that within the potential core of the jet, the turbulent intensity levels are sufficiently low for the density fluctuations caused by the pressure field to dominate the hot wire response. They justify this conclusion with strong radial correlations within the potential core that imply convective velocities of the order of the speed of sound. Spectra were measured in the potential core and the mixing layer. Spectral humps were found in the potential core that were believed to be the result of "extra" energy associated with some combination of the presence of the hydrodynamic pressure field of the large eddies in the mixing layer and local increases in turbulent intensity. This hump was observed to begin at  $X/D = 0.5$  and to increase moving downstream. However, the hump was gradually masked by a build-up of low frequency turbulence as the end of the potential core was approached. The frequency of this spectral peak measured within the potential core agreed with the frequency in the spectra of the radiated sound

field outside the jet. These frequencies corresponded to Strouhal numbers based upon jet diameter and initial mean flow velocity of roughly from 0.5 to 0.7. The peak of the spectra in the mixing layer was observed to occur at a lower frequency than the peak inside the potential core. Thus the results indicated that the eddies in the mixing layer generated a sound field that acted upon the flow within the potential core as well as on the surroundings.

Pressure measurements in and around the initial region of a circular jet were performed by Fuchs (1972). Correlations of pressure signals from two microphones and of a velocity and a pressure signal from a hot wire probe and a microphone were performed. Some of the correlations were performed between signals narrow band filtered at frequencies corresponding to the spectral peak. The correlations revealed that the fluctuating pressure field originating in the mixing layer has a very high coherence over a cross section of the jet, particularly filtered at the frequency corresponding to the spectral peak. This behavior was found to be restricted to the initial region of the jet, within eight diameters of the mouth.

Planchon (1974) performed measurements of the fluctuating static pressure in a round jet using a sophisticated pressure transducer. The transducer bleeds a flow of air out through a probe similar to a static pressure tube. The bleed flow rate is controlled by the static pressure

at the bleed flow holes on the probe and measured by a hot film sensor mounted upstream of the transducer probe. The results of a comparison of measurements of pressure fluctuation intensities and longitudinal turbulent intensities measured along the centerline of the jet potential core indicate that Ko and Davies (1971) conclusion about the hot wire signal in this region is partially correct. Ko and Davies claimed that the density fluctuations associated with an acoustic pressure field dominated the velocity fluctuations in a hot wire signal in the potential core. Planchon's results indicate that the density fluctuations may dominate up to  $X/D = 3$ , by which point the velocity fluctuations have grown to the same order of magnitude. Thus the claim of Ko and Davies appears to be valid for roughly the first half of the potential core. Recall that they also noted peaks in the hot wire spectra inside the potential core and that the frequency of these peaks was very close to that exhibited by the spectra in the mixing layer. A detailed explanation of the origin of these peaks was not provided. This explanation falls in the province of stability theory and is discussed in the next section.

#### B. Instability of Jets and Mixing Layers

The papers reviewed in the previous section presented flow field measurements that indicate that a plane jet does not become self-preserving before it reaches at least

thirty nozzle widths from the mouth. Preceding the self-preserving region, the flow structure grows and adjusts. The rate and frequency dependence of the initial growth in the mixing layers bordering the potential core can be estimated from the results of experimental and theoretical studies of hydrodynamic stability. Such papers are reviewed in this section.

The basic goal of hydrodynamic stability theory is to offer a means of predicting the transition from laminar to turbulent flow. Schlichting (1968) gives a good historical review of the subject, tracing its origins to Osborne Reynolds' initial studies of transition in flow in pipes. The problem is shown to be a question of whether a disturbance introduced into a given laminar flow will experience growth or decay; if the disturbance decays the flow is stable with respect to the particular disturbance, and if it grows the flow is unstable and possibly may become turbulent. Mathematical attacks upon the problem have followed two paths. The first, originating with Reynolds, seeks to analyze the energy interactions of the disturbance with the mean flow to find whether the energy of the disturbance gains more through its action on the mean flow than is lost through viscous dissipation. This path has not proven as successful as the second, and is primarily of value for qualitative purposes.

The second path originated with Lord Rayleigh at nearly the same time as the first, and employs the equations of motion to predict the behavior of a disturbance. In practice, the disturbance is generally restricted to a small perturbation about the mean motion. After substitution into the two-dimensional equations of motion, the lower order terms and the mean flow solution are removed leaving linear equations. Solutions are assumed to have the form of travelling waves that are exponential in time (temporal) or space (spatial). The resulting equation is called the Orr-Sommerfeld equation, and using its boundary conditions it may be solved for eigen values giving wave numbers, propagation speed, and amplification factor. Alternatively, the viscous terms may be dropped along with two boundary conditions, and the inviscid solution found. If the amplification is positive the disturbance grows, and if negative it decays. The linearized version of this technique has enjoyed considerable success both inviscidly and viscously, while the much more difficult non-linear analysis has seen restricted application.

It is very important to realize that although successful analyses can be performed, they do not apply to the entire transition process. The linearized analysis applies to the initial stages of growth or decay of perturbations in a laminar flow, and results in information about the behavior of perturbations only in this region of linear

(exponential) growth. Between this region and the region of fully turbulent flow is a region of complicated non-linear phenomena which is not readily analyzed. This restriction must be remembered in considering the reviewed instability papers which generally deal with two-dimensional linear theory and experimental determinations of behavior in the linear region. Monin and Yaglom (1971) review instability theory and note that in 1933 H. B. Squire was the first to conclude that plane parallel flows disturbed with two-dimensional disturbances become unstable at lower Reynolds numbers than when disturbed with three-dimensional disturbances. For this reason, most interest has remained concentrated upon the two-dimensional case.

Sato (1960) performed an experimental study of stability which included measurements from the linear to the fully turbulent region. The subject of the study was a plane jet with a well developed initial velocity profile. Two modes of sinusoidal velocity fluctuations were observed, one at higher frequencies being symmetric with respect to the jet centerline and the other asymmetric. It was observed that the frequencies of fluctuation depended upon the initial velocity with wide nozzles exhibiting a dependence of frequency upon the three-halves power of velocity and narrow nozzles exhibiting a direct proportional relation. Instability frequencies are usually considered in non-dimensional form as Strouhal numbers. The Strouhal

number is defined as follows:

$$St = \frac{fL}{U} \quad (\text{II-6})$$

where  $f$  = frequency

$L$  = a characteristic length

$U$  = a characteristic velocity

The characteristic velocity used is the initial mean velocity at the mouth of the jet. There are, however, two choices for the characteristic length. One is the width of the nozzle, and the other is a width characteristic of the boundary layer thickness at the mouth. Sato notes that for his case of a narrow nozzle with a fully developed velocity profile, the boundary layer completely fills the nozzle and thus has a constant thickness. In this case the frequency was directly proportional to the velocity, so a Strouhal number calculated with the boundary layer thickness (a constant) is constant. For his case of a wide nozzle, the boundary layer did not fill the nozzle, and the boundary layer thickness varied with the inverse square root of the Reynolds number which is proportional to the inverse square root of the velocity. Using this boundary layer thickness dependence with the frequency proportional to the three-halves power of the velocity again yields a constant Strouhal number. Analyzing his experimental results by calculating a Strouhal number based on boundary layer momentum thickness,  $\theta$ , Sato found both the symmetric and anti-symmetric modes correspond roughly

to a constant Strouhal number,  $St_{\theta} = 0.015$ , over a range of Reynolds numbers based on slot width of 1500 to 8000. Sato also studied the instability behavior when the jet was subjected to acoustic forcing at various pure tone frequencies, and found that disturbances grew faster, reaching the non-linear region closer to the nozzle. The mean velocity profiles for the forced case also indicate that the width of the jet increased with forcing. Sato also performed inviscid linearized calculations of temporal instability modes and found good agreement with his experimentally measured values. It should be noted that some of the comparisons of experiment and theory were based upon a transformation of the theoretical temporal results to spatial form. Later analysis (Gaster (1965), reviewed further on in this section) showed that this transformation is not valid and as a result is somewhat inaccurate.

The same transformation was employed by Wille (1963) in analyzing an extensive study of transition in round and plane jets. Wille's study was concerned with the entire transition process from jet mouth to three-dimensional turbulence. Assuming that the initial boundary layer leaving the nozzle is laminar, the process is described as beginning with the laminar instability of the shear layer which results in the formation of two-dimensional vortices. Then through mutual interaction and instability

these two-dimensional vortices are transformed to three-dimensional turbulence. Measurements in the round jet covering a wide range of velocities and diameters indicated that for a range of Reynolds numbers based on jet diameter of  $10^4$  to  $10^5$ , the Strouhal number based on shear layer momentum thickness remains essentially constant for the frequency of maximum disturbance growth. The round jet experimental frequency results exhibited good agreement with inviscid linearized temporal stability theory. The amplification rates did not exhibit such good agreement. The lack of agreement might be attributed to the use of the transformation which Gaster (1965) reports to be improper. The frequency agreement was attributed to the high Reynolds number of the flow, but an apparent effect of viscosity was noted. It was found that for very small wave numbers, acoustic excitation did not lead to instability as predicted by the inviscid theory. The applied sound was found to regulate the vortices, hasten their growth, and increase their intensity. The experiments did confirm the rolling up of vorticity. An interesting behavior was acoustically forced upon the jet with two speakers driven  $180^\circ$  out of phase. They were positioned at opposite sides of the jet with their axes along a diameter. This type of forcing resulted in vortices which appeared like halves of the normally produced toroidal vortices. These vortices were produced alternately on one side and then the other of the jet.

Symmetric and asymmetric modes were also observed in the plane jet studied by Wille. It was found that for a sufficiently wide jet, the two shear layers acted independently; if only one were disturbed, the other underwent a natural transition process. Both acoustic forcing and vibrational disturbance with a vibrating ribbon in the nozzle boundary layer were employed, but it was found that the vibrating ribbon produced very unusual dips in disturbance amplitudes. It was speculated that this was a spurious, unnatural phenomenon caused by the wake of the ribbon. Measured natural frequencies agreed well with Sato's (1960) results; a constant Strouhal number based on momentum thickness of 0.0161 was found for slot Reynolds numbers greater than  $1.5 \times 10^4$ . The Strouhal number was found to decrease for lower Reynolds numbers. Inviscid calculations of temporal instability were performed using a velocity profile composed of straight line segments and the comparison with experimental results was poor. It was speculated that the neglect of viscosity, the non-parallel flow, and the crude velocity profile approximation were responsible for such poor results. The disturbance amplification factors, which were transformed improperly, also displayed poor agreement. An unusual result was that the maximum amplification rate did not occur at the natural frequency, corresponding to a Strouhal number of 0.0161, but at  $St_\theta = 0.0295$ . No explanation for this occurrence was offered.

Vortex fusion was observed, as a disturbance was seen to drop to one-half its original frequency by approximately 50 momentum thicknesses downstream. Vortex fusion or coalescence is the coming together or rolling up of two vortices to form one larger vortex with twice the initial wave length. This phenomenon is considered in more detail in Section D. It was observed that the application of sound moved the entire process closer to the nozzle.

The final stage of this transition is the instability of the two-dimensional vortices and their breakdown to full three-dimensional turbulence. Theory and experiment were employed in an attempt to determine a "critical initial circulation" by extrapolation. At this critical circulation, the vortex would break down to turbulence. The experiments and theory were applied to the easily measurable case of a Karman vortex street. The agreement was good, but the question of whether the result could be applied to jets required further study.

This process of vortex instability studied by Wille is the last process in the transition to turbulence. In order to reach the state at which this process occurs, the initial laminar shear layer has to exhibit instability. Sato and Sakao (1964) investigated the instability of plane jets at very low Reynolds numbers. They performed careful experiments with laminar jets in a very low disturbance environment. They found that for Reynolds numbers based

on nozzle slot width and maximum velocity, jets were completely laminar at Reynolds numbers less than 10. For Reynolds numbers between 10 and 50, damped periodic velocity fluctuations were observed, and above 50 the regular fluctuations developed into irregular turbulent fluctuations which did not necessarily result in fully developed turbulence. The same range of Reynolds numbers was investigated experimentally using acoustic disturbances and compared with theoretical results yielding fairly good agreement. A very complicated technique was required for the theoretical calculations, for at the very low Reynolds numbers of the study all terms change very fast in the region near the mouth. The spatial amplification results were obtained through integration in the downstream direction. An appreciation of some of the fine points of the temporal to spatial instability transformation appears to have been expressed. The existence of a critical Reynolds number of 4 was not verified experimentally due to an inability to perform accurate measurements of very low level amplitudes.

The problem involved in the transformation of temporal instability results to a spatial form has been mentioned several times. The awareness of these difficulties may be attributed to Gaster (1965). The assumed solution for the perturbation stream function is:

$$\Psi(y;x,t) = \Omega(y)e^{i(ax - \beta t)} \quad (\text{II-7})$$

For the temporal solution it is assumed further that

$$\alpha = \alpha_r \quad \text{Real only}$$

$$\beta = \beta_r + i\beta_i \quad \text{Complex}$$

Thus

$$\Psi(y;x,t) = \Omega(y) e^{\beta_i t} e^{i(\alpha_r x - \beta_r t)} \quad (\text{II-8})$$

where  $\beta_i$  is the temporal amplification factor

$\beta_r$  is the real frequency

$\alpha_r$  is the real wave number

Hence  $\beta_i$  is the growth with respect to time. Experimentally measured amplification factors are spatial rather than temporal, and so a large number of researchers attempted to convert temporal amplification factors to spatial factors to allow comparison of the results of temporal theory with the spatial experimental results. This was often done by assuming that

$$\frac{dx}{dt} = \frac{\beta_r}{\alpha_r} = C_r \quad (\text{II-9})$$

and then converting to obtain a spatial amplification factor. Letting,

$N$  = amplitude

$$\beta_i = \frac{dN}{dt}$$

$$\frac{dN}{dx} = \frac{dN}{dt} \frac{dt}{dx}$$

$$\frac{dN}{dx} = \frac{\beta_i \alpha_r}{\beta_r} \quad (\text{II-10})$$

This last term is the spatial amplification factor.

Gaster points out that this is in fact "the spatial growth apparent to an observer moving with the wave at speed  $C_r$  relative to the plate, and there is no justification for using this relation to compare the measured growth with the calculated parameter  $\frac{\beta_i \alpha_r}{\beta_r}$ ." This applies to instabilities in a boundary layer (over a plate), but also applies to free shear flows. Gaster shows that a relatively simple transformation is possible to get the correct spatial amplification factors for flows with low amplification rates such as boundary layers. This transformation applies for all the unstable cases. However for other flows with small amplification rates the transformation applies only close to the neutral (zero amplification rate) curve. For flows with large amplification rates such as free shear flows, transformation is not possible, and the equations must be solved for the spatial modes. This is done by assuming the solution

$$\psi(y;x,t) = \Omega(y) e^{i(\alpha x - \beta t)} \quad \text{as before,}$$

but with

$$\begin{aligned} \alpha &= \alpha_r + i\alpha_i && \text{Complex} \\ \beta &= \beta_r && \text{Real only} \\ \alpha_r &&& \text{real wave number} \\ \alpha_i &&& \text{spatial amplification factor} \\ \beta_r &&& \text{real frequency} \end{aligned}$$

Resulting in

$$\Psi(y;x,t) = \Omega(y) e^{-\alpha_i x} e^{i(\alpha_r x - \beta_r t)} \quad (\text{II-11})$$

Gaster presents spatial amplification factors obtained from spatial instability calculations and compares them with experimental spatial amplification factors and calculated temporal amplification factors incorrectly transformed. The differences displayed are significant. Gaster notes however that the neutral amplification curves resulting from the two cases are identical.

Michalke (1965) presents an interesting discussion of the history of the application of the faulty transformation. He observes that the application of this transformation resulted in comparisons with experimental results that in many cases showed agreement only to within an order of magnitude. These discrepancies disturbed theoreticians, and were blamed on numerous factors to no avail. Michalke performed temporal calculations of the instability in jet mixing layers and obtained disappointing results. Following Gaster (1965) he performed the spatial instability calculation reported in the paper. The details of the calculation are presented, and a comparison is made with improperly transformed results of a temporal calculation, showing an error in amplification factor of roughly 20% for the most strongly amplified disturbance. The vorticity distribution and streakline patterns are illustrated for the most strongly amplified frequency with a small disturbance applied. It may be seen that the streaklines exhibit a tendency to roll up. Estimates of the errors in these

linearized calculations are presented, and it is estimated that the theory holds reasonably well for distances up to 1.5 disturbance wavelengths from the mouth. A comparison with experimental results is also shown, and it is concluded that the spatial theory gives generally better predictions than temporal theory, particularly at low frequencies. The experimental results used in the comparison were obtained by Freymuth.

Freymuth (1966) gives a more thorough comparison of his data with temporal and spatial theory calculations. The data resulted from a study of the entire transition process in the laminar mixing layer on the edge of a jet. The layer was disturbed by an acoustic source, and it was observed that the amplification factor was independent of the sound pressure level applied, but that the origin of growth shifted. No dependence upon small changes in Mach number was observed, nor upon the position of the loudspeaker supplying the disturbances. The transition was found, within an accuracy of  $\pm 10\%$ , to be independent of the Reynolds number based on nozzle velocity and initial shear layer momentum thickness for a range of  $61 \leq Re_\theta \leq 334$ . This behavior was claimed to justify inviscid treatment. The dependence upon Strouhal number based on momentum thickness was found to be very strong. The transition process was, with the aid of smoke pictures, classified into four regions. First was the region of the

transformation of the nozzle boundary layer into a free mixing layer, second the region of exponential (linear on a log scale) growth, third the non-linear region characterized by the appearance of vortices, and fourth the fully turbulent region. The theoretical spatial instability calculations of Michalke (1965) are then presented and discussed with the same conclusions reached as in Michalke's paper. An interesting final statement by Freymuth claims that because of the observed Reynolds number independence of the transition process, the vortex break down cannot be characterized by a critical Reynolds number based upon circulation as discussed by Wille (1963) and previous workers. Freymuth's observations were that the vortices broke down through mutual interaction.

The laminar free shear layer was also the subject of experimental study by Browand (1966). The study was performed in an open return wind tunnel on a free shear layer formed from a laminar boundary layer flowing off a step to become a free shear layer. As in Freymuth's study, the shear layer was disturbed by sound. The behavior observed was similar as was the agreement with spatial instability theory. The major additions in Browand's paper were the emphasis upon the study of the spectra of the disturbances and the tests for the appearance of a spanwise periodic structure. The three-dimensional periodicity reported by earlier workers was not observed. The energy spectra of

the velocity in the non-linear growth region of the shear layer revealed interesting behavior. A strongly intermittent subharmonic (half-frequency) component of the disturbance frequency was observed in the spectra in the non-linear region. Numerous harmonics and a weak subharmonic of the subharmonic were also observed. It was noted that the appearance of the subharmonic was not caused by the acoustic forcing, for it was observed without forcing. Forcing served to "sharpen" the appearance of the spectra. It also was emphasized very strongly that the appearance of the subharmonic, which had been mentioned in passing by some earlier workers, was an inherent part of the instability phenomenon and not a result of instrumentation problems. It was observed that the flow was two-dimensional before subharmonic growth began, and that as the amplitude of the subharmonic component in the spectrum grew, the amplitude of the fundamental component decreased. A change in the distribution of properties across the shear layer was observed to accompany the appearance of the subharmonic. "A division of the primary wave disturbance seems to be occurring in the initial stage of subharmonic growth. A portion of the wave train moves upward and is convected at a higher velocity, and a portion moves downward with a decrease in velocity." In addition, high frequency bursts were observed on oscilloscope traces of the fluctuations in the region of subharmonics. It was speculated that

these bursts were the result of some form of secondary instability. It appears that these bursts could be a sign of breakdown to three-dimensional turbulence.

The significance of Browand's work is discussed by Mollo-Christensen (1967), his major professor. Observing that Browand's spectra were smoother without forcing, he states that "the smoothing most probably results from phase randomization of the fundamental instability. Therefore, although the velocity signal now is random, one should expect to see intermittently a rather regular spatial structure in the shear layer." He further suggests that "turbulence, at least as far as some of the lower-order statistical measures are concerned, may be more regular than we think it is, if only one could find a new way of looking at it." He also raises the question of the possibility of the early jet responding to its own downstream pressure fluctuations. The comments regarding the need for a new way of looking at turbulence provide a preview of the topic which is reviewed in Section D.

Returning to the results of Browand, Kelly (1967) is responsible for putting the concept of subharmonics on a respectable mathematical footing. Starting from Sato's (1960) observation of a subharmonic, Kelly employs temporal stability theory to examine the possible interactions of waves of different wavelengths on both sides of the wavelength of maximum amplification. The mechanism uncovered

"arises directly from the finite-amplitude growth of the fundamental instability." Essentially, it is found that at some point in its growth, the fundamental instability frequency can interact with a small disturbance at half its frequency and begin to reinforce it. Kelly goes through a complicated calculation to determine the point at which the phenomenon can begin, and using Sato's conditions finds that the fundamental must reach an amplitude of 12% of the mean velocity. Sato's experimental results indicate the phenomenon begins with the amplitude at 10%, so the agreement is rather good. Kelly also analyzes the possibility of using spatial theory for this prediction but concludes that spatial theory is not as well suited for the analysis and does not make the process appear as likely as does temporal theory.

Theory and experiment are combined in the paper by Beavers and Wilson (1970). Flow visualization studies of plane and round jets were performed in a water tunnel using dye to make the vortices visible. A regular periodic vortex structure was observed for both jets in the range of Reynolds number based on nozzle width or diameter from 500 to 3000. The plane jet displayed symmetric pairs of vortices at frequencies corresponding to Strouhal numbers based on nozzle width of 0.43. The circular jet produced vortex rings at a Strouhal number based upon nozzle diameter of 0.63. Both nozzles had sharp edges, but it was

found that rounding the edges did not affect the phenomena. Vortex coalescence was observed in the round jet. "As the rings move downstream, the flow pattern becomes irregular and breaks up, often as a result of one vortex ring catching up with the one ahead and moving inside it." Similar behavior was observed in the plane jet. Both jets were observed to be sensitive to external disturbances in the form of building vibrations. A round jet subjected to a vibration frequency below its natural frequency exhibited a sudden shift to twice the normal wavelength at about three diameters downstream. This appears to be equivalent to the formation of a subharmonic. The plane jet displayed a much longer vortex pattern before break-up when subjected to vibration at a frequency higher than the natural frequency. The influence of disturbances was also considered in the theoretical part of the study. Two infinite parallel vortex sheets were modelled by lines of point vortices, subjected to an initial disturbance, and numerically allowed to move with time. The velocity at each point resulting from the position of all the vortices was calculated and assumed constant over a short time interval allowing the calculation of a displacement for each vortex. The procedure was repeated through a time interval, and it was observed that the vortex lines rolled-up symmetrically and maintained their position in space. The symmetry of the process was observed for asymmetric initial

disturbances as well as symmetric ones. The finding that the vortices maintain their position, that is, that they are not carried downstream is somewhat surprising, but the authors did not question it.

Spatial theory is employed in linear inviscid form by Mattingly and Criminale (1971) in an analysis of a plane turbulent jet. Their calculations compare well with the results of Sato (1960). The calculations are based upon a  $U_0 \text{sech}^2(y)$  velocity profile for the whole jet. Their analysis indicates that disturbances symmetric about the jet centerline are more unstable than asymmetrical disturbances. The results are utilized in an analysis of vorticity, Reynolds stress and disturbance kinetic energy distributions. The vorticity distributions are used as a basis for a statement that the behavior resembles the classic Karman vortex street. The authors very advisedly caution that the analysis applies only in the region of exponential growth of small disturbances. Thus it must be noted that the conclusion about Karman-like vortices is based upon the changes in relative vorticity magnitude and not upon absolute magnitude. The strength of the fluctuations relative to the mean flow in this case is certainly less than that in a wake exhibiting a classic vortex street.

An experimental study of the entire transition process in a mixing layer between two moving streams was performed

by Miksad (1972). Unforced disturbances were found to exhibit subharmonic formations similar to those observed by Browand (1966). Most of the study was performed with the instability forced acoustically. The entire transition process was observed to occur in a distance equivalent to five wavelengths of the disturbance. Miksad observed that transition could be divided into six regions. The first region was that of exponential growth of the fundamental disturbance in accord with linearized theory. The agreement of the measured amplification factors with spatial theory was good at low frequencies and within roughly 10% to 20% near the most unstable frequency. Phase agreement across the layer was also good near the beginning of the region. This region covered roughly 14% of the distance required for the complete transition process. The second region covered about 6% of the transition length and was marked by the appearance of non-linear phenomena; the growth of harmonics of the disturbance frequency and the subharmonics and  $3/2$  harmonic. The growth rates of these parts of the spectra were greater than that of the fundamental frequency which continued to grow exponentially. It is noted that when the same apparatus and instrumentation were used for measurements in the plate wake, subharmonics were not observed. (A wake results when the velocities are the same on both sides of the plate.) Thus it was concluded that the subharmonics were an inherent

feature of free shear layers. The third region covered roughly 27% of the transition length and was characterized by the end of exponential growth of the fundamental, harmonics, and subharmonics. All modes appeared to stop growing. The fourth region displayed renewed growth of the subharmonic and  $3/2$  harmonic while the fundamental remained at the same level and the harmonics began to decay. This region covered 10% of the transition length. The next 26% was called the fifth region, and it was characterized by the beginning of three-dimensional distortion, the decay of the fundamental, and decreases in the growth rates of the subharmonic and the  $3/2$  harmonic. The possibility that the three-dimensional effects were in part caused by the span-wise dimensions and walls of the test facility was raised. The final transition to full three-dimensional turbulence occurred in the last 16% of the transition length. In this region the spectrum lost its discrete appearance, becoming continuous as the flow became truly three-dimensional. It was noted that the high frequency bursts observed by Browand (1966) were not observed. Thus, this study presents a good description of the spectral behavior observed during transition in a mixing layer. The subharmonic formation is verified and found to conform to Kelly's (1967) model.

The breakdown process of plane jets was studied over the Reynolds number (based on nozzle width) range from 1860

to 10,800 by Rockwell and Niccolls (1972). A water tunnel was employed with hydrogen bubble flow visualization techniques and motion picture photography. Four zones of jet growth were observed corresponding to those identified by Freymuth (1966). Vortex coalescence was observed to occur both early in the vortex lifetime and at a later stage. The natural breakdown process cycled between symmetric and asymmetric modes at higher Reynolds numbers, and the vortices were seen to move downstream at a velocity roughly one-half the initial mean velocity. The motion pictures revealed that the "apparent time mean widening of the jet in the region immediately downstream of the nozzle exit is characterized by the formation and subsequent coalescence of vortices formed outside the nozzle exit." In addition, the breakdown Strouhal number based on slot width was found to be proportional to the square root of the Reynolds number. A discussion was published with the paper, and in the discussion O. K. Oseberg and S. J. Kline noted that in a similar study they performed at Stanford in 1971, the effect of the differing conditions at the mouth of their jet "vanished" by  $X/D = 13$ . Oseberg and Kline's report has not been obtained.

The models of instability behavior which have been utilized in these reviewed papers have been linearized and generally have neglected viscosity. Grant (1974) performed numerical calculations including viscous and non-linear

effects. The numerical integration of the equations of motion was carried out for a coarse grid averaging one-half of a round jet. The equations were written in terms of a stream function and vorticity. Different initial velocity profiles and Reynolds numbers were used, and some calculations were seen to exhibit large effects of numerical error. The successful calculations did agree well with experimental studies and showed that the instability mechanism was not dependent upon three-dimensional effects. The flow field was observed to be dominated by a large scale toroidal vortex structure, in agreement with experiments. The Strouhal numbers and wavelengths of the resulting structures agreed with experimental values except for one experiment by Crow and Champagne (1971) reviewed later in this chapter. Crow and Champagne's Strouhal number is approximately one-half of that obtained by Grant. Streaklines were calculated, and did exhibit a rolling up. It was pointed out that the rolling up of the streaklines was a necessary but not a sufficient condition for the existence of vorticity concentrations, and that this should be kept in mind in interpreting flow visualization experiments.

### C. Disturbed Plane Jets and Related Flows

The history of the study of the effects of sound upon jets was surveyed in the previous chapter, and it was shown that the classical studies were chiefly concerned with effects upon the laminar-turbulent transition process.

Modern studies of the effects of sound upon flows have considered several other phenomena. A considerable body of literature has considered the effect of sound upon heat transfer, particularly heat transfer from circular cylinders. The present study is concerned only with the effects of sound upon incompressible free shear layers, and the literature dealing with effects upon heat transfer is not reviewed. Similarly, papers dealing with the effects of sound upon supersonic jets are not reviewed. Examples of such studies are those of Glass (1968) and Lebedev and Telenin (1970). These studies indicate that large changes in jet structure result from acoustic pressure waves radiated by the strong pressure fluctuations downstream in supersonic jets. The acoustic waves apparently travel through the surrounding air to control the structure in the initial region of the jet. The control process involves changes in such things as oblique shock structure, and thus the phenomenon is of little relevance to incompressible flow jets.

The transition of laminar incompressible plane jets was studied by Chanaud and Powell (1962). Using flow visualization techniques in water jets and velocity measurements in air jets, they constructed families of constant disturbance level curves of Strouhal number of disturbance versus Reynolds number for transition. Their most interesting result was that in the water jet they always

observed asymmetric modes of vortex growth, and never the symmetric modes observed by others.

Measurements of changes in the turbulent structure of round jets were made by Vlasov and Ginevskii (1967). Measuring on the centerline at  $X/D = 8$ , they found that in the Reynolds number range between  $6.5 \times 10^3$  to  $5.2 \times 10^4$ , applied sound at frequencies corresponding to Strouhal numbers based on nozzle diameter of 0.2 to 1 decreased the mean velocity and increased the turbulent intensity. Strouhal numbers of 1 to 5 had the opposite effect, and the application of white noise had little effect. These results were obtained in nozzles with an initial turbulent intensity of less than 1%. It was found that sound could cause lower amplitude changes of the same type even when the nozzle boundary layers were artificially tripped resulting in an initial turbulent intensity of 11%. The lateral distributions of Reynolds stress, mean velocity, and the turbulent intensities were also measured. The Reynolds stresses were found to reach their highest relative value for the no sound case. The mean velocity profiles showed that decreases in centerline mean velocity were accompanied by increases in jet width and vice versa. The turbulent intensities at a Strouhal number of 0.38 were all above the no sound values with those at 3.8 below the no sound values. Distributions of the mean velocity and turbulent intensity along the centerline for these

three cases revealed that in the low Strouhal number cases the centerline mean velocity decayed fastest, followed by the no sound, and the high Strouhal number case. The low Strouhal number turbulent intensity grew fastest to the highest level while displaying a peculiar hump at  $X/D = 8$ . Intensities were measured to a distance of 48 diameters downstream. The high Strouhal number case grew slowest with the no sound case in the middle. The authors speculated that these effects might be caused by the interference of the disturbances in the turbulent energy cascade process. The cascade process is a hypothesis about turbulent energy transfer. It states that the turbulent energy gained from the mean flow through the large eddies is successively transferred through smaller and smaller eddies until it is dissipated by molecular viscosity. It was speculated that the energy input at the disturbance frequencies interfered by producing changes in the energy gradient through the cascade. Energy spectra at  $X/D = 3$  did show peaks at the disturbance frequency and its first harmonic. The peaks were not visible at  $X/D = 9$ .

A round jet was also studied by Becker and Massaro (1968). Their experiments relied upon flow visualization techniques to determine the effects of sound on a round jet at Reynolds numbers from 600 to 20,000. The jet had a "top hat" initial velocity profile and exhibited sinuous modes of instability below a Reynolds number of 2300 and

axisymmetric modes above. The frequencies which had maximum effect upon the jet were found to follow the relation:

$$St_D = 0.012 \sqrt{Re_D} \quad (II-12)$$

where both the Strouhal number and the Reynolds number were based on jet diameter. The frequencies did however follow a pattern of stair-step increase, and the authors did advance the possibility of a resonance phenomenon. These frequencies caused the spreading angle of the jet to increase and the point of breakdown to three-dimensional turbulence to move closer to the nozzle. At Reynolds numbers above 2800, vortex coalescence processes were observed, and above 10,000 the clarity of the vortex behavior was obscured by the turbulence. Details of the vortex growth process including the distances required for various parts of the process to occur were also reported.

An interest in fluidic devices and sound motivated a study by Roffman and Toda (1969). They noted that sound can be used to switch bistable fluidic amplifiers, and that environmental noise could adversely affect other fluidic devices utilizing jets. They performed measurements and took flow visualization photographs of an acoustically disturbed plane jet at Reynolds numbers from 200 to 4000 based on slot width. Pressure profiles measured at  $X/D = 15$  revealed that sound decreased the peak pressure and widened the profile. Flow visualization revealed that sound caused the jet to widen at a greater rate and closer

to the nozzle, as well as to display more regular vortex patterns. The frequency of maximum sensitivity was found to correspond to a constant Strouhal number,  $St_D = 0.14$ . One reason offered for the constant Strouhal number was an effect of a plenum resonance. It would, however, appear that if an acoustic resonance were involved, the frequency rather than the Strouhal number would remain constant. The location of the interaction was investigated with the use of a local sound source consisting of a plastic tube transmitting sound from a remote speaker. It was found that the jet was sensitive to the low level sound from the tube only within one nozzle width of the mouth. Actual fluidic amplifiers were also exposed to sound and their performance was found to exhibit effects of sound relatively smaller than the structural changes produced in the jet itself. The design geometry of the devices was responsible for this relative insensitivity.

The effects of relatively low frequency sounds upon a heated round jet issuing from a diffuser were studied by Ivanov (1970). Frequencies corresponding to Strouhal numbers of 0.03 to 0.05 were applied to the jet at a constant Reynolds number of approximately  $5 \times 10^4$ . The dimensionless parameters were based upon exit diameter. Both mean velocities and longitudinal turbulent intensities were observed to be lower than the undisturbed case.

Reports of the effects of sound on round jets, plane jets and jets controlled by acoustic feedback edgetones were surveyed by Rockwell (1971). He observed that the disturbance of round jets had been found to produce toroidal vortices, and he presented a plot of  $St_D$  versus  $Re_D$  for the region of sensitive frequencies found by several investigators. For plane jets, induced eddy shedding and growth were reported for frequencies in the sensitive region, while at higher frequencies transition was retarded and mean velocity profiles were narrowed. The sensitive frequencies found for plane jets by several investigators were plotted on a  $St_D$  versus  $Re_D$  diagram. The resulting sensitive region appeared somewhat larger than that for circular jets. It was observed that generally the largest effect upon a jet was obtained by disturbing it at its natural frequency of self-excitation. It was observed that the plotted Strouhal numbers based on width or diameter of the nozzle allowed calculation of the most sensitive frequency at best to within a factor of 2. It was pointed out that the flow was dependent upon the conditions inside the nozzle and that these conditions could be partially accounted for by utilizing a nozzle boundary layer parameter such as the momentum thickness in place of the nozzle width or diameter in forming a Strouhal number. Rockwell summarized the various investigators' results as showing that disturbing a jet at a relatively low Strouhal number

tends to widen the mean velocity profile, decrease the centerline mean velocity, and increase the turbulent intensity on the axis while disturbing with a relatively high Strouhal number tends to bring about the opposite changes.

Kaiser (1971) and Goldschmidt and Kaiser (1971) studied the interaction of transversely applied pure tone sounds with a plane turbulent jet. The interaction was studied for jet Reynolds numbers of 4500 to 6000 and Strouhal numbers of roughly 0.2 to 2.0. The effect was studied throughout the region from the mouth to  $X/D = 70$ . It was reported that the jet was very sensitive to the proper frequency, with the geometric origin, the widening rate, and the decay rate all showing effects of the disturbance. The mean velocity profiles were found to maintain similarity. The widening rate was found always to exceed the no sound value when the jet was disturbed. The maximum widening rate was roughly 20% higher. The frequency dependence of the changes was found to exhibit a number of relative maxima, giving a suggestion of periodic behavior. The question of whether the periodic behavior was caused by an acoustical resonance or standing wave was resolved by careful acoustical measurements of the flow field which did not indicate such phenomena. The frequency dependence also did not exhibit similar behavior at the different Reynolds numbers. For Reynolds numbers based upon nozzle width of 4500, 5150, and 6000, the most

sensitive frequency corresponded to Strouhal numbers based upon nozzle width of 0.38, 0.37, and 0.42 respectively. The longitudinal turbulent intensity at the mouth was found to be unchanged by sound, indicating no effect upon the flow inside the nozzle. However, outside the nozzle, the intensities of the disturbed case were higher than the undisturbed case all the way along the centerline to  $X/D = 70$ . Thus both the mean profiles which determine the widening rate and the turbulent intensities were found to display the results of the interaction with sound to a distance of 70 nozzle widths downstream of the mouth.

A study of the effects of applied sound on curved wall jets was performed by Rockwell and Toda (1971). Fluidic switching devices allow jets to be attached to one side wall or the other depending upon the input control signal. The effect of sound on the attachment process was studied. The result of interest to general studies of the effect of sound on jets is the finding that by applying sounds at very high amplitudes the jet was found to be affected by frequencies well below the conventional sensitive frequencies.

The studies reviewed so far have utilized relatively low disturbance levels in modifying the jet structure. It is interesting to observe the effects of very large disturbances to attempt to obtain a view of a limiting process in disturbed jets. Binder and Favre-Marinet (1973)

have performed such a study. They pulsed a round jet with a rotating butterfly valve mounted upstream. The pulsing could reach a value of 40% of the mean velocity at the mouth. The Reynolds numbers of the study were greater than 10,000. The main findings were that the length of the potential core was reduced from an undisturbed length of 5 to 6 diameters to only 1 diameter by large amplitude pulsing. Pulsing at a Strouhal number 0.18 and an amplitude of 0.25 caused an increase of roughly 40% in the widening rate and roughly 20% in the centerline velocity decay. The asymptotic rates also were reached by 7 diameters while the unpulsed case required 13 diameters to reach its asymptote. It was observed that a small pulsing (3%) reached its asymptotic rate faster but had the same slope as the unpulsed case. A sophisticated phase-averaging technique was used to separate the pulsation contribution to the turbulent intensity from the random turbulence. It was found that the contribution by the pulsations had decayed to zero at 4 diameters from the mouth. The turbulent intensity on the centerline in the case of 25% pulsing reached an asymptotic value of 31% which it appeared to maintain, at least through 20 diameters downstream. The unpulsed jet reached a turbulent intensity of 23% at  $X/D = 20$ . The phenomenon did show a dependence upon Strouhal number of the pulsing; it was not an effect of large turbulent intensity only. The authors state that the

"remarkable fact is the apparently indefinite persistence of the improved mixing in pulsating jets although the pulsation is completely washed out at  $10 d_0$  [diameters] downstream." It should be noted that the measurements presented in the paper apparently extended to 25 diameters downstream. The idea that jets may exhibit a subrange of mean flow behavior before reaching their final asymptotic widening and decay rates was proposed by Heskestad (1965) in a paper reviewed earlier in this chapter. It would seem that such a phenomenon could occur in this case. Accompanying the paper by Binder and Favre-Marinet (1973) was a flow visualization study of a pulsed jet performed by Curtet and Girard (1973) under slightly different conditions in a different set up. The pictures, including one of an undisturbed round jet, illustrate the entrainment process and the chaotic motions that actually make up the mean profiles.

Another study which used flow visualization techniques to gain an understanding of the interaction between a disturbance and a plane jet was performed by Rockwell (1972). Hydrogen bubble flow visualization was utilized with a plane jet in a water tunnel. The jet was disturbed by an oscillating plate positioned some distance away from the nozzle. The jet was observed over a range of Reynolds numbers from 1860 to 10,800, for various disturbance Strouhal numbers. The behavior of the jet indicated that

the response to the disturbances could be classified into five regimes, with the natural undisturbed jet breakdown serving as a reference behavior. The highest Strouhal number regime was called the "upper zone regime." This regime corresponded to disturbance Strouhal numbers at least three times the natural breakdown Strouhal number. In this regime it was observed that the jet was essentially unaffected except for small insignificant vortices whose formation was induced by the disturbance on the outer edges of the jet. The next lower regime was termed the "preservation regime." The disturbance Strouhal numbers in this regime were from three times the natural Strouhal number down to almost the natural number at higher Reynolds numbers. The regime was marked by the formation of small vortices which underwent controlled coalescence while the jet potential core was relatively preserved. The next regime was that in which the disturbance frequency was the same as the natural breakdown frequency. It was named the "matched excitation" regime. This regime was marked by increased vortex formation, growth, and coalescence which resulted in very strong distortion (bending) of the potential core. This effect was observed to be strongest at the lowest Reynolds numbers with behavior at high Reynolds numbers approaching that of the preservation regime. Rockwell noted the contrast between the behavior of the plane jet disturbed at its natural frequency and the behavior of

round jets. The plane jet behavior is characterized by asymmetric behavior while the round jet displays axisymmetric modes. At frequencies of approximately one-third the natural frequency the behavior appeared to justify the title, "forced fusion regime." The disturbance caused the formation of large vortices which appeared to cause the natural vortices "to become squeezed together" and around the large vortices as "frills." Rockwell noted this behavior appeared as though it could increase the width of the mean profile and increase the turbulent intensity near the half width point of the profile in accordance with quantitative measurements by other researchers in this regime. The final regime occurs at frequencies less than one-tenth the natural frequency and is termed the "low frequency zone regime." The disturbances in this regime appeared to have no effect. Rockwell made a number of comparisons in this study with previous quantitative and qualitative studies and found general agreement. He also remarked that the numerical vortex sheet computations of Beavers and Wilson (1970) display many features similar to those shown in his motion pictures. The study gives good descriptions of the phenomena which occur in the initial region of the jet, and offers plausible explanations for observations made farther out in the jet beyond the scope of the study ( $X/D \approx 6$ ). These explanations suggest that the disturbance effects which have been measured in the main region of

are the results of interactions in the initial region. This view of the interaction process is widely held, and the literature suggests that it is, at least in part, correct.

Morkovin and Paranjape (1971) have proposed a mechanism that offers an explanation of the manner in which vortices are generated by the action of sound. Their hypothesis is based upon experiments performed in a plane jet with movable "local" acoustic sources. Two of these sources were two-dimensional line sources located on either side of the nozzle. It was found possible to excite symmetric modes with these sources. The other two sources were "point" sources which could be located anywhere in the jet. A probe tube microphone was used for "point" measurements of sound pressure level. Experiments were performed using the point sources positioned symmetrically about the jet centerline. It was found that moving the point sources while maintaining the sound pressure level at the nozzle lip constant resulted in the same amplification factors for the disturbances in the shear layers. Thus it was concluded that the interaction occurs at the nozzle lips. Experiments performed with only one of the point sources produced conflicting results that eventually led to the conclusion that the growth was not dependent upon the amplitude of the acoustic pressure, but upon the spatial gradient of the acoustic pressure. Experimental

results were obtained that suggested the validity of the hypothesis. A physical model for the interaction process was suggested.

One idealized model, which suggests this dependence on the [acoustic] pressure gradient near the detachment of the jet from the curving lip, visualizes back-and-forth motion of the detachment point under the dynamic action of the driving acoustic field. This model simultaneously provides a mechanism for the conversion of irrotational waves to vorticity fluctuations since the variable contact with the solid surface would cause a time-varying vorticity discharge past  $x = 0+$ .

Miksad (1972) in his study of shear layer instability advanced a similar model. His apparatus, partially described in Section B, consisted of two streams separated by a splitter plate, with a loudspeaker placed upstream in the plenum of one stream with its axis perpendicular to the plane of the splitter plate. He stated the following:

It is believed that the principal effect of the loudspeaker excitation was to shift the location of the [leaving] stagnation point on the splitter plate up and down, thus injecting vorticity in the free shear layer. This supposition is supported by our observation that a loudspeaker placed at the downstream end of the wind tunnel was rather ineffective in exciting shear-layer disturbances and, in particular, antisymmetric disturbances.

This statement appears to suggest a model that agrees with Morkovin et al. The mechanism seems to agree with experiments and thereby must be considered as a possible initial phase of the interaction process.

A very different interaction process was hypothesized by Simcox (1969) and Simcox and Hoglund (1971). The direct interaction of sound with the flow through vortex

stretching and convection by the acoustic field was considered theoretically. Series expansions of the flow field pressure and velocity were performed and substituted into the Navier-Stokes equations. The acoustic "particle" velocity and pressure were added to the respective first order expansion terms in the equations. The equations were converted to vorticity form and terms were ordered. It was found that acoustic particle velocity interacted with the first order vorticity in the second order vorticity equation. Note that an equivalent term involving the first order flow field velocity also was present. The interaction term was considered separately, averaged over an interaction period, and then substituted back into the original equation. Further analysis yielded the result that the interaction was maximized when the acoustic wave number equalled the flow wave number. Consideration was given to the turbulent energy spectrum, and the Reynolds stresses. It was concluded that the interaction would have no direct effect upon the Reynolds stresses. It was hypothesized that the major effect of the interaction on the flow occurred through its alteration of the spectral energy content and resulting interference in the energy cascade. The same hypothesis has been discussed earlier in this chapter in connection with the paper of Vlasov et al. (1967).

This hypothesis was also considered in a paper by Borisov and Rozenfeld (1971). Their paper surveyed effects of sound upon several types of flows, concentrating upon stability considerations. They noted the hypothesis expressed by Vlasov et al. and reported that another researcher had analyzed the problem and concluded the frequency dependence of the effects observed by Vlasov was more readily explained in terms of the jet instability frequency than by energy cascade interference.

Another direct interaction mechanism has been proposed by Ajagu (1976). Recall that a two-dimensional turbulent jet is bounded by a moving interface which separates it from the non-turbulent surroundings. Entrainment is mass crossing this interface, and it has been suggested that the first phase of this crossing involves an engulfment of non-turbulent fluid by a contortion of the interface termed a "fold-over." The jet studied by Ajagu was well documented by Jenkins (1974) and Mulej (1975) who had studied its intermittent properties. The objective of the study of Ajagu was to measure various properties of the behavior of the interface with particular emphasis upon determining the extent of fold-over. As part of this study, a limited series of measurements were performed with an acoustic disturbance applied transversely in the main region of the jet. Increases in the widening rate of the jet were found to be accompanied by increases in the

percentage of fold-over. Changes in the intermittency distribution were also reported. These results must be interpreted with caution, for they were the product of limited measurements. In particular, their comparison with the undisturbed case made use of disturbed mean flow parameters such as the jet half width. This also resulted from limited measurements. The uncertainties in the disturbed results are considerably larger than those in the undisturbed case results.

The reviewed papers indicate that jets and related flows can be affected by the application of a disturbing sound field. The effects have been reported to include changes in the mean and turbulent structure, and several theories of the interaction mechanism have been proposed. The reviewed flow visualization studies indicate that the vortex structure may play an important role in the interaction. Studies of the role of large scale vortex structure in turbulent flows are reviewed in the next section.

#### D. Large Scale Orderly Structures in Turbulent Flows

Large scale orderly structures have always been present in some turbulent flows, and a survey of the older literature reveals that many researchers recognized and commented on various aspects of large scale behavior. The current interest in large scale structures stems from findings of recent years indicating that some turbulent flows are more orderly than previously believed.

Experiments utilizing flow visualization and specialized measurement techniques have shown that the structures maintain their coherence over greater distances than previously revealed by standard measurement techniques.

Townsend (1956, 1966) is generally credited with being one of the first to recognize the important role played by the large scale components of the flow. In modelling a free shear flow, he recognized the role of the large eddies.

...the observed rate of spread of free turbulent flows is largely due to a large-scale mixing motion by an easily distinguished group of eddies whose scale is very considerably larger than the scale of the eddies containing most of the turbulent energy. These large eddies by contorting the bounding surface of the fully turbulent fluid allow entrainment to proceed over a considerably larger surface than would otherwise be possible, and so control the rate of spread of the whole flow.

He also suggested that the large slow eddies that he described served to convect the smaller scale turbulence. A further hypothesis was that the large scale eddies controlled the turbulence level through a role as intermediary between the mean flow and the smaller scale energy containing eddies.

Grant (1958) studied the large scale structure in a cylinder wake and a flat plate boundary layer through correlation measurements. Only the wake results are considered here, for this survey covers only free shear layer structures which are directly relevant to the present study. In the wake he concluded that two types of large scale structure were in evidence. One type was vortex

pairs rotating in opposite directions with their axes normal to the plane of the wake. Along with these vortices, jets of turbulent fluid projected from the wake core were apparent. It was suggested that these jets resulted from an instability of the turbulent shear stress.

Large eddies resembling the mixing jets observed by Grant in wakes were found to be present in the initial region of a circular jet studied by Bradshaw et al. (1964). Mollo-Christensen (1967) reviewed his own work in jet noise studies and that of his student, Browand (1966) in shear layer instability, concluding that, as previously quoted, a new method of studying turbulent flows might uncover greater regularity in the flow structure.

A new method was not needed by Brown and Roshko (1974), and Roshko (1975). They performed a flow visualization study of the turbulent incompressible mixing layer formed between two gases at a pressure of 10 atmospheres. This pressure and the choice of gases (nitrogen and helium was one combination) allowed very detailed shadowgraph pictures to be taken. The pictures, first published in 1971, revealed a very regular structure in the turbulent mixing region. The structure appeared similar to a sequence of breaking ocean waves. The behavior was observed to have some similarities to that exhibited in the late non-linear regions of laminar shear layer instability. However, this of course, was a fully turbulent flow. Roshko stated that

the pictures initially were surprising and that it was thought they they resulted from vibrations in the set up or some other experimental problem. Eventually it was concluded that the pictures truly revealed the structure of the flow. Brown and Roshko stated:

It seems astonishing that many years of research on mixing layers, much of it with the help of sophisticated methods of hot-wire anemometry, had not drawn a picture of such clearly defined, distinctive structures. There is often no substitute for direct flow visualization.

Analysis of their motion pictures revealed that the eddies moved at nearly constant speed and increased their size and spacing through coalescence. The coalescence process was occasionally observed to involve as many as four eddies at one time. Their work generated considerable interest in the phenomenon.

At approximately the same time, Crow and Champagne (1971) reported results of a study of orderly structure in a round jet. Using flow visualization and quantitative measurements, they uncovered the existence of large scale orderly axisymmetric turbulent "puffs." These puffs occurred at a Strouhal number based on nozzle diameter of approximately 0.3 and Reynolds numbers greater than  $10^4$ . They were a turbulent phenomena that were formed even when the laminar nozzle boundary layer was tripped. The difference between these puffs and the laminar shear layer instability behavior was emphasized. The laminar instabilities scale upon the nozzle boundary layer thickness while

the puffs scaled upon the jet diameter. The puffs were observed to be formed by the repeated coalescence of vortices which had resulted from the non-linear phases of the initial instability process. The puffs grew rapidly near the end of the potential core at four diameters downstream from the nozzle. The puffs were much more intermittent than the laminar instability waves. In order to study the process in detail, the flow was forced by a loudspeaker which excited resonances of the plenum upstream of the nozzle, resulting in rms fluctuation amplitudes at the mouth of up to 2%. It was found that the  $St = 0.3$  mode was the preferred mode in that it reached the highest amplitude at saturation. The peak amplitude occurred at  $X/D = 4$  and then decayed. The disturbance imposed upon the jet was observed to control the phase of disturbances out to approximately  $X/D = 8$ , beyond which it was ineffective. Forcing at  $St = 0.6$  resulted in violent subharmonic formation at  $X/D = 4$ . This subharmonic was, of course, at the preferred mode frequency,  $St = 0.3$ . This preferred mode was believed to reach its high amplitude because it was the wave least capable of generating a harmonic. The generation of a harmonic slows the growth of the fundamental and leads to amplitude saturation. Forcing this mode was observed to increase the entrainment in the initial region, increase the turbulent intensities in the potential core and the outer half of the shear layer, slightly

increase the jet spreading, and move the origin of the velocity decay inwards two diameters toward the nozzle. The energy spectra revealed that the turbulent energy was concentrated in spikes at the fundamental and its first two harmonics, with the broadband background turbulence suppressed over the unforced case. Comparisons with stability theory for non-linear dispersive waves surprisingly revealed a much better agreement with temporal theory than with spatial theory. This documentation of an orderly structure in the turbulent region of a round jet was of great interest to researchers in turbulence and in jet noise. A number of papers on jet noise produced by modelling of orderly structures followed.

Round jets exhibit many similarities with plane jets, but an important distinction between the two exists in the initial region. The round jet potential core is surrounded by a single annular mixing layer while the plane jet potential core is bounded by two separate plane mixing layers. The question of whether plane jets had such an orderly structure present was addressed by Thompson (1975). A plane jet was forced by a loudspeaker exciting a resonance in the plenum. The Strouhal number based on nozzle width was varied from 0.15 to 0.60 by changing the initial velocity, resulting in a Reynolds number that ranged from 31,600 to 8000. The nozzle boundary layer was not tripped as Crow and Champagne (1971) had done, and hence some Reynolds

number dependence was retained for the shear layer and mean flow behavior. Symmetric shear layer modes were excited by the symmetric forcing. In the Strouhal number range studied, a preferred mode of the type observed by Crow and Champagne was not found. The forcing frequency component of the turbulent intensity found by Thompson did not approach the high levels found by Crow and Champagne. However, his method of finding this component apparently used a much narrower effective bandwidth than theirs. The results from the linear regions of the shear layer growth were found to compare well with Michalke's (1965) linear inviscid theoretical calculations except for phase behavior which disagreed with Michalke and with Freymuth's (1966) measurements as well. Results of the forcing on the mean velocity profiles, turbulent intensity profiles and related properties were presented. The mean profiles displayed small effects. The centerline mean velocity had small changes, as did the half widths. It should be noted that the Reynolds-number effects were nearly as large as the forcing effects in these parameters. In addition, measurements of these parameters were performed only to a distance of 15 nozzle widths downstream. It also appears that the jet was unbounded by confining plates and hence was asymptotically approaching three-dimensional behavior. The jet aspect ratio was quite large though. The mass flux and entrainment rate showed much

smaller effects than those found by Crow and Champagne (1971). Thus a similar mode of orderly structure was not found in this plane jet. The lack of boundary layer tripping and the sizable Reynolds number variations may have had an effect upon these results. Also, the Strouhal number of maximum amplification in the shear layer, 0.45, was not studied in the detail used on 0.18 and 0.30. The instability calculation agreement with spatial theory cannot be compared with Crow and Champagne's calculations for turbulent non-linear instability; the cases are different. A question may also be raised about the symmetric forcing of the shear layers, for the asymmetric mode is more common at high Reynolds numbers. Thompson's recommendations for future study included study of the asymmetric case.

The results of Crow and Champagne (1971) were duplicated and extended to higher Strouhal numbers by Hussain and Zaman (1975). They found that Crow et al.'s preferred mode of 0.3 could be attained in their rig when the nozzle boundary layer was tripped, but that when untripped 0.4 was preferred. Their data with the tripped nozzle essentially duplicated that of Crow et al. It was found that forcing moved the turbulent intensity peak upstream with little effect upon the centerline mean velocity. Noticeable changes in the mass flux, momentum flux, and jet half width were observed in the initial region of the jet. For

the untripped nozzle, a strong subharmonic of  $St = 0.8$  was formed as a result of the coalescence of vortical puffs. Higher Strouhal numbers were studied without tripping, so comparisons must be viewed with this difference in mind. Through  $St = 1.2$ , turbulent intensities were found to be increased. Beyond 1.2, the turbulent intensities decreased and the peak of the axial profile shifted downstream.  $St = 1.6$  exhibited the strongest turbulence suppression. Higher Strouhal number forcing did not appear to suppress turbulence as much as some of the literature suggests. The major contribution of this paper is its confirmation of Crow and Champagne's results in a different set up at different Reynolds numbers.

Other measurements reporting coherent structures in turbulent round jets have been reported by Wooldridge and Wooten (1971). They concentrated upon measurements in the initial region of the jet, measuring mean velocities, turbulent intensities, spectra, and correlations. From the measurements, convective velocities were calculated for the entire flow spectrum and for various octave frequency bands. It was found that the radial distribution of the broad band convective velocity did not vary as much as the mean velocity. The narrow band convective velocities tended to exhibit smaller changes than the broad band. A continuation of this study was reported by Wooldridge, Wooten, and Amaro (1972). Mean velocities, turbulent

AD-A071 261

PURDUE UNIV LAFAYETTE IND RAY W HERRICK LABS  
ACOUSTIC INTERACTION WITH A TURBULENT PLANE JET. (U)  
AUG 77 F W CHAMBERS, F WILLIAMS  
HL-77-31

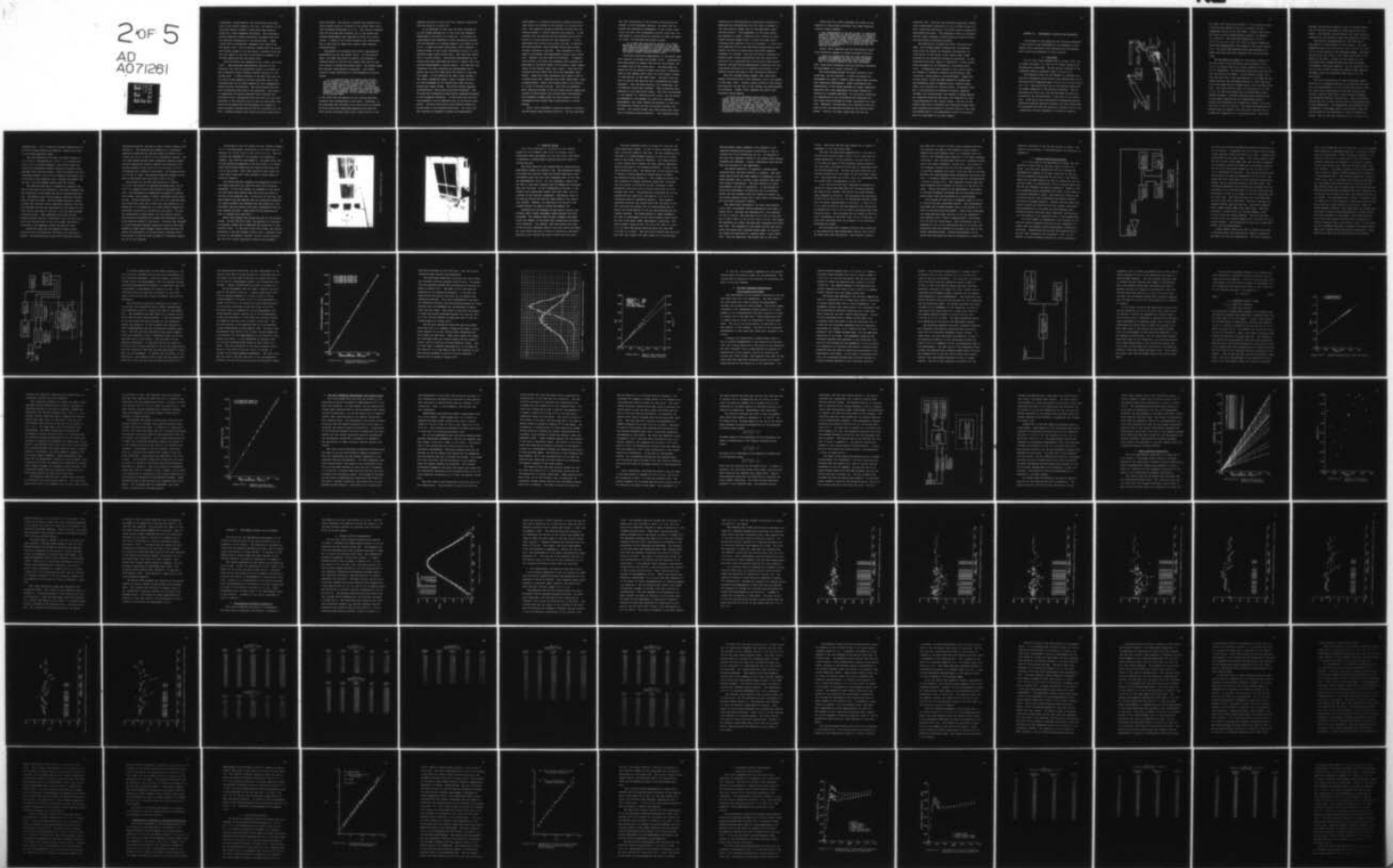
F/6 20/4

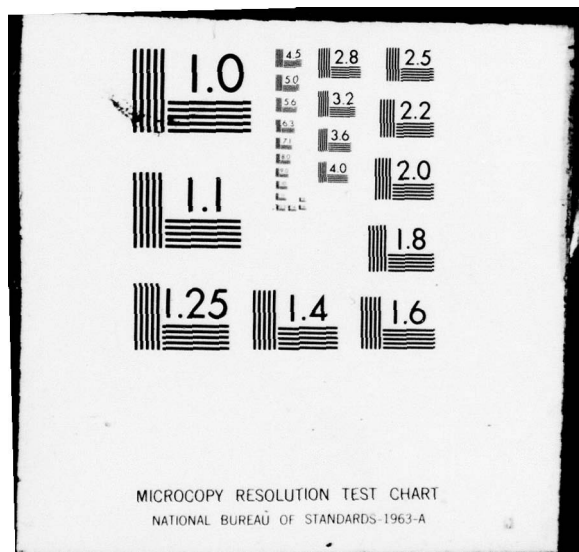
UNCLASSIFIED

N00014-67-A-0226-0025  
NL

2 OF 5

AD  
A071261





intensities, energy spectra, and correlations were measured in the initial region of the jet. The spectra in the core were found to exhibit a peak which was gradually buried by a lower frequency turbulence. The correlation results indicated strong correlation throughout the core and decaying correlations in the mixing layer. These results were in substantial agreement with those of Ko and Davies (1971), and the authors claimed that the results lent further support to Ko and Davies' contention that the hot wire signal in the core is dominated by pressure fluctuations emanating from the mixing layer.

This contention was disputed by Lau, Fisher, and Fuchs (1972). They performed measurements primarily in the potential core and the entrainment region in an effort to gain information about possible orderly structure in the mixing layer. A simple analysis of the mass flux over the hot wire in the potential core was presented, and it was concluded that for low Mach numbers the wire predominantly sensed velocity fluctuations. The term arising from density fluctuations was shown to be negligible. The results of comparisons of spectra obtained from a quarter inch microphone with a streamlined nose cone and a hot wire both operating in the potential core as well as other tests were cited as confirming that the microphone did respond to static pressure fluctuations and did not interfere with the flow. Pressure-velocity and velocity-velocity correlations

were performed. The results indicated the presence of an evenly spaced array of vortices in the mixing layer which were convected downstream at  $0.6 U_0$ . The results suggested that the vortices were toroidal, but it was stated that further measurements were required to prove this conclusively. A model of the vortex structure was constructed, and it was found to agree with certain other measured characteristics.

This model was evaluated with further experimental measurements by Lau and Fisher (1975). In the previous paper, the model was found to predict the presence of observed spikes in the hot wire signal when the wire was just inside or outside the mixing layer. The spiked signal was analyzed using reduction techniques. The results allowed a better description of the phenomenon to be presented.

It is suggested that the leading edge of each vortex induces a transfer of high velocity fluid to the low speed side of the mixing layer, while the trailing edge causes the transfer of low velocity fluid towards the jet potential core. Qualitatively, this is shown to account for both the Reynolds shear stress and the observed "spikey" nature of the signals observed, in particular, on the potential-core side of the mixing layer.

It was found that the spacing of the vortices was more irregular than hypothesized in the model. Otherwise, it was concluded that the model of an axial array of toroidal vortices convecting downstream sweeping fluid back and forth across the mixing layer gave a good account of the

dominant structure in the first few diameters downstream from the mouth of a round jet.

It is important to note that the model proposed by Lau and Fisher applies only to the first few diameters downstream of the mouth of a round jet. Previously reviewed papers have discussed a vortex coalescence process, and this process is noticeably absent in the model of Lau et al. A paper by Winant and Browand (1974) presents a detailed study of the vortex coalescence process in a low Reynolds number plane mixing layer. The study was conducted in a water channel. Traditional measurements of the mixing layer were performed and found to compare well with previous measurements in mixing layers. The same flow was visualized with dye injection and photographed with a camera that could be towed above the channel at the mean flow speed. It was observed that small waves formed in the linear instability region, grew to become vortices, and then proceeded to roll around each other and pair, forming one larger vortex. The entire process appeared two-dimensional, and pairing continued downstream. The vortices were distorted as they paired, becoming elongated in the streamwise direction. It was noted that this process appeared to be an important part of the mixing layer growth. Velocity fluctuations were measured across the mixing layer at one distance downstream. The velocities were obtained as ensemble averages from measurements

conditioned on a velocity fluctuation outside the mixing layer which was related to the passage of a vortex structure. The resulting velocity profiles revealed that two vortices offset in lateral position were passing. It was observed that the pairing process depended upon non-uniformity in vortex spacing and time separation. It was speculated that forcing the process and thereby reducing the non-uniformity, would decrease mixing layer growth through a decrease in pairing. This statement at first seems to contradict some experimental results with forced jets. However, the two cases are different. It appears that forcing a jet fixes the frequency and increases the amplitude of the waves formed in the initial linear theory region of the laminar shear layer region. Thus the fluctuations saturate faster and non-linear phenomena begin sooner. These non-linear phenomena would seem to lead to irregularities that, combined with higher amplitudes, could increase growth. Winant and Browand seem to be referring to a case of forcing vortices. Thus they are speaking about applying forcing to the non-linear region; generating uniform vortices rather than uniform small disturbances. They proposed a simple model for the process of vortex coalescence which relied upon irregularities in vortex spacing.

Acton (1976) performed a detailed analysis of modelling the mixing layer through vorticity. He also concluded

that the irregularity of the vorticity distribution was central to the coalescence process. He noted that the process was essentially independent of the initial conditions, and that this independence offered little hope for some means of controlling the structure in order to reduce jet noise. He described the growth process:

It is seen that the pairing process is a likely mechanism for the growth of a turbulent mixing layer. The irregularities caused in the layer by any coalescence would be sufficient to provoke further pairings, thus ensuring continual amalgamation events to produce the smooth linearly growing mixing layer.

Continued conditional measurements in the mixing layer were reported by Browand and Weidman (1976). Measurements were conditioned by signals from two hot film probes; one on either side of the mixing layer. The amplitudes and phases of the two detector signals were used to determine when to read signals from a split hot film sensor located at some position in the shear layer. The split film was able to resolve the velocity into a streamwise and normal component. Thus the mean velocity, the intensities, and the Reynolds stress were obtained. These properties were measured at two conditioned states. The first corresponded to the passage of a recently paired vortex, and the second corresponded to the passage of a pairing in progress. Measurements were taken forward and backward in time from the detection instant so that the entire structure was defined. The results showed that these events were important in Reynolds stress production. "Net Reynolds-stress

production is characterized by significant correlation of momentum-flux contributions over the time of passage of the large scales, rather than by high amplitude, short duration bursts." This dependence on the large scales was observed to cause a similarity with results for much higher Reynolds number flows, in which the small scale turbulence was expected to be very different. It was noted that modelling of the flow had proven quantitatively unsuccessful and that an interacting vortex model appeared necessary for success. Thus the two papers coauthored by Browand report visual observations that the large scale structure is an important part of the mixing layer growth process, and quantitative measurements indicating that the large scale structure is an important contributor to the Reynolds stress and hence to the turbulence production.

Thus the reviewed papers suggest that large scale orderly structures play a very important role in the growth of free shear flows. Several recent surveys of the subject have analyzed the way that it has changed the understanding of turbulence. Roshko (1976) examined the effect upon turbulent energy spectra.

In trying to understand energy spectra, it has always been difficult to explain the sources of the energy contributions to the low wave numbers, which contain most of the energy. Clearly, important scales are furnished by eddy spacings and eddy lifespans, but even larger scales (lower wave numbers) will be introduced by the vortex coalescence events and the resulting disruptions of order along the shear layer; three-dimensional effects on all these may also play a role.

Davies and Yule (1975) discussed the effect of the theories of large scale structures upon ideas regarding spectral energy transfer.

...the repercussions of the new concept of turbulence structure have made the ideas regarding the interpretation of fixed point wave number spectra in terms of different scales of motion less physically realistic. In particular, the concept of an energy cascade process from large to smaller scales of motion derived from fixed point measurements is not compatible with the observed structure...

Laufer (1975) observed that the importance of large scale structures appears to extend throughout the flow.

...there are indications that the large structures dominate the dynamics not only in fully developed, so-called equilibrium turbulent shear layers but also in the early phases of the flow development.

Thus, large scale structures could be important throughout the development of a plane turbulent jet.

The relationship between the areas covered in this review may now be clarified. A plane jet begins its development as a pair of laminar shear layers which develop small amplitude disturbances. These disturbances grow exponentially in the region governed by linear instability equations until they experience non-linear effects and saturate at a maximum amplitude. By this point, harmonics and subharmonics of the disturbance have developed and such large scale processes as vortex coalescence are occurring. Meanwhile, the potential core turbulence level has grown as the core has been narrowed by the growing shear layers. Finally, the shear layers meet and end the

potential core. The flow then proceeds downstream, perhaps with a complicated interaction of the two shear layers and their large eddy structures, and tends toward an asymptotic self-preserving state. This asymptotic state is characterized by linear widening, linear centerline velocity decay, and self-similar turbulence profiles.

The application of sound can affect the entire process. The reviewed papers indicate that a disturbing sound field can modify the frequency and amplitude of fluctuations in the region of the laminar shear layer governed by the linearized instability equations. In the following non-linear region of instability, vortex coalescence processes may be affected by a disturbing sound field. Accompanying these changes in the initial region are changes in turbulent intensity distributions, mean velocities, energy spectra, and entrainment. Beyond the initial region, sound has been reported to change mean flow parameters such as widening rates, velocity decay rates, and locations of virtual origins. Structural changes in distributions of turbulent intensity, Reynolds stresses, and intermittency, and changes in energy spectra and interface fold-over have also been reported for locations downstream of the initial region. The goal of the present study was to determine the mechanism through which sound produces such effects in the main region of the flow. The methods used in the experimental study of this phenomenon are described in the next chapter.

### CHAPTER III EXPERIMENTAL APPARATUS AND TECHNIQUES

Descriptions of the apparatus and techniques employed in the course of the investigation are presented in this chapter while analysis of the techniques and the measurement results are presented in later chapters.

#### A. Flow Field

The jet flow field assembly used by Kaiser (1971) was no longer available, so a new jet of similar geometry was designed and constructed. The new system consisted of the components shown in schematic form in Figure III-1.

The turbulent plane jet was formed by a smoothly contracting rectangular nozzle with an exit aspect ratio of 48. The nozzle exit dimensions were 6.35 mm (0.25 in) by 0.305 m (12.0 in). The nozzle exit was in the vertical plane with the larger dimension in the vertical direction. The jet exhausted into still air, and the entrained flow was constrained by two vertical walls in the plane of the nozzle exit. These walls were constructed of fiberglass acoustic absorption material backed by plywood, and they constrained the entrained flow near the nozzle to approach the jet with a negligible velocity component in the axial direction.

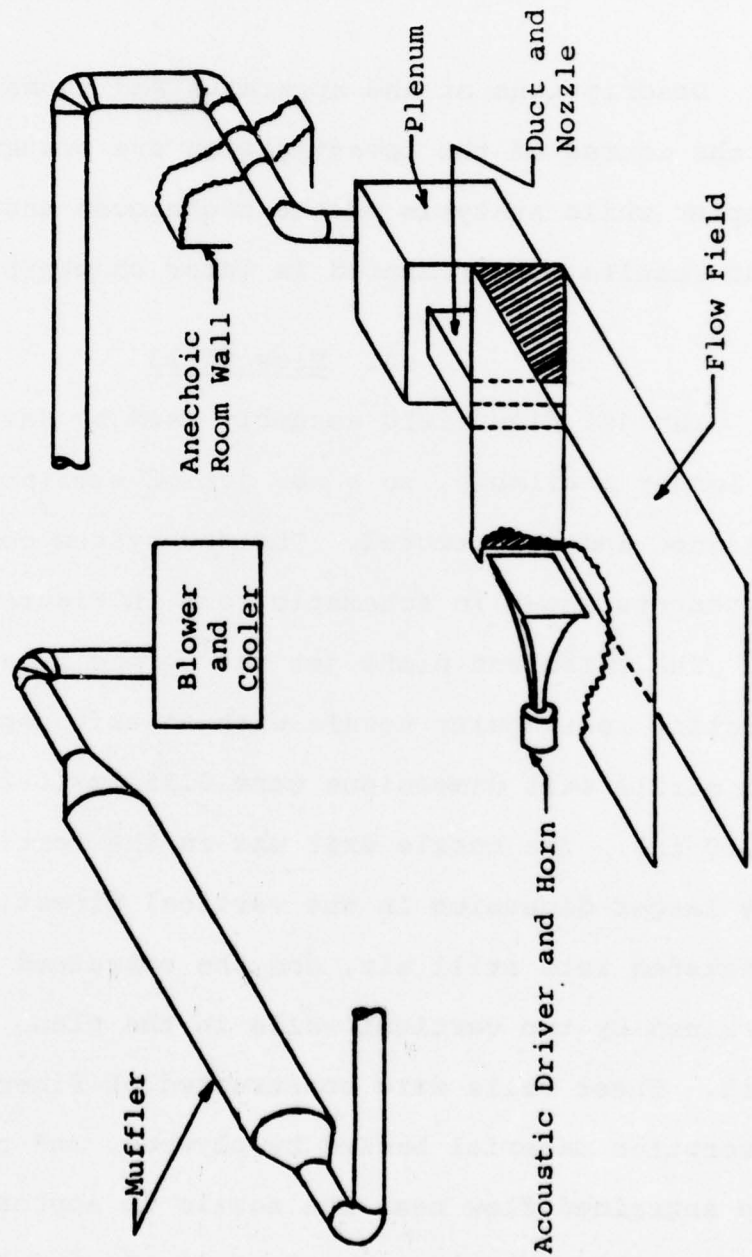


Figure III-1 Schematic Diagram of Experimental Facility

Two sheet steel walls were mounted in the horizontal planes at the top and bottom of the jet to preserve the two-dimensional nature of the flow field. Without these walls, the plane jet would asymptotically approach the behavior of a round jet. The walls had dimensions of 0.914 m (36.0 in) by 1.52 m (60.0 in), with the smaller dimension positioned symmetrically with respect to the nozzle centerline. The nozzle and confining walls were mounted in an angle iron frame that also supported the traversing mechanism.

The mechanism was capable of traversing a section of the flow field in the horizontal plane extending 0.38 m (15 in) on either side of the nozzle centerline and 1.27 m (50 in) downstream. The horizontal positioning was achieved with two electric dc motors. The downstream (axial) position was read from a steel tape measure on the frame and the lateral position was available from both a steel tape measure on the frame and the voltage across a ten turn potentiometer. The tapes could be read to an accuracy of  $\pm 0.2$  mm ( $\pm 0.01$  in) and the voltage from the potentiometer gave a similar accuracy. Vertical positioning was limited by the various probe supports and was accomplished manually. Heights were measured with a machinist's square to an accuracy of  $\pm 0.4$  mm ( $\pm 0.02$  in). The traversing mechanism was mounted atop the frame of the flow field, and the various probes were supported on a cantilevered arm. This whole

assembly was mounted on wheels so that it could be moved from the anechoic room where all measurements were performed. The anechoic room was shared with other projects, necessitating the ability to move the apparatus in and out.

The acoustic characteristics of the room will be described in a later section of this chapter. The room dimensions were 3.66 m (12 ft) by 3.66 m (12 ft) by 3.66 m (12 ft) to the points of the fiberglass wedges. The metal grating floor was 0.305 m (1 ft) above the points of the wedges on the floor. Except for one unique run, all instruments were located outside the room with probes and speakers controlled remotely. The air supply for the jet was also located outside the anechoic room, assuring extremely quiet and controlled conditions in the jet environment.

The air was provided by a large centrifugal blower enclosed in a concrete block box in a corner of the acoustics lab approximately 9 m (30 ft) from the anechoic room. The blower drew conditioned air from the acoustics lab through a muffled inlet with a servo-controlled damper, and discharged through a cooling coil. Water was passed through the coil to cool the air from the blower back down to room temperature. The temperature was monitored with a thermometer in the supply duct in the anechoic room, and once adjusted at the beginning of a test it proved very steady. The air left the cooling coil in a 0.15 m (6 in)

diameter duct. A "Y" in the duct allowed bleeding part of the flow through restrictive exhausts, keeping the blower in its steady operating range.

The air continued in the duct and passed through a 6.1 m (20 ft) long muffler of 0.18 m (7 in) internal and 0.41 m (16 in) outside diameter. The annular space was filled with fiberglass acoustic absorption material which absorbed noise from the blower. After the muffler the flow continued through a 0.15 m (6 in) diameter sheet metal duct to the wall of the anechoic room. Between the muffler and the wall, the flow passed through three 90° elbows.

The anechoic room was on a foundation separate from that of the rest of the laboratory, and hence isolated from the vibrations of the blower and the air conditioning system. The massive walls of the anechoic room were concrete block filled with sand. The flow passed through a length of duct that was built into a removable section of the wall. The removable section was constructed of two sheets of plywood, one on each side of the wall, with the space between filled with sand. Sand completely encircled the duct passing through the wall, anchoring it into the wall structure, and ensuring that it did not transmit appreciable vibration to the apparatus inside the anechoic room.

Inside the room, the flow passed through another section of duct including two 90° elbows and entered the plenum. The plenum box was lined with fiberglass acoustic

absorption material, and did not have a direct acoustic path through it. The entering flow impacted on a fiberglass absorption faced barrier and was forced to diffuse into a 0.406 m (16 in) by 0.305 m (12 in) rectangular passage. The flow then passed through three turbulence reducing screens and was accelerated through a smooth two-dimensional contraction ending in the 0.102 m (4 in) by 0.305 m (12 in) rectangular duct leading to the nozzle. The plenum box was 0.71 m (28 in) long. The distance from the entrance to the duct to the nozzle exit plane was 0.635 m (25 in).

The entrance to the duct was filled by a 0.0825 m (3.25 in) long section of aluminum honeycomb with 6.35 mm (0.25 in) diameter pores which served to straighten the flow. The honeycomb was immediately followed by a medium-fine screen, which helped to reduce turbulence levels downstream. Farther downstream, 0.42 m (16.5 in) upstream from the nozzle exit plane was a final very fine screen of 17.3 meshes per cm (40 meshes per in) which further reduced the turbulence intensity at the mouth of the nozzle. The duct was constructed of sheet metal, and the parallel section containing the honeycomb and screens was reinforced to minimize possible flexing of the walls. The walls had "windows" in which fiberglass acoustic absorption material was flush mounted to lower sound pressure levels within the duct and reduce the possibility of strong acoustic standing waves. This section of the duct was inclosed in a carefully sealed box of 3/4 inch plywood.

Downstream of the last screen the duct formed a gradual 16 to 1 two-dimensional contraction to the nozzle exit dimensions of 6.35 mm (0.25 in) by 0.305 m (12 in). The contraction was composed of two circular arcs joined by a tangent. The first arc was formed in the sheet metal duct, and the second was machined in the two 51 mm (2 in) square steel blocks which formed the two sides of the final section of the nozzle. This final section of the nozzle had a very short (less than 6 mm) parallel section ending in sharp 90° corners.

The nozzle and duct assembly was permanently bolted to the frame supporting the confining walls and traversing mechanism. In this way changes in alignment of the nozzle and flow field were reduced when the set up was moved in and out of the anechoic room. To move out of the room, the probe support arm was removed from the traversing mechanism, the nozzle assembly was unbolted from the plenum box, and the plenum box and circular duct were disconnected from the duct through the wall. These parts of the system may be seen in Figures III-2 and III-3.

These last figures also illustrate part of the acoustic system. As with the flow field, the objective in designing the acoustic system was to duplicate the conditions of the previous study. In the case of the flow system, the results presented in the next chapter confirm that a turbulent plane jet with an undeveloped "top-hat" initial velocity profile and very low initial turbulence intensity was produced.

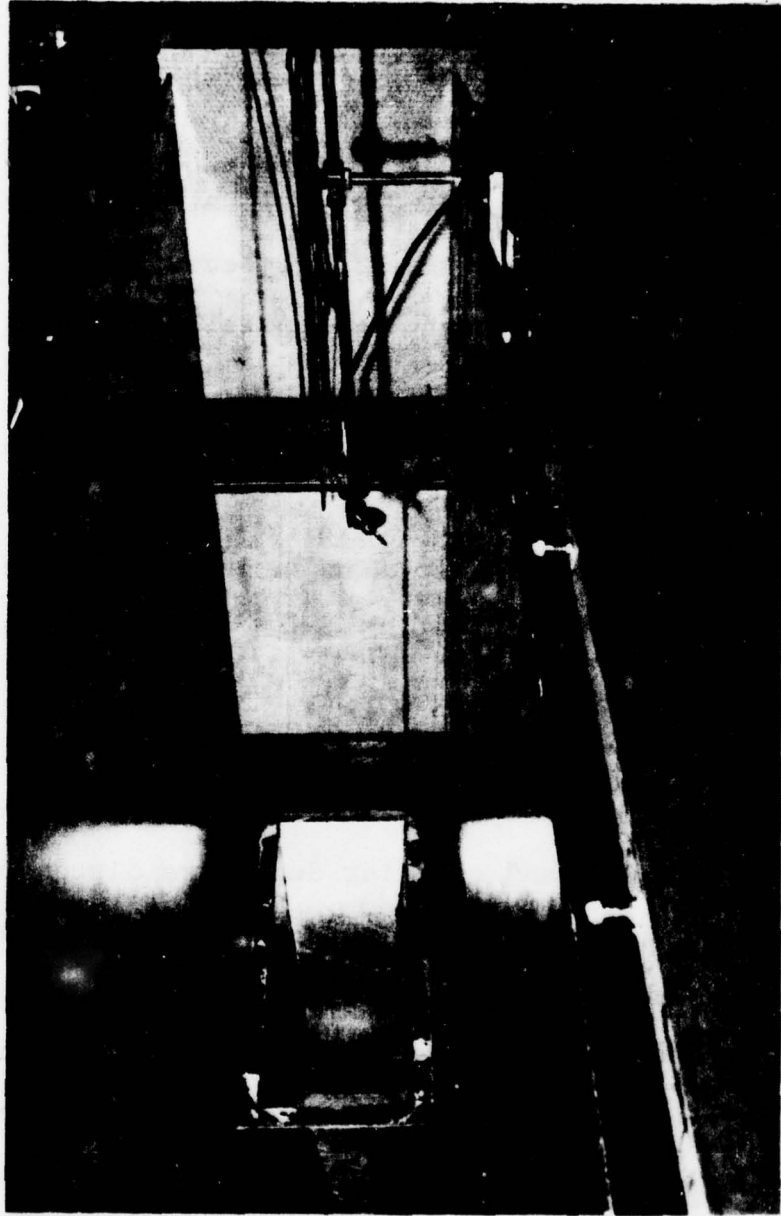


Figure III-2 Experimental Flow Field



Figure III-3 Experimental Facility

### B. Acoustic System

The prime objectives in the design of the acoustic system for this research were first to provide a quiet, disturbance free environment for the flow field, and second to generate a uniform plane traveling wave with which to disturb the jet.

The first objective was accomplished by conducting the experiments inside the anechoic room. The fiberglass wedges with which the room was lined had acoustic absorption characteristics such that the lower frequency limit of the room was approximately 100 Hz. At this frequency, roughly ten per cent of the sound incident upon the wedges was reflected back into the room. As the frequencies of interest in the research were appreciably higher than this limit, the performance of the room was acceptable. The massive walls of the room insulated the interior from sounds in the laboratory outside. However, the room had to be linked to the outside through its need to intake and exhaust air.

Allowance for the exhaust air was made by leaving the conduits used to pass instrument cables through the walls unplugged. The conduits were of small diameter and ended within the wedges, so the sound they transmitted was essentially absorbed. Furthermore, they were behind the plane of the vertical confining walls of the flow field, and hence any noise would have had to follow a reflective, and hence absorptive path through the room to reach the flow field.

The major possible source of intake air noise was the large centrifugal blower. It had 16 radial straight blades and a rotational speed of 3640 rpm. The two characteristics resulted in a blade passage frequency of 925 Hz, at which much of the blower noise was expected. The prime solution to this problem was to employ the large annular absorptive muffler described in the preceding section. It had a very large absorptive area. The second part of the solution was to design a baffled absorptive plenum having no direct, non-reflective path through it. This plenum box served the dual purposes of further absorbing sounds from the blower and flow noises in the ducts, as well as making a fluid mechanical transition from a circular duct flow to a rectangular duct flow. The plenum was constructed of 3/4 inch plywood and was lined with a minimum of 0.1 m (4 in) of fiberglass acoustic absorption material. More acoustic absorption material was placed flush with the walls in the duct following the plenum, but its prime purpose was to absorb the sounds applied to the jet and reflected and diffracted upstream. The effectiveness of these treatments was seen in measurements of the sound pressure level within the flow field under normal experimental conditions. The sound pressure level at  $X/D = 50$ ,  $Y/D = 20$ , and  $Z = 0.115$  m (4.5 in) above the bottom confining plate was less than 75 dB SPL re  $20 \mu\text{N}/\text{m}^2$ . The true sound pressure was certainly less than this figure, for when viewed on an oscilloscope,

the microphone signal appeared to be composed of non-radiating pseudo-sound pressure fluctuations in the entrained flow field surrounding the jet. No evidence of any pure tone component related to the blower blade passage frequency was observed. A quiet, disturbance free environment was provided for the experiments.

The second objective, to generate a uniform plane traveling wave, was more difficult to achieve. The ideal sound source would have been capable of generating a high sound pressure level, uniform, plane traveling wave over a wide range of frequencies. The most difficult of these requirements was that of uniformity. It was decided to relax this requirement, allowing the use of an acoustic driver and horn assembly which was capable of generating high sound pressure levels over a wide range of frequencies, but with some directional effects.

The system used consisted of an Altec 290E acoustic driver and a rectangular section exponential horn shown in Figure III-3. The horn was designed with a low frequency cut off of 166 Hz. The horn was 0.712 m (28 in) long and had a mouth 0.184 m (7.25 in) by 0.483 m (19 in). The signal was generated by a Bruel and Kjaer Beat Frequency Oscillator Type 1022. The frequency of the signal was set and continuously monitored with a Systron Donner Model 114 Counter. The signal was amplified by a Marantz Model 9 Power Amplifier. From the amplifier, the signal went to the Altec

driver. The driver and horn were supported on stands independent of the flow field frame.

The horn was positioned perpendicular to the axis of the jet with its exit plane 0.559 m (22 in) away from the nozzle centerline. At this position, the horn was 0.1 m (4 in) from the edges of the horizontal plates confining the flow field, and hence the horn was not completely blocking the entrained flow. The horn was positioned with its vertical centerline at the height of the flow field centerline. The centerline was 0.343 m (13.5 in) downstream from the nozzle mouth, corresponding to  $X/D = 54$ .

A one inch Bruel and Kjaer condenser microphone connected to a Bruel and Kjaer Type 2107 Frequency Analyzer was used to set, monitor, and control the sound pressure level produced by the horn. The microphone was positioned at  $X/D = 50$  (0.318 m or 12.5 in) downstream from the nozzle with its sensor perpendicular to the axis. It was 0.127 m (5 in) from the axis on the side opposite that of the horn. Its height was 0.115 m (4.5 in) above the bottom flow field confining plate. The microphone was not placed in the vertical centerplane of the flow field, for if it had been, it would have interfered with the movement of the traversing mechanism and probes.

The microphone and frequency analyzer were calibrated at the beginning of each measurement session with a Bruel and Kjaer Type 4220 Pistonphone. The frequency analyzer

was used with a 20 Hz to 40 kHz linear weighting function. The analyzer was used in the frequency analysis mode to measure the sound pressure level in a frequency band centered at the frequency being generated in the beat frequency oscillator. The 3 dB down band width was a constant percentage of the center frequency, six per cent. The output of the frequency analyzer was fed into the compressor circuit of the beat frequency oscillator, which was used to actively maintain the sound pressure level produced by the driver and horn. A schematic diagram of the acoustical instrumentation is given in Figure III-4. The compressor circuit kept the sound pressure level constant to within  $\pm 0.3$  dB SPL re  $20 \mu\text{N}/\text{m}^2$ . During the course of the measurements, the output of the beat frequency oscillator and the unfiltered microphone output were both monitored on an oscilloscope.

This system was used over a frequency range of 200 Hz to 4200 Hz and gave acceptable results. Most measurements were made with a sound pressure level of 105 dB SPL re  $20 \mu\text{N}/\text{m}^2$  at the monitoring microphone. Under these conditions the sound pressure along the axis of the jet appeared to vary smoothly over a range of approximately 7 dB between  $X/D = 80$  and the nozzle mouth. This distribution was not measured for all of the frequencies used in the study, and deviations from this behavior are probable for some of the higher frequencies used. Detailed measurements of the sound field were made for the two frequencies at which the

turbulent structure of the jet was studied in detail. The results of the acoustic field measurements are presented in Appendix B.

### C. Pressure Profile Measurements

As a first step in the experimental program, the frequencies to which the jet was most sensitive had to be found. This was most conveniently done by studying the dependence of changes in the basic structure of the jet. The two parameters describing the jet flow in the similar region are the mean velocity at the jet centerline, and the jet half width, or alternatively the jet velocity decay rate and the jet widening rate may be considered. Those are the two parameters which Goldschmidt and Kaiser (1971) found to be greatly affected by sound. The centerline velocity and the half width are both obtainable from lateral velocity profiles or pressure profiles. Several profiles would give several centerline velocities and half widths, and enable the determination of the decay rate and widening rate. Pressure profiles were most easily measured, and following is a description of the technique used in their measurement.

The large number of frequencies to be studied, and the need for several pressure profiles at each frequency demanded that the pressure profile measurement technique be efficient. Constructing the profile from measured points was too time consuming to be considered. Thus, it was decided to obtain pressure profiles by slowly traversing

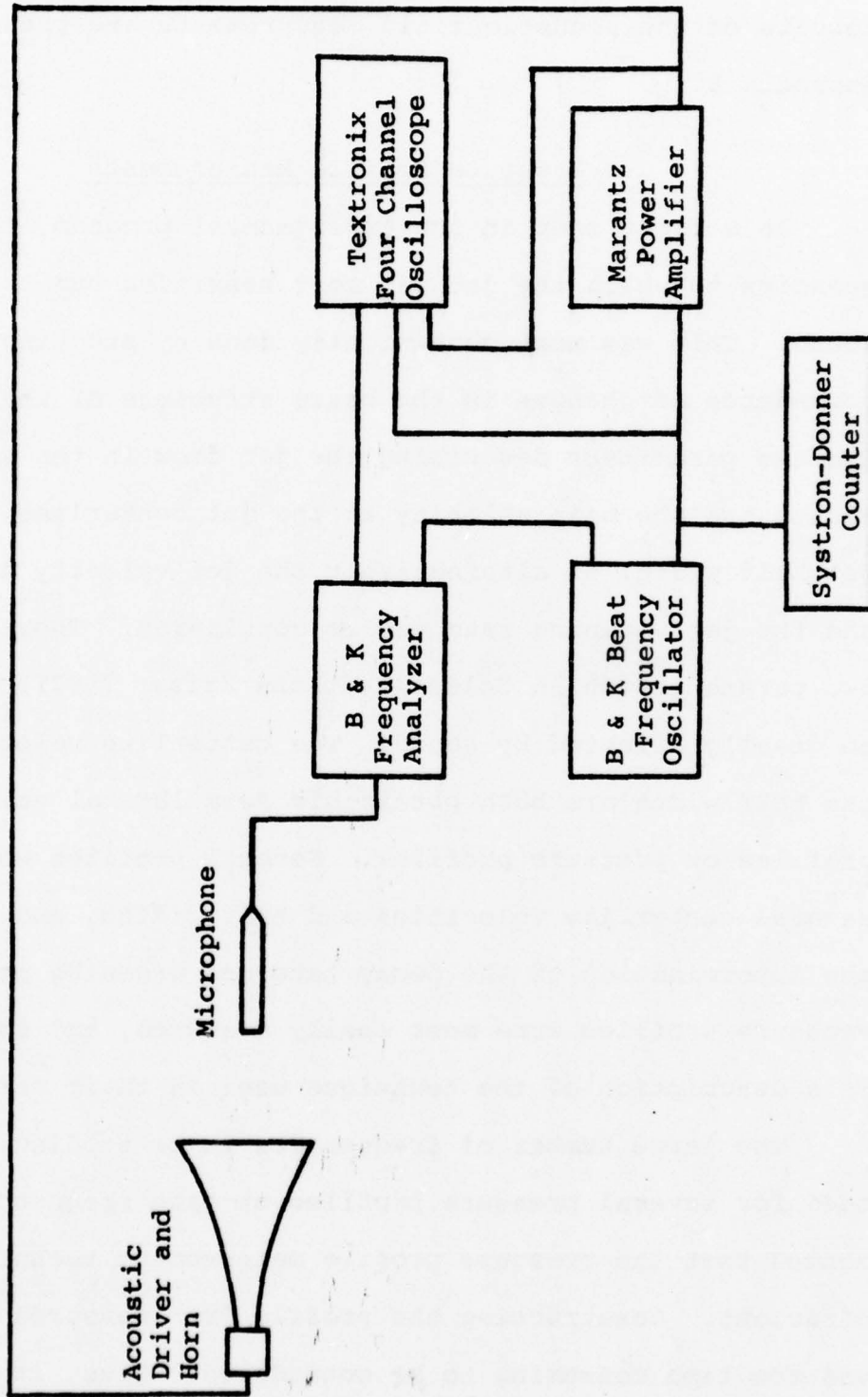


Figure III-4 Schematic Diagram of Acoustical Instrumentation

the flow and plotting the measured pressure distribution on an X-Y plotter. A Honeywell 580 X-Y-Y plotter was available, so two profiles could be plotted at one time. A support was constructed for two pitot tubes. Pitot tubes could be used for the jet was a free shear flow, and the static pressure in the similar region was essentially the ambient pressure. The two pitot tubes were mounted so that one was 0.127 m (5 in) downstream of the other. This allowed plotting pressure profiles at stations separated by an X/D of 20. The probes were both positioned in the horizontal plane midway between the two confining plates of the flow field. The traversing mechanism could traverse slowly enough for this technique in only one direction, so the rear pitot tube was positioned 25.4 mm (1 in) closer to the jet centerline than the front tube. This kept the tube out of the wake from the first tube while traversing. The front tube was also somewhat smaller than the rear one. Both were stainless steel, sharp, square edged total head tubes. The front tube had a 1.08 mm (0.041 in) outside diameter, and a 0.46 mm (0.018 in) inside diameter. The rear tube had a 1.52 mm (0.060 in) outside diameter and a 0.81 mm (0.032 in) inside diameter. The differences in size had no observable effect upon the measurements.

Large diameter tubing was used to connect both tubes to Whittaker Model P7D Differential Pressure Transducers and Model CD10 Carrier Demodulators. The front transducer

had a 1 psi diaphragm, and the rear had a 0.1 psi diaphragm. The difference in diaphragm range had no observable effect upon the measurements. These transducers remained in the anechoic room, where the open side of the differential pressure transducer was exposed to the ambient pressure inside the anechoic room (which was slightly higher than that outside). The output voltage of each carrier demodulator was fed to either a Thermo Systems 1076 voltmeter or a "time constant box." The traversal speed was 0.28 mm/s (0.011 in/s), and it was found that subjecting the signal to a one second time constant did not alter the plotted mean profile other than to remove some of the fluctuations. When the Thermo Systems voltmeters were used, they were set to the one volt dc scale and their time constant was set to one second. The instrumentation is shown in schematic form in Figure III-5. The voltmeters' outputs were then connected to the two Y-axis inputs of the plotter. When the Thermo Systems voltmeters were unavailable the signals were first fed to simple resistance-capacitor low pass filters with time constants of one second. From those time constant boxes the signals were each sent in parallel to a digital voltmeter and to the plotter Y-axis. In this case, the two voltmeters used were a Keithley 160 Digital Multimeter and a CALICO Series 8300 Digital Multimeter. These meters were used only for monitoring and calibration.

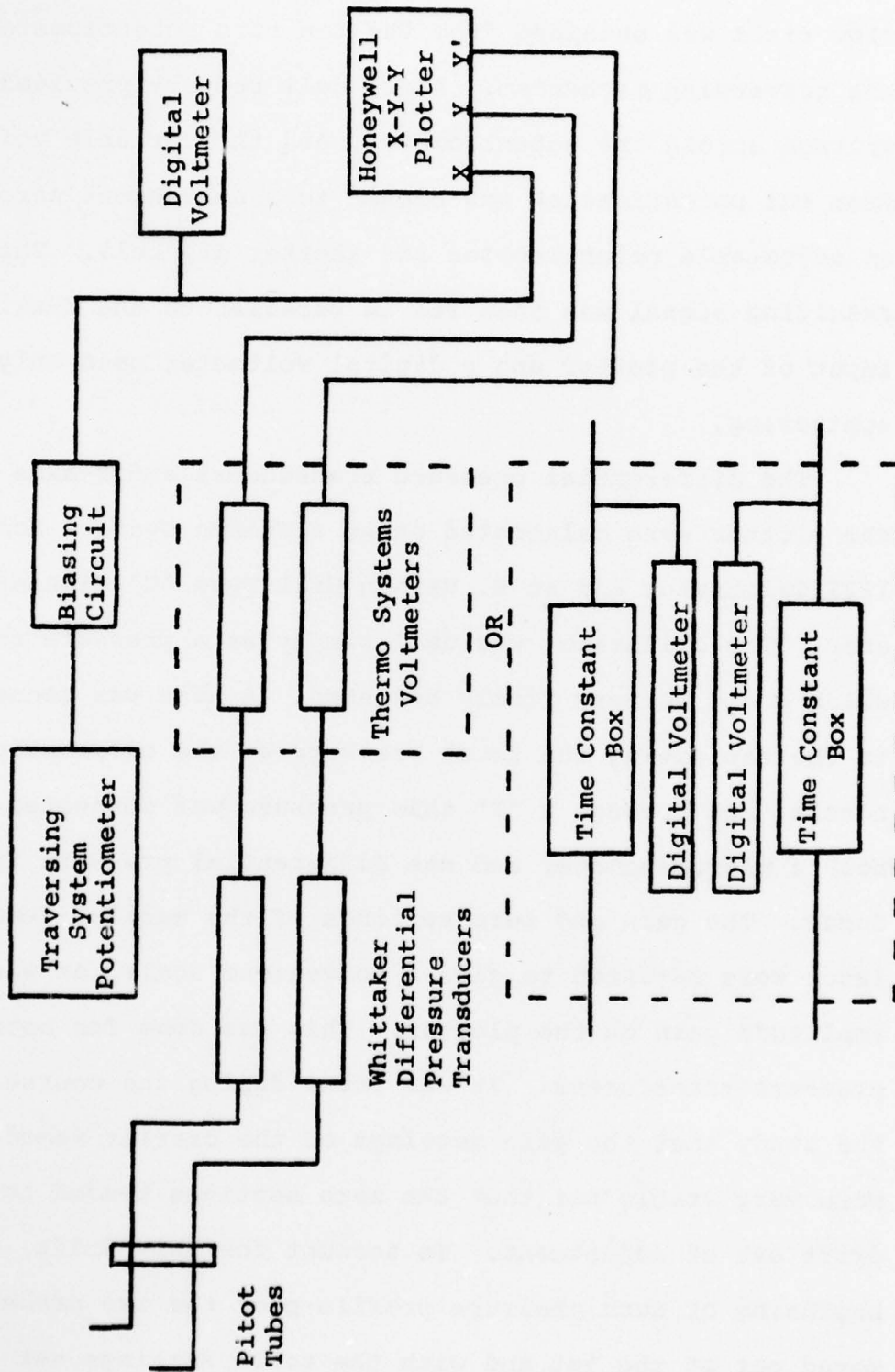


Figure III-5 Schematic Diagram of Pressure Profile Instrumentation

A voltage proportional to the lateral position in the flow field was obtained from the ten turn potentiometer on the traversing mechanism. A dry cell battery provided the voltage across the potentiometer, and the variable voltage from the potentiometer was biased to a convenient zero with an adjustable potentiometer and another dry cell. The resulting signal was then fed in parallel to the X-axis input of the plotter and a digital voltmeter used only for monitoring.

The differential pressure transducers and Y-axes of the plotter were calibrated using a Thermo Systems Model 1125 Calibrator and an E. Vernon Hill Type "C" Micromanometer. The calibrator was used simply as a pressure source which could be very finely adjusted. A hose was connected to the tap giving the total pressure at the calibration nozzle, and through a "T" this pressure was connected to both a micromanometer and one differential pressure transducer. The gain and zero settings of the carrier demodulator were adjusted to give a convenient scale, as was the amplitude gain on the plotter. This was done for both pressure transducers. It was found during the course of the study that the gain settings of the carrier demodulators were very stable but that the zero settings tended to slowly drift out of adjustment. To account for this drift, at the beginning of each pressure profile plot the two probes were moved out of the jet and with the scale settings set for

the appropriate X/D positions, the zero adjustments on the plotter were used to bring the pens to a reference level on the paper that was used as the zero in reading the plots. At the end of a measurement session, the calibrations were checked. Typical calibrations are shown in Figure III-6.

The micromanometer was also used to monitor the total head at the mouth of the jet. A square edged pitot tube with an outside diameter of 1.52 mm (0.060 in) and an inside diameter of 0.81 mm (0.032 in) was positioned at a height of 25.4 mm (1 in) above the bottom confining plane on the nozzle centerline in the exit plane of the jet. The pitot tube was connected to the micromanometer with large diameter tubing, and the top of the micromanometer column was connected to a hose which was inserted through the anechoic room wall into a corner of the room. This was done because it was observed that the flow generated a small overpressure in the anechoic room. The pitot tube measurements were found to be in error through comparison with straight hot wire measurements of the velocity in the nozzle exit plane. A 4.8% difference in velocity, with the hot wire readings being higher by this amount, was found. This was attributed to the static pressure distribution at the mouth of the jet, which, of course, is ignored in the total pressure measurement. The total pressure was used to set the flow rate in all the measurement sessions, and the resulting velocities and Reynolds numbers

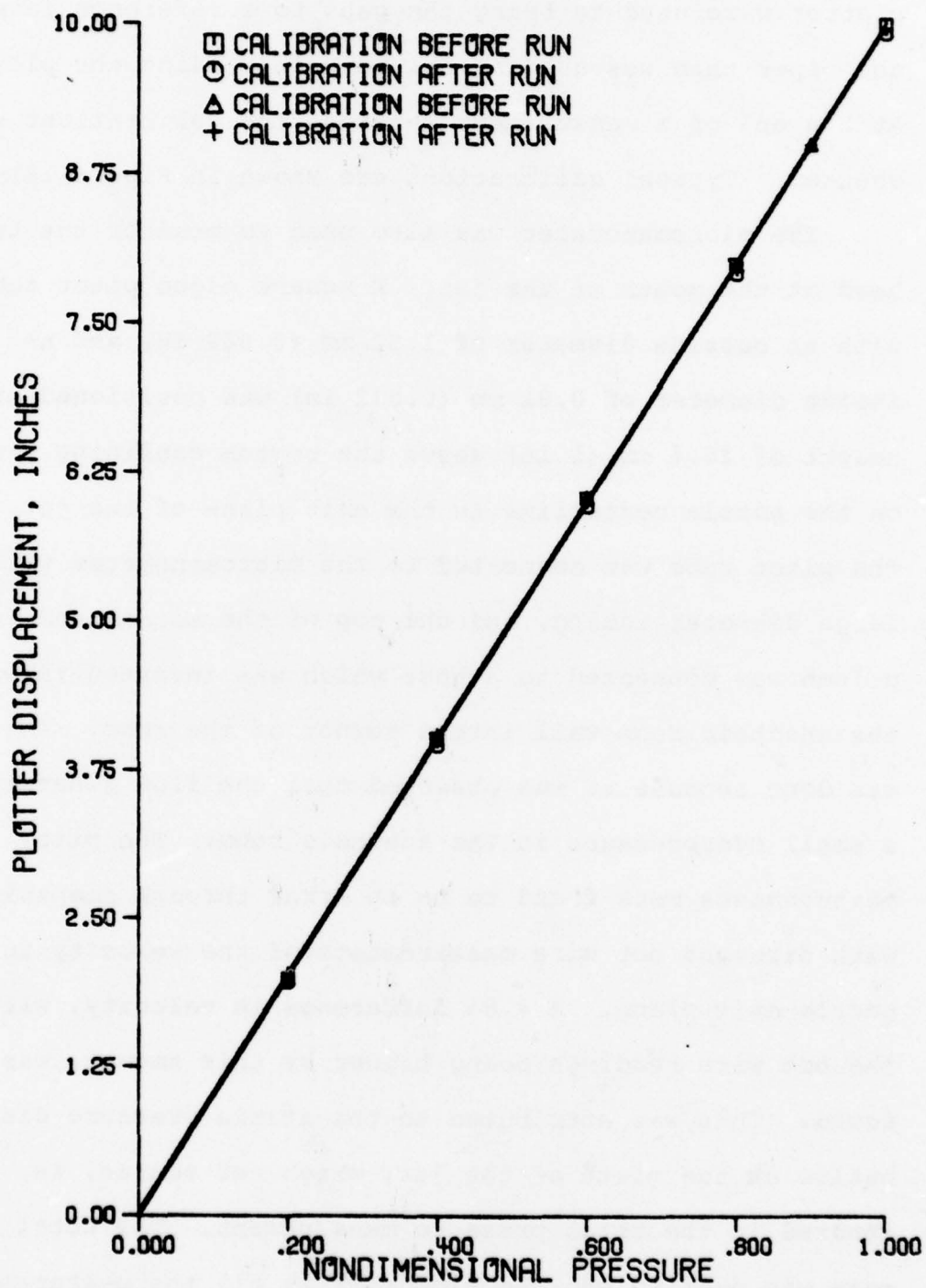


Figure III-6 Typical Differential Pressure Transducer Calibration

have been corrected to the 4.8% error. Thus the initial centerline mean velocity was determined.

The downstream centerline velocities and half widths were obtained from the pressure profile plots. An average line was sketched through the fluctuations of the plot as shown in Figure III-7. The peak of this line gave the magnitude of the centerline pressure. A line was then drawn across the plot at the level of one quarter this centerline pressure. This line corresponded to one half the centerline velocity, and the distance between its intersections with the sketched line was measured to obtain twice the half width. The X-axis of the plots was scaled to twice the actual traversed distance for plots at X/D's up to 80, and was reduced to eighty per cent of the traversed distance at larger X/D's.

The measured centerline velocities and half widths were then input to a computer program which made a linear least squares fit to the velocity decay parameters and half widths for each case. These least square fit slopes and intercepts were the velocity decay rate and velocity origin, and the widening rate and geometric origin. Also for each case, a computer generated plot of the data and the lines fit to it was made so that the linearity of the data and the goodness of the fit could be observed. A typical plot is shown in Figure III-8.

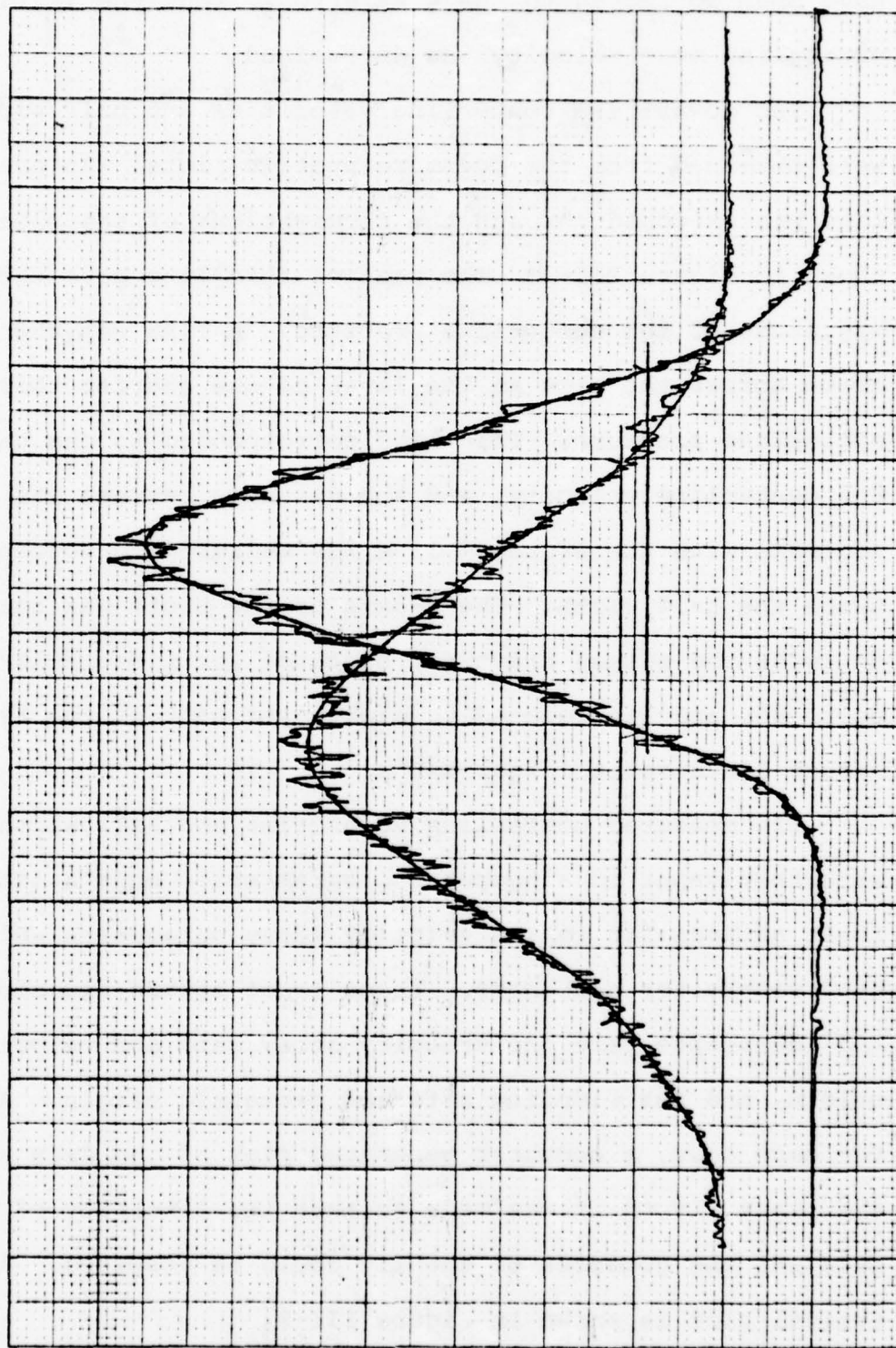


Figure III-7 Typical Pressure Profiles with Measured Half Widths

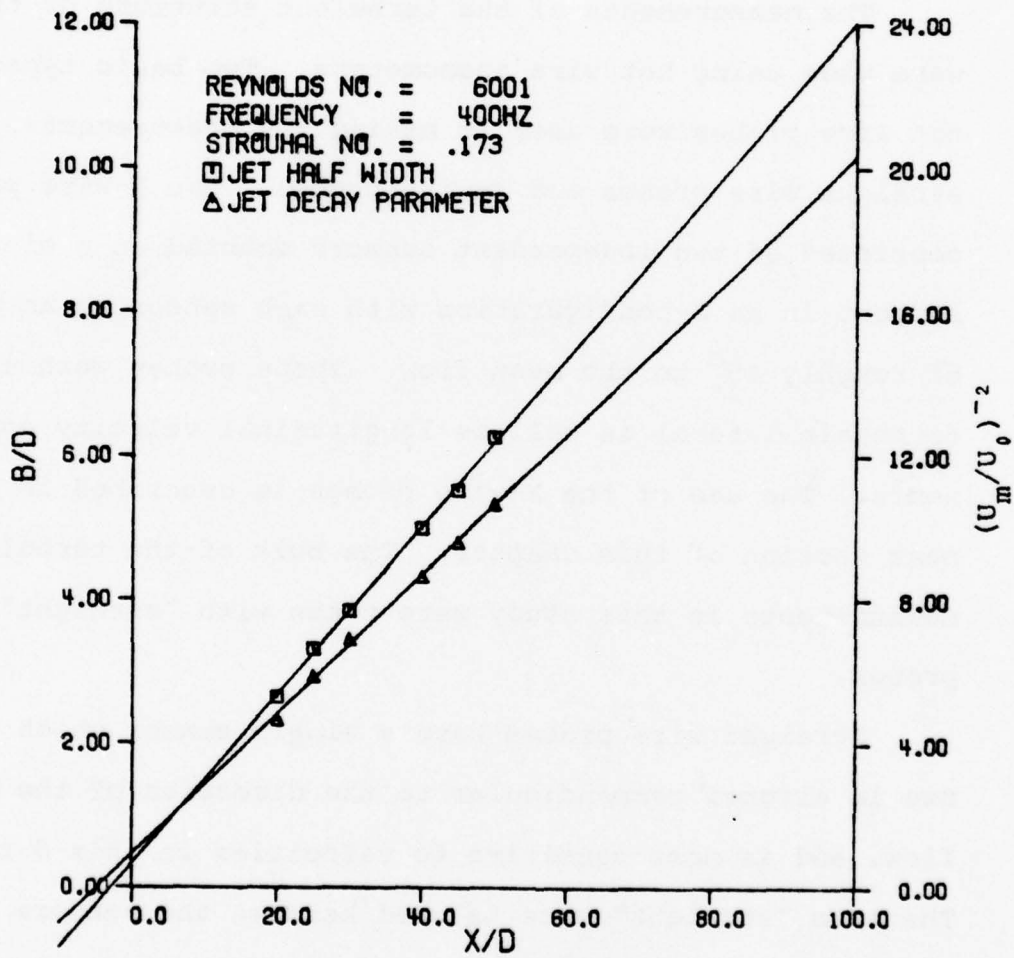


Figure III-8 Typical Half Width and Velocity Decay Results

In this way, the frequency dependence of the acoustic effects upon the turbulent plane jet was determined. The results and an analysis of the accuracy of this method are given in the next chapter.

D. Hot Wire Anemometer Measurements  
with Straight Wire Probes

The measurements of the turbulent structure of the jet were made using hot wire anemometers. Two basic types of hot wire probes were used in making the measurements, straight wire probes and X-wire probes. The X-wire probes consisted of two independent sensors mounted on a single support in an X-configuration with each sensor at an angle of roughly  $45^{\circ}$  to the mean flow. These probes were used to obtain lateral as well as longitudinal velocity components. The use of the X-wire probes is described in the next section of this chapter. The bulk of the turbulence measurements in this study were taken with "straight" wire probes.

Straight wire probes have a single sensor which in use is aligned perpendicular to the direction of the mean flow, and is most sensitive to velocities in this direction. The term "straight" wire is used because the sensors are perpendicular to the support, and not at angles as are X-wires and "slant" wires. The straight wires used in this study were DISA type 55F11 miniature probes with sensors either mounted at the factory or in the laboratory. The

factory mounted sensors were 5  $\mu\text{m}$  (0.0002 in) diameter platinum plated tungsten wire with an overall length of 3 mm (0.12 in) and with the sensor ends gold and copper plated to reduce the sensitive wire length to 1.25 mm (0.049 in). The sensors mounted in the laboratory had similar dimensions but were 3.8  $\mu\text{m}$  (0.00015 in) diameter etched tungsten wire with copper plated ends.

The probes were operated in the constant temperature mode at a resistance of 1.8 times their ambient resistance by Thermo Systems Type 1050 or 1050A anemometers. The anemometer outputs were used directly for turbulence intensity measurements and were linearized with a DISA Type 55D10 Linearizer for mean velocity measurements. Calibration was performed using a Thermo Systems Model 1125 calibrator (with the probe in the low turbulence core of a free jet the calibrator generated from the laboratory compressed air supply), an E. Vernon Hill Type "C" Micro-manometer, and a Thermo Systems Model 1076 True RMS meter operating in a dc range. The anemometer stability and frequency response were adjusted in the calibration flow using an oscilloscope and the anemometer's built-in square wave generator at a velocity high enough to ensure stable operation over the range of velocities encountered in the experimental flow field. In the case of linearized operation, the linearizer settings were adjusted through the iterative method detailed in the linearizer operating

manual. The velocities corresponding to dynamic heads of 15.25 mm (0.60 in) and 3.82 mm (0.15 in) of water were used in this set up procedure. The linearizer was adjusted until the first velocity yielded an output voltage of  $10.000 \pm 0.005$  volts and the second (one half the first velocity) resulted in an output of  $5.000 \pm 0.008$  volts as indicated on the Thermo Systems voltmeter for the dynamic heads measured on the micromanometer. The calibration procedure following this point was the same for the linearized and non-linearized cases. The dynamic pressure and output voltage (of the anemometer or the linearizer, or both in some cases) were then noted for at least five values of the dynamic pressure between 15.25 mm (0.60 in) and 0.512 mm (0.02 in) of water. The same calibration points were remeasured at the end of the measurement session.

The following procedure was used to measure longitudinal turbulence rms velocity levels and mean velocities using the non-linearized anemometer output voltage. In these cases, the wire was placed horizontally, so that it was sensitive primarily to the longitudinal velocities. Figure III-9 is a schematic of the instrumentation used in this measurement. The mean value of the anemometer output voltage was measured from a Thermo Systems Model 1076 True RMS Voltmeter set to the one volt dc scale with a sufficiently long time constant setting to obtain a steady reading. The rms of the turbulent fluctuations of the

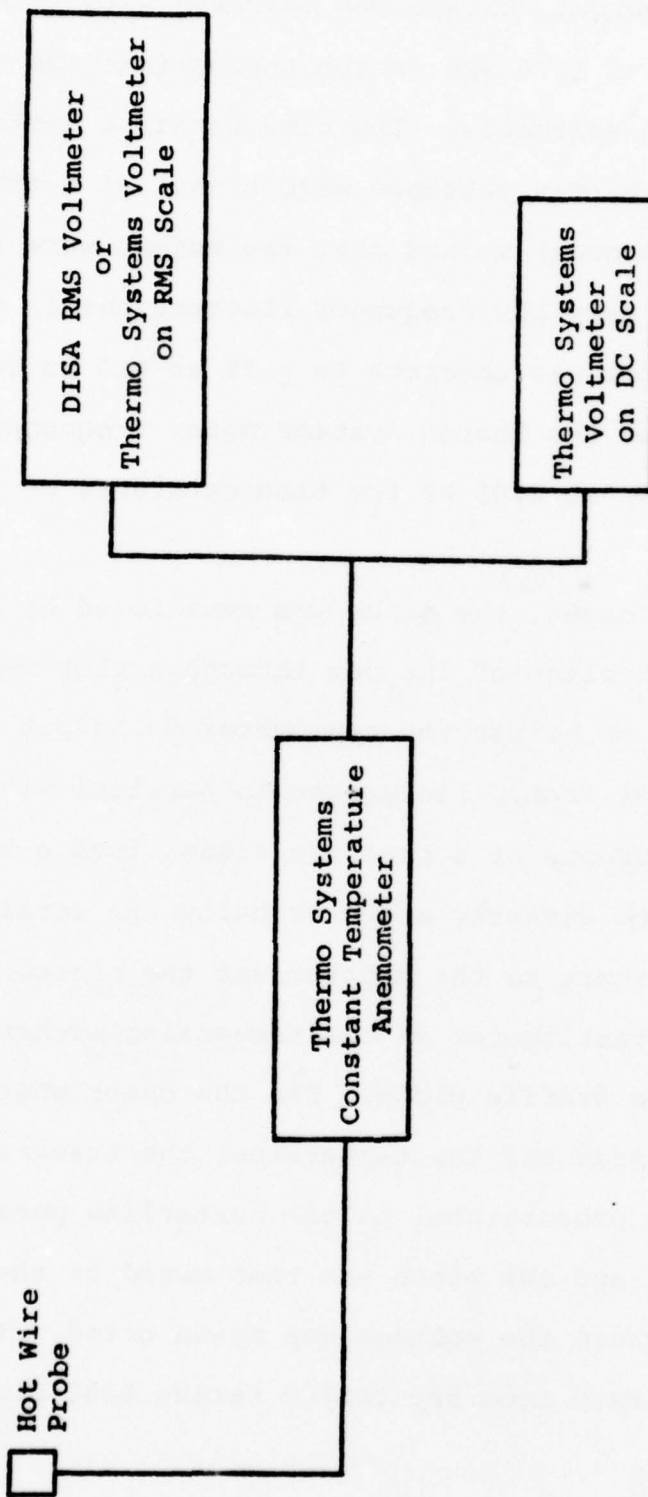


Figure III-9 Schematic of Longitudinal Turbulence Intensity Instrumentation

anemometer output voltage was measured with either another Thermo Systems 1076 set on the appropriate rms scale or a DISA D35 RMS Voltmeter. The time constant settings used in reading the rms voltages were always at sufficiently high ( $\geq 10$  seconds) values that the meters were able to measure the very low frequency fluctuations in the flow. The DISA meter was accurate to  $\pm 2\%$  at 0.5 Hz for such settings, and the Thermo Systems meter frequency response was 3 dB down at 0.06 Hz for time constants of 10 seconds or greater.

In all cases, the probe was positioned by first finding the centerline of the jet through a plot made with an X-Y plotter of either the anemometer dc output voltage, the dc output from a linearizer in parallel with the measuring instruments or a pressure signal from a total head probe mounted directly above or below the straight wire. The X-axis input to the plotter was the biased voltage from the potentiometer on the traversing mechanism, as for the pressure profile plots. For the cases where measurements were made off the centerline, the traversing mechanism voltage proportional to the centerline position was first read, and the probe was then moved to the measuring position, where the voltage was again noted. This voltage was always read from the CALICO Series 8300 Digital Multi-meter.

The rms and dc voltages obtained in this manner were then converted to turbulence intensity and mean velocity using the digital computer. The Collis and Williams (1959) type equation for the relation between the anemometer output voltage and the velocity was found to give a good fit to the calibration points. The equation is

$$E^2 = Z_1 + Z_2 U^{0.45} \quad (\text{III-1})$$

where

$E$  = anemometer output voltage

$Z_1, Z_2$  = empirical constants

$U$  = mean flow velocity

The calibration voltages were squared in the computer and the dynamic pressures were converted to absolute velocities and then taken to the 0.45 power. A linear least squares fit was then made to these points, yielding the constants  $Z_1$  and  $Z_2$ . A typical calibration and the line fit to it is shown in Figure III-10. The equation was solved for velocity and the constants  $Z_1$  and  $Z_2$  were used to calculate mean velocities from the dc voltages measured. The turbulence intensities were calculated by using the slope calculated from the Collis and Williams equation at the given dc level. It was assumed that this voltage/velocity slope was constant over the range of the turbulent velocity fluctuations considered. This was not the case, and was the source of some error. The error attributable to this assumption is analyzed in the next chapter, where the results of the mean

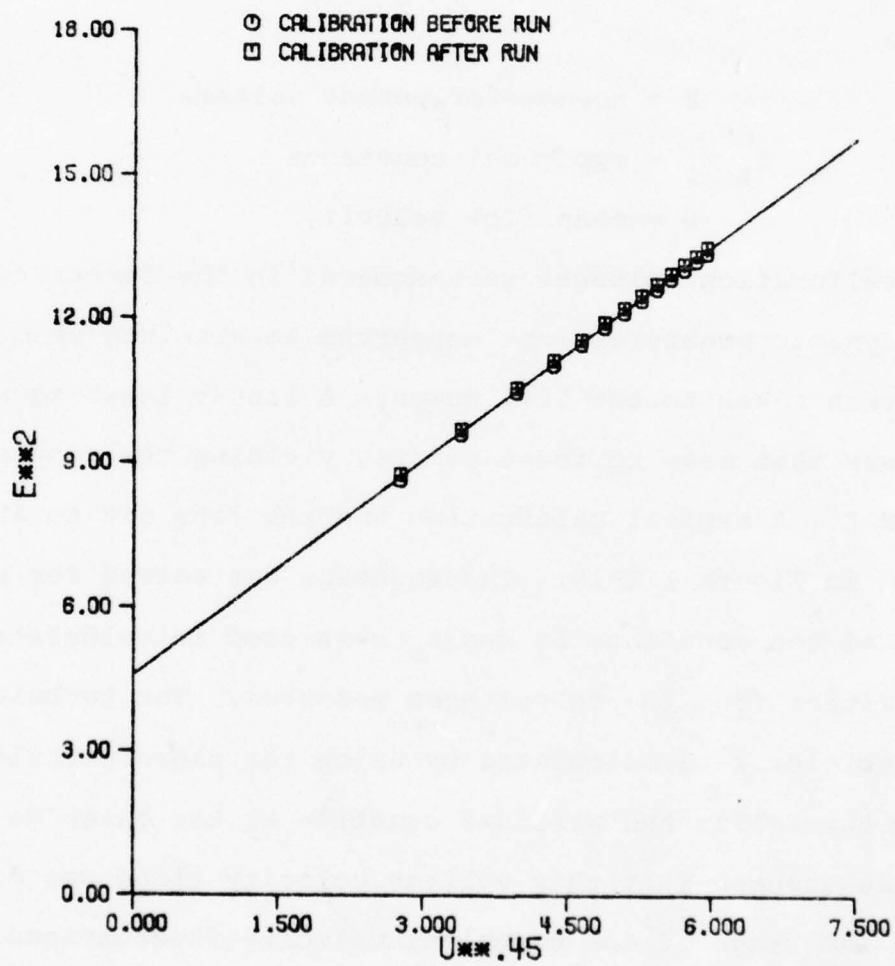


Figure III-10 Typical Straight Wire Probe Calibration

velocity and turbulence intensity measurements with non-linearized straight wires are presented.

The linearized straight wire output was used to measure mean velocity profiles and to position the probe at particular points on the velocity profile, notably the centerline, and the half velocity point ( $Y/B = 1$ ). Linearized straight wires were used to measure the velocity profile very near ( $X/D \approx \frac{1}{4}$ ) the mouth of the jet, and the boundary layer profile on the wall of the nozzle at  $X/D = -0.5$ . For these shear layer and boundary layer measurements, the space resolution of the probe was increased by placing the wire sensor in a vertical plane. The standard traversing mechanism did not have sufficient accuracy to traverse the extremely thin shear layer at the mouth or the boundary layer within the nozzle, so the probe was traversed through this region manually using a support moved by a micrometer, the whole assembly clamped to the flow field support framework. These measurements were made with the experimenter inside the closed anechoic room, traversing the probe and reading the linearized dc voltage from a Thermo Systems 1076 voltmeter inside the room. The linearized voltage from the linearizer outside the room was brought through the wall with a long cable.

The measured linearized mean voltages were converted to velocities using the digital computer. The calibration points were input to the computer and a linear least squares

fit was made to them. The intercept and slope obtained from the least squares fit were then used to calculate the velocities from the measured dc voltage. A typical calibration and the line fit to it is shown in Figure III-11. The mean velocity results obtained with linearized straight wires are presented in the next chapter, along with an analysis of their accuracy.

The methods with which straight wires, both with linearized outputs and without, were used for absolute measurements have been described. In addition to these applications, for which the probes were very carefully calibrated, the straight wires were used for some experiments that did not require any calibration. One of these applications was to sense the fluctuating turbulent signals for display on an oscilloscope along with the trace of the applied sound frequency. Photographs of the oscilloscope traces were taken to illustrate the changing wave shapes as the flow moved downstream. These photos are presented in the next chapter. Uncalibrated straight wire probes were also used to supply the signal for the energy spectrum measurements described in section F. Thus the straight wire anemometer probes were used in a number of ways. However, the straight wires could give no indication of the lateral components of the velocity fluctuations or the Reynolds stresses. These characteristics of the flow had to be measured with X-wire probes. The technique used for measurement with these probes is described in the next section.

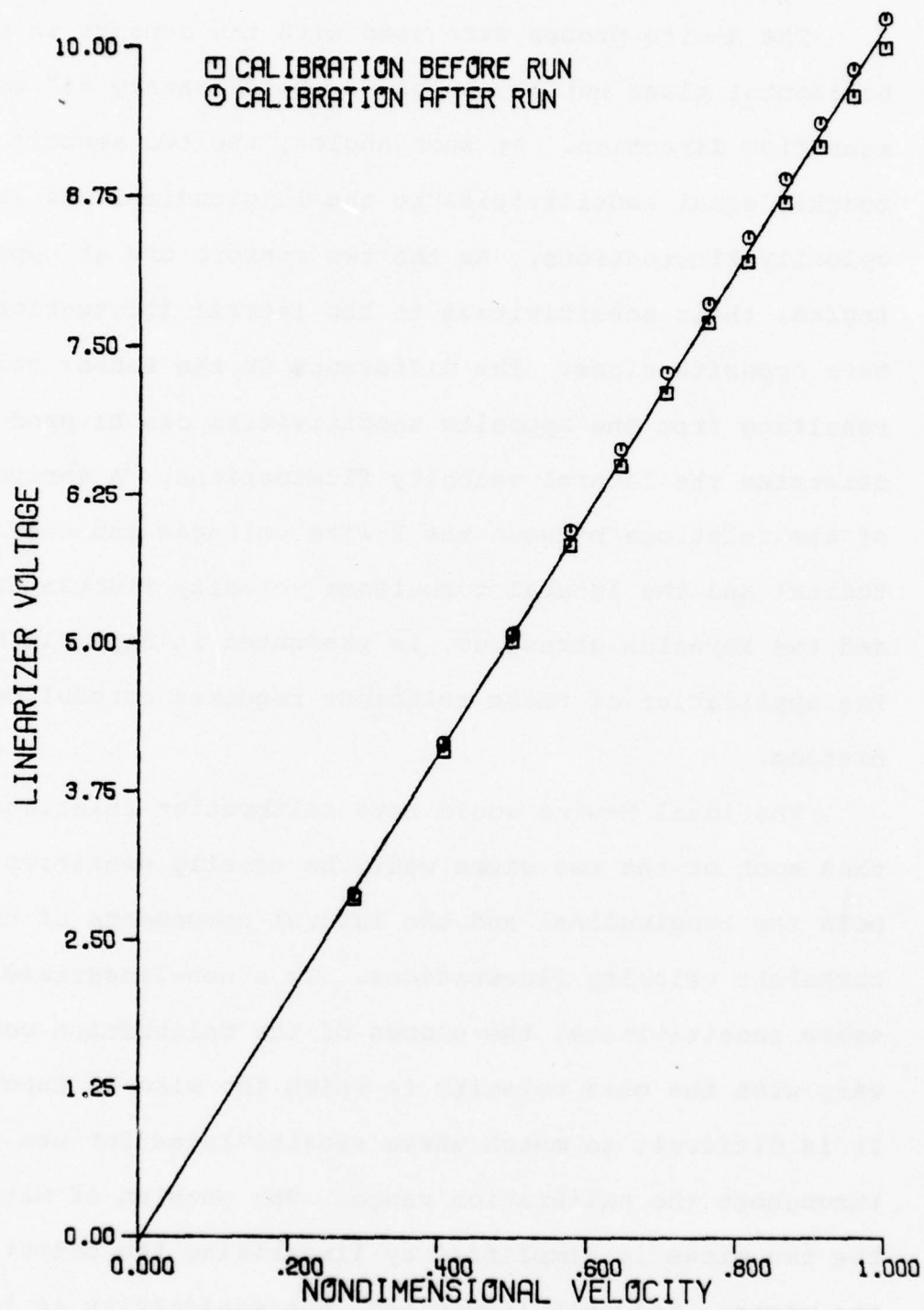


Figure III-11 Typical Straight Wire  
Probe Linear Calibration

### E. Hot Wire Anemometer Measurements with X-Wire Probes

The X-wire probes were used with the sensors in the horizontal plane but at angles of approximately  $45^\circ$  to the mean flow direction. At such angles, the two sensors have roughly equal sensitivities to the longitudinal and lateral velocity fluctuations. As the two sensors are at opposite angles, their sensitivities to the lateral fluctuations have opposite signs. The difference in the sensor voltages resulting from the opposite sensitivities can be used to determine the lateral velocity fluctuations. A derivation of the relations between the X-wire voltages and the longitudinal and the lateral turbulence velocity fluctuations, and the Reynolds stress  $\overline{uv}$ , is presented in Appendix D. The application of these relations requires careful calibration.

The ideal X-wire would have calibration relations such that each of the two wires would be equally sensitive to both the longitudinal and the lateral components of the turbulent velocity fluctuations. In a non-linearized wire, these sensitivities, the slopes of the calibration curve, vary with the mean velocity to which the wire is exposed. It is difficult to match these sensitivities for two wires throughout the calibration range. The problem of matching the two wires is simplified by linearizing the output of the wires. Properly linearized, the sensitivity is independent of mean velocity. The benefits of linearization

are considerable in this case, and any errors involved in the linearization can easily be justified as being smaller than the errors in sensitivities that are inherent in not linearizing. Thus, in this research, the X-wires used were linearized.

Measurements were made with Thermo Systems Model 1241 T1.5 X-wire probes. These probes had 4  $\mu\text{m}$  (0.00015 in) diameter platinum coated tungsten wires with a sensing length of 1.25 mm (0.050 in) and a total length of 1.5 mm (0.06 in). The calibration procedures followed were similar to those used for linearized straight wires.

All of the measurements were done using Thermo Systems Constant Temperature Anemometers, and the two channels used were either a 1050 and a 1050A, or two 1050's. One difference in the initial set up of the X-wires was in the resistance measurements. The probe supports could not be shorted, so the two cables were shorted and the anemometer zero adjustments were set to balance the bridge. The probes were then connected, and the resistance of the complete probe and support assembly was measured. The internal resistances stamped on the probe and support were used with the resistances indicated by the balanced bridge to set the probe operating resistances at 1.6 times the ambient resistance.

The next step in the calibration of the two wires was the linearization. This was done for each wire with the

probe aligned such that the sensor being linearized was perpendicular to the flow from the calibrator. The same iterative procedure of improving the linearization was followed with the X-wires as for the straight wires. The wires were linearized so that a velocity corresponding to a dynamic pressure of 15.3 mm (0.6 in) of water gave a linearizer output of 10.00 volts. This was of course for flow normal to the wire, and the wires were to be used to measure flows at angles of roughly  $45^{\circ}$  to the normal. The calibration or sensitivities at these angles were needed. Various empirical formulae for angular sensitivities are available, such as those of Friehe and Schwarz (1968) and Champagne (1966). These formulae require that the geometry of the wire be accurately known. The angles on one X-wire probe were measured by mounting the probe in the negative carrier of a photographic enlarger and measuring the angles of the projected image. The accuracy of this technique was questionable, and it was concluded that in this case the sensitivities could best be found directly by calibrating the angular response of the X-wire probe.

The sensitivities that were actually needed for each wire were the sensitivity to longitudinal velocities and the sensitivity to lateral velocities. These sensitivities were found, as for the straight wire, by measuring the linearizer voltage versus velocity with the Thermo Systems Model 1125 Calibrator. The need to rotate the probe was

met by mounting it in a milling machine crosshead. The crosshead was capable of linear motion in two perpendicular directions and rotation within the same plane. The longitudinal direction sensitivities were found by mounting the X-wire probe so that its axis roughly coincided with the axis of the flow from the calibrator, and adjusting the angle so that the dc voltages from the two wires were identical. This was done for a velocity corresponding to a dynamic pressure of 15.3 mm (0.60 in) of water. The angle at which the two probes were balanced then served as the zero degree reference angle, and a linearized calibration was measured at this angle. The probe was supported on the crosshead in such a way that after calibrating this longitudinal response, the crosshead was rotated in  $15^\circ$  increments at which the calibrations of both wires were measured. This was repeated to  $90^\circ$ , which corresponded to the lateral sensitivity calibration. At the end of a measurement session, the longitudinal calibration was repeated after again balancing the dc voltage of the two wires by carefully adjusting the angle of the probe relative to the calibration jet.

After calibration, the probe was moved to the jet where it was positioned at a height of 0.15 m (6 in), and on the jet centerline at  $X/D \approx 1$  in the jet potential core. The support assembly for the probe had been built with provision for adjusting the angle of the probe. This adjustment to

the angle between the probe axis and the flow axis was used to balance the dc voltages from the two wires, at which point the probe was assumed to be aligned with the jet centerline at the same angle as it had been with the calibration rig centerline. Measurements were then begun.

Two different methods were used to take the measurements which were needed to determine  $u'$ ,  $v'$  and  $\overline{uv}$ . For the ideal X-wire, the mean square of the sum of the fluctuating voltages is directly proportional to the horizontal fluctuation mean square.

$$\overline{(e_1 + e_2)^2} \propto \overline{u^2}$$

The mean square of the difference of the fluctuating voltages is proportional to the lateral fluctuation mean square.

$$\overline{(e_1 - e_2)^2} \propto \overline{v^2}$$

The mean of the difference of the squares is proportional to the Reynolds stress.

$$\overline{(e_1^2 - e_2^2)} \propto \overline{uv}$$

These are the relations for the ideal X-wire. As shown in Appendix D for the X-wire probe with unequal sensitivities, these relations are somewhat more complicated. However, three measured quantities are sufficient to calculate the three unknown quantities. The three voltage terms were measured in two different ways. One employed digital

techniques, and the other analog readouts. The digital technique was implemented with a Hewlett Packard 5450A Fourier Analyzer System. The Fourier Analyzer was programmed to digitize the two analog voltages  $e_1$  and  $e_2$ , algebraically form instantaneous sums, differences, and differences of squares, and then sum these terms to form averages. The resulting sums were then printed out for further reduction on the large digital computer. The measurements analyzed digitally were done at X/D's of 20, 40, and 60 and Y/B's from 0 to 2. The input was ac coupled at a 3 dB down high pass frequency of 5 Hz, the frequency resolution was 10 Hz, the maximum frequency was 2560 Hz, and the averaging time was 30 seconds. The program used in the analyzer for this case is given in Appendix D. The digital analysis was checked in one case by parallel analog analysis. A schematic of the digital and analog analysis instrumentation is given in Figure III-12.

The heart of the analog instrumentation was a Thermo Systems Model 1015C Correlator. The two linearized wire voltages were the inputs to it, and it took the sum and difference of the two signals. The sum was fed to one Thermo Systems Model 1076 True RMS Voltmeter and the difference was fed to another one. The rms voltages were averaged with the 100 second time constant. As the third signal needed to solve for the Reynolds stress, the rms of the voltage from one of the wires was used. This rms

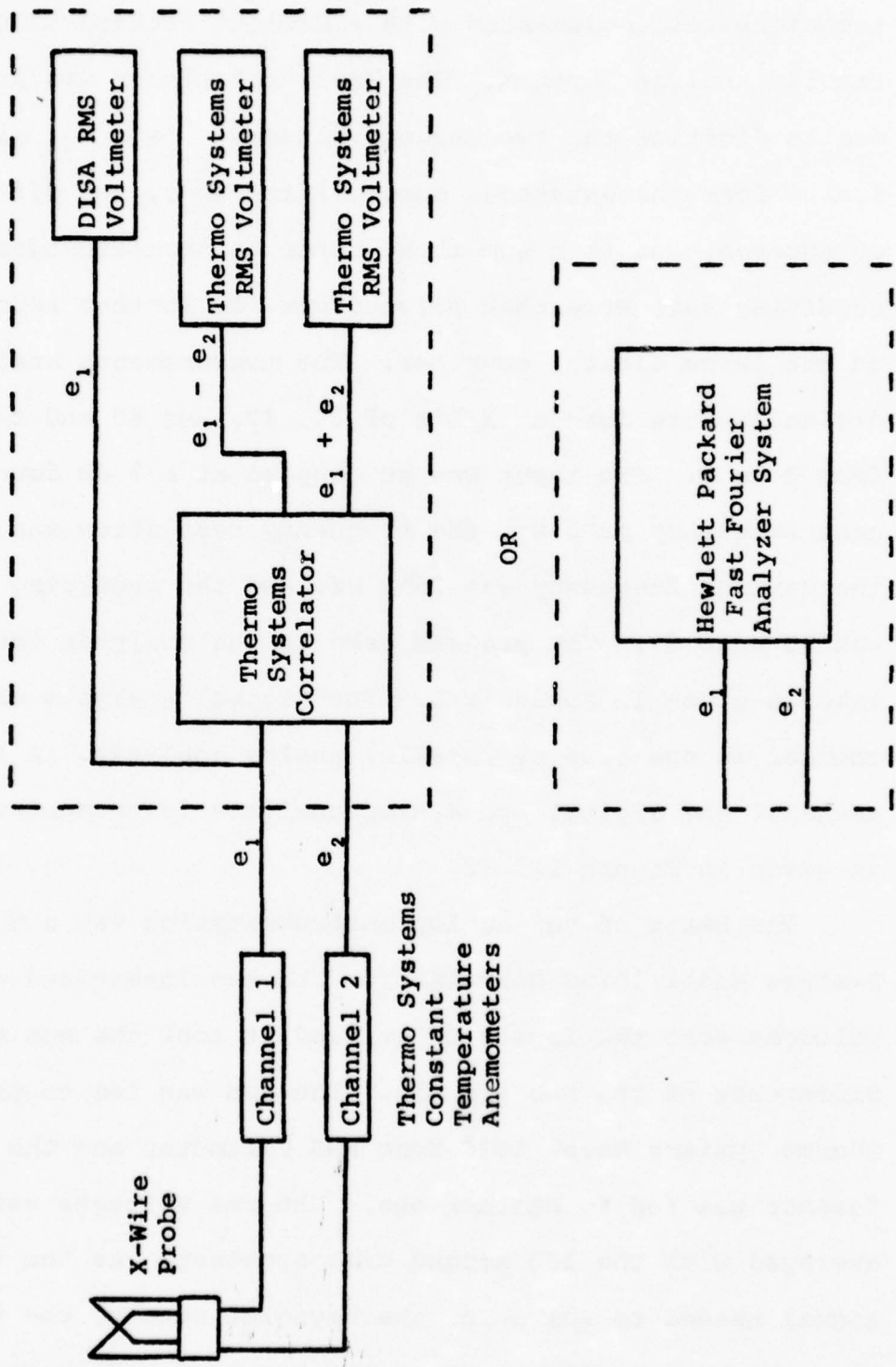


Figure III-12 Schematic Diagram of X-Wire Measurement Instrumentation

voltage was measured with a DISA Type 55D35 RMS Voltmeter, also using a 100 second time constant. The major difference between the analog and digital evaluations of the three quantities was that in the analog case the correlator was ac coupled at 0.1 Hz and essentially all the very low frequency components of the signals were analyzed, while the digital evaluation was weighted to components with frequencies above 5 Hz.

Another set of data was taken and analyzed solely by analog means. Measurements of the longitudinal and lateral turbulence intensities were made along the jet centerline from  $X/D = 0$  to  $X/D = 80$ , and laterally at  $X/D = 20, 40,$  and  $60$  for  $Y/B$  of  $0$  to  $2$ . The longitudinal results were compared by simultaneous measurements with a non-linearized straight wire mounted  $12.7$  mm ( $0.5$  in) above the X-wire. Only the rms values of the sum and difference voltages were measured for the X-wire. For both sets of data measured with the X-wire, the jet centerline was found by traversing and plotting the dc coupled sum of the X-wire linearized voltages, smoothed by the one second time constant of one of the Thermo Systems Model 1076 Voltmeters, on the X-Y-Y recorder. The results of the X-wire measurements are presented in the next chapter.

The results were calculated on the digital computer using one of the relations derived in Appendix D. The sensitivities for the X-wires were obtained by fitting

linear least squares fits to the calibration points. A typical example of these fits is given in Figure III-13. The angular sensitivity distribution is shown in Figure III-14. The calibrations did exhibit small amounts of drift from the beginning to the end of the measurement sessions, and the averages of the before and after longitudinal sensitivities were used. The lateral sensitivities, which were not checked at the end of the measurement session, were scaled by the ratio of the average longitudinal sensitivities to the initial longitudinal sensitivities. These sensitivities were then input to the computer program which calculated the final values for the longitudinal and lateral turbulence intensities and Reynolds stresses. These results are presented in the next chapter along with a detailed analysis of their accuracy.

#### F. Energy Spectrum Measurements

The final experimental technique to be described in this chapter is the method used to measure the energy spectra of the longitudinal turbulent velocity fluctuations. These one-dimensional spectra were measured in order to obtain an indication of the frequency distribution of the energy in the longitudinal turbulent fluctuations.

The signals used for the spectra were obtained from non-linearized straight wires. The signal was first fed to an SKL Model 302 Variable Electronic Filter where it was low pass filtered twice at a frequency just under the

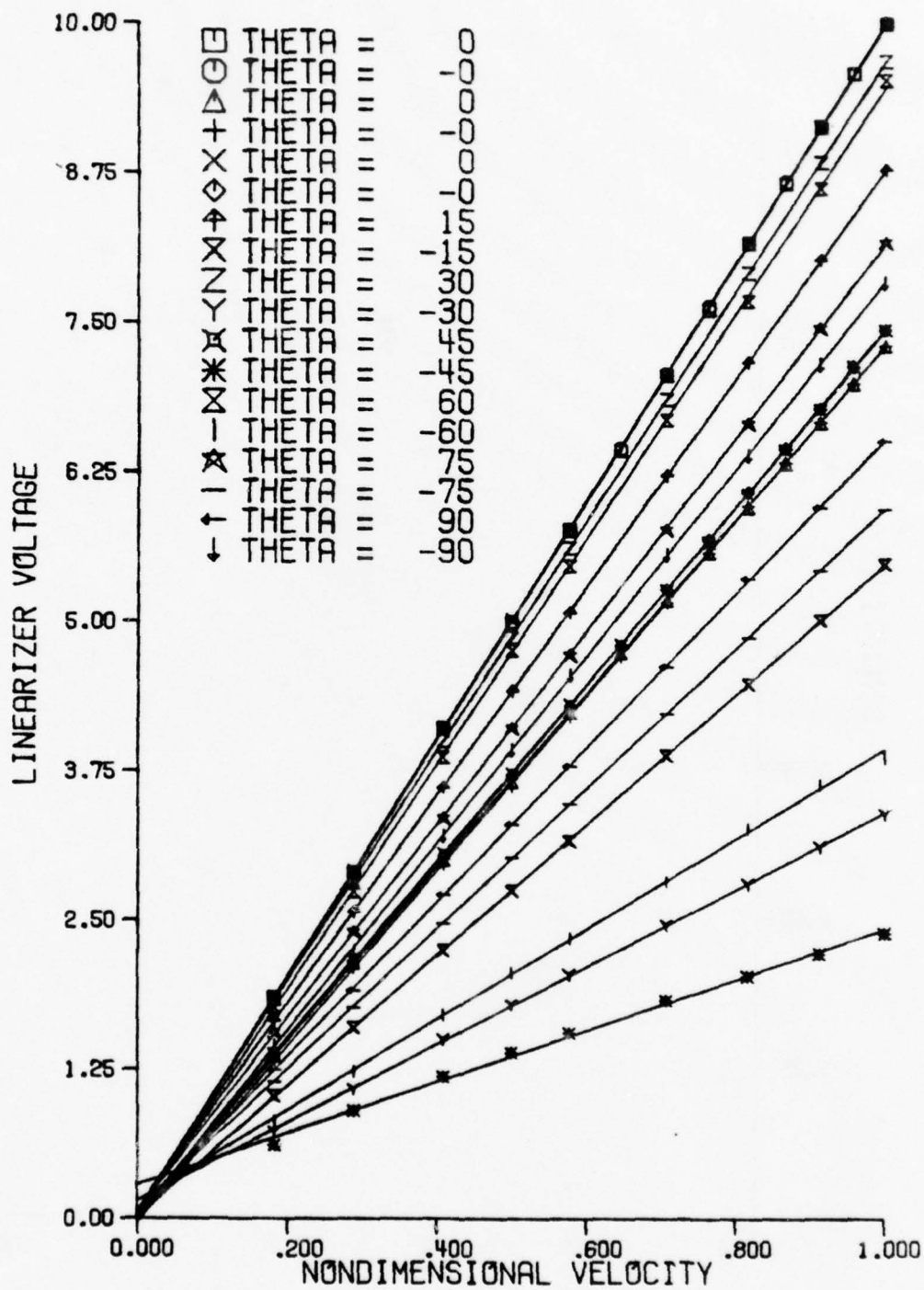


Figure III-13 Typical X-Wire Probe  
Linearized Calibration

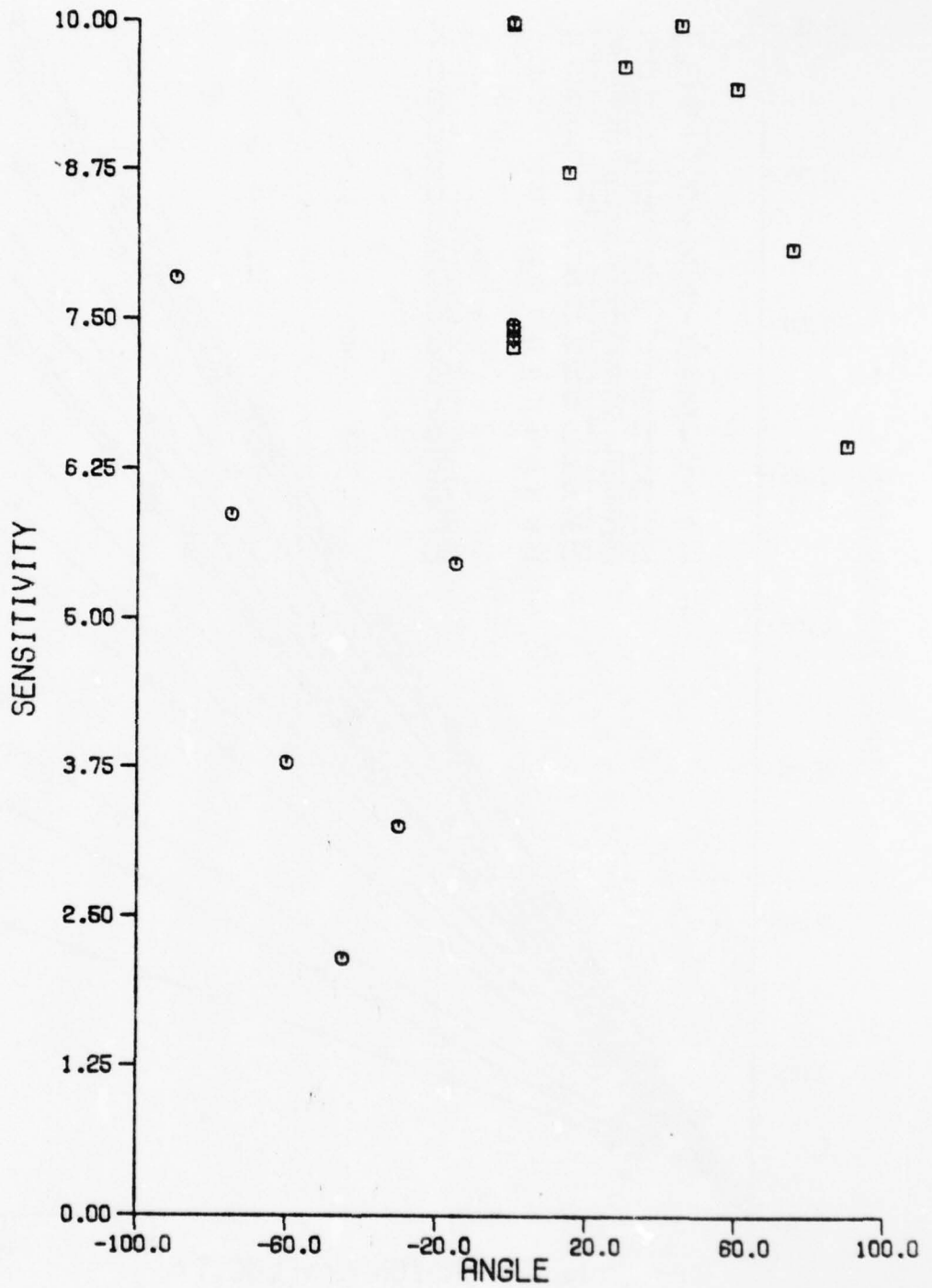


Figure III-14 Typical X-Wire Probe Sensitivity Calibration

maximum frequency to be calculated in the spectrum. This filtering was done to remove any high frequency components of the signal that would be folded over and aliased in the digitally calculated spectrum. From the filter, the signal was connected to the Channel A input of the Hewlett-Packard 5450 A Fourier Analyzer System.

The signal was ac coupled to the input with the coupling having a 3 dB down lower frequency limit of 5 Hz. Before beginning the program to calculate the spectrum, the input attenuator of the analog to digital converter section was adjusted to eliminate any overloading. The sampling parameter controls were adjusted to the desired values. Nearly all of the spectra presented in the next chapter were obtained using a frequency resolution of 10 Hz, which corresponds to a sample time of 0.1 second. A block size of 512 positions was used, and this resulted in a maximum frequency of 2560 Hz, generally higher than any component of the signal that had an observable magnitude.

When these preliminary steps were completed, the program was begun. The listing of the program is given in Appendix F. The program began by first clearing all storage locations. A loop was then begun which first sampled a 0.1 second long section of the signal. A discrete finite Fourier transform of the digitized signal was then performed. The transform was then multiplied by its complex

conjugate to form an energy spectrum, and this spectrum was added to the summation of the previous spectra. The loop was then repeated. This was done 300 times, so that the total record length sampled was 30 seconds. This 30 second record length, combined with the 10 Hz resolution bandwidth of the spectra, results in a random error of less than 6% according to a relation derived by Bendat and Piersol (1971). The sum of the 300 spectra was then normalized by dividing by 300 and then by its integral. The resulting normalized energy spectrum was then displayed on the system oscilloscope display, and punched out on a high speed paper tape punch for later analysis. This process took roughly twenty minutes to complete, for the arithmetic operations are performed very slowly. The resulting energy spectra were limited by the analyzer's 40 dB dynamic range. This resulted in some zeros in the final normalized spectra.

The spectra were prepared for analysis on the digital computer by having computer cards punched from the paper tapes. The computer was then used to prepare linear or log, normalized or absolute spectra for plotting on the CALCOMP plotter. The results of these measurements are presented in the next chapter, with discussions of their trends and analyses of the measurement errors.

## CHAPTER IV EXPERIMENTAL RESULTS AND DISCUSSION

The results of the experimental measurements of the effects of applied sound on the plane turbulent jet are presented in this chapter. The presentation includes discussion of the trends evidenced by the data, and of inaccuracies attributed to various sources. An analysis of the implications of these trends and their relation to the relevant theories is saved for presentation in Chapter V.

The results presented in this chapter are divided into two sections. Kaiser and Goldschmidt's (1971) study of the effect of sound upon the gross properties of a turbulent plane jet was the stimulus for this research, and Section A contains the results of measurements to confirm their findings. Section B is a presentation of the results obtained from the measurements of the effects of certain frequencies of sound on the turbulent structure of the jet. These measurements were the major goal of the experimental phase of the research. A summary of all results presented is given in Section C.

### A. Measurements of Frequency Dependence

This section presents the results of measurements which were made to determine the frequency dependence of

the effects of the pure tone sounds on the jet. The frequency dependence was measured through the changes in the jet mean pressure profiles at distances from the nozzle of 20 to 50 slot widths.

#### 1. Pressure Profile Measurements

The jet mean total pressure profiles were measured in order to determine the sound induced changes in the jet widening rate and velocity decay rate. The pressure profiles were measured using the technique described in Chapter III which utilized two pitot tubes, two differential pressure transducers, and an X-Y-Y plotter. A typical pressure profile plot is shown in Figure III-7. In the far region of the jet ( $X/D \geq 20$ ), the mean velocity profiles should display similarity, and the distributions of the turbulence intensities and Reynolds stresses should also approach similarity, although generally at greater distances from the mouth. The mean velocity profile similarity was checked with points measured from pressure profiles taken at  $X/D$ 's of 20, 30, and 40 for no applied sound, and 105 dB SPL re  $20 \mu\text{N}/\text{m}^2$  sound at frequencies of 700 Hz and 1600 Hz. The pressure profile points were taken from the "average lines" sketched over the profiles, as shown in Figure III-7. The velocities were scaled by the local mean centerline velocity,  $U_m$ , and the distance from the centerline was scaled by the jet half width,  $B$ . The resulting scaled velocity profile is shown in Figure IV-1

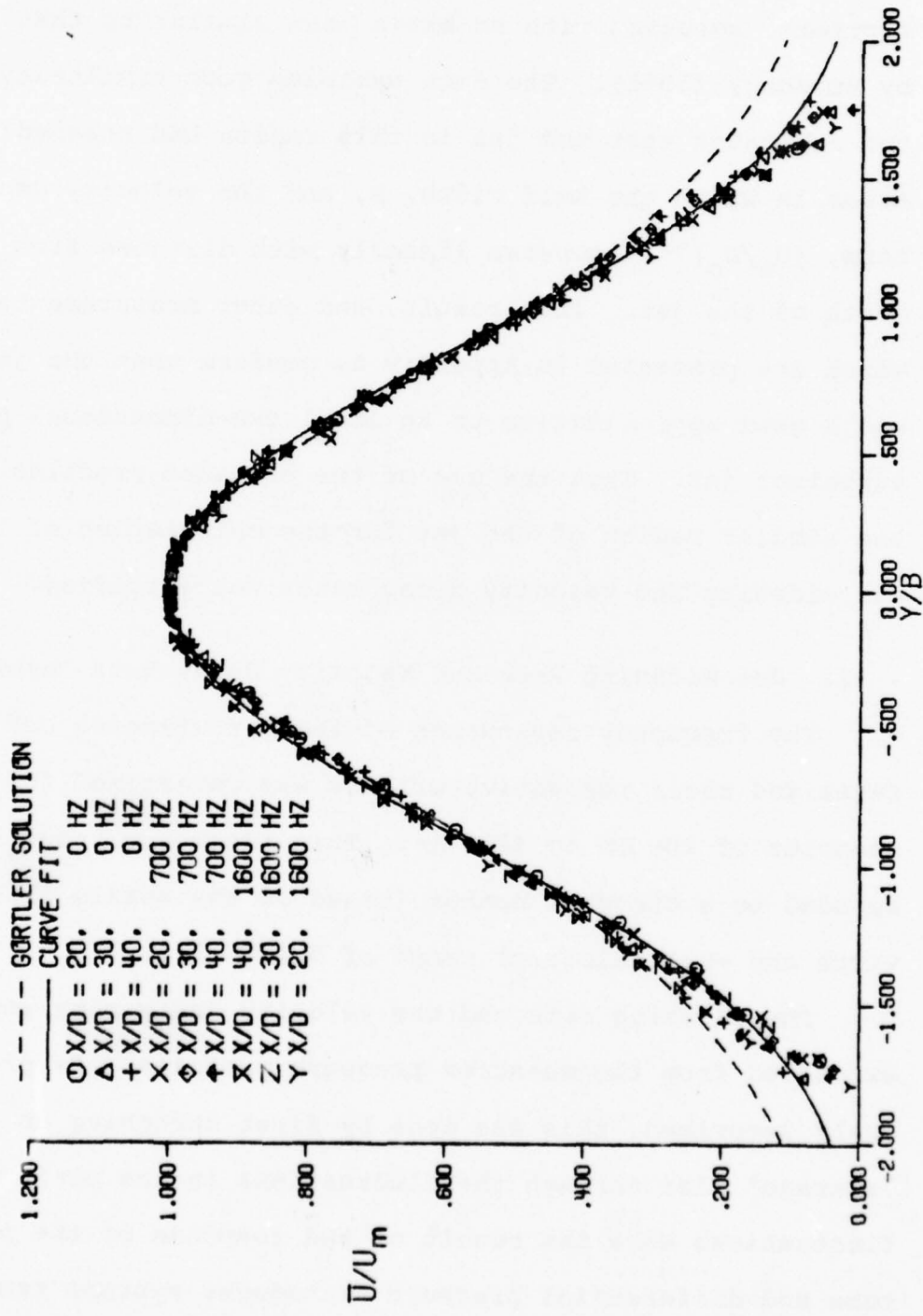


Figure IV-1 Mean Velocity Profiles

along with Görtler's (1942) classical solution for the profile and an empirical fit to the profile using the form of Görtler's solution with an extra term similar to that used by Bradbury (1965). The data exhibits good similarity, and indicates that the jet in this region had reached the stage in which the half width,  $B$ , and the velocity decay term,  $(U_m/U_o)^{-2}$ , increase linearly with distance from the mouth of the jet. This result, and other measurements which are presented in Appendix A, confirm that the jet was a good approximation to an ideal two-dimensional plane turbulent jet. Thus the use of the pressure profiles in the similar region of the jet for the calculation of linear widening and velocity decay rates was justified.

## 2. Jet Widening Rate and Velocity Decay Rate Results

The frequency dependence of the jet widening and decay rates and their respective origins was determined for frequencies of 200 Hz to 4200 Hz. This frequency range corresponded to a Strouhal number (based on the nozzle slot width and exit velocity) range of 0.1 to 1.8.

The widening rate and the velocity decay rate were extracted from the measured pressure profiles. As previously described, this was done by first sketching an "average" line through the fluctuations in the plots. The fluctuations were the result of the response of the pitot tube and differential pressure transducer systems response to the low frequency fluctuations in the turbulent flow

field. The pressure measuring system had a frequency response that was 3 dB down at about 5 to 8 Hz, and this sensitivity generally resulted in small fluctuations in the pressure profile plots. These small fluctuations were easily averaged out in the sketch, as shown in Figure III-7. The sketching technique was used on well over one thousand pressure profiles, and a high degree of uniformity in the application of the technique was developed. The accuracy of the half width and centerline mean total pressure measured from the profiles varied with the level of fluctuations in the plot. The level of fluctuations varied with the X/D position of the profile and the frequency of applied sound. In the applied sound frequency range between roughly 800 Hz and 1400 Hz, large fluctuations were present in the pressure profile plots. These fluctuations were largest at approximately 1100 Hz. These fluctuations were carefully investigated, for at first they were believed to be the result of faulty instrumentation or vibrating mechanical apparatus. The fluctuations were found to be random intermittent changes in the mean flow that could not be averaged away. The flow appeared to be alternating randomly between two modes of response to the applied sound. The study of this phenomenon is described in Appendix C. Pressure profiles were measured for frequencies in this region, and the plots were treated in the same manner as all the others. The region corresponds to Strouhal numbers

from 0.4 to 0.7, with the largest fluctuations in roughly the middle of the region.

The measured half widths and centerline pressures were input to a computer program which calculated the velocity decay ratio, and then calculated linear least squares fits to the half width and velocity decay ratio points. The resulting fits were checked via a computer generated plot of the points and the least squares fit lines. The slope and intercept of these two lines gave the widening rate and geometric origin and the velocity decay rate and velocity origin. Early measurements were made using four pressure profiles at each frequency, and the final measurements were made using six pressure profiles for each frequency.

The resulting plots of widening rate, geometric origin, velocity decay rate, and velocity origin versus Strouhal number are presented in Figures IV-2 through IV-9. The numerical results in these plots are tabulated in Tables IV-1 through IV-8. Figures IV-2 through IV-5 include points obtained from measurements of both four and six profiles, and Figures IV-6 through IV-9 include only the results obtained from measurements of six profiles. A number of trends may be observed in these plots. The most obvious is that the applied sound can have a large effect upon the gross structure of the jet in the region from  $X/D = 20$  to  $X/D = 50$ .

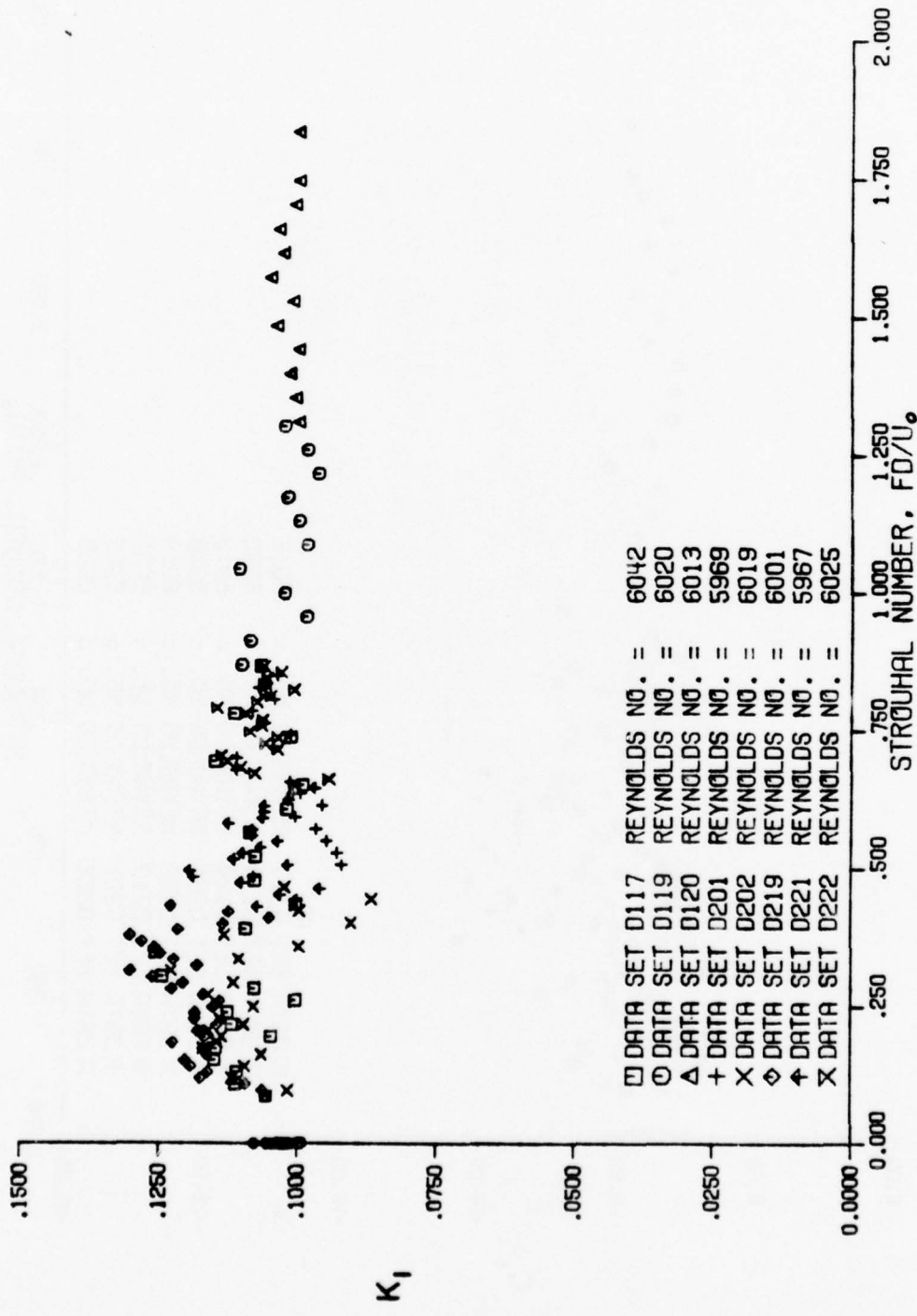


Figure IV-2 Strouhal Number Dependence of Widening Rate for all Data

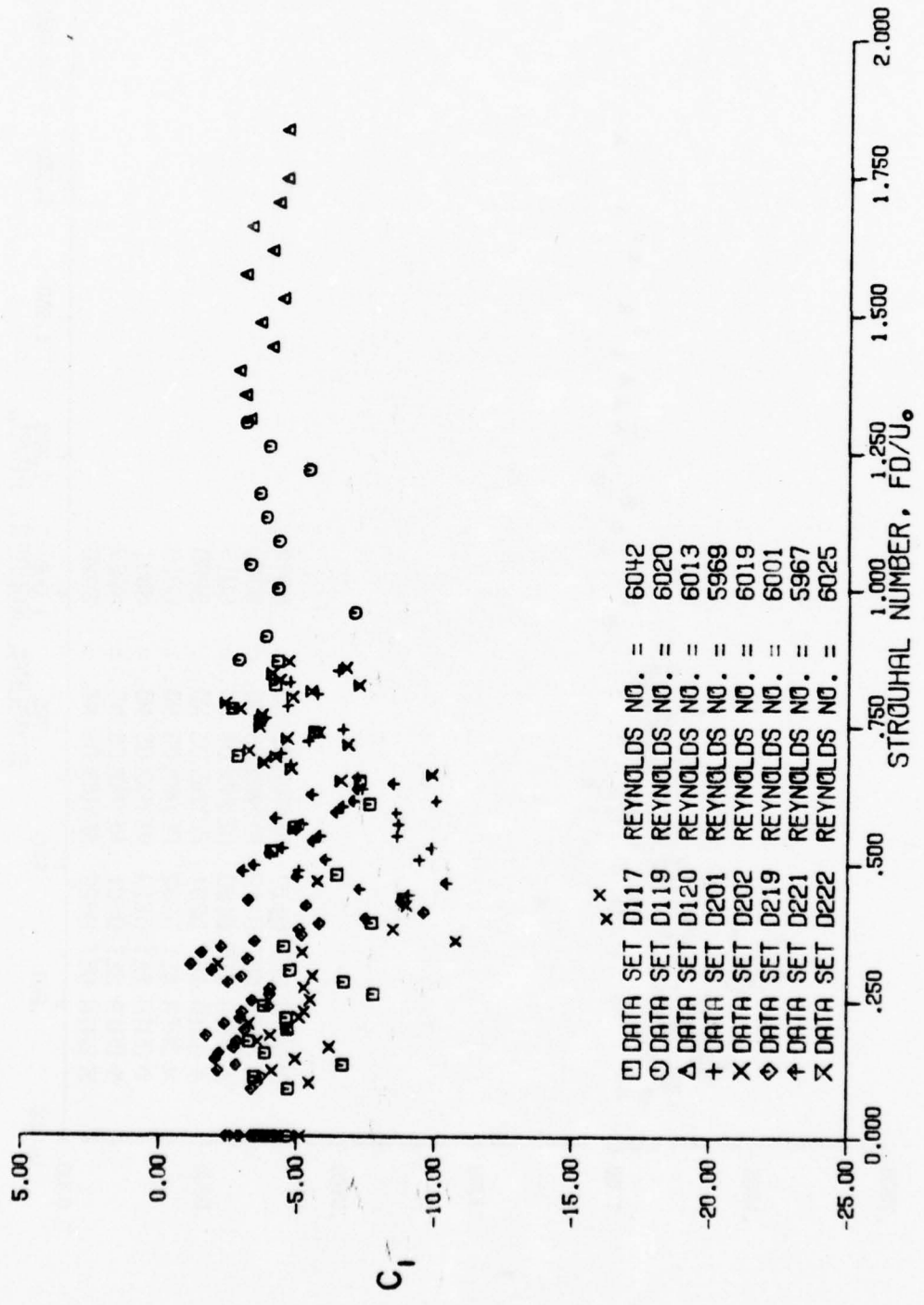


Figure IV-3 Strouhal Number Dependence of Geometric Origin for all Data

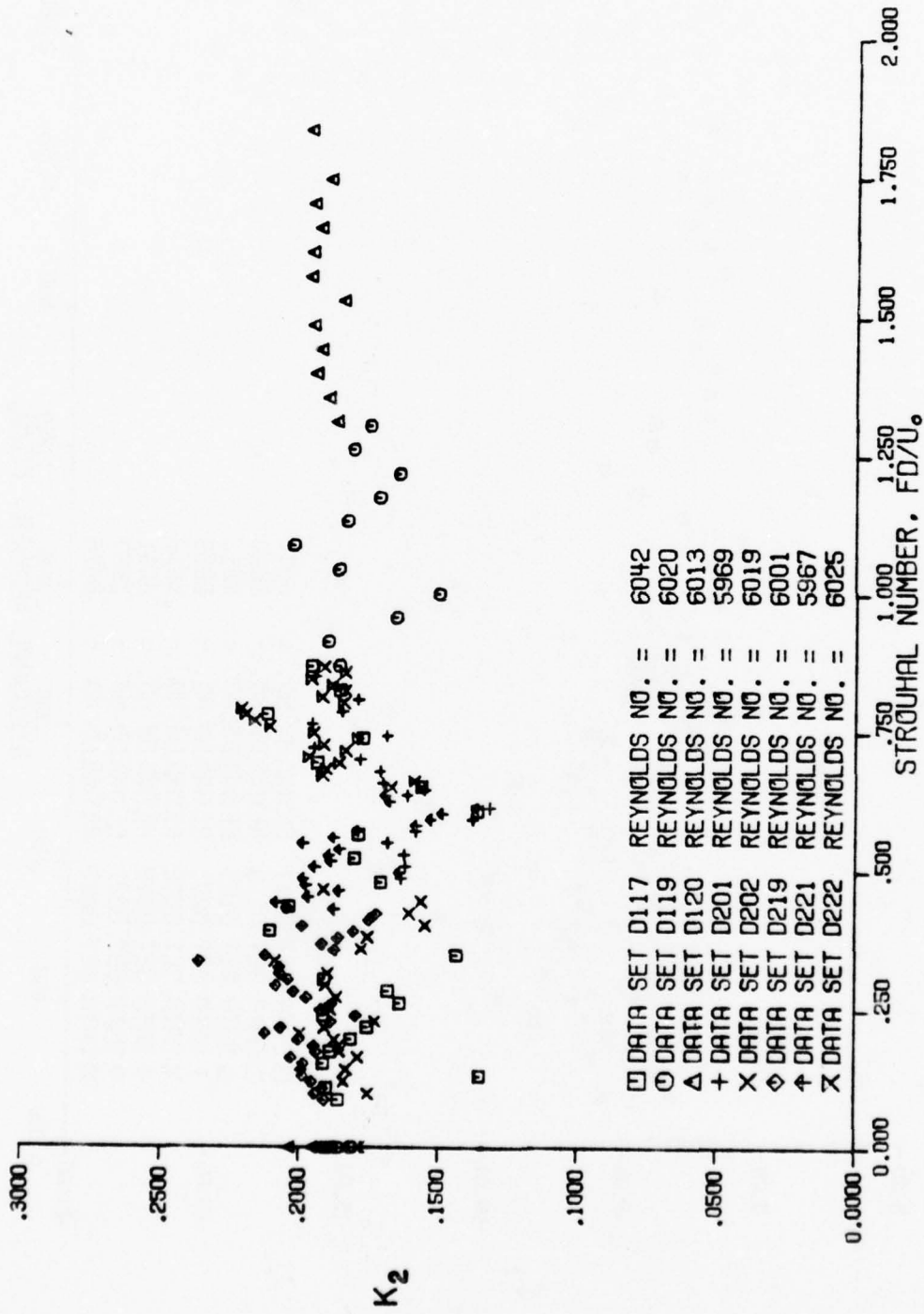


Figure IV-4 Strouhal Number Dependence of Velocity Decay Rate for all Data

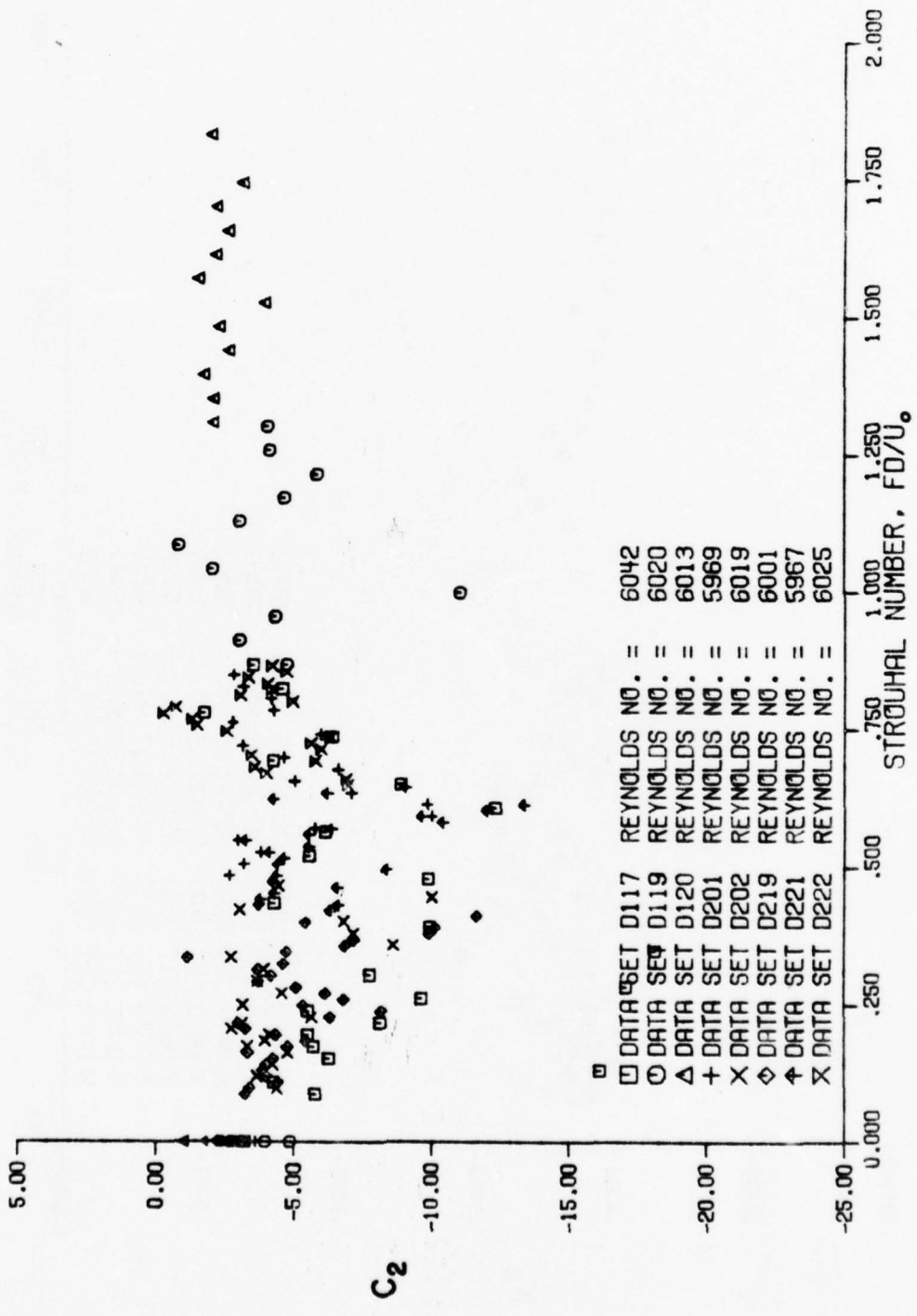


Figure IV-5 Strouhal Number Dependence of Velocity Origin for all Data

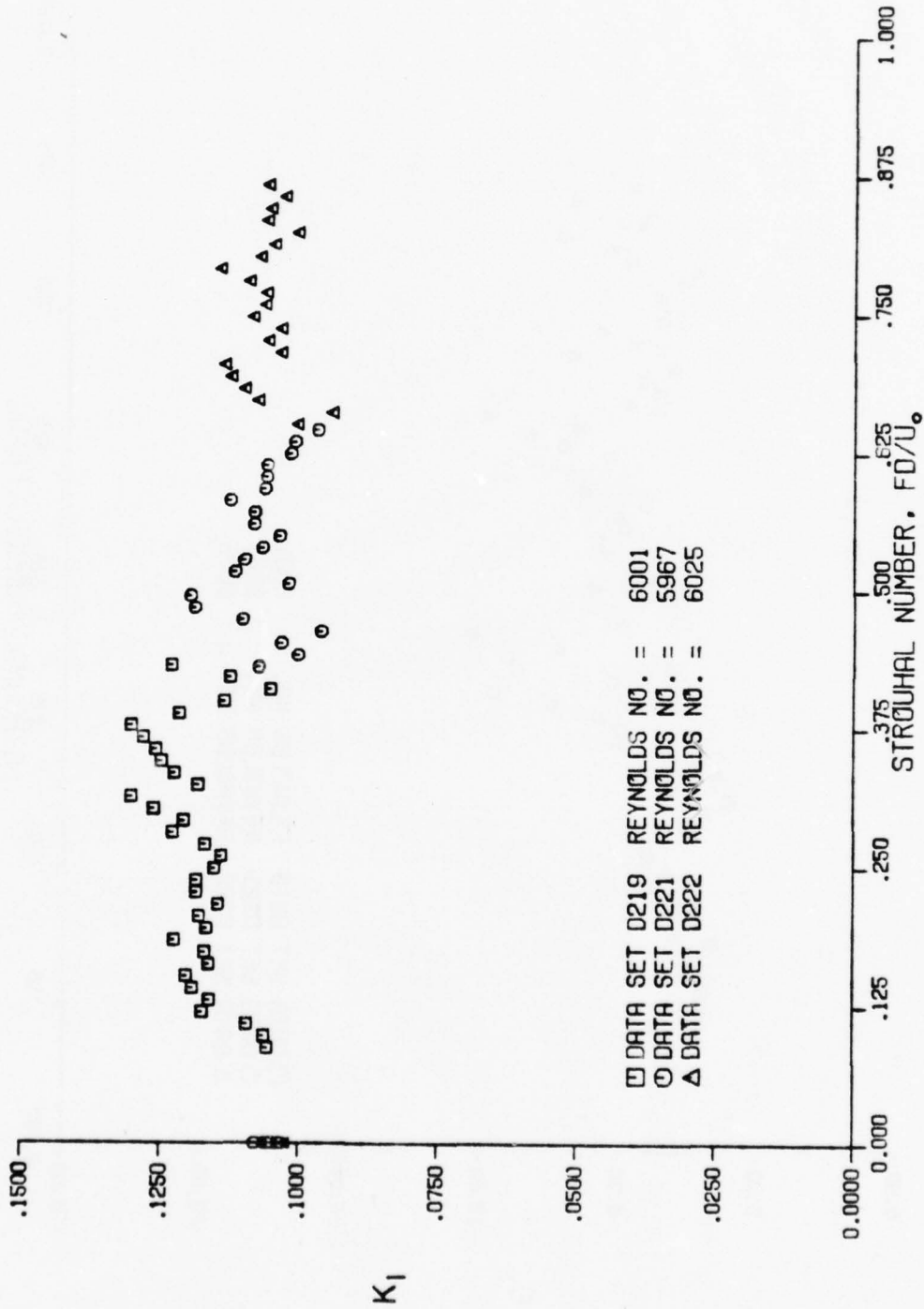


Figure IV-6 Strouhal Number Dependence of Widening Rate for Six Profile Data

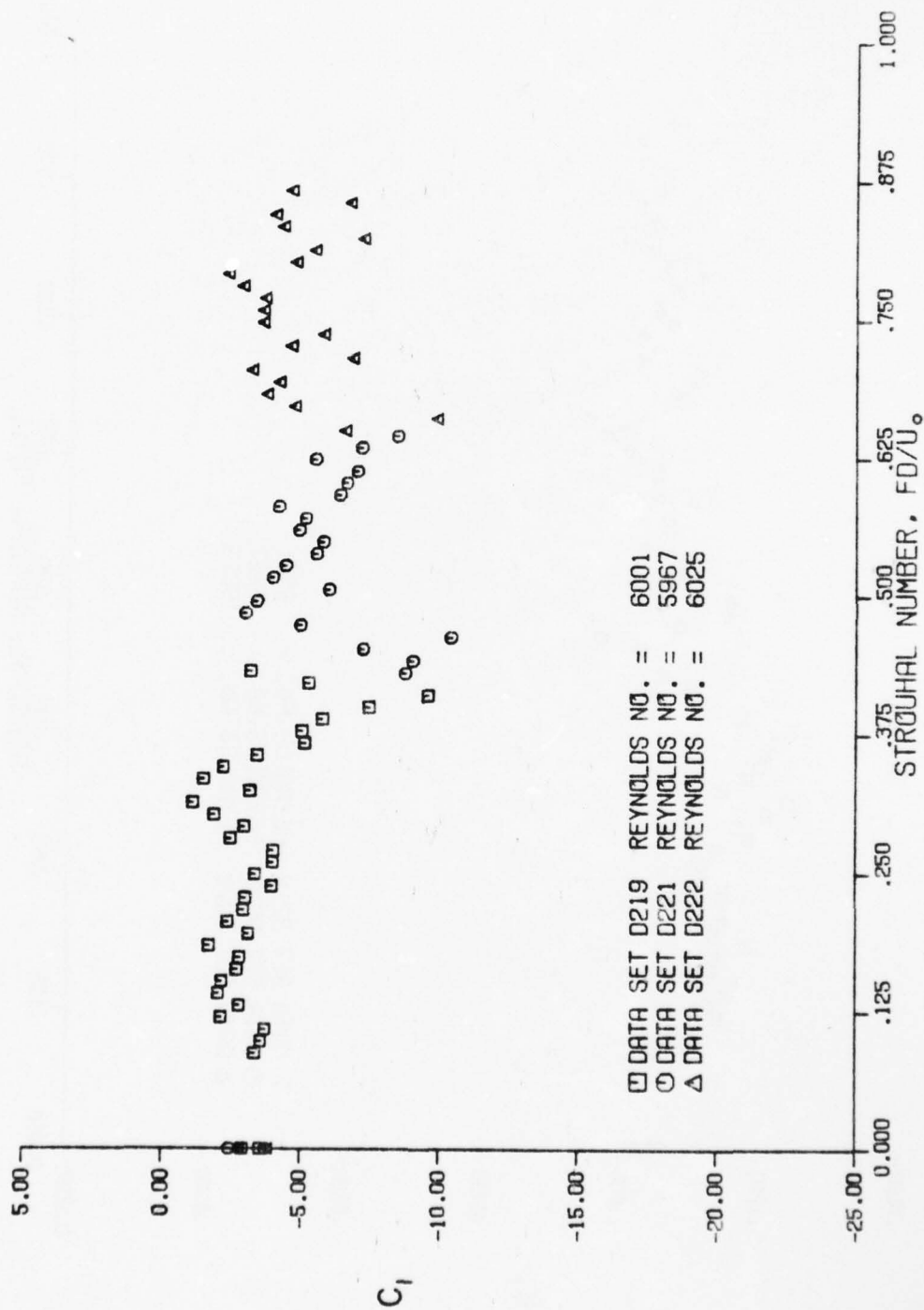


Figure IV-7 Strouhal Number Dependence of Geometric Origin for Six Profile Data

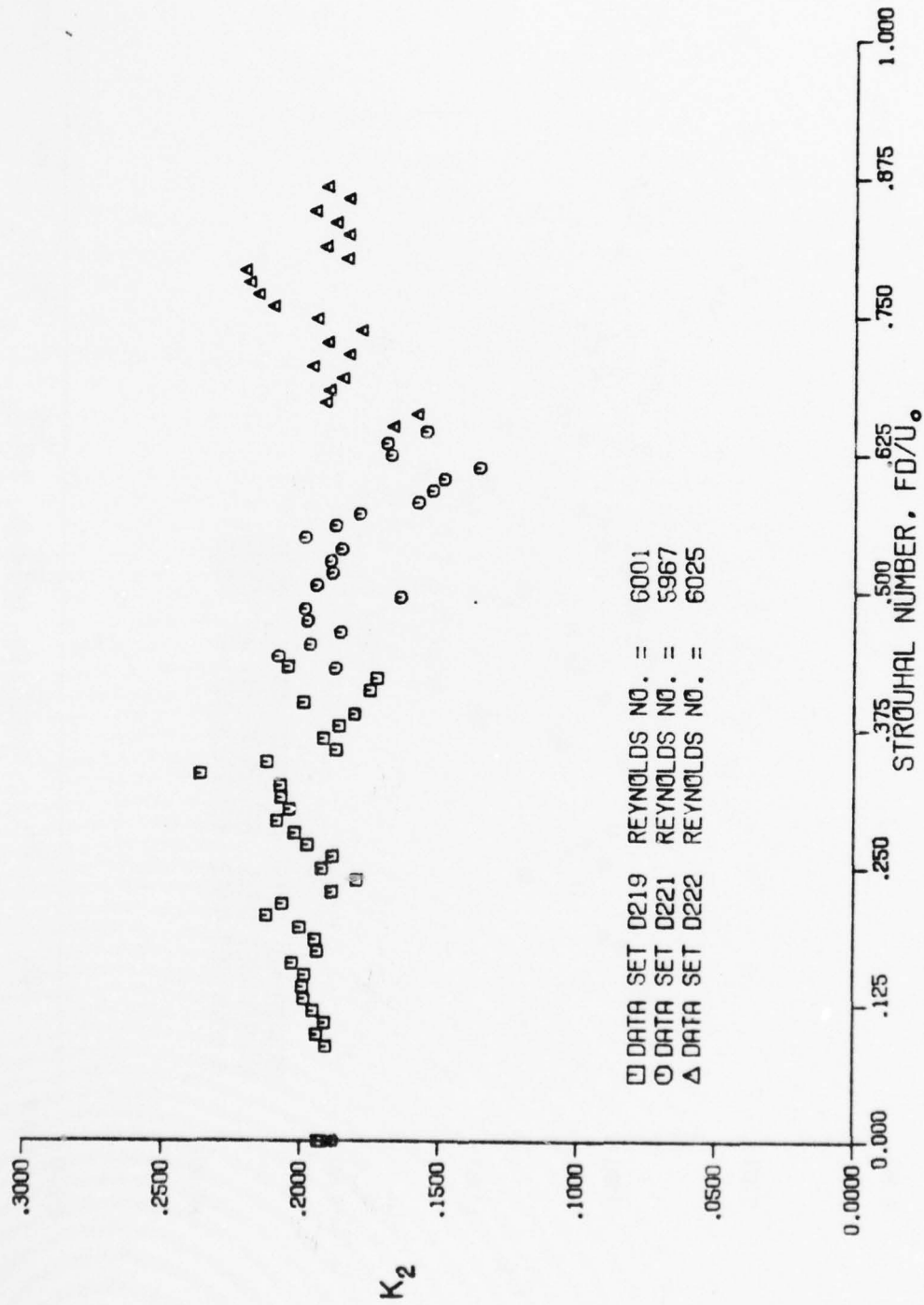


Figure IV-8 Strouhal Number Dependence of Velocity Decay Rate for Six Profile Data

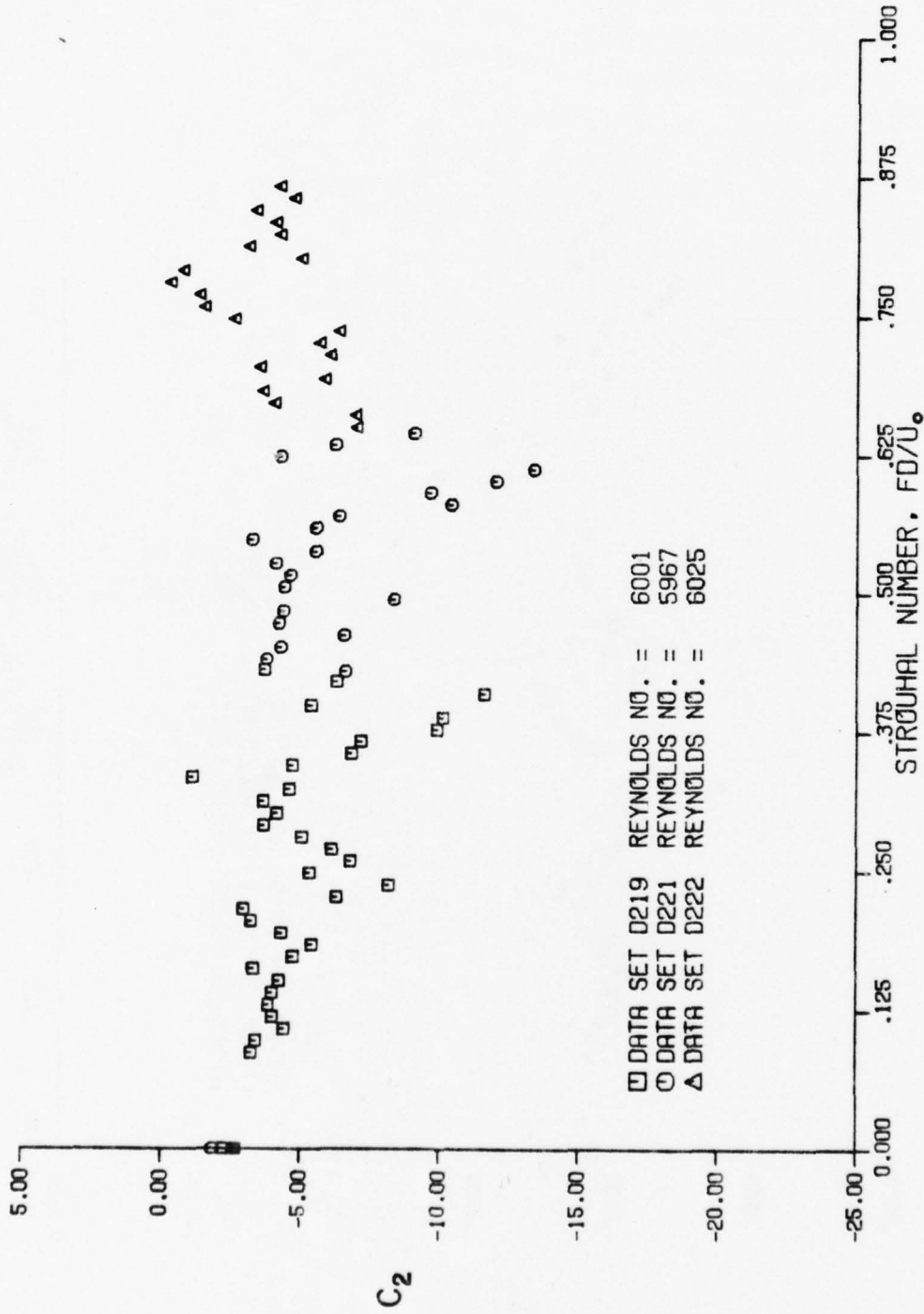


Figure IV-9 Strouhal Number Dependence of Velocity Origin for Six Profile Data

TABLE IV-1  
DATA SET D117 RESULTS  
REYNOLDS NO. = 6042

STROUHAL NUMBER ST	WIDENING RATE K1	GEOMETRIC ORIGIN C1	DECAY RATE K2	VELOCITY ORIGIN C2
0.0000	.1023	-4.0274	.1900	-3.2130
0.0000	.1029	-3.6540	.1881	-3.2369
.0867	.1055	-4.6919	.1859	-5.7794
.1084	.1111	-3.4564	.1902	-4.2933
.1301	.1108	-6.6516	.1351	-16.1451
.1518	.1149	-3.8381	.1913	-6.2731
.1734	.1146	-3.2635	.1888	-5.7153
.1951	.1047	-4.6609	.1814	-5.5092
.2168	.1118	-4.6243	.1756	-8.1408
.2385	.1126	-3.8100	.1913	-5.5306
.2602	.1004	-7.7789	.1640	-9.6443
.2819	.1078	-5.6376	.1682	-17.0792
.3035	.1244	-4.7508	.1911	-7.7686
.3469	.1257	-4.5187	.1434	-13.1353
.3903	.1093	-7.7036	.2104	-9.9545
.4336	.1003	-8.8435	.2035	-4.3142
.4770	.1077	-6.4345	.1707	-9.0947
.5204	.1076	-4.0739	.1833	-5.5771
.5637	.1086	-4.8711	.1783	-6.1453
.6071	.1019	-7.6153	.1361	-12.3247
.6504	.0991	-7.2553	.1562	-8.9137
.6938	.1148	-2.8049	.1935	-4.2802
.7372	.1012	-5.6127	.1773	-6.4112
.7805	.1113	-2.6235	.2117	-1.7672
.8239	.1058	-4.1777	.1857	-4.6104
.8672	.1065	-4.2589	.1958	-3.5462

TABLE IV-2  
DATA SET D119 RESULTS  
REYNOLDS NO. = 6020

STROUHAL NUMBER ST	WIDENING RATE K1	GEOMETRIC ORIGIN C1	DECAY RATE K2	VELOCITY ORIGIN C2
0.0000	.1030	-3.4466	.1859	-3.1431
0.0000	.1027	-3.5833	.1908	-3.9732
0.0000	.0995	-4.6734	.1815	-4.9756
.9678	.1101	-2.9520	.1859	-4.7588
.9112	.1035	-3.8849	.1899	-3.0099
.9546	.0983	-7.0357	.1684	-1.3384
.9980	.1022	-4.2357	.1497	-11.0633
1.0414	.1104	-3.2599	.1960	-2.3977
1.0847	.0932	-4.3075	.2021	-1.8497
1.1281	.0997	-3.8415	.1800	-3.3339
1.1715	.1018	-3.6051	.1715	-1.6650
1.2149	.0953	-5.2586	.1645	-5.8345
1.2583	.0933	-3.3369	.1811	-4.1326
1.3017	.1024	-3.0859	.1751	-3.0441

TABLE IV-3  
DATA SET D120 RESULTS  
REYNOLDS NO. = 6013

STROUHAL NUMBER ST	WIDENING RATE K1	GEOMETRIC ORIGIN C1	DECAY RATE K2	VELOCITY ORIGIN C2
0.0000	.1010	-4.2574	.2034	-.9951
0.0000	.1035	-3.6232	.1954	-2.4819
1.3086	.0999	-3.2132	.1872	-2.0541
1.3522	.1005	-3.0348	.1902	-2.0750
1.3958	.1016	-2.7953	.1948	-1.7322
1.4395	.1000	-4.0000	.1931	-2.6422
1.4831	.1040	-3.5577	.1959	-2.2878
1.5267	.1011	-4.3917	.1852	-3.9300
1.5703	.1051	-3.0352	.1970	-1.5350
1.6139	.1028	-4.0078	.1954	-2.1613
1.6576	.1035	-3.2367	.1934	-2.6189
1.7012	.1006	-4.2147	.1958	-2.1948
1.7448	.0999	-4.5145	.1899	-3.1553
1.8320	.1000	-4.5500	.1968	-2.0181

TABLE IV-4  
DATA SET D201 RESULTS  
REYNOLDS NO. = 5969

STROUHAL NUMBER ST	WIDENING RATE K1	GEOMETRIC ORIGIN C1	DECAY RATE K2	VELOCITY ORIGIN C2
0.0000	.1074	-2.8492	.1777	-3.3277
0.0000	.1018	-4.2927	.1774	-3.6047
.4840	.1079	-5.0602	.1634	-2.6959
.5055	.0921	-9.4354	.1619	-3.2074
.5270	.0929	-9.8601	.1623	-3.8297
.5485	.0948	-8.6181	.1684	-2.9878
.5700	.0967	-8.6660	.1582	-5.7864
.5915	.1004	-8.5757	.1377	-10.0145
.6131	.0956	-10.0314	.1318	-9.8739
.6346	.0995	-7.3367	.1612	-7.1258
.6561	.1014	-7.1598	.1701	-5.0677
.6776	.1110	-4.7297	.1709	-6.6360
.6991	.1109	-4.3823	.1782	-4.6685
.7206	.1043	-5.3889	.1947	-3.1748
.7421	.1012	-6.6502	.1686	-5.9957
.7636	.1058	-3.8469	.1955	-2.8033
.7851	.1091	-4.6151	.1847	-4.3089
.8066	.1041	-5.7051	.1790	-4.2052
.8282	.1070	-4.7196	.1876	-3.1909
.8497	.1036	-6.4575	.1945	-2.8465

TABLE IV-5  
DATA SET D202 RESULTS  
REYNOLDS NO. = 6019

STROUHAL NUMBER ST	WIDENING RATE K1	GEOMETRIC ORIGIN C1	DECAY RATE K2	VELOCITY ORIGIN C2
0.0000	.0999	-5.1151	.1782	-3.1195
0.0000	.1034	-4.1199	.1831	-2.5056
.0975	.1017	-5.4376	.1752	-4.4128
.1191	.1117	-4.1003	.1840	-3.6823
.1408	.1094	-4.9452	.1831	-4.2451
.1624	.1064	-6.1654	.1788	-4.7922
.1733	.1169	-3.5586	.1954	-3.0279
.1841	.1144	-4.0297	.1853	-3.9711
.1949	.1136	-4.6587	.1874	-4.1408
.2058	.1160	-3.2759	.1997	-2.7472
.2166	.1097	-5.0866	.1909	-3.1682
.2274	.1140	-5.2632	.1729	-5.6431
.2491	.1079	-5.4773	.1888	-3.1761
.2707	.1161	-5.2455	.1868	-4.5931
.2924	.1115	-5.5613	.1907	-3.7029
.3140	.1228	-3.1335	.1699	-3.9373
.3357	.1105	-5.1899	.2087	-2.7466
.3574	.0997	-10.7823	.1776	-3.6853
.3790	.1131	-3.4752	.1755	-3.1757
.4007	.0903	-16.2459	.1547	-6.3211
.4223	.0886	-9.9759	.1605	-3.1611
.4440	.0866	-15.9815	.1503	-10.0273
.4657	.1023	-5.7280	.1810	-4.4337

TABLE IV-6  
DATA SET D219 RESULTS  
REYNOLDS NO. = 6001

STROUHAL NUMBER ST	WIDENING RATE K1	GEOMETRIC ORIGIN C1	DECAY RATE K2	VELOCITY ORIGIN C2
0.0000	.1047	-3.5653	.1921	-2.7016
0.0000	.1055	-2.9005	.1934	-2.2419
.0662	.1056	-3.3627	.1908	-3.2592
.0571	.1062	-3.5855	.1942	-3.4243
.1079	.1093	-3.7211	.1913	-4.4445
.1187	.1174	-2.1373	.1955	-4.0336
.1235	.1161	-2.7908	.1986	-3.8740
.1403	.1191	-2.0424	.1991	-4.0178
.1510	.1202	-2.1697	.1983	-4.2603
.1618	.1162	-2.7177	.2028	-3.3438
.1726	.1169	-2.8151	.1938	-4.7749
.1834	.1224	-1.7017	.1947	-5.4410
.1942	.1166	-3.1221	.2002	-4.3698
.2050	.1179	-2.3814	.2122	-3.2692
.2158	.1145	-2.9621	.2065	-2.9959
.2266	.1184	-3.0257	.1887	-6.3279
.2374	.1184	-3.9968	.1797	-8.1854
.2481	.1152	-3.3778	.1922	-5.3583
.2589	.1140	-4.0351	.1883	-6.8223
.2697	.1169	-4.0409	.1974	-6.1535
.2805	.1236	-2.5073	.2020	-5.1005
.2913	.1206	-2.9909	.2083	-3.7405
.3021	.1261	-1.9103	.2039	-4.2060
.3129	.1301	-1.1468	.2062	-3.7187
.3237	.1181	-3.1972	.2071	-4.6439
.3345	.1224	-1.5324	.2042	-1.1645
.3453	.1247	-2.2451	.2121	-4.7563
.3561	.1257	-3.4602	.1872	-6.8517
.3669	.1279	-5.1333	.1812	-7.1593
.3777	.1301	-5.0677	.1800	-9.0021
.3884	.1212	-5.7356	.1815	-10.1250
.3992	.1131	-7.4764	.1804	-5.4318
.4100	.1050	-9.5873	.1742	-11.0069
.4208	.1123	-5.3133	.1784	-8.3349
.4316	.1229	-3.2287	.2044	-3.7561

TABLE IV-7  
DATA SET D221 RESULTS  
REYNOLDS NO. = 5967

STROUHAL NUMBER ST	WIDENING RATE K1	GEOMETRIC ORIGIN C1	DECAY RATE K2	VELOCITY ORIGIN C2
0.0000	.1079	-2.4663	.1934	-1.8751
0.0000	.1031	-2.7312	.1879	-2.7013
.4298	.1071	-8.7889	.1875	-6.6437
.4405	.1001	-9.0519	.2080	-3.8184
.4513	.1031	-7.2684	.1966	-4.3316
.4620	.0959	-10.4331	.1857	-6.5952
.4728	.1101	-5.0195	.1976	-4.2739
.4835	.1187	-3.0465	.1935	-4.4184
.4943	.1194	-3.4550	.1640	-8.3889
.5050	.1017	-6.0300	.1945	-4.4034
.5158	.1114	-4.0336	.1887	-4.6671
.5265	.1097	-4.4813	.1894	-4.1441
.5373	.1056	-5.5831	.1805	-5.5643
.5480	.1035	-5.8213	.1988	-3.2283
.5587	.1081	-4.9626	.1877	-5.5647
.5695	.1081	-5.1855	.1790	-6.3881
.5803	.1124	-4.2249	.1580	-10.4213
.5910	.1062	-6.4100	.1528	-9.6500
.6017	.1050	-6.6476	.1486	-12.0153
.6125	.1059	-7.0378	.1359	-13.3960
.6232	.1016	-5.5341	.1677	-4.3136
.6340	.1009	-7.1884	.1693	-6.2483
.6447	.0989	-9.4833	.1550	-9.1833

TABLE IV-8  
DATA SET D222 RESULTS  
REYNOLDS NO. = 6025

STROUHAL NUMBER ST	WIDENING RATE K1	GEOMETRIC ORIGIN C1	DECAY RATE K2	VELOCITY ORIGIN C2
0.0000	.1056	-2.7994	.1888	-2.5769
0.0000	.1025	-3.8455	.1886	-2.6362
.6495	.1006	-6.5625	.1671	-6.9884
.6503	.0944	-9.8827	.1585	-6.9430
.6718	.1077	-4.7457	.1917	-4.0445
.6820	.1101	-3.7678	.1904	-3.6225
.6923	.1126	-4.2047	.1856	-5.8229
.7035	.1136	-3.2191	.1985	-3.5035
.7144	.1035	-6.8357	.1834	-6.0239
.7253	.1038	-4.6241	.1912	-5.8570
.7361	.1036	-5.7891	.1790	-6.3467
.7469	.1086	-3.6228	.1949	-2.6041
.7576	.1064	-3.6277	.2105	-1.5234
.7685	.1082	-3.7111	.2151	-1.5419
.7794	.1093	-2.9109	.2193	-1.2955
.7902	.1103	-2.3799	.2239	-1.7435
.8011	.1073	-4.8158	.1542	-4.6301
.8119	.1043	-5.4953	.1919	-3.1058
.8227	.1036	-7.2480	.1837	-4.2250
.8335	.1061	-4.3503	.1632	-4.0377
.8443	.1054	-4.0786	.1953	-3.3003
.8550	.1089	-6.7369	.1837	-4.7546
.8660	.1059	-4.6351	.1912	-4.2407

In Figure IV-2 (as well as Figure IV-6) it may be seen that an appropriate frequency and intensity applied sound can increase the jet widening rate up to 25% over the average of the cases without applied sound. The cases with no applied sound are plotted at a Strouhal number of zero. Figures IV-4 and IV-8 show that the velocity decay rate can be increased up to approximately 18% over the average no sound case. The figures show that these effects are frequency dependent. The widening rates and geometric origins show little change for the larger Strouhal numbers, while displaying large rather peaked changes at the lower Strouhal numbers. The velocity decay rates and velocity origins show somewhat similar behavior. The characteristics of the frequency dependence will now be discussed.

The widening rates generally show increases above the no sound rates, and the increases are most noticeable for Strouhal numbers below 0.4. The widening rates between 0.4 and 0.62 exhibit a large amount of scatter. This region is the one which displayed the intermittent fluctuations previously mentioned. From 0.62 to 1.08 the widening rates display four relative maxima. The region between 0.62 and 0.87 shows very good repeatability. Beyond 1.1, the widening rates differ very little from the no sound values, indicating that the sound has little effect in this region.

The geometric origin plot also exhibits small changes as compared to the no sound values in the region beyond a Strouhal number of 1.1. In general, the geometric origin appears to be less affected by the applied sound than the widening rate. The geometric origin results show that the origin tended to move upstream when affected by the applied sound, although at the Strouhal numbers corresponding to the largest widening rates, the trend is the opposite with slight downstream shifts. These results exhibit more scatter than the widening rates, but this is expected from geometric considerations. A widening rate change of 2% for a fixed half width at  $X/D = 20$  will result in roughly a 10% change in the geometric origin assuming typical conditions. The geometric origin results show very large scatter in the region of the intermittent fluctuations, and this may be attributed to this large sensitivity to small changes in the widening rate. The geometric origin results do however, like the widening rates, show their best repeatability in the range between 0.62 and 0.87. The changes in this region are relatively small, though. All of the geometric origins are negative, that is, the jet appeared to widen from zero width upstream of the nozzle mouth.

The velocity decay results also give origins upstream of the nozzle mouth. The velocity decay rate results are similar to the widening rate results in terms of regions

of scatter, of good repeatability, and of little apparent effect, but the results also differ in some ways. The decay rate plot shows many more cases of significant decreases in the decay rate than the widening rate plot shows of decreases in the widening rate. Also, except for one point at a Strouhal number of 0.33, the highest decay rate occurs at 0.79. The lowest decrease repeatably present in the decay rate occurs at a Strouhal number of 0.61. A relatively repeatable upstream shift in the velocity origin is also indicated at this Strouhal number.

As in the case of the geometric origins, the majority of the changes in the velocity origins appear to be in the upstream direction. However, as with the geometric origins, the largest decay rates appear to be accompanied by small downstream shifts in the origin. The magnitude range and the apparent scatter are larger for the velocity origin results than for the geometric origins, but like them, all the resulting values are negative.

Thus the frequency dependence results show that in the region from  $X/D = 20$  to  $X/D = 50$ , the appropriate frequency and sound pressure level can produce large changes in the parameters describing the mean flow behavior of the turbulent plane jet. The effects are tabulated in Table IV-18 in the summary at the end of the chapter. These results display a fairly large amount of scatter, but the trends are relatively clear. The scatter may be attributed to two sources.

The first source is the inaccuracies in the measurements. It is estimated that the mean pressure at the jet centerline was measured to an accuracy of roughly  $\pm 2\%$ . This error contributed to errors in measurements of the half widths by roughly the same amount through inaccurate positioning of the quarter pressure or one half velocity level on the pressure profiles. The half widths were measured to an accuracy of roughly 2.5%, so the total accuracy of the half width measurements was approximately 4.5%. The worst possible case of maximally inaccurate half widths arranged in order with errors of  $-4.5\%$  at  $X/D = 20$  and  $+4.5\%$  at  $X/D = 50$  would give a widening rate error of about 10%. A random distribution of the errors in the half width measurements would reduce this error considerably. The measurement results confirm the conservatism of this estimate, for the measurements of the no sound widening rates fall within  $\pm 4.5\%$  of their original value. All of the no sound velocity decay rates fall within  $\pm 6\%$  of the average except for one which is 8.5% higher than the average. The greater range of the decay rates may be based upon the fact that they were dependent upon the level of the pressure, and hence upon the absolute magnitude of the pressure transducer calibration, while the widening rates were dependent only on the linearity of the transducer response. The sensitivity of the origins to small changes in the two rates was discussed previously.

The second source of errors or scatter in the results was possible changes in the experimental apparatus. As the apparatus was periodically removed from the anechoic room and then returned, small changes in alignment occurred. The alignment of the traversing mechanism, the jet flow field confining walls, and the nozzle was very good, for they were bolted together. The alignment of the acoustic source and the flow field was a more likely source of errors in the cases of applied sound. The acoustic driver and horn assembly and the flow field were supported separately, and thus had to be realigned after each disassembly. It is estimated that the sound source had alignment errors of the following magnitudes. The center point of the exit plane of the horn was positioned to within  $\pm 3$  mm (0.125 in) in the three axes of the flow field. The angular misalignments possible were less than  $\pm 1^\circ$  in the X-Y and X-Z planes and less than  $\pm 2^\circ$  in the Y-Z plane. These misalignments, in combination with the directionality of the sound source may have resulted in two contributions to the error. The first of these is an error in the measurement of the sound pressure level at the controlling microphone; but this is estimated to be small, as the microphone was positioned nearly on the axis of the horn in a relatively flat region of the directivity curve. The second contribution to errors may have stemmed from the misalignment's resulting in effectively different applied

sound pressure levels in the regions of the jet most sensitive to the effects of sound. It is believed that such an occurrence may have been a contributor to the scatter in the results. Other factors which could have made small contributions to the scatter are the inaccuracy of the pitot tube alignment with the mean flow direction, the inaccuracy of the longitudinal spacing between the two pitot tubes, and the inaccuracy of the longitudinal positioning of the pitot tube assembly.

An extensive list of other possible sources of small errors might be compiled, but it is believed that the most important ones have been presented. However, the accumulated inaccuracies that the various sources appear to represent do not approach the levels of scatter in the results. The scatter in the results could well be attributed to the nature of the phenomenon. The jet was disturbed with relatively (compared to other works such as Thompson (1975)) low levels of sound, and the literature suggests that the effect of sound on jets is disturbance level dependent. Hussain and Zaman (1975) suggest that there are critical levels above which disturbance produces stable effects. It is speculated that the levels used in this study of the mean flow frequency dependence may have been below possible critical levels over parts of the frequency range studied, resulting in relatively large levels of scatter in the measured widening rates, decay rates,

and the geometric and velocity origins.

Despite the scatter, the frequency dependence results show that in the region from  $X/D = 20$  to  $X/D = 50$ , the appropriate frequency and sound pressure level can produce large changes in the parameters describing the development of the mean flow field of the turbulent plane jet.

The measurements of the frequency dependence of the jet widening and decay rates were undertaken for two reasons. The first reason was to compare the most sensitive Strouhal numbers obtained from measurements in this jet to those results in the literature for other disturbed jets. This is done in the next chapter. The measurements also were taken to enable a good choice of the frequencies to be used in the detailed study of the effects of the applied sound on the turbulent structure of the jet. Two frequencies were to be chosen, and the following criteria were used in the choice. The first criterion was that both frequencies used had to have significant effects upon the widening rate of the jet. The widening rate effect was chosen as the prime criterion, for the widening rate results were both the most dramatic and the most accurately measured of the frequency dependent parameters obtained. The second criterion was that the effects of the two frequencies be very repeatable. Thus the frequencies within the range of the large intermittent fluctuations were eliminated. A third criterion was that the frequencies be

widely separated and that one not be a harmonic of the other. This criterion was imposed in the interest of gaining a broader knowledge from the limited amount of data to be taken, for it seemed possible that harmonic frequencies could exhibit similar effects upon the turbulent structure. This criterion was of a precautionary nature, for the frequency dependence results did not exhibit a clearly harmonic nature. The last criterion considered was related to the convenience of measurement and comparison of results. This criterion was that the chosen frequencies be multiples of fifty Hz. The imposition of this criterion simplified the setting of filters in the acoustic system, and allowed simpler comparisons of the turbulent energy spectrum results which are presented in a later section.

The two frequencies chosen were 700 Hz and 1600 Hz, corresponding to Strouhal numbers of 0.30 and 0.69 respectively. The two frequencies met the first criterion by producing widening rates approximately 22% and 9% above the average no sound rates. The decay rates increased only slightly; approximately 2% at 700 Hz, and 1% at 1600 Hz. The second criterion was also well satisfied. Both frequencies corresponded to the most repeatable regions of the widening rate versus Strouhal number results. Another factor adding to the repeatability of the points chosen was that they appeared to be in relatively flat regions of the widening rate as a function of Strouhal number curve.

Using the points displayed in Figures IV-2 and IV-4 to take averages of the chosen points and the two points on each side of the points, the widening rate at 700 Hz is only 2.9% larger than the average of the five points, and the decay rate is 1.8% larger. The widening and decay rates at 1600 Hz are only 0.6% and 1.0% above the average for it and the four surrounding points. Thus slight changes in the sound frequency or velocity at the mouth of the jet resulting in small changes in the Strouhal number would not be expected to result in large changes in the effect upon the flow. That the other two criteria were met is self evident.

The results of detailed measurements of changes in the structure of the jet produced by the two frequencies are presented in the next section.

#### B. Measurements of Changes in the Turbulent Structure

The results presented in the preceding section give an indication of the magnitude of the effects of the applied sounds on the development of the mean velocity profiles of the jet in the region from  $X/D = 20$  to  $X/D = 50$ . The results also show the dependence of these effects upon the frequency of the sound. They do not, however, give indications of the form of the interaction between the sound and the jet flow. An experimental study of the changes in the turbulent structure of the disturbed jet was deemed necessary to uncover the interaction mechanism.

Measurements were performed at Reynolds numbers of approximately 6000 based on the nozzle slot width and exit velocity. The measured turbulent properties were the longitudinal and lateral turbulence intensities from  $X/D = 0$  to  $X/D = 80$  along the centerline, the energy spectra of these longitudinal intensities along the centerline from  $X/D = 0$  to  $X/D = 30$ , the longitudinal and lateral turbulence intensities transverse to the jet from  $Y/B = 0$  to  $Y/B = 2$  at  $X/D = 20, 40,$  and  $60$ , and the Reynolds stress  $\overline{uv}$  at the same transverse locations. In addition, mean flow measurements of the pressure profiles were carried out for  $X/D = 20$  to  $X/D = 170$ . The mean flow measurements are presented first.

#### 1. Jet Half Width Results

The frequency dependence results were based upon measurements of the pressure profiles between  $X/D = 20$  and  $X/D = 50$ , at the beginning of the similar region of the jet. To answer the question of whether the increased widening rates measured in this region continued downstream, pressure profiles were measured for each of the three cases from  $X/D = 20$  to  $X/D = 170$ . The resulting distributions of half widths are plotted in Figure IV-10. The widening rate is proportional to the slope of a line connecting the half widths, and it is apparent that particularly for the two cases of applied sound the slopes are not constant. The slopes appear to begin a decrease between  $X/D = 60$

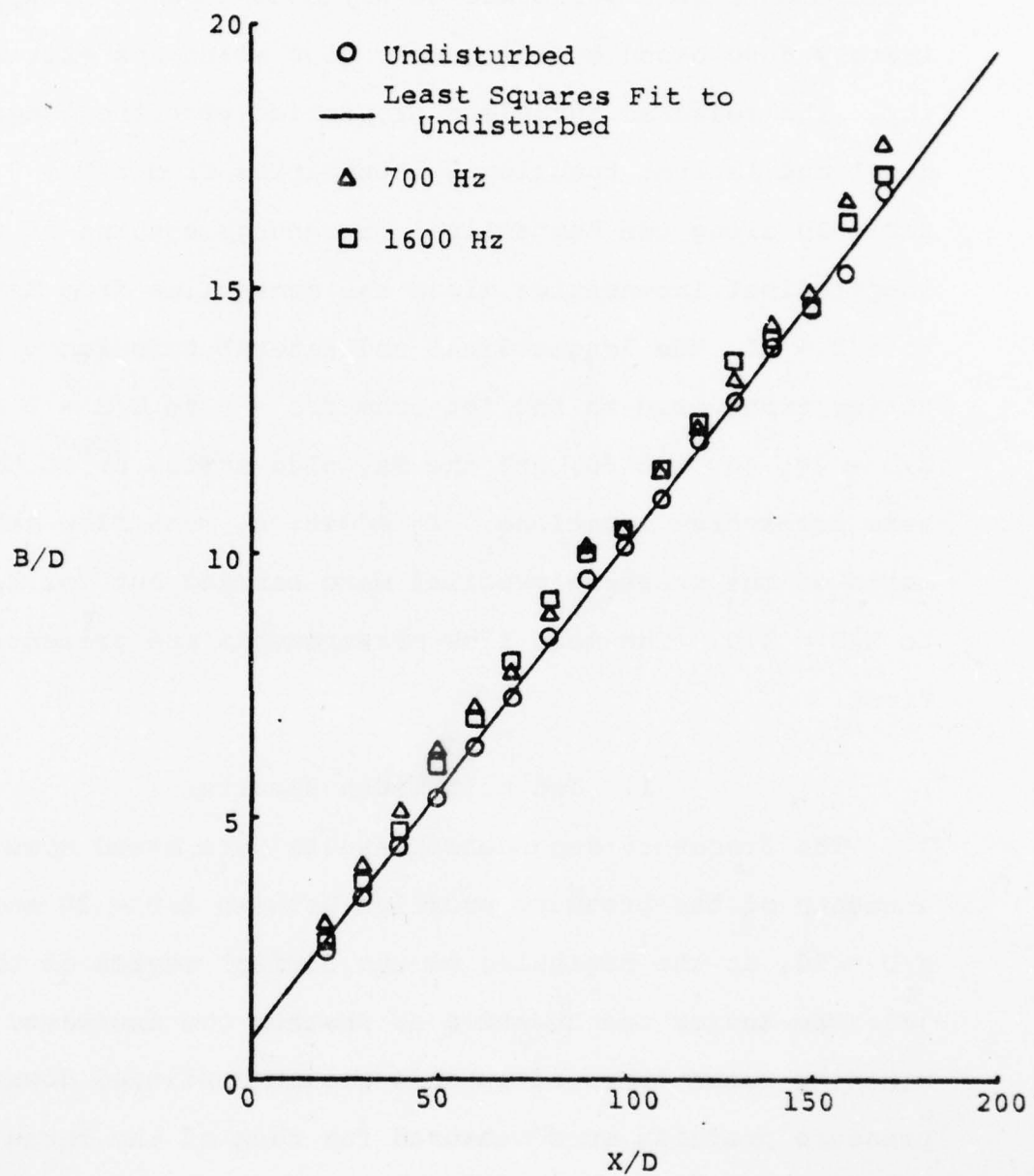


Figure IV-10 / Jet Half Width Growth With and Without Disturbance

and 80, tending towards slopes similar to that of the no sound case. The half widths beyond  $X/D = 120$  to 130 display a high degree of scatter which may be attributed to the extremely low mean velocities in this region. The accuracy of the data in this region does not justify a quantitative comparison of slopes. Qualitatively, the only conclusion that may be drawn is that for the two frequencies studied, the high initial widening rates appear to decrease to values approaching that of the undisturbed case at large distances from the nozzle, indicating that the effect of sound upon the widening rates may be confined to the region where  $X/D < 80$ . This result raises the question of whether the widening rate decreased only because that part of the flow showing the decrease was in a region of low sound pressure level downstream of the sound source. This question was answered by repeating the measurements of the 700 Hz case with the acoustic source and controlling microphone both moved 50  $X/D$  downstream. The sound pressure level at the microphone was 105 dB SPL re  $20 \mu\text{N}/\text{m}^2$  as in all the other measurements. The results of this measurement are presented in Figure IV-11 along with the results for the same frequency with the acoustic source in the normal position for comparison. The downstream location of the acoustic source does not appear to increase the widening rate in the downstream area. The half widths display the same behavior as for the case with the acoustic

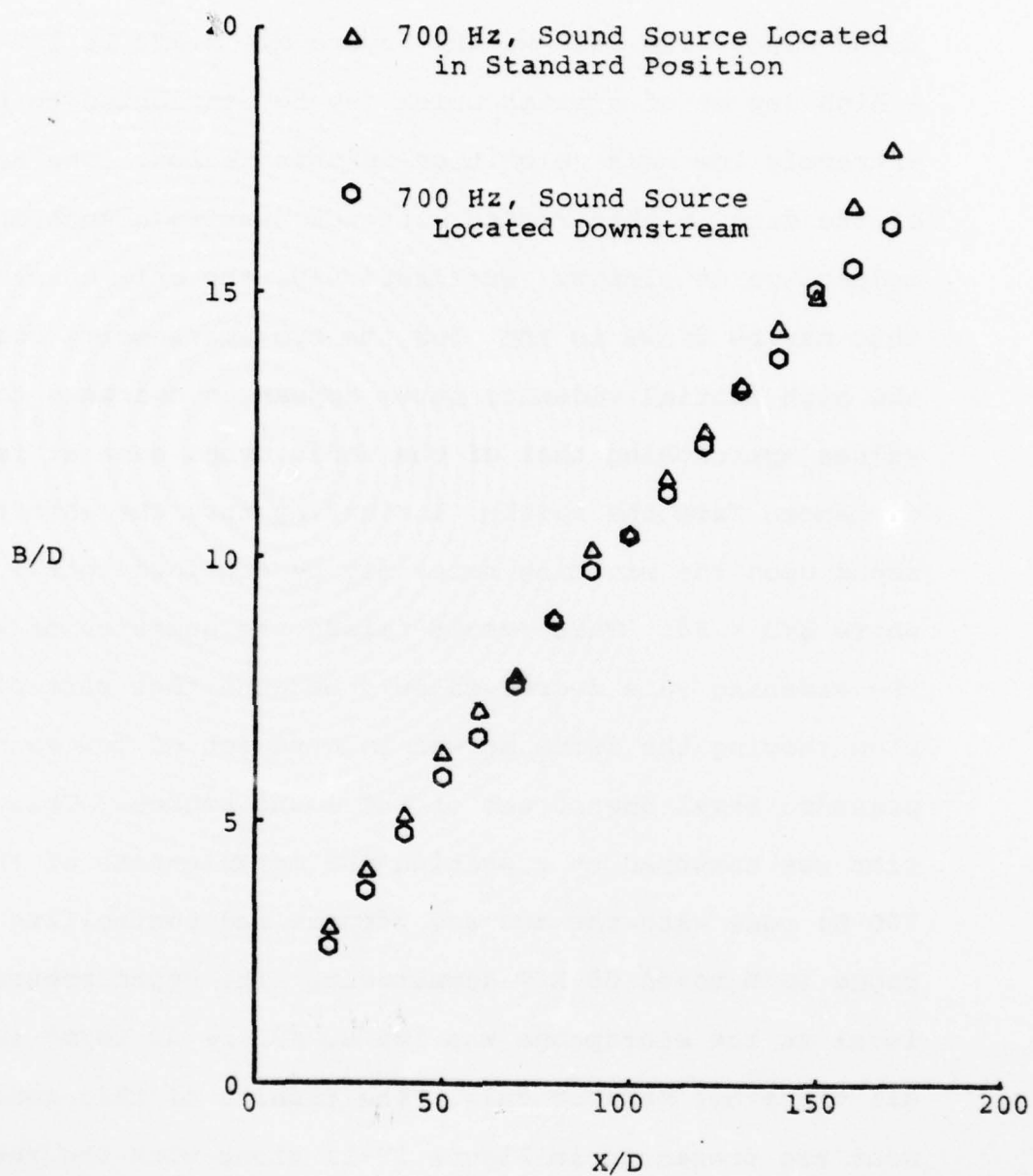


Figure IV-11 Comparison of 700 Hz Case Half Widths Resulting from Different Acoustic Driver Location

source in the normal position. The major difference is that the half widths for the downstream case are smaller than those for the normal case. The initial widening rates appear similar, but the plots seem to be displaced by a shift in the geometric origin in the downstream source case.

Thus, the half width measurements for large  $X/D$ 's indicate that the applied sound increases the jet widening rate in the region up to  $X/D = 80$ , and that beyond this point, the widening rates decrease, approaching that of the no sound case. A shift of the sound source downstream does not appear to change this behavior.

The same error analysis applies to these measurements as to the frequency dependence measurements, except that greater errors are present at the larger  $X/D$ 's because of the greater relative effect of drafts in the room. Alignment errors were not present in the measurements with the acoustic source in the normal position, and only acoustic source misalignments were present in the case with the source downstream, for the measurements were done in one session without disassembly of the apparatus.

The mean profile measurements thus indicate that the effect of sound is concentrated in the region inside  $X/D = 80$ . Measurements of the turbulent structure of the jet were carried out inside  $X/D = 80$  to reveal the details of the effect and the mechanism from which it results.

## 2. Turbulence Intensity Measurements along the Jet Centerline

The single parameter that by itself most fully describes the character of a turbulent flow is the turbulent intensity, the ratio of the rms of the turbulent velocity fluctuations to a characteristic mean velocity. The turbulence intensity and its distribution within a flow give indications of the growth and decay of the turbulence. The longitudinal turbulence intensity,  $u'/U_m$ , and the lateral turbulence intensity,  $v'/U_m$ , were measured along the jet centerline from  $X/D = 0$  to  $X/D = 80$ . The results of these measurements are presented in this section.

The longitudinal intensities presented were measured with a non-linearized straight wire, and the lateral intensities presented were measured with a linearized X-wire. Analog techniques were used for these measurements, the results of which are shown in Figures IV-12 and IV-13. The numerical results are given in Tables IV-9, IV-10 and IV-11. It may be seen that the sound produces large changes in the longitudinal turbulence intensity distribution along the jet centerline.

All three cases have approximately the same very low turbulence intensities at  $X/D = 0$  in the exit plane of the nozzle. The turbulence intensities at the mouth are all under 0.5%, indicating that the sound fields studied did

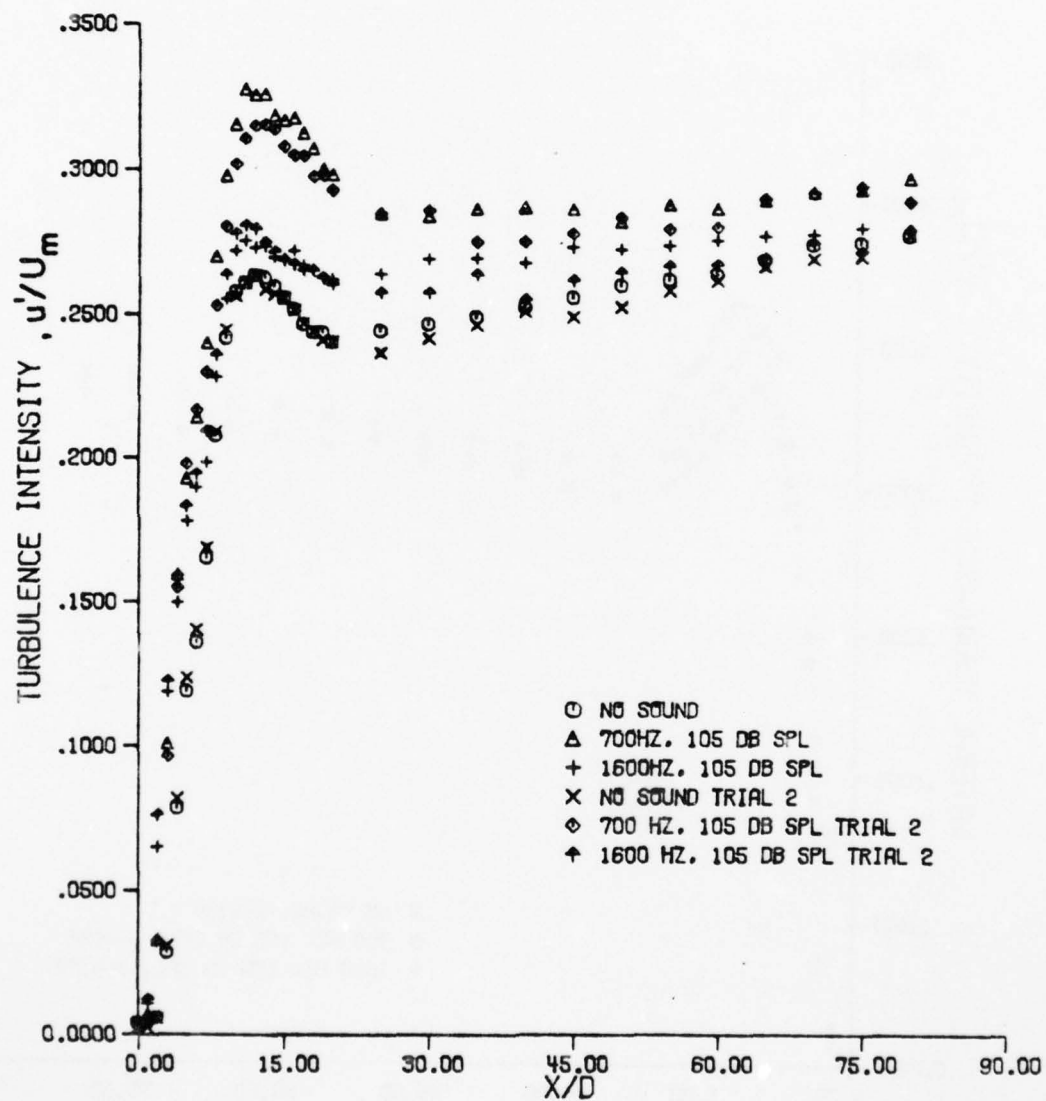


Figure IV-12 Distribution of Longitudinal Turbulence Intensity along the Jet Centerline

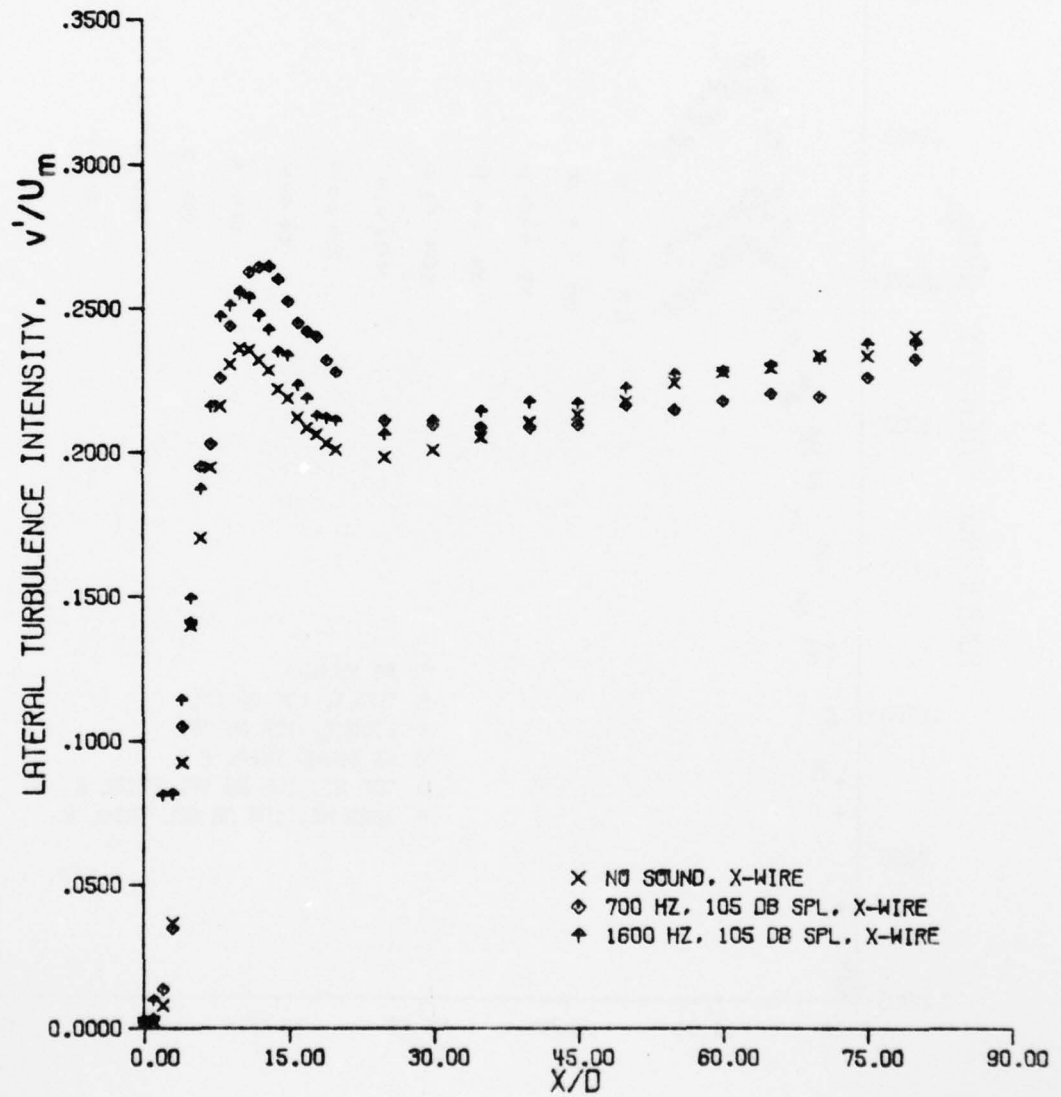


Figure IV-13 Distribution of Lateral Turbulence Intensity along the Jet Centerline

TABLE IV- 9  
 TURBULENCE INTENSITIES ALONG THE CENTERLINE  
 NO SOUND CASE

X/D	LONGITUDINAL INTENSITY TRIAL 1	LONGITUDINAL INTENSITY TRIAL 2	LATERAL INTENSITY
0.0	.0041	.0025	.0019
1.0	.0042	.0025	.0024
2.0	.0060	.0055	.0081
3.0	.0286	.0309	.0362
4.0	.0786	.0818	.0924
5.0	.1191	.1232	.1401
6.0	.1360	.1402	.1703
7.0	.1652	.1688	.1946
8.0	.2078	.2091	.2160
9.0	.2419	.2448	.2305
10.0	.2579	.2562	.2353
11.0	.2609	.2610	.2355
12.0	.2634	.2634	.2320
13.0	.2627	.2586	.2294
14.0	.2596	.2570	.2217
15.0	.2557	.2555	.2196
16.0	.2519	.2514	.2121
17.0	.2466	.2469	.2084
18.0	.2438	.2442	.2061
19.0	.2438	.2412	.2030
20.0	.2405	.2405	.2009
25.0	.2443	.2366	.1982
30.0	.2466	.2416	.2007
35.0	.2492	.2464	.2051
40.0	.2523	.2503	.2105
45.0	.2558	.2490	.2132
50.0	.2600	.2525	.2177
55.0	.2619	.2582	.2242
60.0	.2638	.2616	.2277
65.0	.2687	.2664	.2292
70.0	.2740	.2691	.2336
75.0	.2747	.2698	.2335
80.0	.2772	.2772	.2403

TABLE IV-10  
 TURBULENCE INTENSITIES ALONG THE CENTERLINE  
 700 HZ CASE

X/D	LONGITUDINAL INTENSITY TRIAL 1	LONGITUDINAL INTENSITY TRIAL 2	LATERAL INTENSITY
0.0	.0043	.0028	.0020
1.0	.0072	.0058	.0035
2.0	.0330	.0326	.0139
3.0	.1009	.0965	.0349
4.0	.1593	.1549	.1051
5.0	.1929	.1979	.1410
6.0	.2141	.2166	.1950
7.0	.2401	.2297	.2029
8.0	.2699	.2530	.2257
9.0	.2979	.2803	.2439
10.0	.3154	.3018	.2559
11.0	.3276	.3107	.2627
12.0	.3256	.3148	.2645
13.0	.3258	.3154	.2647
14.0	.3185	.3136	.2601
15.0	.3168	.3078	.2523
16.0	.3176	.3049	.2448
17.0	.3124	.3047	.2418
18.0	.3072	.2974	.2401
19.0	.3002	.2978	.2319
20.0	.2981	.2929	.2277
25.0	.2950	.2846	.2110
30.0	.2840	.2857	.2093
35.0	.2865	.2751	.2086
40.0	.2869	.2750	.2085
45.0	.2862	.2778	.2095
50.0	.2822	.2834	.2165
55.0	.2879	.2734	.2149
60.0	.2866	.2801	.2177
65.0	.2894	.2899	.2204
70.0	.2923	.2918	.2194
75.0	.2933	.2942	.2261
80.0	.2971	.2890	.2325

TABLE IV-11  
 TURBULENCE INTENSITIES ALONG THE CENTERLINE  
 1600 HZ CASE

X/D	LONGITUDINAL INTENSITY TRIAL 1	LONGITUDINAL INTENSITY TRIAL 2	LATERAL INTENSITY
0.0	.0043	.0029	.0028
1.0	.0108	.0123	.0100
2.0	.0651	.0760	.0812
3.0	.1189	.1225	.0817
4.0	.1497	.1591	.1142
5.0	.1781	.1831	.1496
6.0	.1898	.1945	.1871
7.0	.1984	.2093	.2159
8.0	.2283	.2357	.2471
9.0	.2554	.2636	.2510
10.0	.2720	.2779	.2551
11.0	.2755	.2808	.2537
12.0	.2731	.2795	.2476
13.0	.2736	.2747	.2425
14.0	.2696	.2715	.2349
15.0	.2691	.2686	.2335
16.0	.2719	.2671	.2232
17.0	.2669	.2650	.2186
18.0	.2654	.2649	.2126
19.0	.2628	.2626	.2118
20.0	.2620	.2602	.2108
25.0	.2639	.2574	.2061
30.0	.2690	.2572	.2110
35.0	.2693	.2636	.2144
40.0	.2675	.2549	.2175
45.0	.2732	.2615	.2171
50.0	.2723	.2642	.2223
55.0	.2738	.2664	.2272
60.0	.2757	.2671	.2282
65.0	.2770	.2692	.2304
70.0	.2778	.2747	.2327
75.0	.2798	.2716	.2378
80.0	.2888	.2792	.2376

not produce large changes in the flow within the nozzle. Measurements of the nozzle boundary layer and the velocity profile at  $X/D = 0.125$  confirm this result. These measurements are presented in Appendix A. Beyond  $X/D = 0$ , the two cases of applied sound exhibit faster turbulence intensity growth than the no sound case. Initially, the 1600 Hz case exhibits the greatest rate of increase, but between  $X/D = 3$  and  $5$ , the 700 Hz case passes the 1600 Hz case. The repeatability of this phenomenon is illustrated by the presentation of two sets of measurements in Figure IV-12. The two sets are labelled as "trial 1" and "trial 2" in the figure. The turbulence intensities in all cases continue to grow and reach peaks between  $X/D = 11$  and  $X/D = 13$ . The 1600 Hz case peak is less distinct, and it appears to occur slightly before the no sound and 700 Hz cases. The peak turbulence intensity is roughly 22% higher than the no sound case for the 700 Hz case and 5% for the 1600 Hz case. These percentages roughly correspond to the percentage increases in widening rates for the two cases. The 700 Hz case had an initial widening rate 22% above the no sound case, and the 1600 Hz case had an 8.9% increase. The implications of this similarity are discussed in the following chapter.

Beyond the peaks, the turbulence intensities decrease to a minimum value between  $X/D = 20$  and  $X/D = 25$ . They then either generally tend to increase or remain nearly

AD-A071 261

PURDUE UNIV LAFAYETTE IND RAY W HERRICK LABS  
ACOUSTIC INTERACTION WITH A TURBULENT PLANE JET. (U)  
AUG 77 F W CHAMBERS, F WILLIAMS  
HL-77-31

F/6 20/4

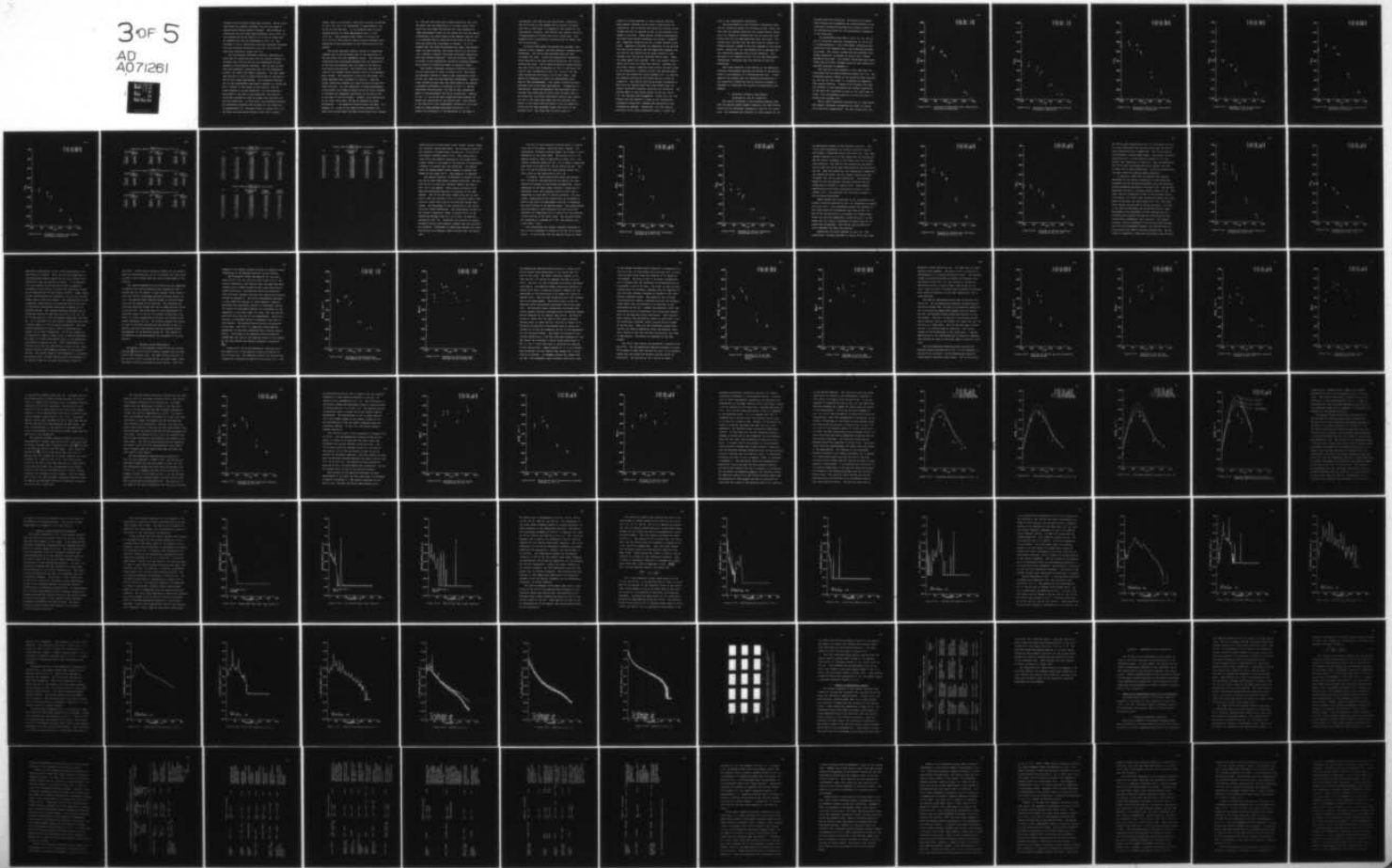
UNCLASSIFIED

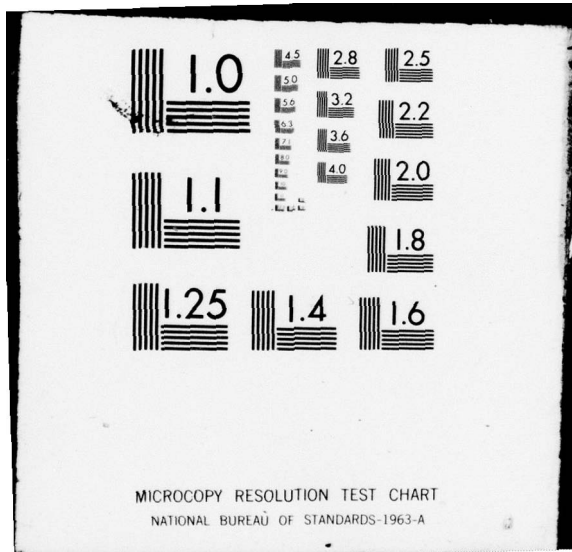
N00014-67-A-0226-0025

NL

3 of 5

AD  
A071261





constant with increasing downstream distance. The no sound case shows the greatest increase, with the two cases of applied sound showing lesser increases. The difference in intensities for the three cases decreases, and at  $X/D = 80$ , the intensities are all within 7.2% of the no sound case, as compared with the 22% difference at  $X/D = 12$ . The increase in the no sound case turbulence intensity indicates that the turbulent structure of the flow field did not reach self similarity inside  $X/D = 80$ .

The longitudinal turbulence intensity distributions along the jet centerline show that the changes produced in the mean flow field of the jet are accompanied by large changes in the turbulent structure. The two sets of data show good agreement, indicating that for the frequencies studied, the effect was highly repeatable. The most important source of errors in these results was the accuracy of the hot wire probe positioning. The transverse distribution of the longitudinal turbulence intensity in a plane jet has a "valley" in the center of the profile, with the local minimum on the jet centerline. If the probe were positioned to the side of the centerline, the measured turbulence intensities would be higher than the values on the true centerline. In this study, the difference between the centerline intensity and the peak off the centerline is approximately 8%. The peak occurs at roughly  $Y/B = 0.4$ , and hence the positioning accuracy could have a greater

effect closer to the nozzle, where the jet width is smaller. At  $X/D = 20$ ,  $Y/B = 0.4$  corresponds to approximately 6 mm (0.25 in) from the axis. It is estimated that the positioning accuracy in these measurements was  $\pm 1.5$  mm (0.05 in). This accuracy could result in an error at  $X/D = 20$  of no more than 2%, and at larger distances downstream the errors attributed to this source would be even smaller.

The second important source of errors in these measurements was in the technique used in the evaluation of the non-linear hot wire anemometer output. The turbulence intensities were calculated assuming that the sensitivity of the wire was constant over the range of the velocity fluctuations encountered. The sensitivity used was the slope of the voltage versus velocity curve at the measured mean voltage. The calibration curves are non-linear, and  $dU/dE$  increases with increases in velocity. Thus the actual sensitivity changes for large velocity fluctuations about the mean. For the conditions of these measurements, a fluctuation five times as large as the rms could increase or decrease the anemometer sensitivity by as much as 65% at the peak of the fluctuation. However, such fluctuations do not occur very often, and may be balanced by large fluctuations in the opposite direction about the mean. For example, an average of two sensitivities obtained from equal fluctuations about the mean giving sensitivity changes

of +65% and -47% would give a mean sensitivity less than 9% higher than the sensitivity at the mean signal level. Since the very large fluctuations are less probable for these measurements along the jet centerline than the smaller fluctuations, the error would be much smaller than 9%, and it is believed that it would be of the order of the error from the positioning inaccuracy or smaller. If it is assumed that the large fluctuations are evenly distributed about the mean velocity, the errors would be in one direction, leading to smaller calculated turbulence intensities than were actually measured. Thus the two major sources of errors in the longitudinal turbulence intensity measurements along the centerline result in opposite trends.

The lateral turbulence intensity distribution along the jet centerline is shown in Figure IV-13. The trends are basically similar to those of the longitudinal intensities, but there are some important differences. Similarities include the fact that the three cases do not exhibit noticeable differences in intensity at  $X/D = 0$ . Moving downstream from the mouth, the 1600 Hz case intensities begin to increase before the 700 Hz intensities. However, by  $X/D = 5$ , the 700 Hz case intensities have reached and passed the intensities of the 1600 Hz case. Also similar to the results for the longitudinal intensities, the three cases all reach maximum amplitudes around  $X/D = 11$ . However the difference in the magnitudes of the peaks is

considerably less than for the longitudinal intensities. The 700 Hz case is the highest and is roughly 13% higher than the no sound case, as compared to 22% higher for the longitudinal intensity. The 1600 Hz case lateral intensity is approximately 8% higher than the no sound case. This compares with a longitudinal intensity peak 5% higher than the no sound peak.

Following these peaks the intensities decrease, come somewhat closer together, and then gradually increase going downstream. The 700 Hz case decreases most and then increases the least. Unlike the longitudinal intensities, which remained in the same relative positions, the lateral intensities cross. The no sound intensities become greater than the 700 Hz case intensities at  $X/D = 45$  and equal the 1600 Hz case intensities at  $X/D = 55$ . At  $X/D = 80$ , the three intensities are within 3.3% of each other. This amount of difference is within the experimental error band of these measurements. The lateral intensities were obtained from X-wire probe measurements. A comparison of longitudinal intensities measured simultaneously using a straight wire probe and an X-wire probe was made, and it was found that the X-wire longitudinal results were generally 5% to 10% lower than those from the straight wire, except in the region near the mouth of the jet where the X-wire results were sometimes higher than those of the straight wire. The three sets of points shown in

Figure IV-13 were measured in three separate sessions. Each session included its own X-wire linearization and calibration, and it follows that there are relative errors between the sets of results as well as the absolute error common to all sets. These lateral intensity measurements were made using analog techniques and average u component and v component sensitivities for a Thermo Systems X-wire probe. Appendix D includes the comparison of the straight wire and X-wire results, and the comparison suggests that the 1600 Hz case results are 2% lower relative to the straight wire than the no sound and 700 Hz cases. These two cases appear well matched. Thus, the results shown in Figure IV-13 must be viewed with caution. Assuming that the X-wire lateral intensity errors follow the same trends as the longitudinal intensity errors, the absolute magnitudes of the results are likely somewhat low. In addition the relative position of the curves may be in error by roughly 2%. The results thus may be safely considered to show that the applied sound has large effects upon the lateral turbulence intensity along the jet centerline. The effects begin in the initial region of the jet, and at  $X/D = 80$  they may have disappeared. Within  $X/D = 25$ , the effects are very similar to those in the longitudinal turbulence intensities, although the magnitudes of the increases are smaller. Beyond  $X/D = 25$ , the relative positions of the three intensities change, a result not

seen in the longitudinal intensities.

The measurements of the turbulence intensities along the jet centerline reveal the following trends. They indicate that the applied sound has the largest effects within  $X/D = 25$ , tending to increase the rate at which the intensities grow and the peak magnitudes that they reach. The results also indicate that the sound does not produce the effects through a change in the flow upstream of the nozzle mouth. Beyond  $X/D = 25$ , the effects tend to decrease and the intensities approach the no sound intensity. This decrease is not complete at  $X/D = 80$  for the longitudinal intensities, indicating that the effects are felt far downstream.

The trends observed in the results of the centerline intensity measurements describe the effects of the applied sound in one dimension of a two-dimensional flow. A knowledge of the effects upon the transverse distribution of the turbulence intensities and the Reynolds stresses is necessary to understand the complete two-dimensional phenomenon.

### 3. Turbulence Intensity Measurements

#### Transverse to the Jet Centerline

The results presented in the preceding sections show that the applied sounds produce changes in the mean profile growth and the turbulence intensities along the jet centerline. The magnitude and character of these changes are not

uniform along the centerline. The question of whether these changes were accompanied by redistributions of the turbulence intensities and Reynolds stresses across the jet provided motivation for the measurements transverse to the centerline.

The measurements were made at  $X/D = 20, 40, \text{ and } 60$ , and at transverse locations corresponding to  $Y/B$ 's from 0 to approximately 2. The longitudinal intensities presented here were measured with a non-linearized straight wire probe. The lateral intensities were measured using analog techniques to process the signal from a Thermo Systems X-wire probe. The lateral intensities were calculated from the X-wire voltages using the four sensitivity equation developed in Appendix D.

The results of the preceding section show that the intensities did not reach similarity before  $X/D = 80$ . The transverse profiles scaled by the centerline mean velocity,  $U_m$ , and the jet half width,  $B$ , illustrate the departure from similar behavior. Figures IV-14 through IV-19 show the profiles of the longitudinal and lateral intensities at the three  $X/D$  locations for each of the three cases of sound. The corresponding numerical results are given in Tables IV-12 through IV-17.

The no sound transverse distributions of longitudinal and lateral turbulence intensities are shown in Figures IV-14 and IV-15 respectively. For both intensities, the

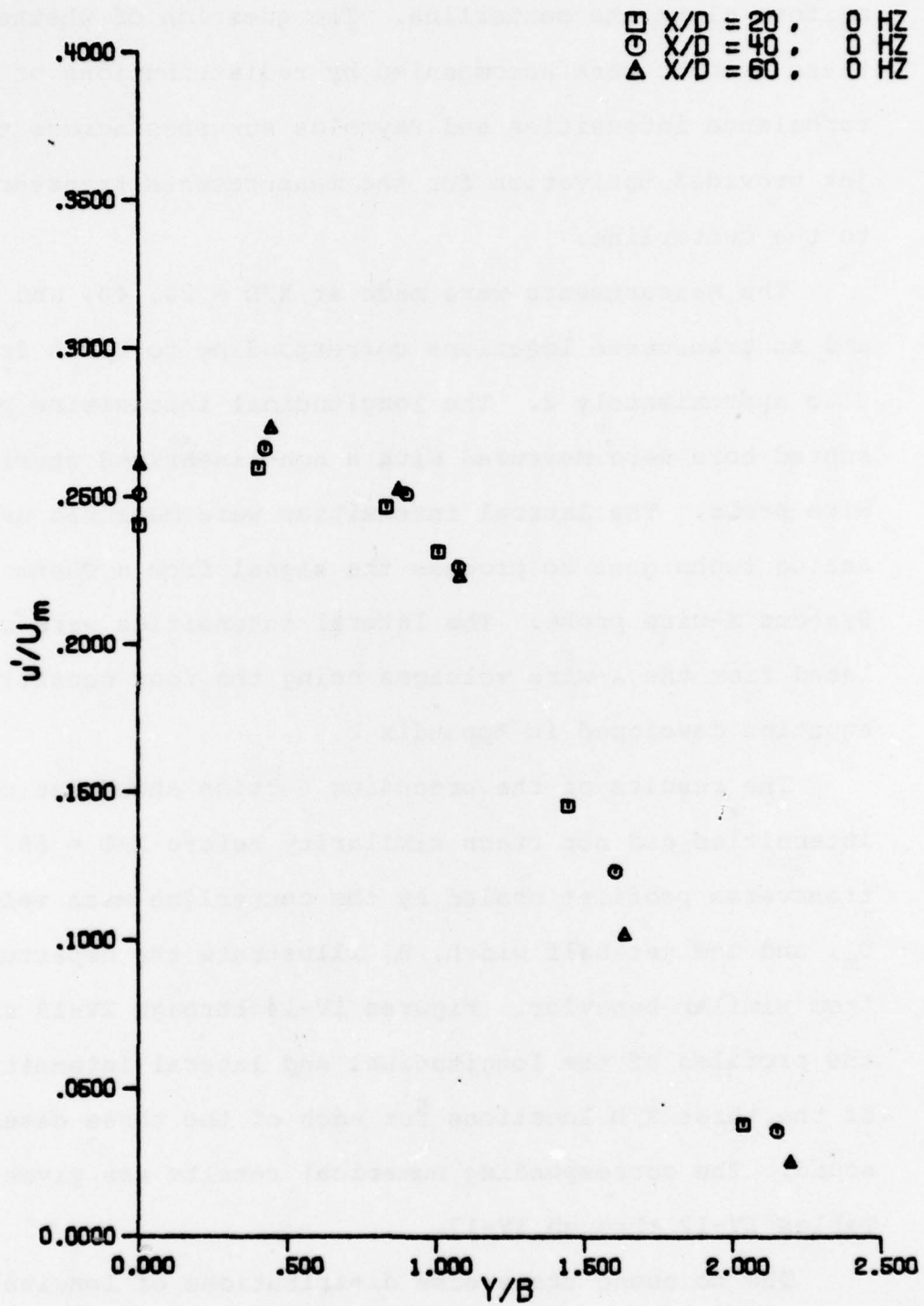


Figure IV-14 Profiles of Undisturbed Case Longitudinal Turbulence Intensities

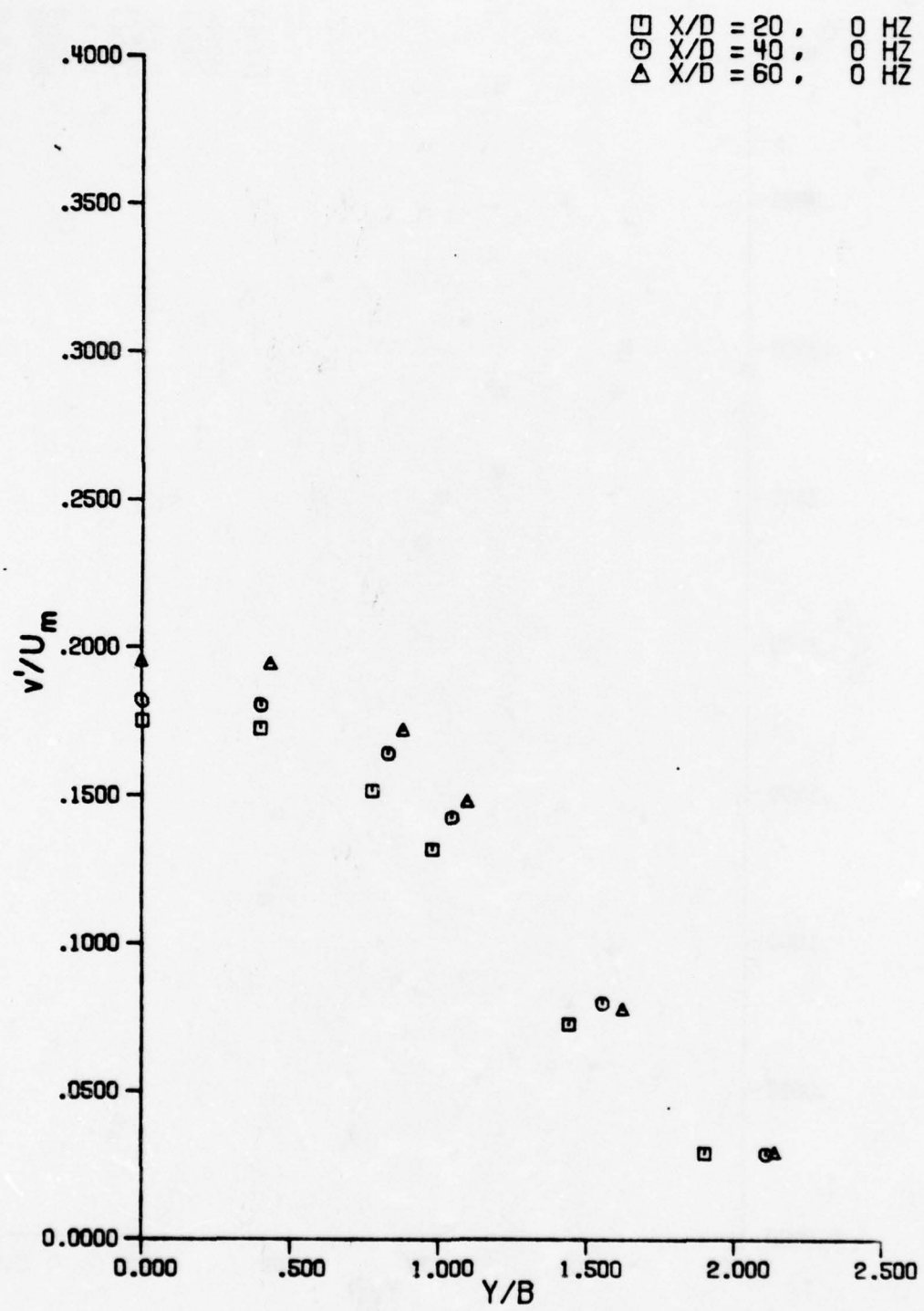


Figure IV-15 Profiles of Undisturbed Case Lateral Turbulence Intensities

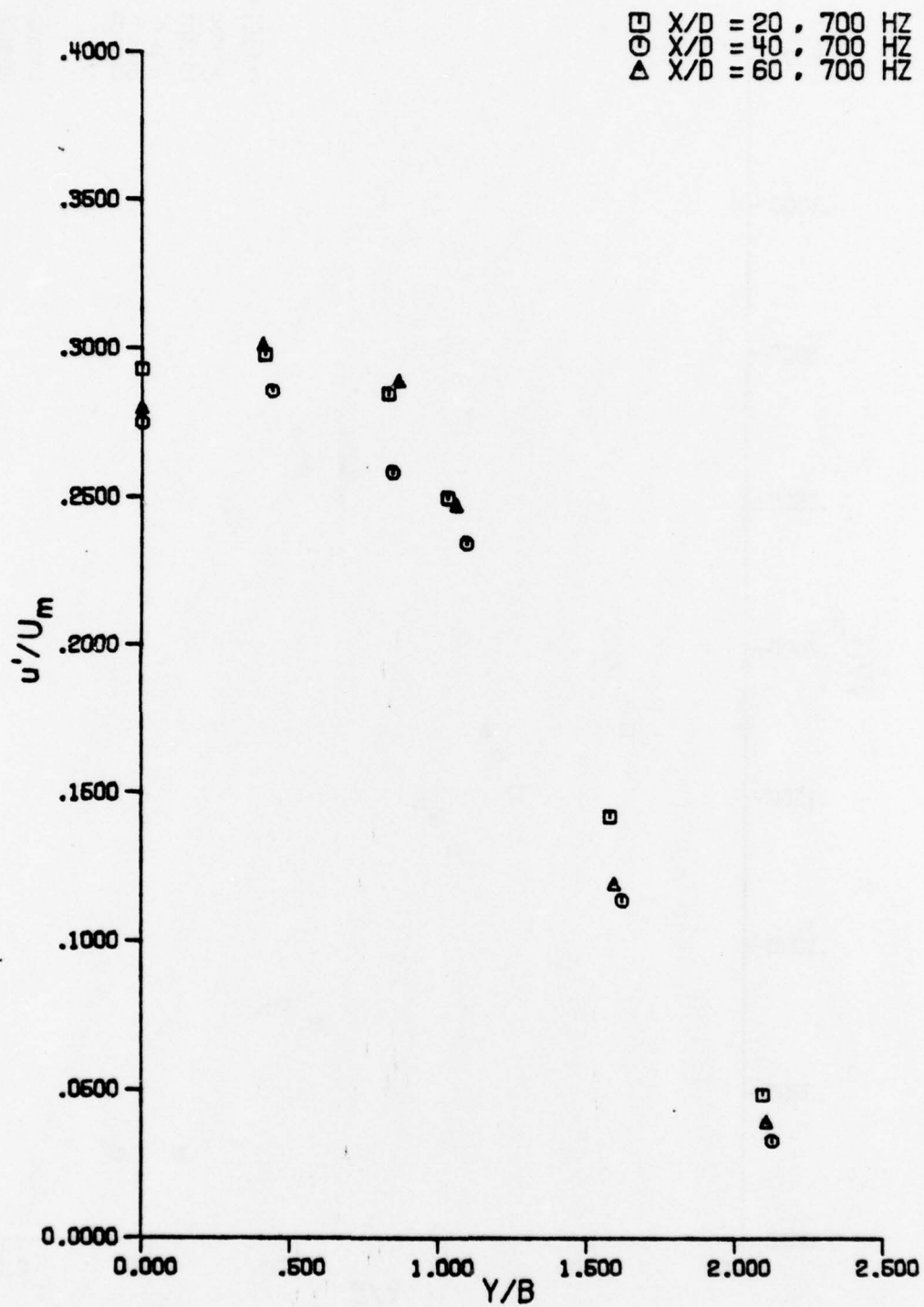


Figure IV-16 Profiles of 700 Hz Case Longitudinal Turbulence Intensities

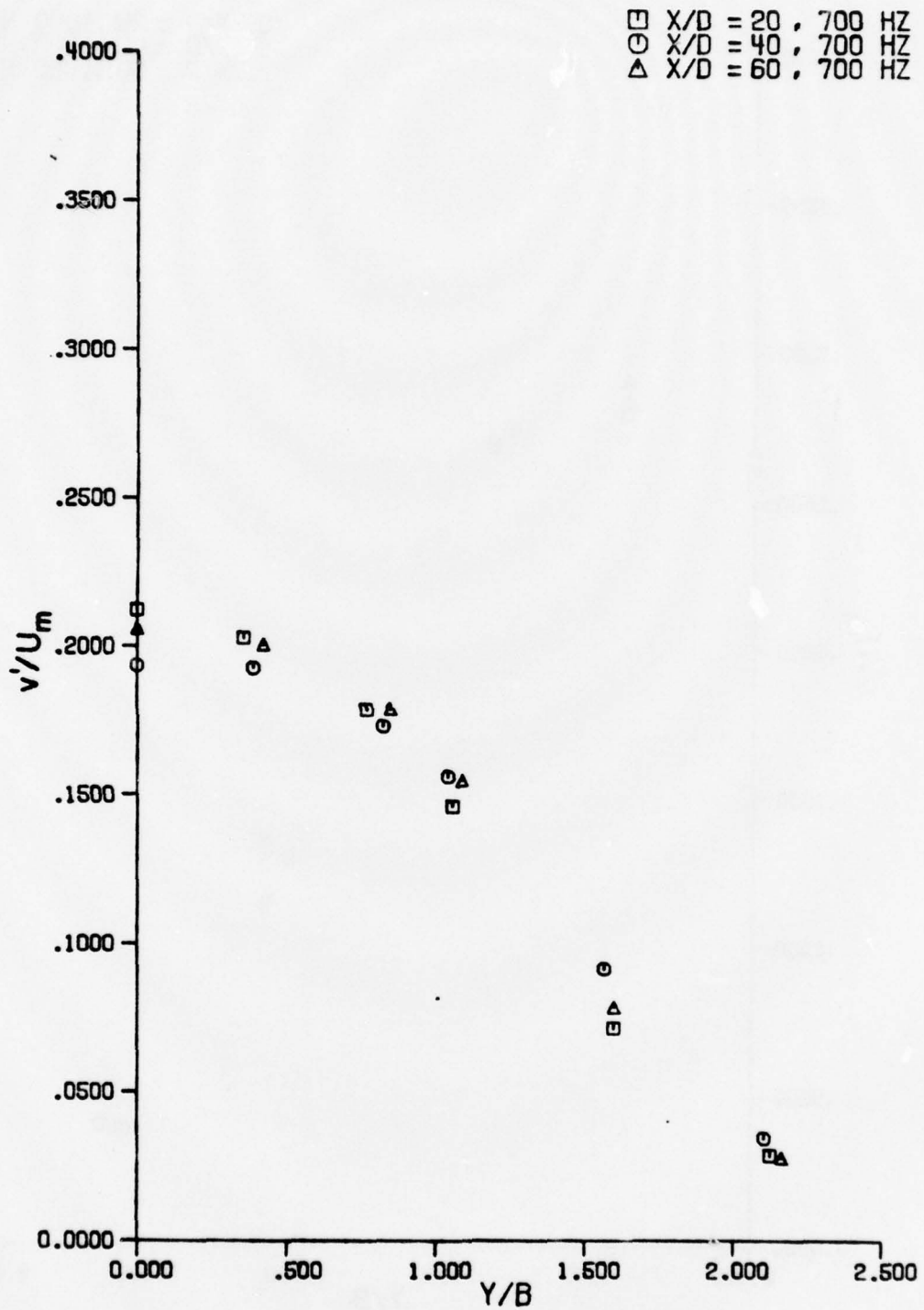


Figure IV-17 Profiles of 700 Hz Case Lateral Turbulence Intensities

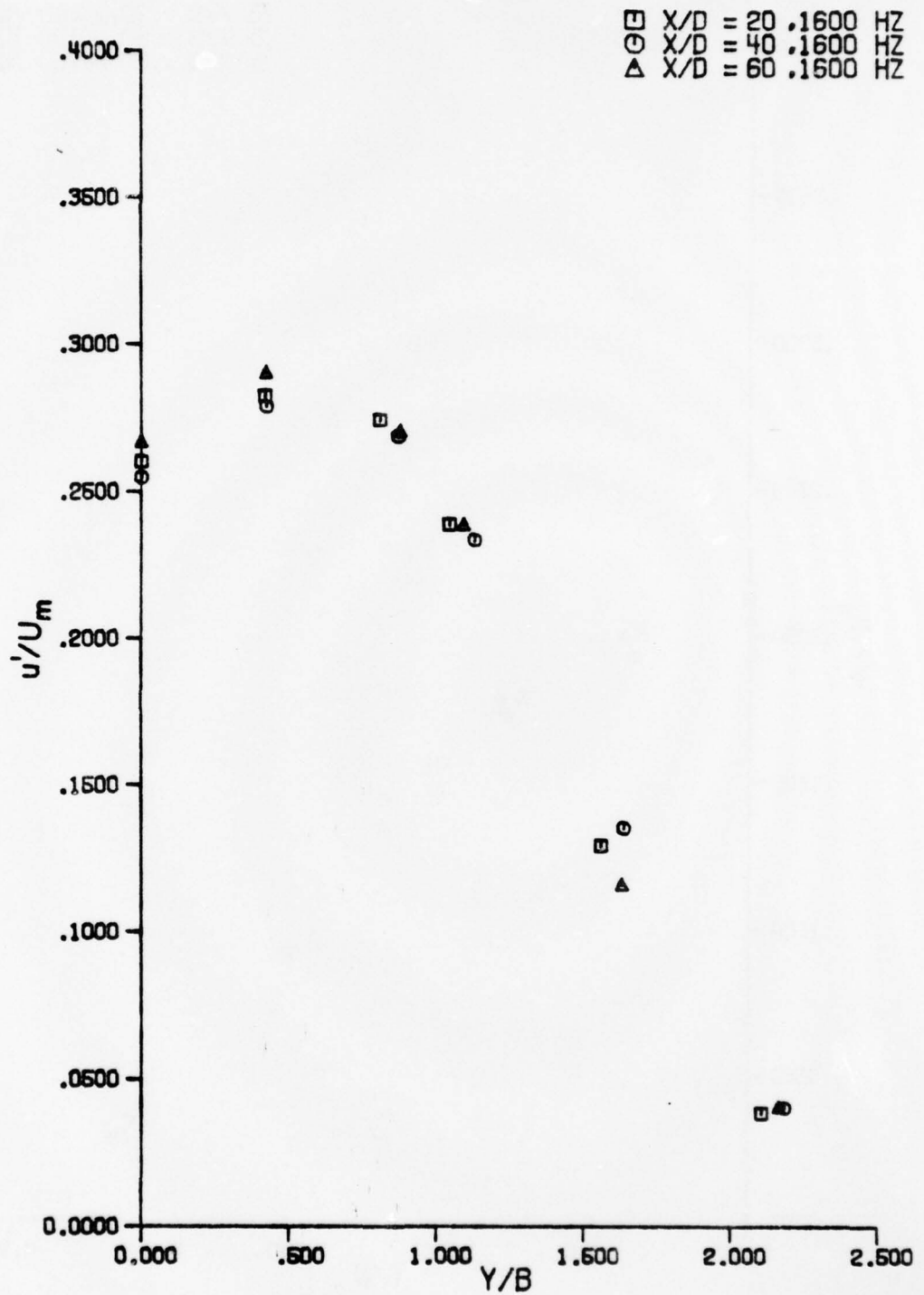


Figure IV-18 Profiles of 1600 Hz Case Longitudinal Turbulence Intensities

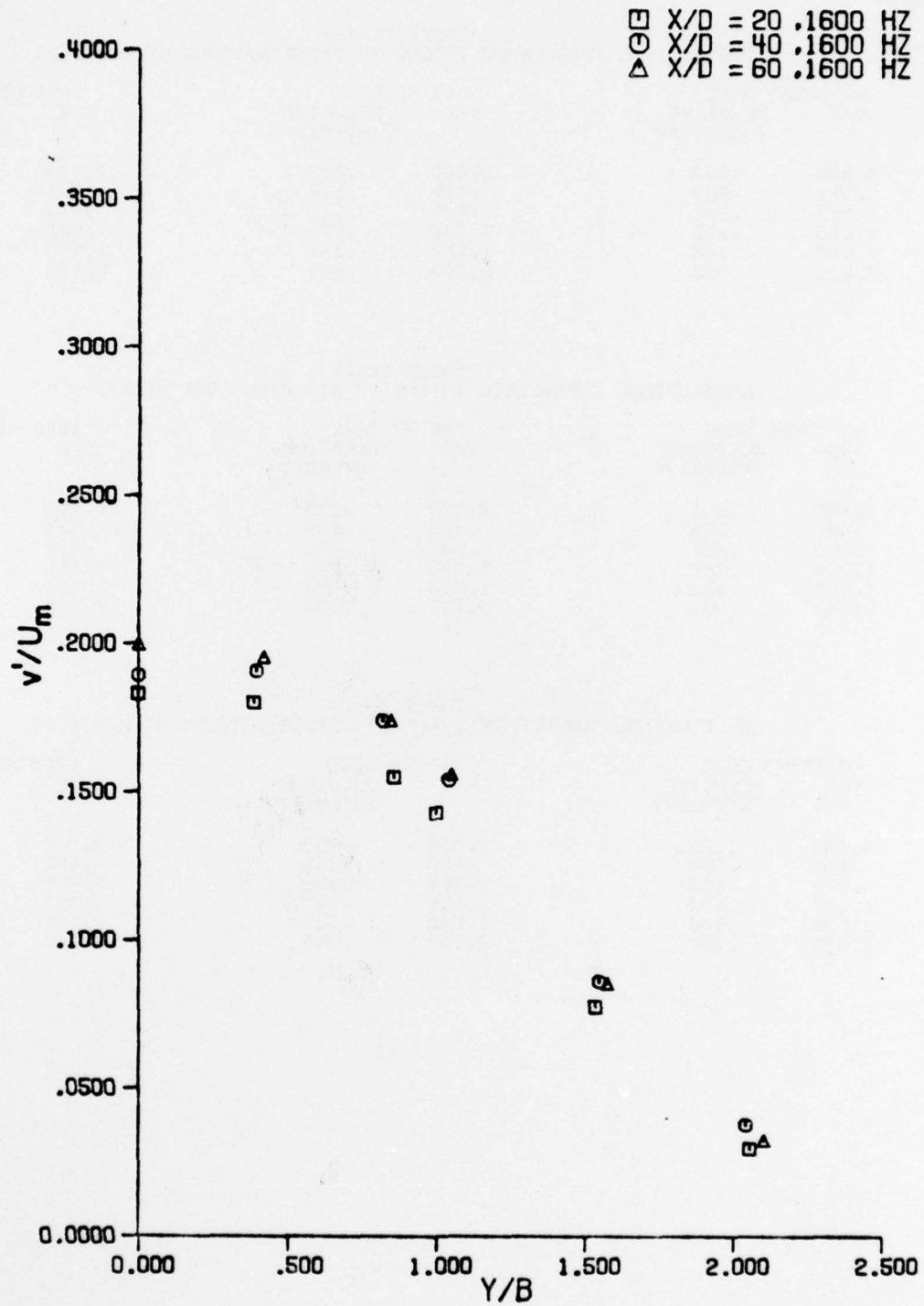


Figure IV-19 Profiles of 1600 Hz Case Lateral Turbulence Intensities

TABLE IV-12  
LONGITUDINAL TURBULENCE INTENSITY DISTRIBUTIONS AT X/D = 20

NO SOUND CASE		700 HZ CASE		1600 HZ CASE	
Y/B	RELATIVE INTENSITY	Y/B	RELATIVE INTENSITY	Y/B	RELATIVE INTENSITY
0.000	.240	0.000	.293	0.000	.260
.399	.260	.415	.298	.420	.282
.829	.247	.830	.285	.810	.274
1.006	.232	1.030	.250	1.045	.239
1.443	.145	1.577	.142	1.560	.129
2.035	.038	2.095	.049	2.105	.039

TABLE IV-13  
LONGITUDINAL TURBULENCE INTENSITY DISTRIBUTIONS AT X/D = 40

NO SOUND CASE		700 HZ CASE		1600 HZ CASE	
Y/B	RELATIVE INTENSITY	Y/B	RELATIVE INTENSITY	Y/B	RELATIVE INTENSITY
0.000	.251	0.000	.275	0.000	.255
.421	.266	.439	.286	.424	.279
.898	.251	.844	.258	.872	.269
1.074	.226	1.093	.235	1.131	.234
1.603	.123	1.618	.114	1.638	.135
2.148	.036	2.127	.033	2.184	.040

TABLE IV-14  
LONGITUDINAL TURBULENCE INTENSITY DISTRIBUTIONS AT X/D = 60

NO SOUND CASE		700 HZ CASE		1600 HZ CASE	
Y/B	RELATIVE INTENSITY	Y/B	RELATIVE INTENSITY	Y/B	RELATIVE INTENSITY
0.000	.262	0.000	.280	0.000	.267
.441	.274	.407	.301	.423	.291
.870	.253	.864	.289	.879	.271
1.077	.224	1.059	.247	1.095	.239
1.634	.102	1.592	.120	1.631	.116
2.193	.026	2.107	.040	2.165	.041

TABLE IV-15  
REYNOLDS STRESS AND LATERAL INTENSITY DISTRIBUTIONS  
NO SOUND CASE

X/D	Y/B	NON-DIMENSIONAL REYNOLDS STRESS	REYNOLDS STRESS CORRELATION	LATERAL RELATIVE INTENSITY
20.0	0.000	.00127	.0330	.1754
20.0	.399	.01526	.3606	.1727
20.0	.777	.01675	.4659	.1516
20.0	.990	.01255	.4391	.1319
20.0	1.442	.00390	.3784	.0728
20.0	1.904	.00023	.1148	.0294
40.0	0.000	-.00017	-.0042	.1620
40.0	.399	.01470	.3275	.1805
40.0	.830	.01765	.4369	.1642
40.0	1.046	.01442	.4471	.1425
40.0	1.555	.00396	.3293	.0798
40.0	2.111	.00090	.4454	.0291
60.0	0.000	-.00337	-.0724	.1956
60.0	.434	.01427	.2850	.1946
60.0	.890	.01690	.3823	.1724
60.0	1.098	.01379	.3999	.1482
60.0	1.622	.00361	.2962	.0781
60.0	2.140	.00070	.3086	.0299

TABLE IV-16  
REYNOLDS STRESS AND LATERAL INTENSITY DISTRIBUTIONS  
700 HZ CASE

X/D	Y/B	NON-DIMENSIONAL REYNOLDS STRESS	REYNOLDS STRESS CORRELATION	LATERAL RELATIVE INTENSITY
20.0	0.000	.00139	.0235	.2122
20.0	.356	.01613	.2787	.2028
20.0	.769	.02012	.4082	.1786
20.0	1.056	.01534	.4394	.1462
20.0	1.600	.00349	.3361	.0716
20.0	2.125	.00052	.2716	.0287
40.0	0.000	-.00371	-.0738	.1934
40.0	.390	.01525	.2972	.1927
40.0	.824	.01994	.4045	.1732
40.0	1.042	.01628	.4125	.1562
40.0	1.567	.00703	.4324	.0917
40.0	2.105	.00130	.4625	.0345
60.0	0.000	-.00319	-.0584	.2039
60.0	.423	.01516	.2727	.2009
60.0	.845	.01688	.3874	.1790
60.0	1.090	.01473	.3833	.1547
60.0	1.601	.00419	.3290	.0783
60.0	2.164	.00112	.5588	.0282

TABLE IV-17  
 REYNOLDS STRESS AND LATERAL INTENSITY DISTRIBUTIONS  
 1600 HZ CASE

X/D	Y/B	NON-DIMENSIONAL REYNOLDS STRESS	REYNOLDS STRESS CORRELATION	LATERAL RELATIVE INTENSITY
20.0	0.000	-.00073	-.0165	.1830
20.0	.389	.01241	.2631	.1801
20.0	.858	.01682	.4262	.1550
20.0	.999	.01304	.3837	.1428
20.0	1.535	.00355	.2989	.0775
20.0	2.058	.00078	.3821	.0298
40.0	0.000	-.00245	-.0536	.1892
40.0	.397	.01465	.2941	.1907
40.0	.819	.01859	.4099	.1740
40.0	1.041	.01630	.4366	.1538
40.0	1.549	.00498	.3487	.0860
40.0	2.043	.00163	.4897	.0378
60.0	0.000	-.00227	-.0466	.1998
60.0	.421	.01355	.2603	.1955
60.0	.846	.01658	.3662	.1742
60.0	1.053	.01408	.3693	.1561
60.0	1.577	.00453	.3177	.0855
60.0	2.105	.00113	.4142	.0326

three profiles in each figure reveal roughly similar shapes but different scaled magnitudes. The centerline longitudinal intensity increases about 9% from  $X/D = 20$  to 60 and the lateral intensity about 11.5%. The intensities at large  $Y/B$ 's also exhibit increases at the larger  $X/D$ 's. A small change in the shape of the profiles of longitudinal intensity is evident near the centerline. The typical plane jet saddle-shaped profile appears to become less humped at the larger  $X/D$ 's. This behavior is expected.

The opposite behavior is exhibited in Figure IV-16 by the 700 Hz case longitudinal intensity profiles. The profile at  $X/D = 20$  has the shallowest saddle, and that at  $X/D = 60$  is the deepest. This unusual increase of the hump with downstream distance is discussed in the next chapter. The 700 Hz case also differs from the no sound case in that the profile at  $X/D = 20$  exhibits larger intensities at large  $Y/B$ 's than do the profiles farther downstream. The magnitudes of the intensities on the centerline also reveal differences. The longitudinal as well as the lateral intensities (shown in Figure IV-17) on the centerline decrease from  $X/D = 20$  to  $X/D = 40$  and then increase to  $X/D = 60$ . Otherwise, the profiles of lateral intensity exhibit less dramatic changes than the longitudinal profiles. Differences in magnitudes between the three  $X/D$  profiles are generally smaller except near the centerline.

The 1600 Hz case intensity profiles shown in Figures IV-18 and IV-19 exhibit relatively small changes. The longitudinal intensity profiles appear the closest to self-similarity of the three cases. The profile at  $X/D = 20$  appears slightly lower in magnitude at large  $Y/B$ 's. The lateral intensity profile at  $X/D = 20$  is lower in magnitude than those at 40 and 60 all the way across the jet. The  $X/D = 40$  and 60 profiles are quite similar except for a lower value on the centerline at  $X/D = 40$ .

In general, these figures have shown that between  $X/D = 20$  and 60, the profiles are not similar for they exhibit differences in both shape and magnitude. Thus a comparison of the three cases involves a comparison of developing flows with changing profiles rather than a comparison of three sets of similar profiles. For this reason, comparisons of the three cases are performed at each of the three  $X/D$  measurement stations to determine the local effects of the applied sound. These measurements were performed at fixed distances from the nozzle and therefore the comparisons do not account for the different virtual origins of the three cases. The various origins are displaced by a maximum of 6  $X/D$ , and generally are within about 3  $X/D$ .

The longitudinal and lateral intensity profiles at  $X/D = 20$  are displayed in Figures IV-20 and IV-21 respectively. It may be seen that the applied sounds do result

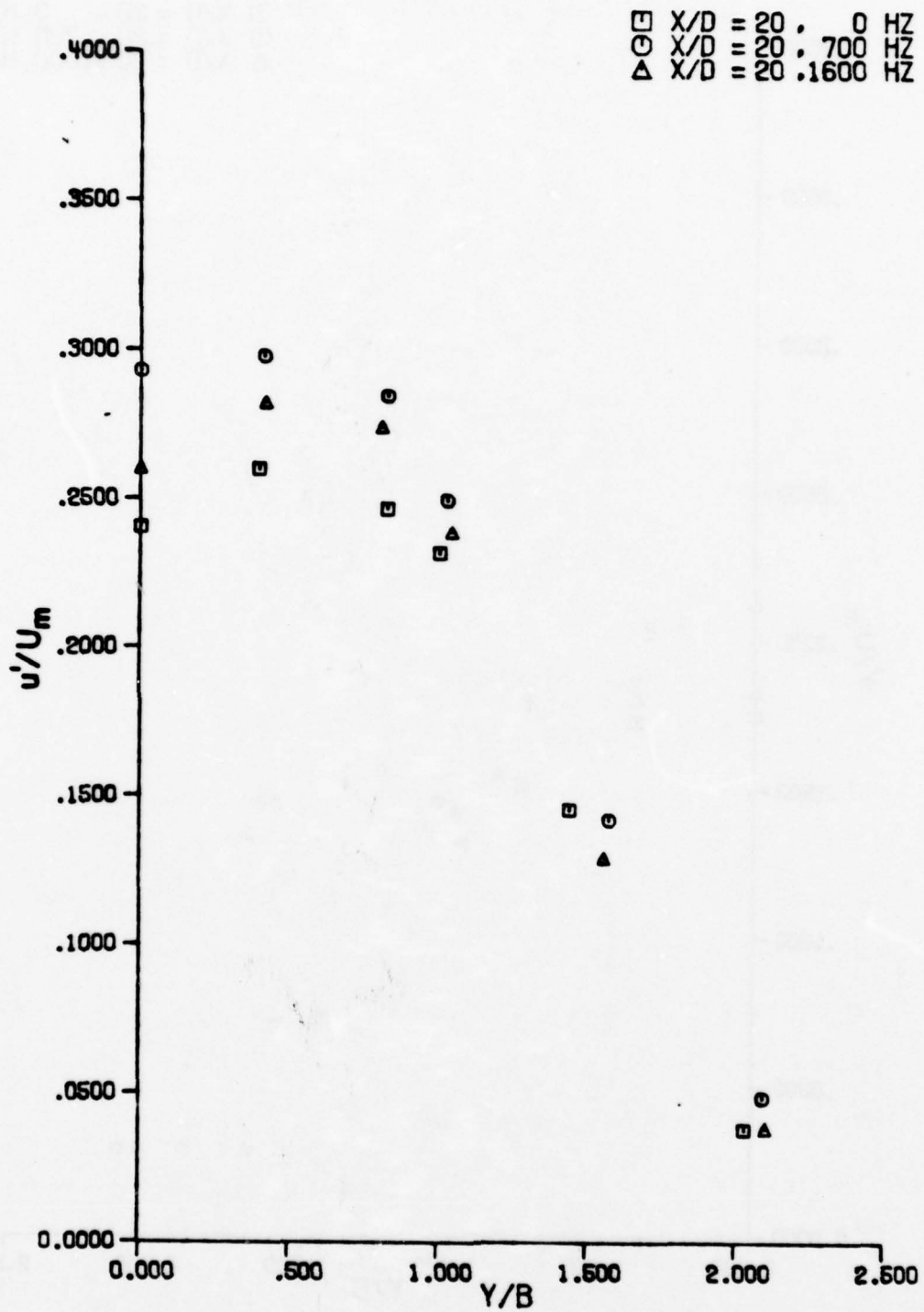


Figure IV-20 Profiles of Longitudinal Turbulence Intensities at  $X/D = 20$

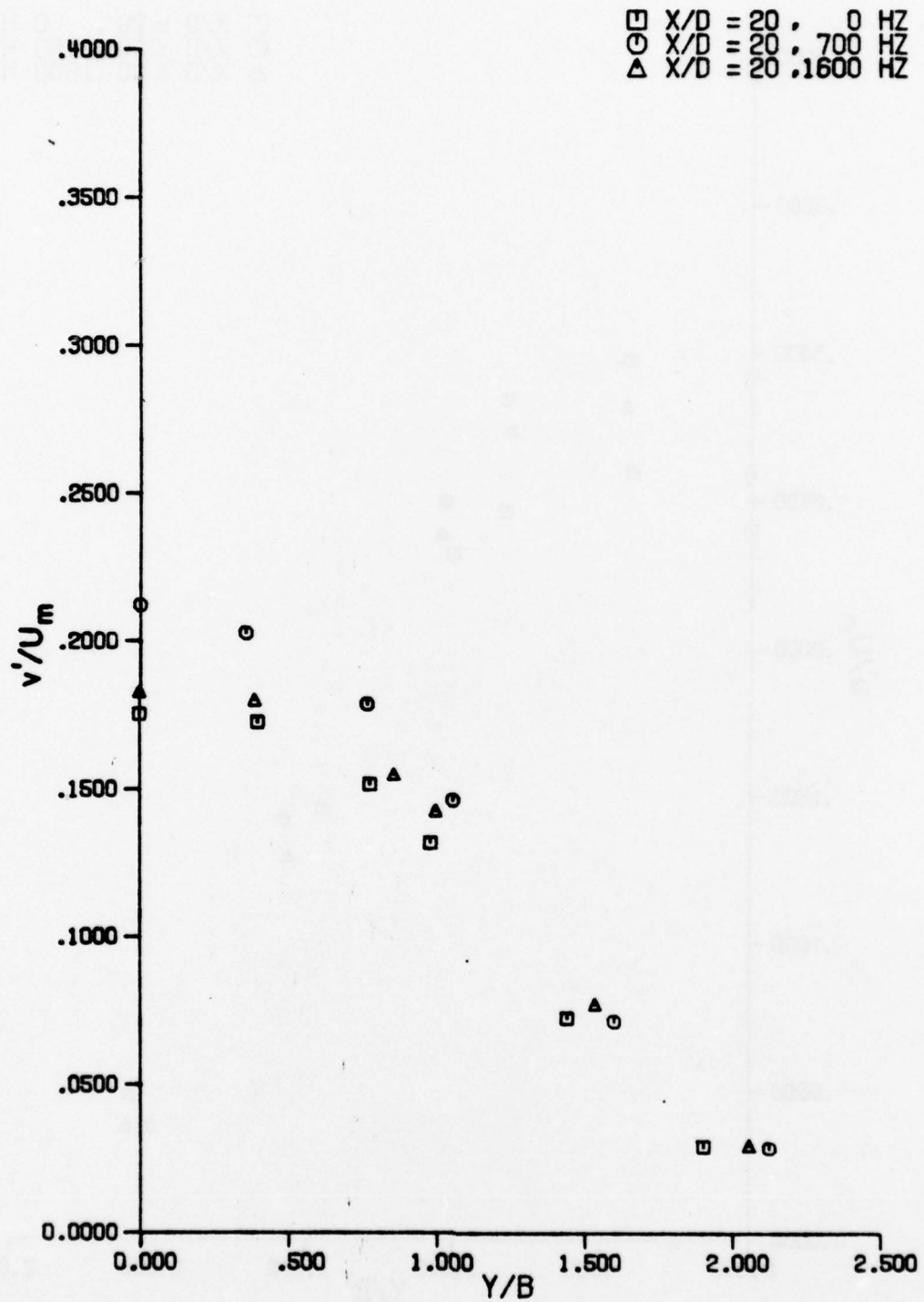


Figure IV-21 Profiles of Lateral Turbulence Intensities at X/D = 20

in significant changes in the intensity profiles. The 700 Hz case longitudinal and lateral intensity profiles are highest in magnitude across the entire jet. The longitudinal intensity is 15 to 22% higher near the centerline, and the lateral intensity is 21% higher than the no sound case intensity. The 1600 Hz case intensities are between the no sound and 700 Hz case intensities all the way across the jet. Near the centerline, the longitudinal intensities are roughly 8% higher, and the lateral intensities only 4% higher than the no sound intensities. The different shapes of the longitudinal intensity profiles near the centerline are evident in Figure IV-20. These saddle-shaped profiles have been discussed previously in this chapter, and it was observed that the shapes changed as the flow moved downstream.

These changes are illustrated in the longitudinal and lateral intensity profiles at  $X/D = 40$ , presented in Figures IV-22 and IV-23. The differences between the profiles of the three cases are considerably less than at  $X/D = 20$ . The 700 Hz case profiles still display the highest magnitudes, but now the longitudinal intensities are 7 to 10% higher and the lateral intensities 6% higher than the no sound case intensities. The 1600 Hz case profiles are still in between the other two profiles.

Differences are still apparent at  $X/D = 60$ . The longitudinal intensity profiles in Figure IV-24 still show

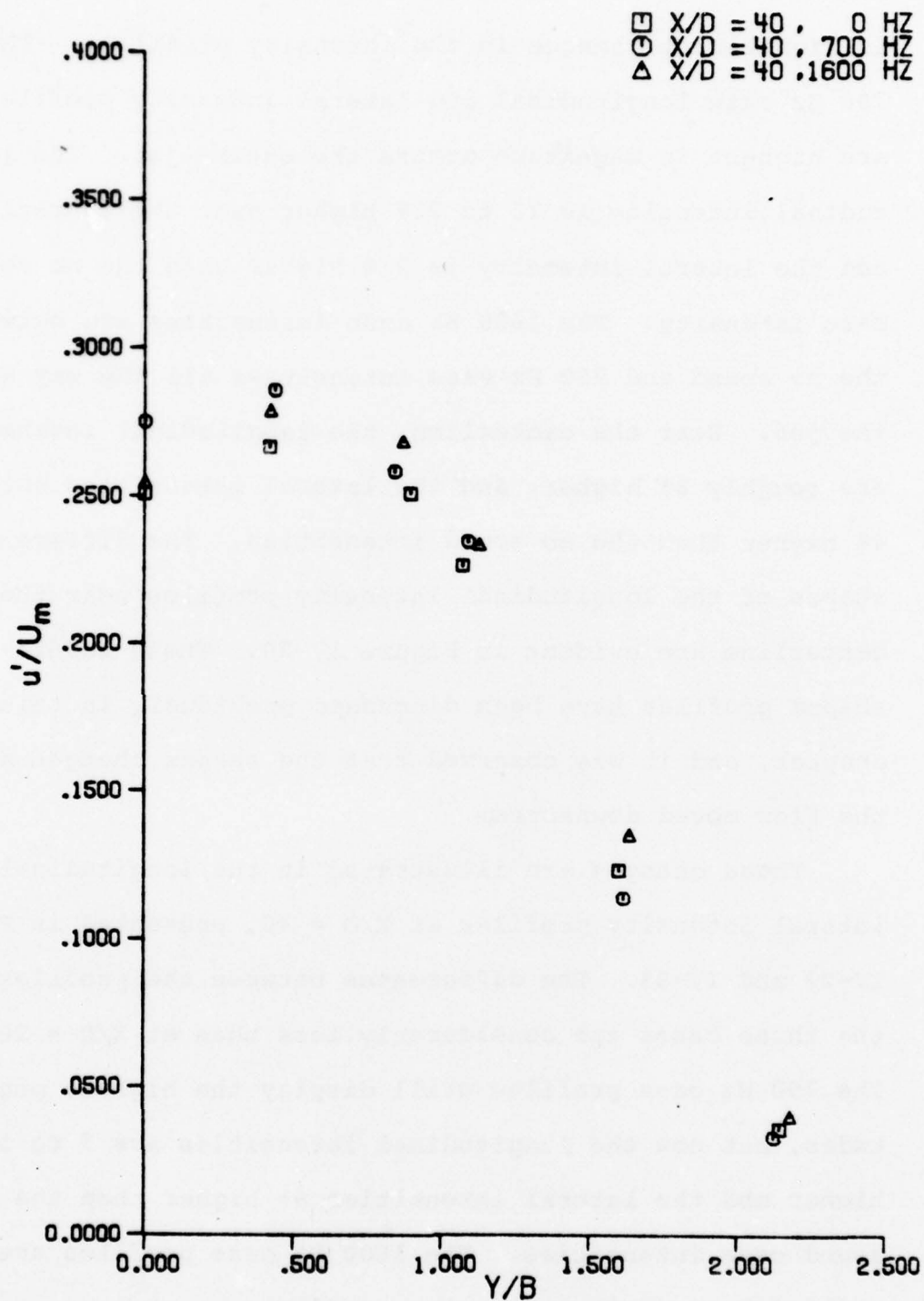


Figure IV-22 Profiles of Longitudinal Turbulence Intensities at X/D = 40

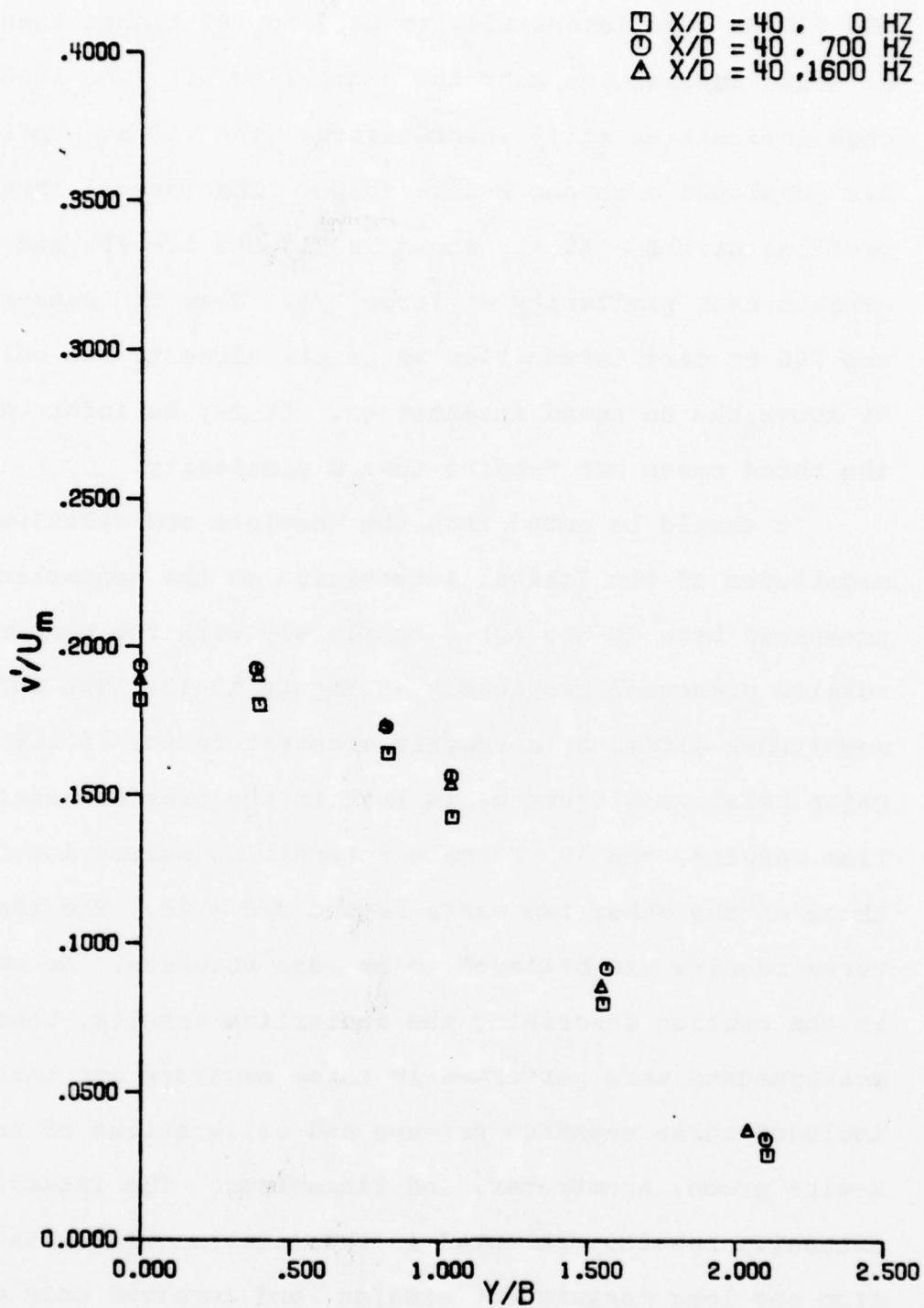


Figure IV-23 Profiles of Lateral Turbulence Intensities at X/D = 40

the 700 Hz case intensities to be 7 to 10% higher than the no sound intensities near the centerline with the 1600 Hz case intensities still intermediate. The 700 Hz profile has developed a strong saddle shape. The lateral intensity profiles at  $X/D = 60$  are shown in Figures IV- 25, and exhibit near similarity at large  $Y/B$ . Near the centerline, the 700 Hz case intensities are still highest, but only 5% above the no sound intensities. It may be inferred that the three cases are tending toward similarity.

It should be noted that the absolute and relative magnitudes of the lateral intensities on the centerline presented here do not agree completely with the centerline results presented previously in Figure IV-13. The absolute magnitudes differ by a roughly constant factor of 11%. The major relative difference is that in the previous centerline results, the 700 Hz case intensities became lower than those of the other two cases beyond  $X/D = 40$ . The transverse results are believed to be more accurate. As noted in the section describing the centerline results, those measurements were performed in three sessions and thus included three separate set-ups and calibrations of the X-wire probe, anemometer, and linearizer. The lateral intensity results presented in this section were obtained from one long measurement session and involved only one X-wire set-up and before and after calibrations. As discussed in Appendix D, there were relatively large absolute

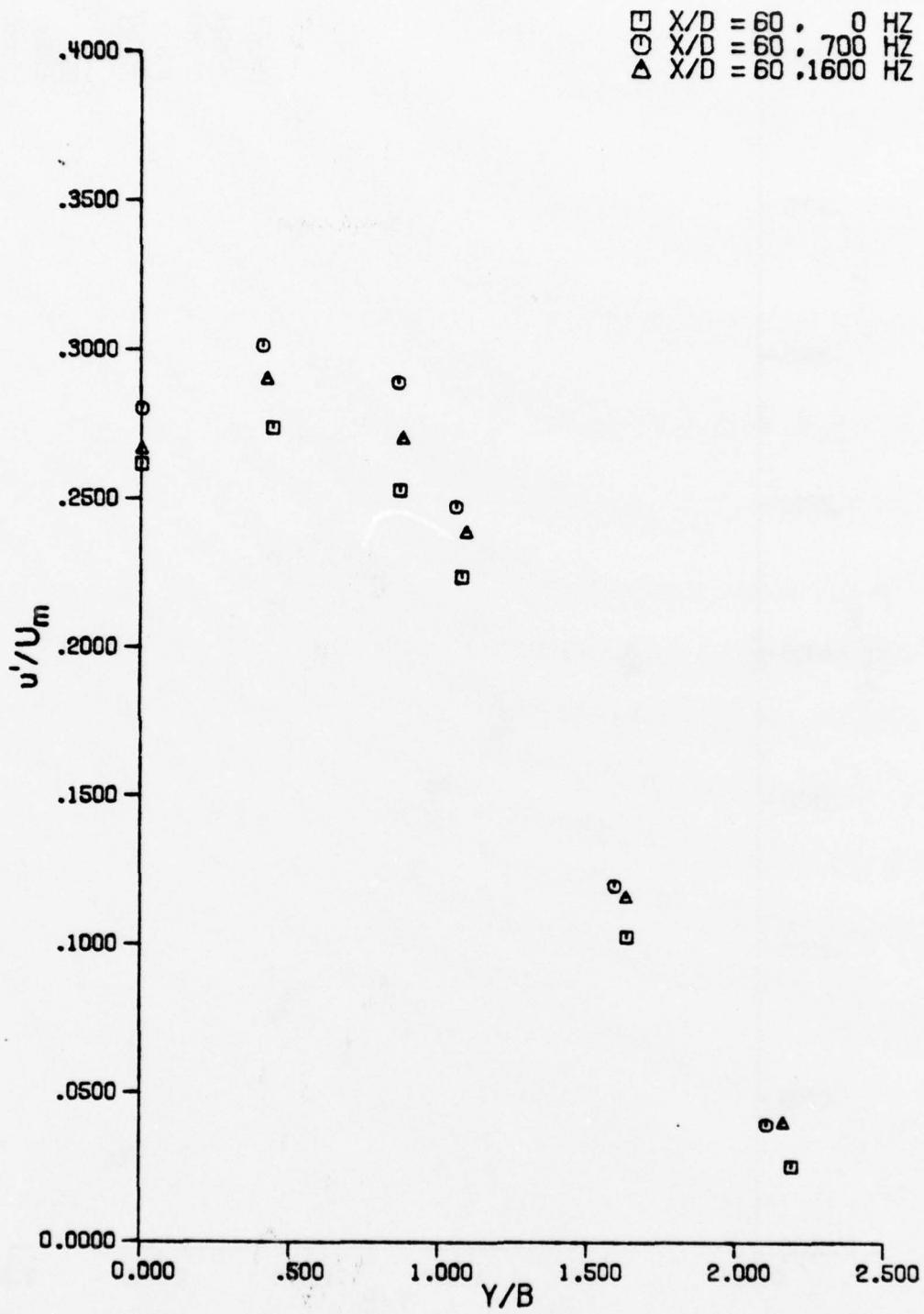


Figure IV-24 Profiles of Longitudinal Turbulence Intensities at X/D = 60

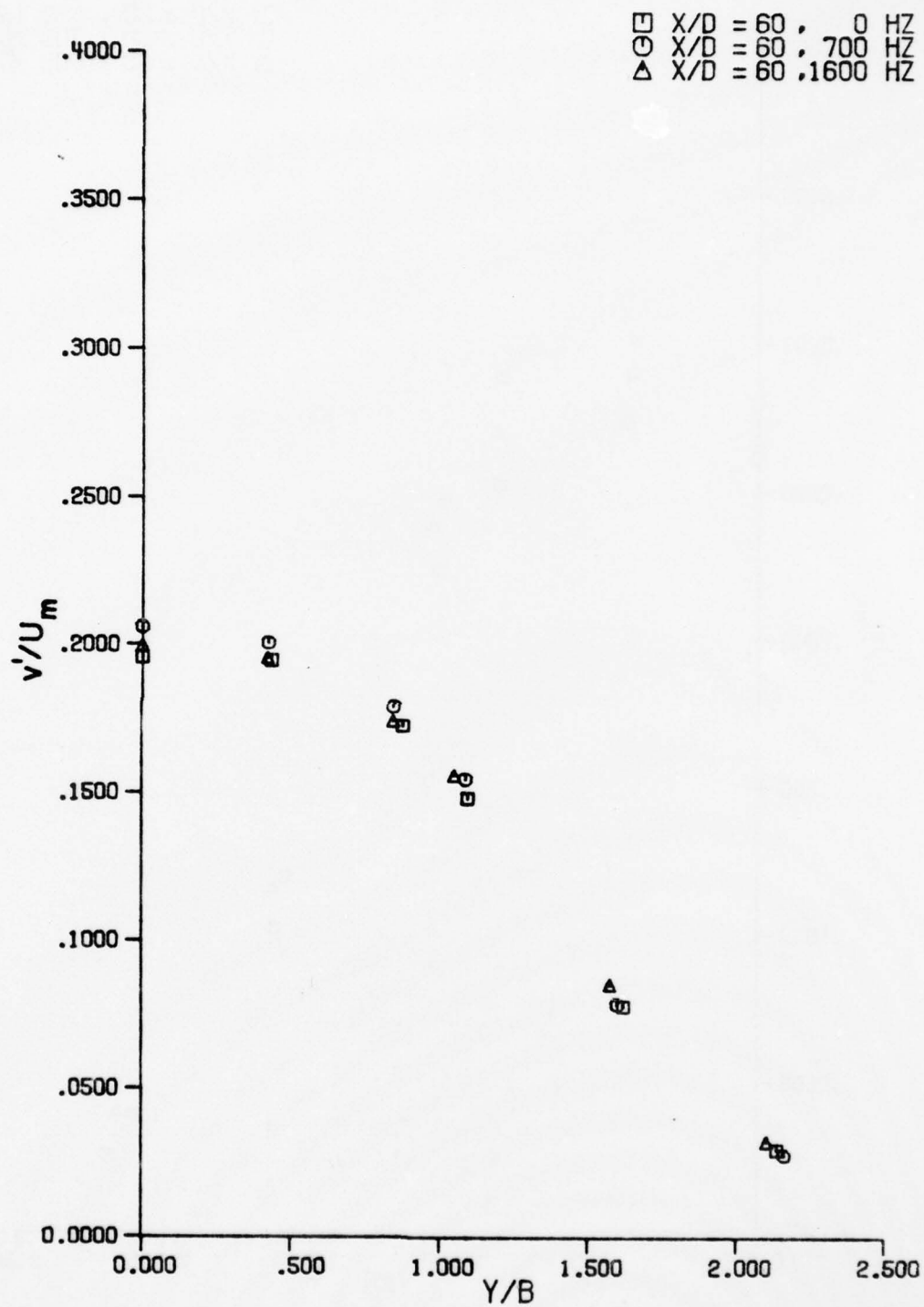


Figure IV-25 Profiles of Lateral Turbulence Intensities at X/D = 60

magnitude uncertainties in the X-wire measurements from one session to another. Thus, the relative magnitudes in one measurement session should be much more accurate than comparisons from one session to another. It is believed that the accuracy of the relative lateral intensities presented in this section is within the uncertainty caused by the repeatability of the acoustic effects. These repeatability uncertainties are estimated to be  $\pm 2\%$  for the half widths used to scale the results. The repeatability of the turbulence intensities may be estimated from the two sets of centerline longitudinal intensities presented in the previous section. The average difference between the two centerline results for each case at X/D's of 20, 40, and 60 is less than 2.5%, with the maximum difference less than 5%. It is estimated that the lateral intensities are within a similar band of  $\pm 2.5\%$  in relative magnitude. The term relative magnitude is used to refer to magnitude with respect to the other intensities. All of the intensities are believed to share a common error in absolute magnitude. The same  $\pm 2.5\%$  error band should apply to the transverse longitudinal intensity results. These measurements with straight wires have the same sources of error as the longitudinal intensity measurements presented in the previous section. The errors caused by the assumption of a constant sensitivity about the mean velocity point are believed to be somewhat larger at the more intermittent large Y/B

positions. Similar errors would be present for all measurements at these positions, and it is believed that they would not have a major effect upon the relative magnitudes of the results.

The results presented in this section may be summarized as showing that the two applied sound frequencies used to disturb the jet did result in large changes in the longitudinal and lateral turbulence intensity profiles across the jet. The applied sound produced changes in both the magnitudes and the shapes of the profiles. The disturbed profiles are generally higher than the no sound profiles across the entire jet. The sound does not just redistribute the turbulent energy in the jet with higher intensities in one region and lower intensities in another, but actually adds energy throughout the jet. The relation between the effects of sound on the mean profiles and the effects on the turbulence intensity distributions was also studied through measurements of the Reynolds stress,  $\overline{uv}$ . The results of the Reynolds stress measurements are presented in the next section.

#### 4. Reynolds Stress Measurements

The product of the Reynolds stress  $\overline{uv}$  and the velocity gradient  $\frac{\partial U}{\partial y}$  gives the rate of energy transfer from the mean flow to the turbulent flow. The mean velocity profiles of the jet were found to be similar for the three cases, hence the scaled velocity gradients are also similar. Thus the

changes in the energy transfer rate may be studied through comparisons of the measured Reynolds stress profiles.

The  $\overline{uv}$  Reynolds stress was measured for the three cases at  $X/D = 20, 40, \text{ and } 60$  at  $Y/B$ 's from 0 to 2. The results presented in this section were obtained from measurements with a Thermo Systems X-wire probe using analog signal processing. The Reynolds stress was calculated from the output voltages with the four sensitivity relation derived in Appendix D. The X-wire measurements performed in this study were subject to large changes in absolute magnitude from measurement session to measurement session. The results of individual sessions are acceptable for the comparison of the three cases (no sound, 700, and 1600 Hz), which was the prime goal of the measurements. The X-wire accuracy is discussed further in Appendix D and later in this section. The Reynolds stress results are presented in two ways. The first is a Reynolds stress made non-dimensional by the local centerline mean velocity squared,  $\overline{uv}/U_m^2$ . The second is the Reynolds stress correlation, formed from the ratio of the Reynolds stress to the product of the longitudinal and lateral turbulence intensities,  $\frac{\overline{uv}}{u'v'}$ .

Figure IV-26 is the non-dimensional Reynolds stress and Figure IV-27 is the Reynolds stress correlation for the no sound case. The numerical results for the Reynolds stresses are tabulated in Tables IV-15 through IV-17. The

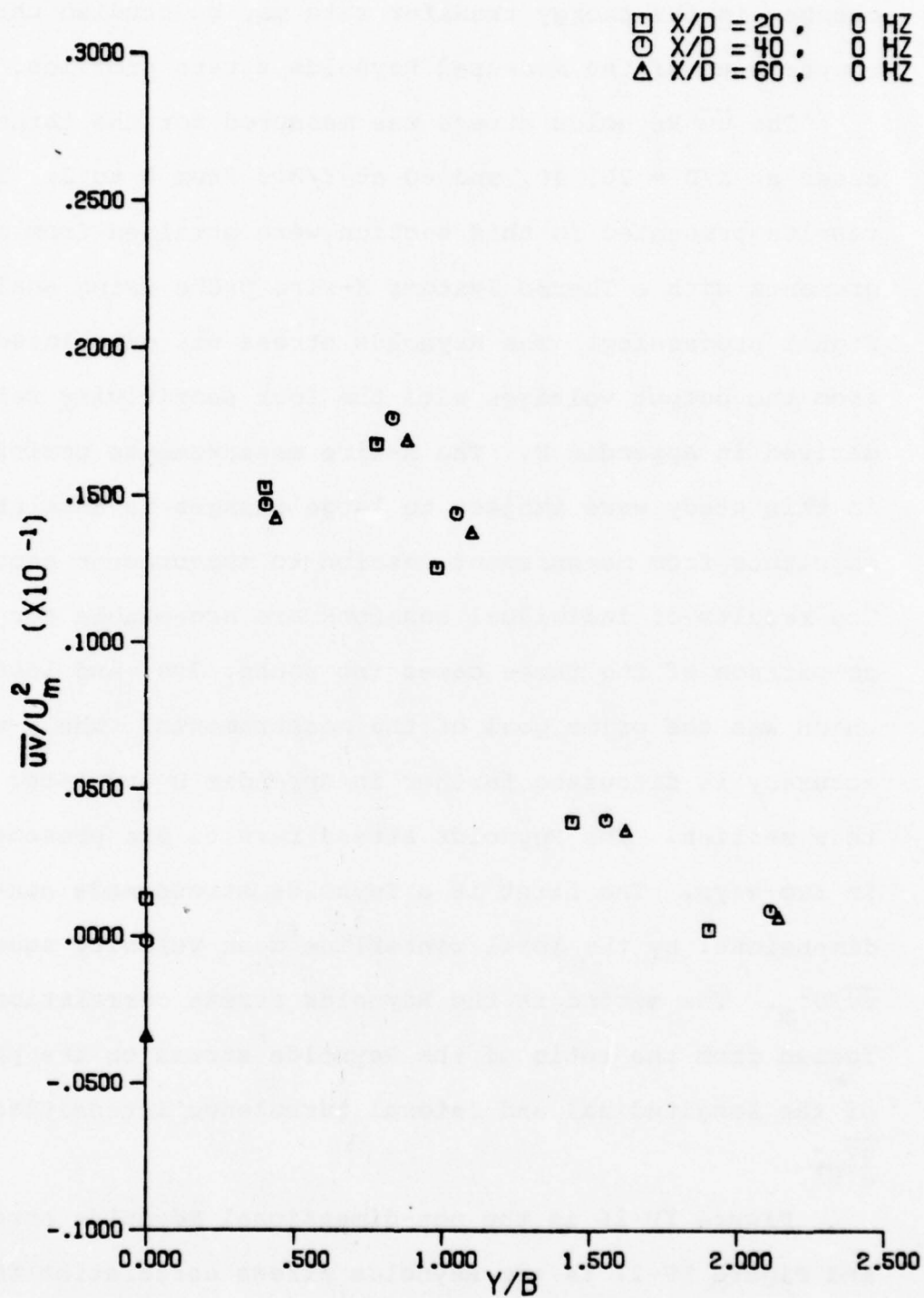


Figure IV-26 Profiles of Undisturbed Case  
Non-Dimensional Reynolds Stresses

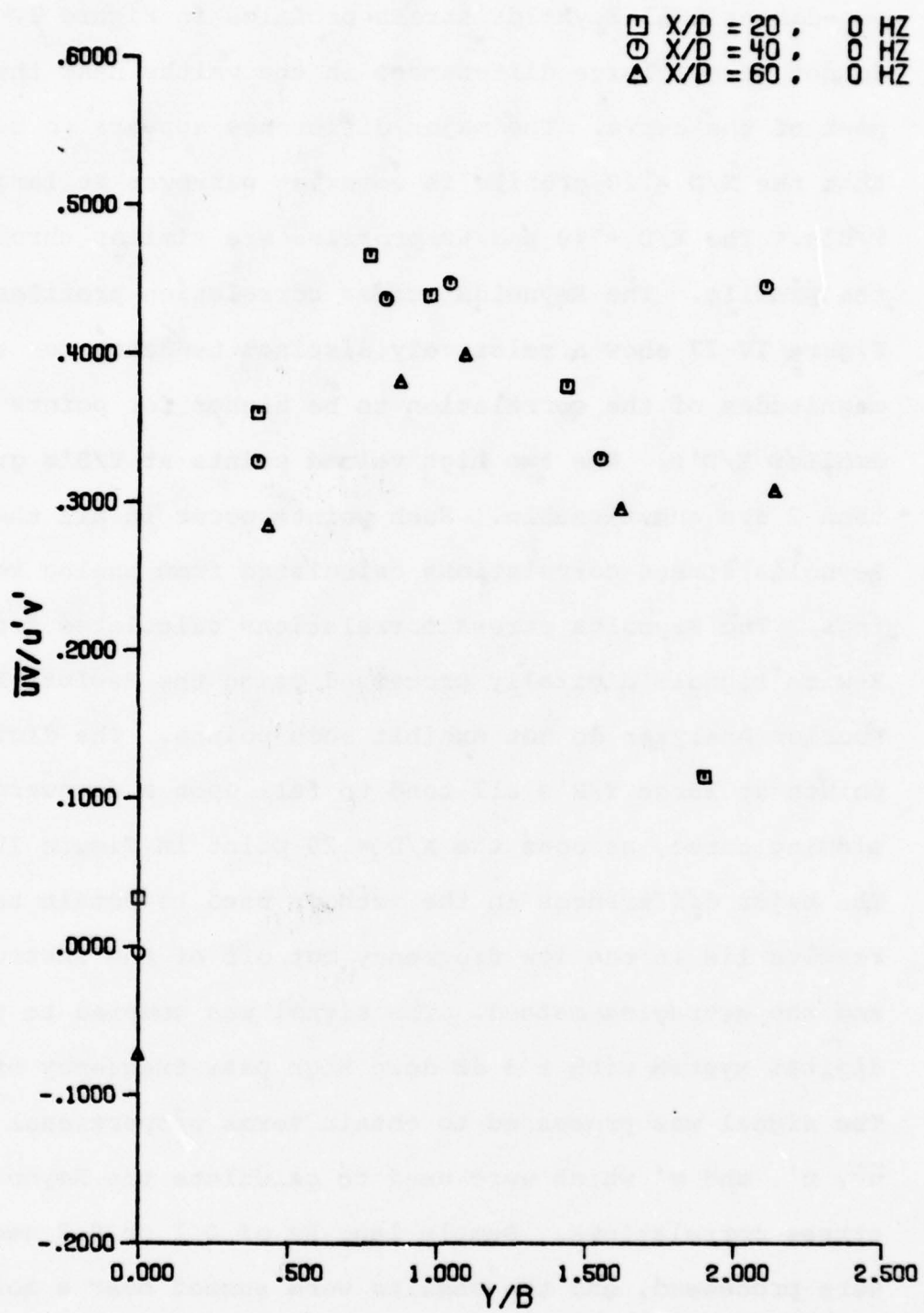


Figure IV-27 Profiles of Undisturbed Case Reynolds Stress Correlations

non-dimensional Reynolds stress profiles in Figure IV-26 do not reveal large differences in the values near the peak of the curve. The major difference appears to be that the  $X/D = 20$  profile is somewhat narrower at large  $Y/B$ 's. The  $X/D = 40$  and  $60$  profiles are similar throughout the profile. The Reynolds stress correlation profiles in Figure IV-27 show a relatively distinct tendency for the magnitudes of the correlation to be higher for points at smaller  $X/D$ 's. The two high valued points at  $Y/B$ 's greater than 2 are questionable. Such points occur in all the Reynolds stress correlations calculated from analog readings. The Reynolds stress correlations calculated from X-wire signals digitally processed using the Hewlett Packard Fourier Analyzer do not exhibit such points. The digital points at large  $Y/B$ 's all tend to fall upon a downward sloping curve, as does the  $X/D = 20$  point in Figure IV-27. The major differences in the methods used to obtain the results lie in the low frequency cut off of the instruments and the averaging method. The signal was coupled to the digital system with a 3 dB down high pass frequency of 5 Hz. The signal was processed to obtain terms proportional to  $\overline{uv}$ ,  $u'$ , and  $v'$  which were used to calculate the Reynolds stress correlations. Sample lengths of 0.1 or 0.2 seconds were processed, and the results were summed over a total time of 30 seconds. An ensemble average was formed from the sum. The voltmeters used to measure equivalent terms

in the analog processed method responded to frequencies as low as 0.5 Hz, and the signals were averaged with a continuous low pass filter type time constant of 30 seconds to 100 seconds. The flow at  $Y/B = 2$  is highly intermittent, and it appears that the difference in correlations may be considered in one of two ways. The first is that the high correlations are erroneous, stemming from the inability of the long time constant averaging to respond to the intermittent turbulent signal. The second is that the high correlations are correct, resulting from the low frequency large eddies that are believed to be important in the entrainment by the jet. Gutmark and Wagnanski (1976) have published results of conditional and conventional measurements of the Reynolds stress correlation. Their measurements display high correlation values at large  $Y/B$ 's, with the conditional turbulent region correlations the higher of the two sets. They note the difference between their results and those of Heskestad (1965) and Bradbury (1965), whose results do not show the high correlations, but offer no explanation. This matter is discussed in the next chapter.

The 700 Hz case results are presented in Figures IV-28 and IV-29. The non-dimensional Reynolds stresses in Figure IV-28 appear to show that the peak for  $X/D = 20$  is somewhat higher than the others and slightly shifted toward the centerline. The profiles at  $X/D = 40$  and 60 appear

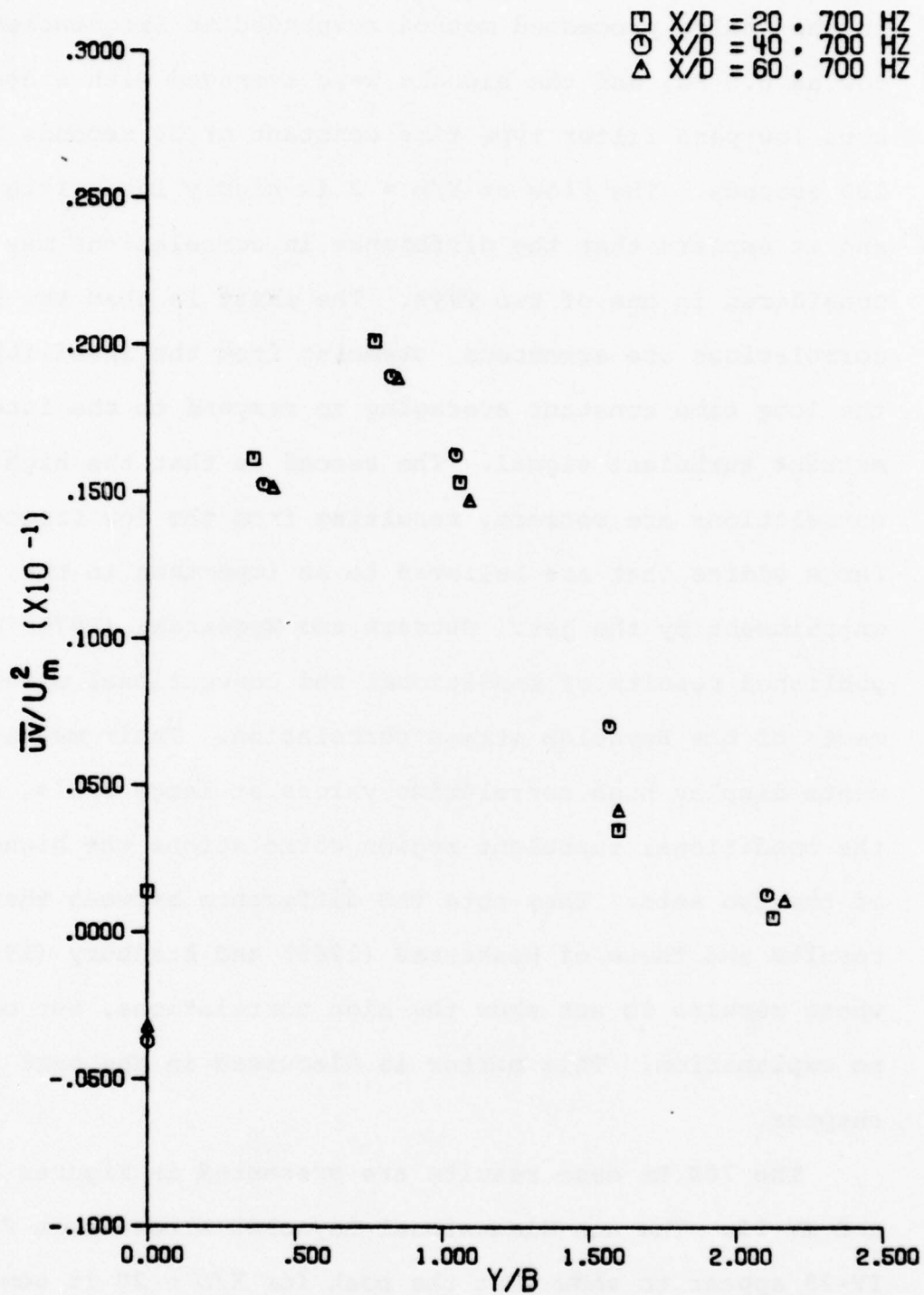


Figure IV-28 Profiles of 700 Hz Case  
Non-Dimensional Reynolds  
Stress

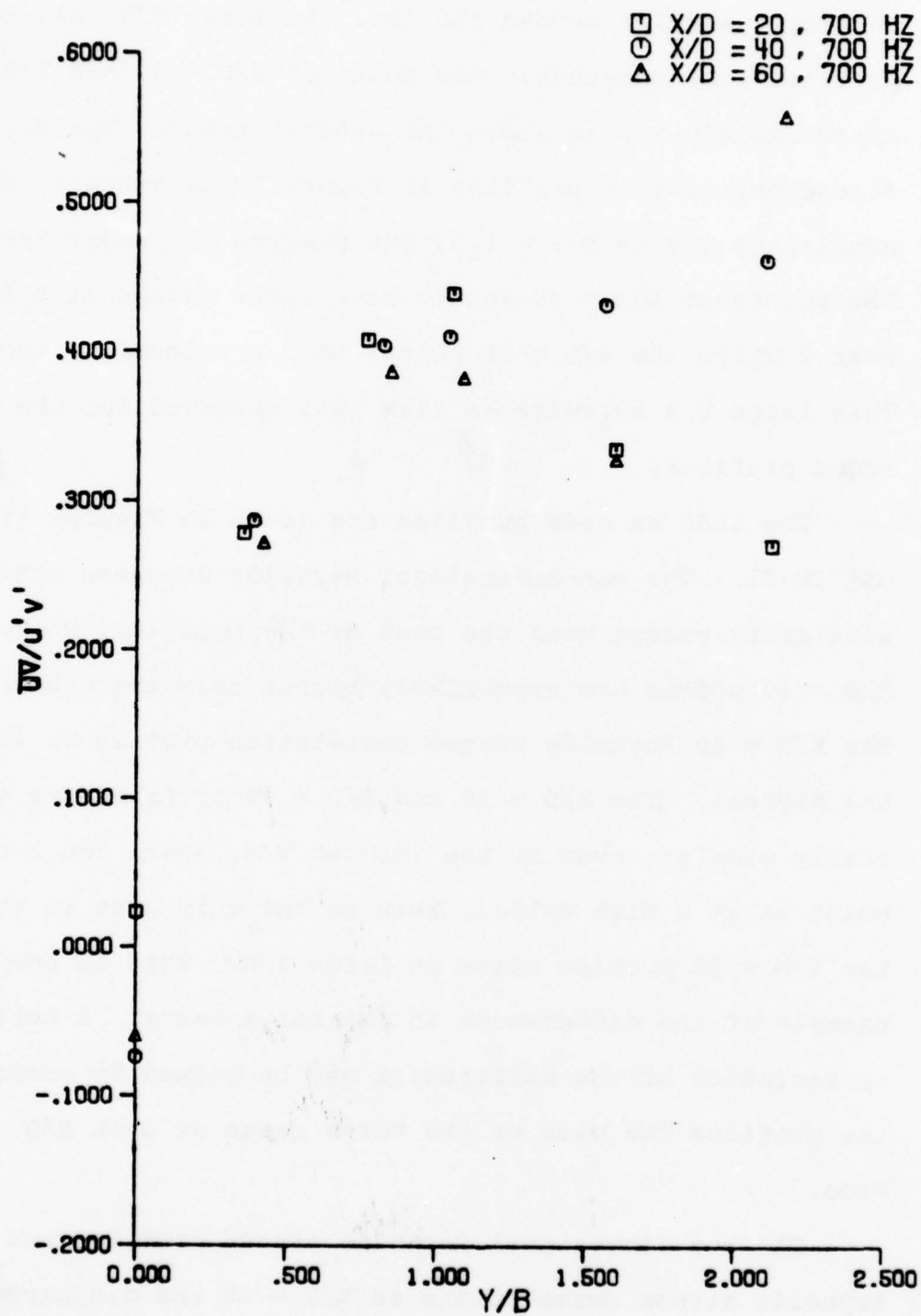


Figure IV-29 Profiles of 700 Hz Case  
Reynolds Stress Correlation

generally similar across the jet. At large  $Y/B$ , all three profiles come together. One point at  $X/D = 40$  and  $Y/B$  of approximately 1.6 is above the general trend. The Reynolds stress correlation profiles in Figure IV-29 exhibit near similarity inside  $Y/B = 1.5$ , but diverge at larger  $Y/B$ . The points at  $X/D = 40$  and 60 have large values at  $Y/B$  near 2 while the  $X/D = 20$  points have continued to decrease. This large  $Y/B$  behavior is like that observed for the no sound profiles.

The 1600 Hz case profiles are given in Figures IV-30 and IV-31. The non-dimensional Reynolds stresses exhibit similarity except near the peak of the profiles, where the  $X/D = 40$  points are appreciably higher than the others. The  $X/D = 40$  Reynolds stress correlation profile is also the highest. The  $X/D = 20$  and  $X/D = 60$  profiles are generally similar, even at the largest  $Y/B$ , where the  $X/D = 20$  point is at a high value. This is the only case in which the  $X/D = 20$  profile rises at large  $Y/B$ . This is one example of the differences in the three cases. A better appreciation of the differences may be gained by comparing the profiles for each of the three cases at each  $X/D$  position.

The non-dimensional Reynolds stress profiles and Reynolds stress correlations at  $X/D = 20$  are displayed in Figures IV-32 and IV-33. The non-dimensional Reynolds stress profile exhibits clear trends. The 700 Hz profile

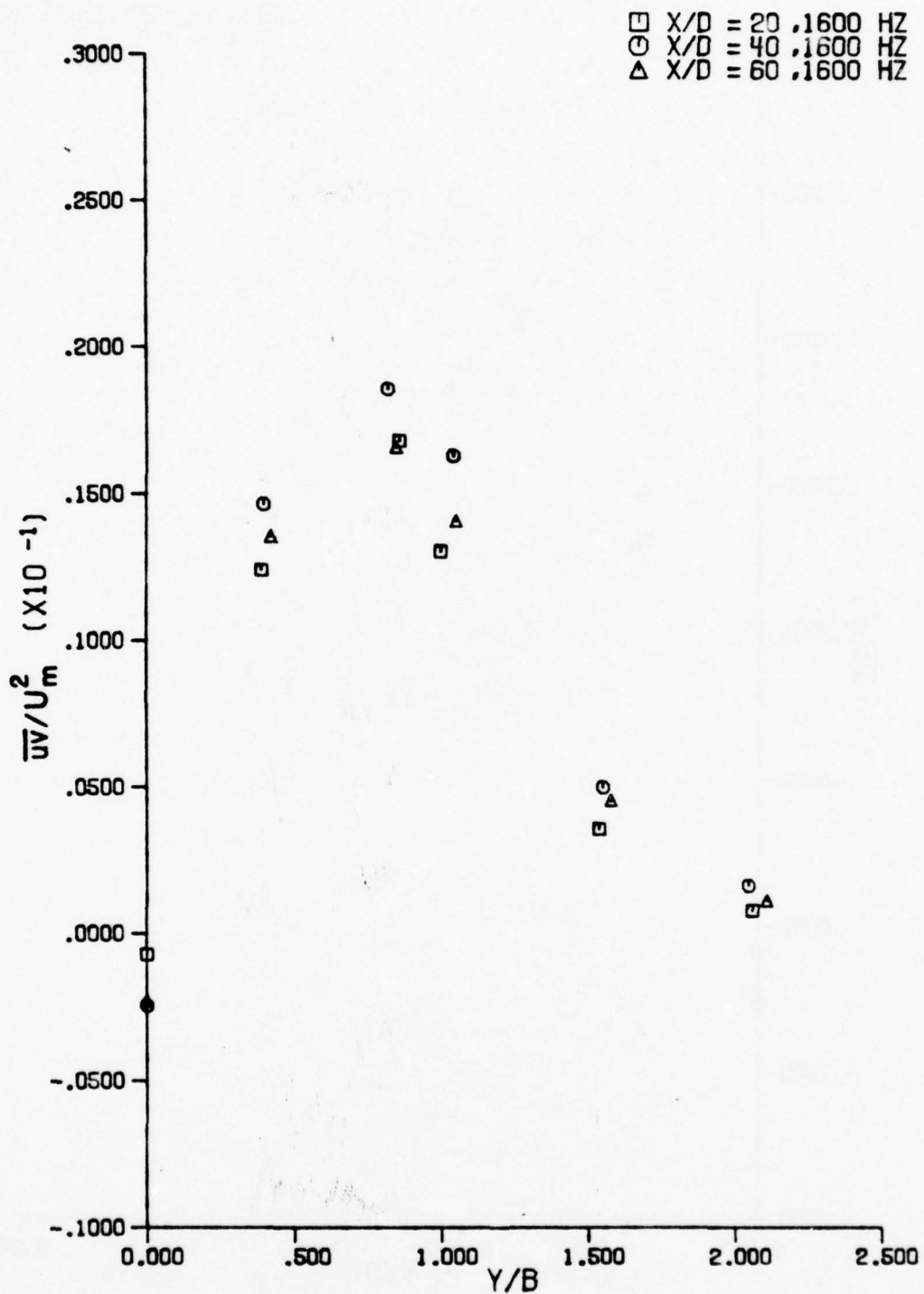


Figure IV-30 Profiles of 1600 Hz Case Non-Dimensional Reynolds Stress

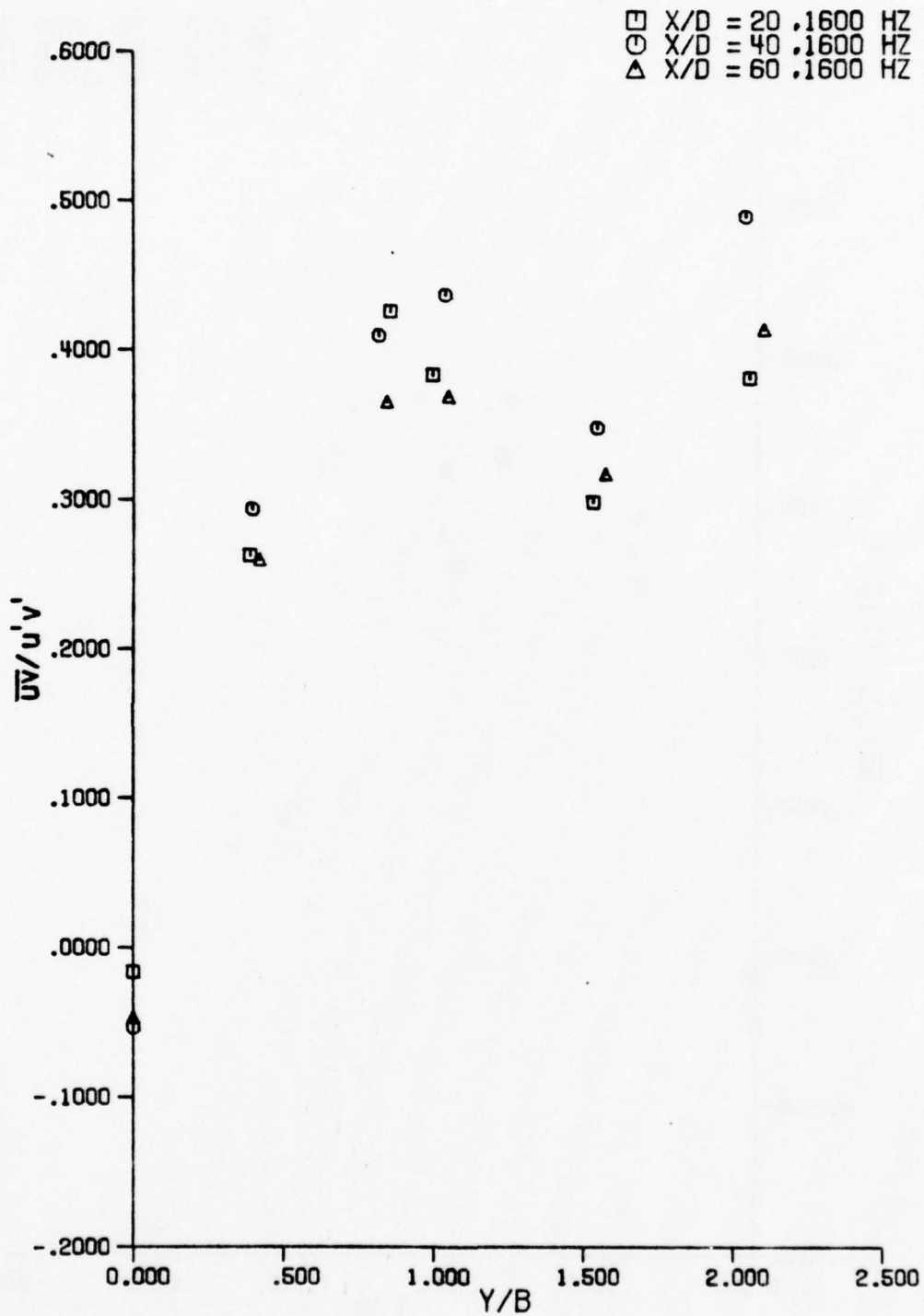


Figure IV-31 Profiles of 1600 Hz Case  
Reynolds Stress Correlation

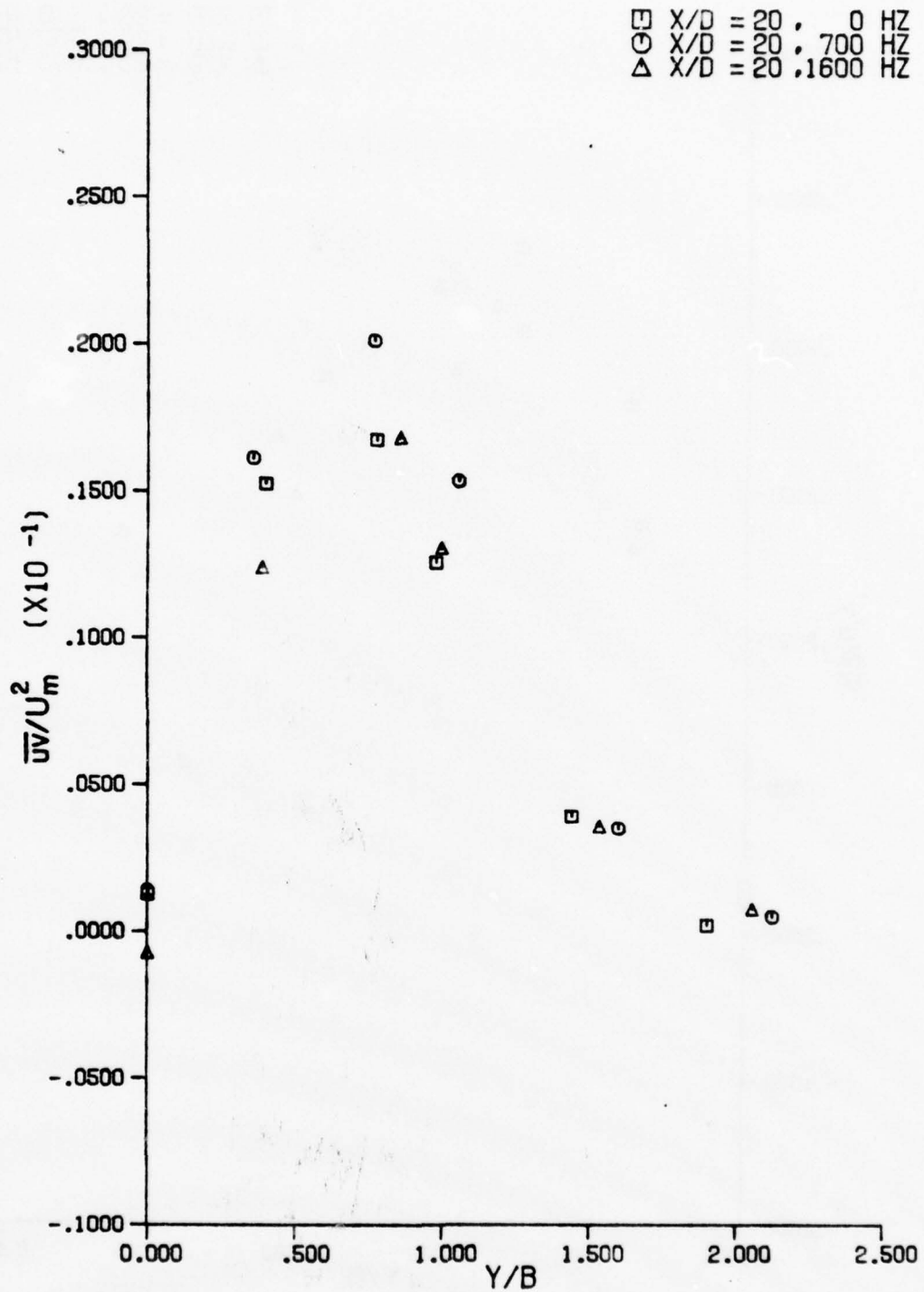


Figure IV-32 Profiles of Non-Dimensional Reynolds Stresses at X/D = 20

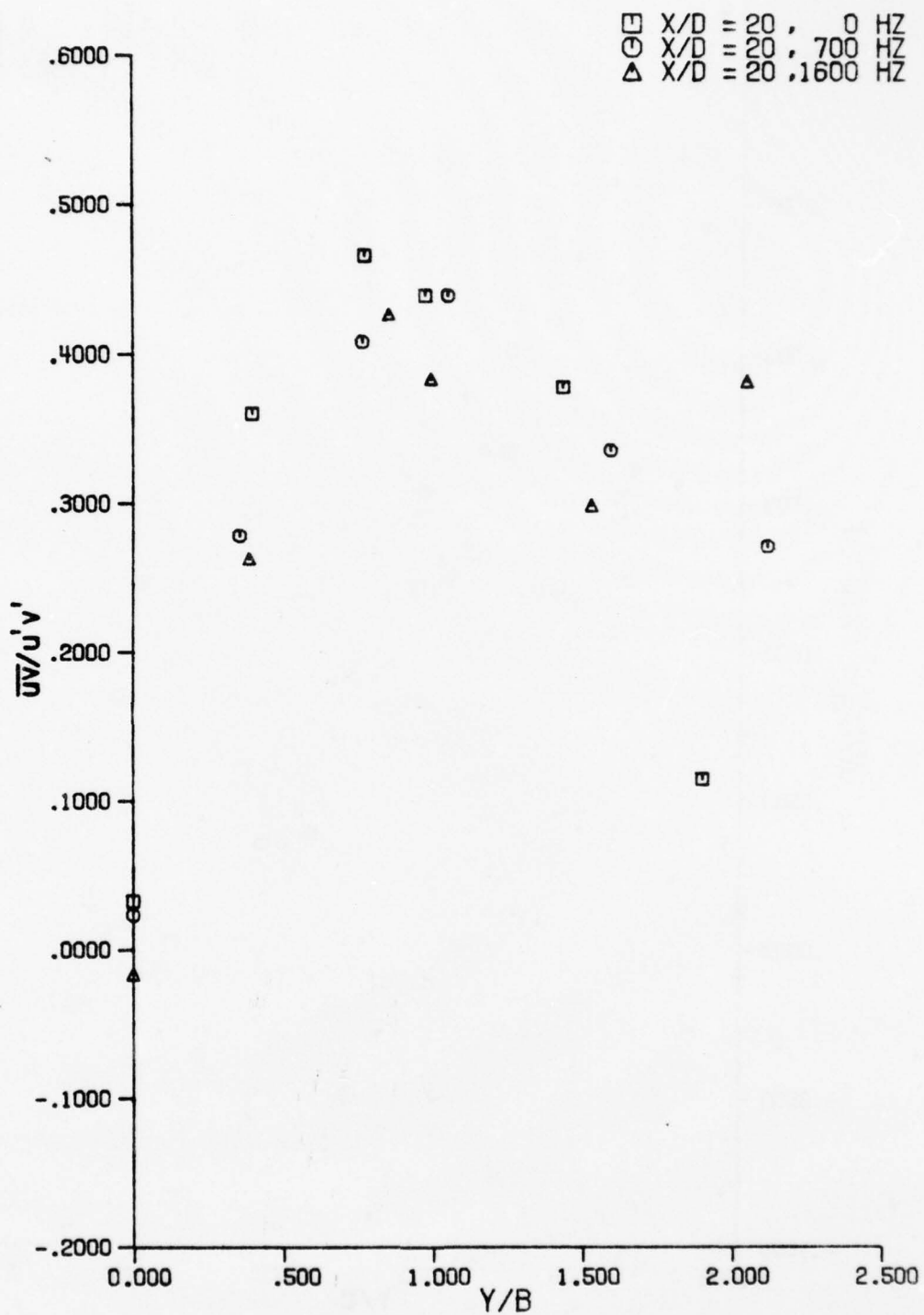


Figure IV-33 Profiles of Reynolds Stress Correlations at  $X/D = 20$

is consistently highest across the jet. Although there are not enough points to clearly define the peaks of the profiles, it appears that the peaks occur at somewhat different distances from the jet centerline. The profiles of the results of the no sound case and the 700 Hz case suggest peaks at a  $Y/B$  of approximately 0.65 while the 1600 Hz case results suggest a peak nearer to  $Y/B = 0.75$ . The points suggest further that the peaks of the no sound case and the 1600 Hz case may be at approximately the same level. However, the difference in the position of the peaks would result in differences in the energy transfer rates from the mean flow to the turbulence.

The slope of the mean velocity profile at  $Y/B = 0.75$  is approximately 7% greater than that at  $Y/B = 0.65$ , and since the energy transfer rate is proportional to  $\left| \overline{uv} \frac{\partial \bar{U}}{\partial Y} \right|$  the rate at the peak for 1600 Hz would be higher. Also, since the maximum of  $\left| \frac{\partial \bar{U}}{\partial Y} \right|$  in this case occurs near  $Y/B = 0.9$ , it appears that the integral of the energy transfer rate would be higher for a peak at  $Y/B = 0.75$ . This would be the result of the shift in the peak shifting the higher values of the Reynolds stress into correspondence with larger values of the slope of the mean velocity profile, thereby increasing the integral of their product. Thus it appears that at  $X/D = 20$ , the two cases of applied sound may transfer energy from the mean flow to the turbulence at greater rates than the no sound case.

The Reynolds stress correlation profiles for the three cases at  $X/D = 20$  are shown in Figure IV-33. The results are somewhat surprising, but illuminating. One might expect that the application of sound to the flow would result in a more ordered flow and a greater correlation between the velocity components at a point. Of course, since the Reynolds stress correlation is a zero time delay correlation, a phase lag between the two perturbations would decrease the correlation. However, one might well expect some ordering of the flow if there were direct interactions between the sound field and the flow throughout the flow field. The results at  $X/D = 20$  do not indicate this. The no sound correlations are generally the highest of the three cases. The 1600 Hz case correlations are generally the lowest, with the 700 Hz correlations in the middle. Thus it appears that the sound field does not order the flow field in this region.

The non-dimensional Reynolds stress profiles at  $X/D = 40$  are presented in Figure IV-34. The 700 Hz case Reynolds stresses are also the highest at  $X/D = 40$ , but the differences between the three cases are smaller than at  $X/D = 20$ . It appears that the 700 Hz case profile is somewhat broader in the region of  $Y/B = 1.5$ , but the peak appears to be only slightly higher than the 1600 Hz case. The no sound case is consistently low. The positions of the peaks of the three profiles are not very well indicated

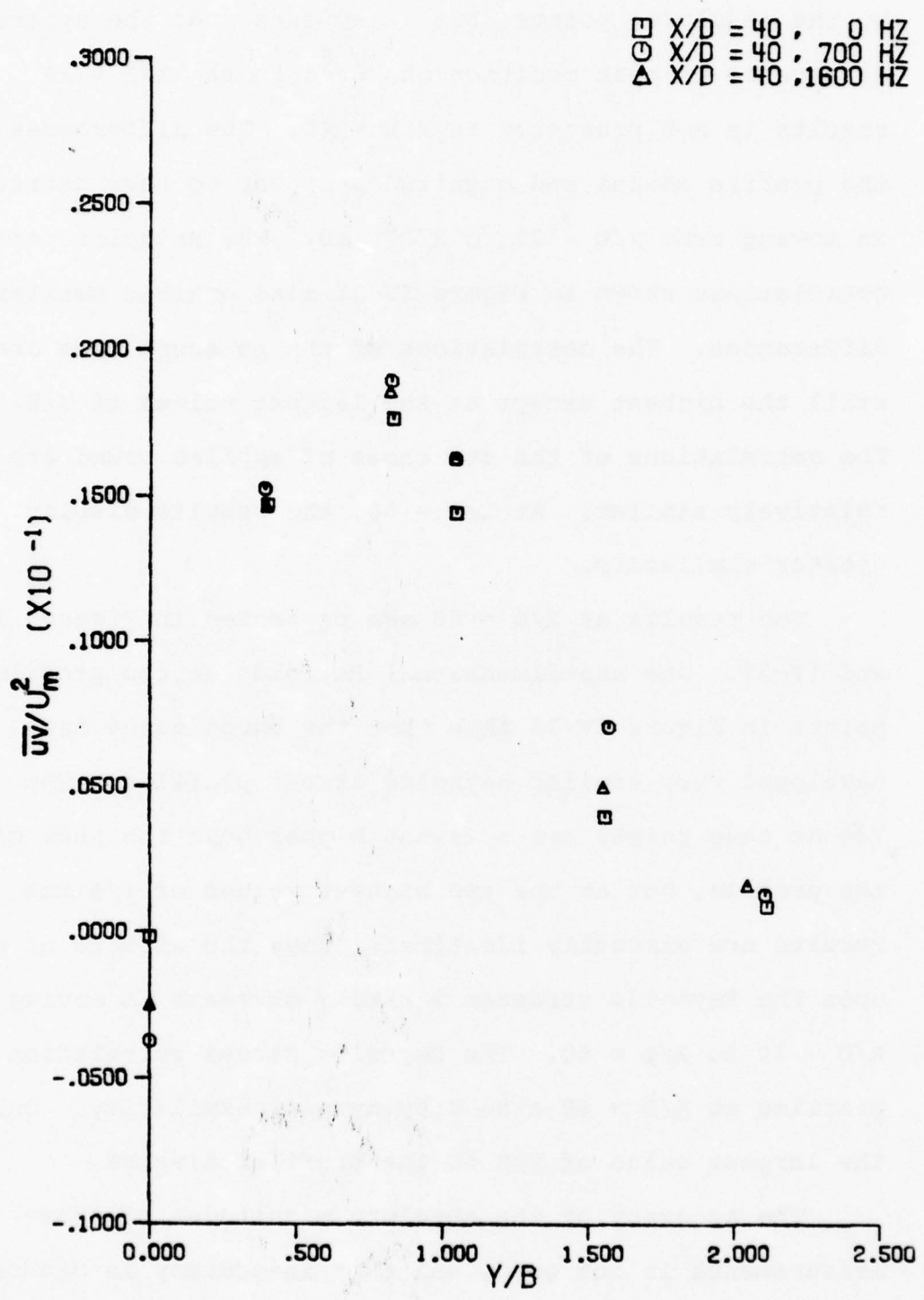


Figure IV-34 Profiles of Non-Dimensional Reynolds Stresses at X/D = 40

by the resulting points, but it appears that the apparent difference in peak position observed in the  $X/D = 20$  results is not presented at  $X/D = 40$ . The differences in the profile shapes and magnitudes appear to have decreased in moving from  $X/D = 20$  to  $X/D = 40$ . The Reynolds stress correlations shown in Figure IV-35 also exhibit smaller differences. The correlations of the no sound case are still the highest except at the largest values of  $Y/B$ . The correlations of the two cases of applied sound are relatively similar. At  $X/D = 60$ , the results display greater similarity.

The results at  $X/D = 60$  are presented in Figures IV-36 and IV-37. The non-dimensional Reynolds stress profile points in Figure IV-36 show that the three cases have developed very similar Reynolds stress profiles. The 700 Hz case points are somewhat higher near the peak of the profile, but at the two highest values of  $Y/B$  the results are virtually identical. Thus the effects of sound upon the Reynolds stresses markedly decrease in moving from  $X/D = 20$  to  $X/D = 60$ . The Reynolds stress correlation profiles at  $X/D = 60$  also display near similarity. Only at the largest value of  $Y/B$  do the profiles diverge.

The accuracy of the absolute magnitudes of these measurements is not good, and this inaccuracy is discussed in detail in Appendix D. The results presented in this section were obtained from X-wire measurements which

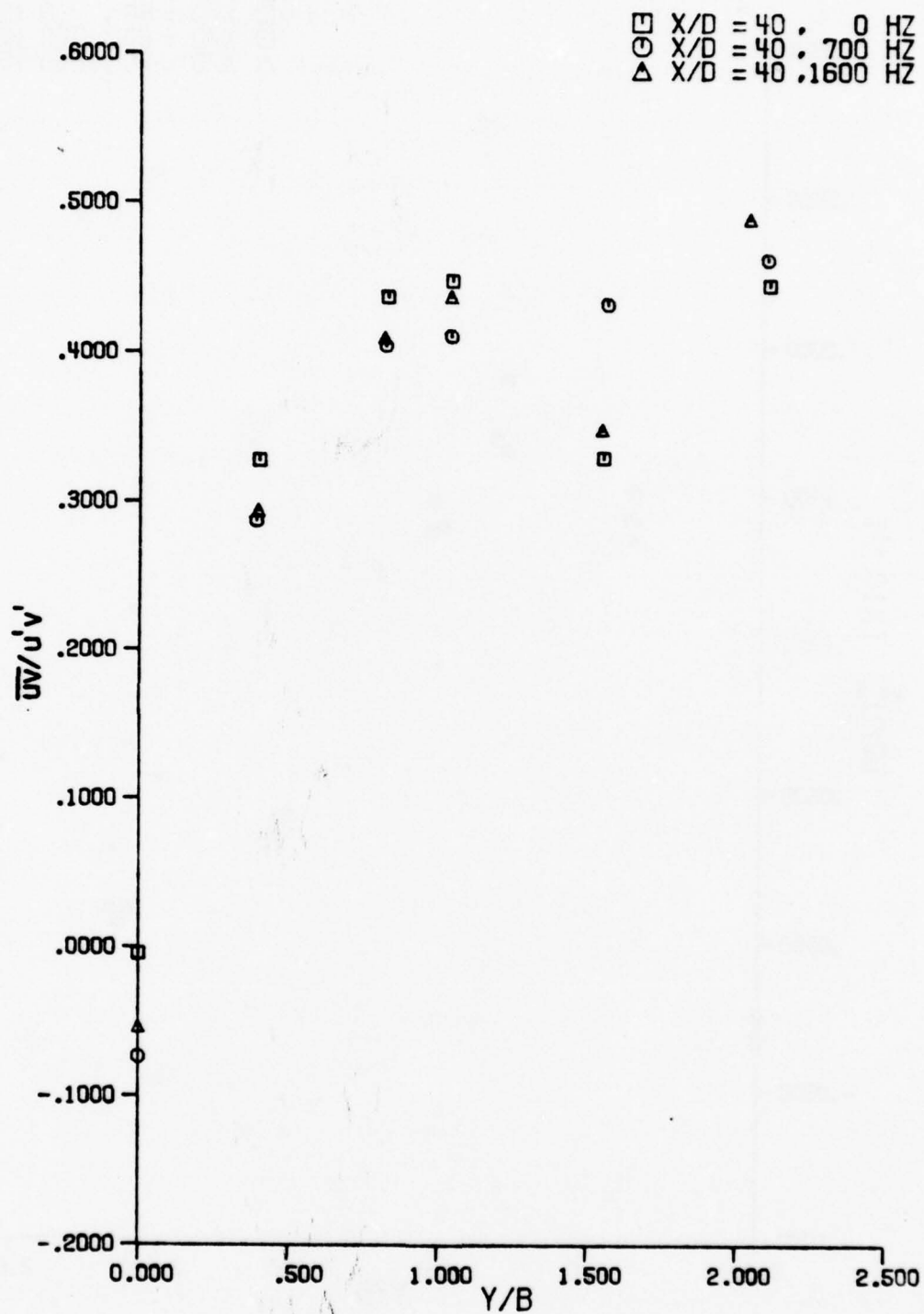


Figure IV-35 Profiles of Reynolds Stress Correlations at  $X/D = 40$

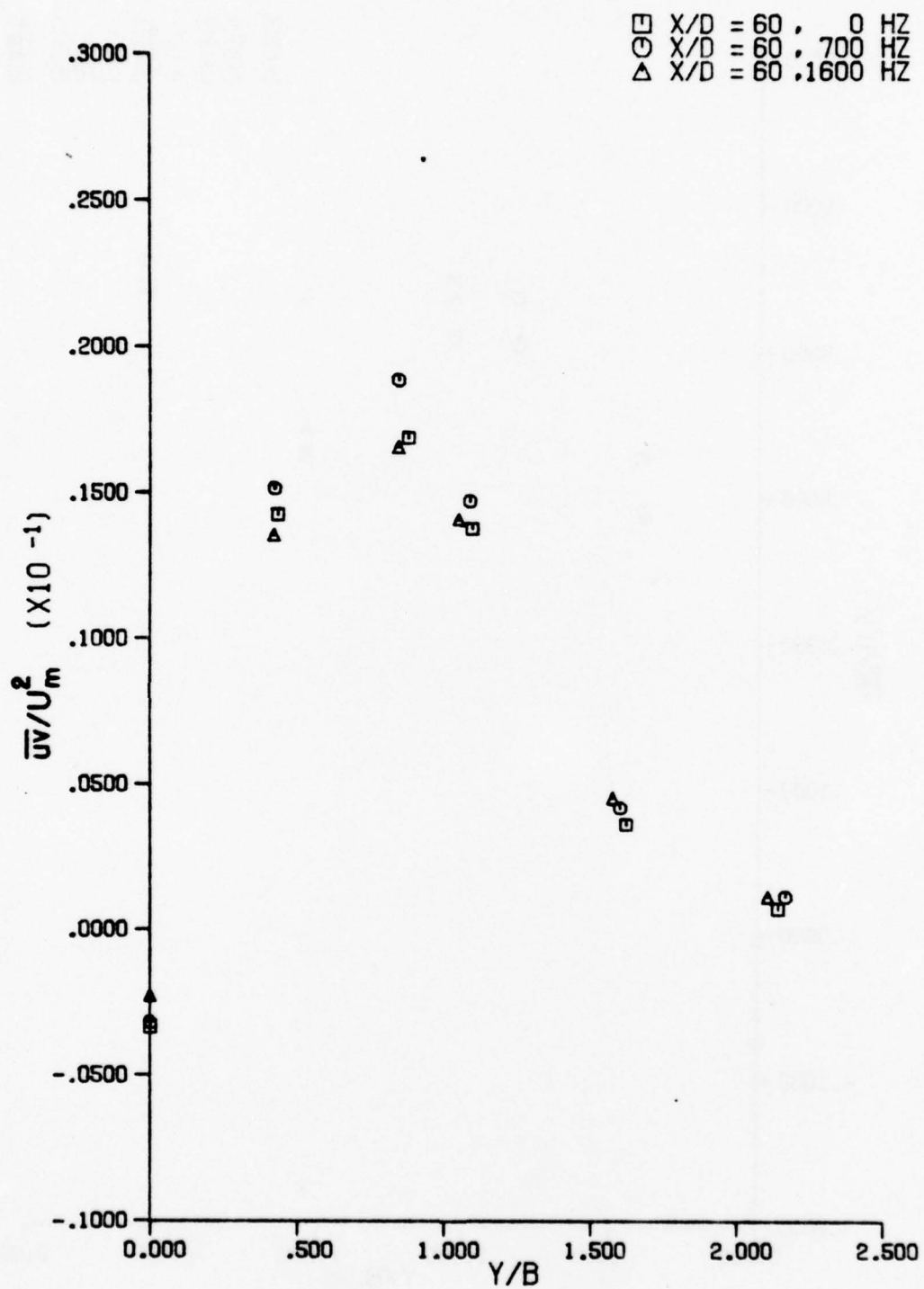


Figure IV-36 Profiles of the Non-Dimensional Reynolds Stresses at  $X/D = 60$

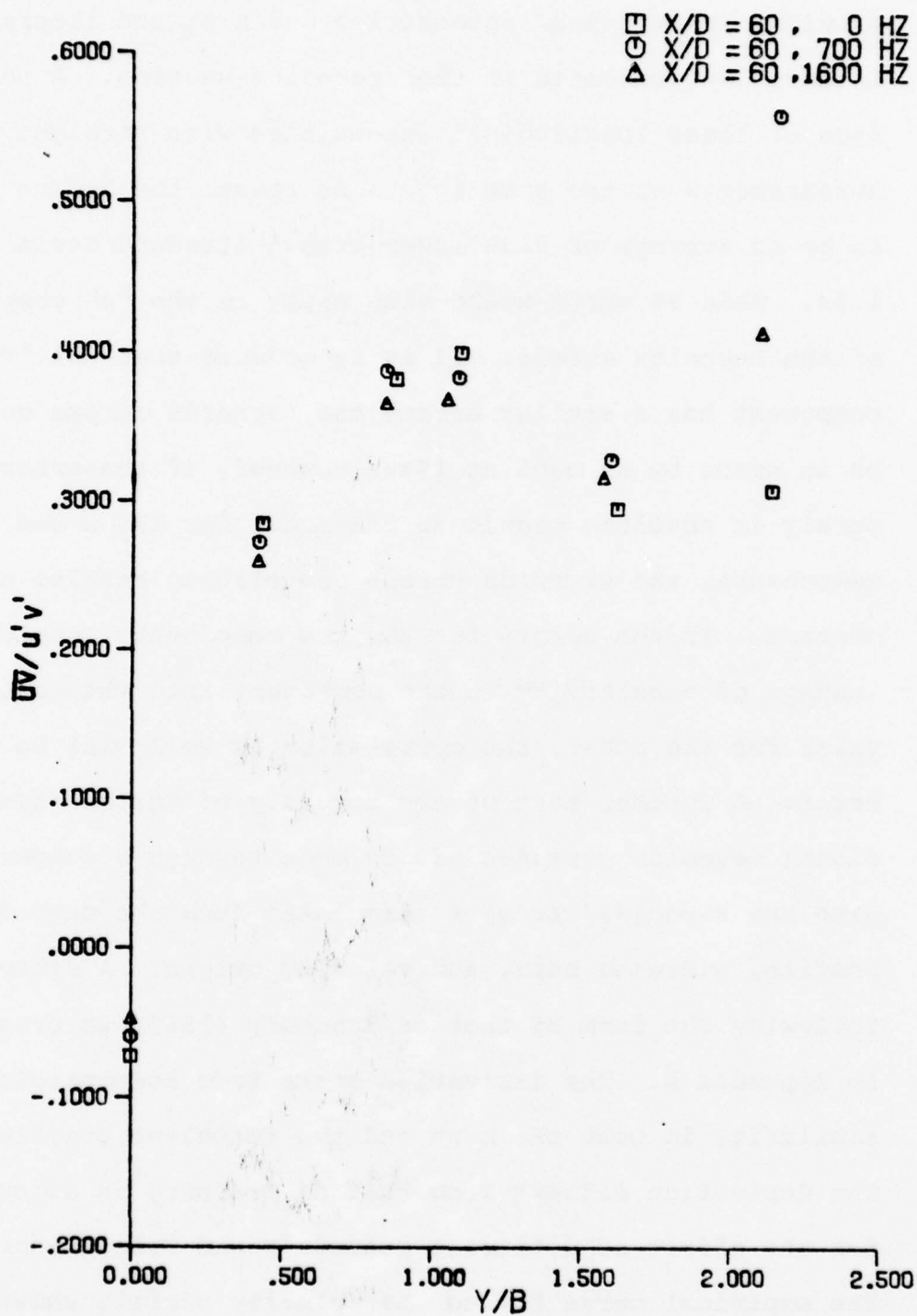


Figure IV-37 Profiles of Reynolds Stress Correlations at X/D = 60

provided longitudinal intensities and also the lateral intensities presented in the preceding section. A comparison of these longitudinal intensities with straight wire measurements at the same locations reveal the X-wire results to be an average of 9.3% lower with a standard deviation of 1.5%. This 9% error would also apply to the "u" component of the Reynolds stress. If it is assumed that the "v" component has a similar error, the Reynolds stress could be in error by as much as 19%. However, if the errors are purely in absolute magnitude and equal for the u and v components, the Reynolds stress correlation results are correct. If the errors for the two components involve a leakage of sensitivity to one component into the resulting value for the other, the correlation as well will be in error. A further test of the accuracy of the non-dimensional Reynolds stresses may be made through a comparison with the Reynolds stresses calculated from the mean velocity profile, widening rate, and velocity origin. A derivation following the form of that of Bradbury (1965) is presented in Appendix E. The derivation stems from assumptions of similarity in both the mean and the turbulent profiles. The derivation differs from that of Bradbury in accounting for the effect of different geometric and velocity origins. The empirical curve fit to the velocity profile shown near the beginning of this chapter was used to calculate the velocities and slopes of the velocity profile for insertion

in the derived equation. The resulting curves are shown along with the results of the measurements presented in this section in Figures IV-38 through IV-40. It may be observed in Figure IV-38 that at  $X/D = 20$ , the calculated Reynolds stresses are roughly 15% higher than the results of the measurements. The errors decrease somewhat at  $X/D = 40$ , but it may be observed in Figure IV-39 that the calculations, based upon assumptions of similarity, do not predict the decrease in the effects of the applied sounds. The same trends may be seen in Figure IV-40, at  $X/D = 60$ . As a test of the possible effects of errors in the curve fit used, the same calculations were performed at  $X/D = 40$  using velocities and slopes graphically obtained from the mean velocity profiles. The resulting curves and the measured points are presented in Figure IV-41. The calculated curves are approximately 25% higher than the results of the measurements. The accuracy of the calculated Reynolds stresses is not readily estimated, for it depends in a complicated manner upon the accuracy of the mean velocity profile slopes used and upon the accuracy of some numerical integrations. It is believed that the errors in the absolute magnitudes of the measured Reynolds stresses are bounded by the difference between them and the calculated curves. The relative errors between the various measured points are believed to be considerably smaller than these absolute errors. The absolute error may be

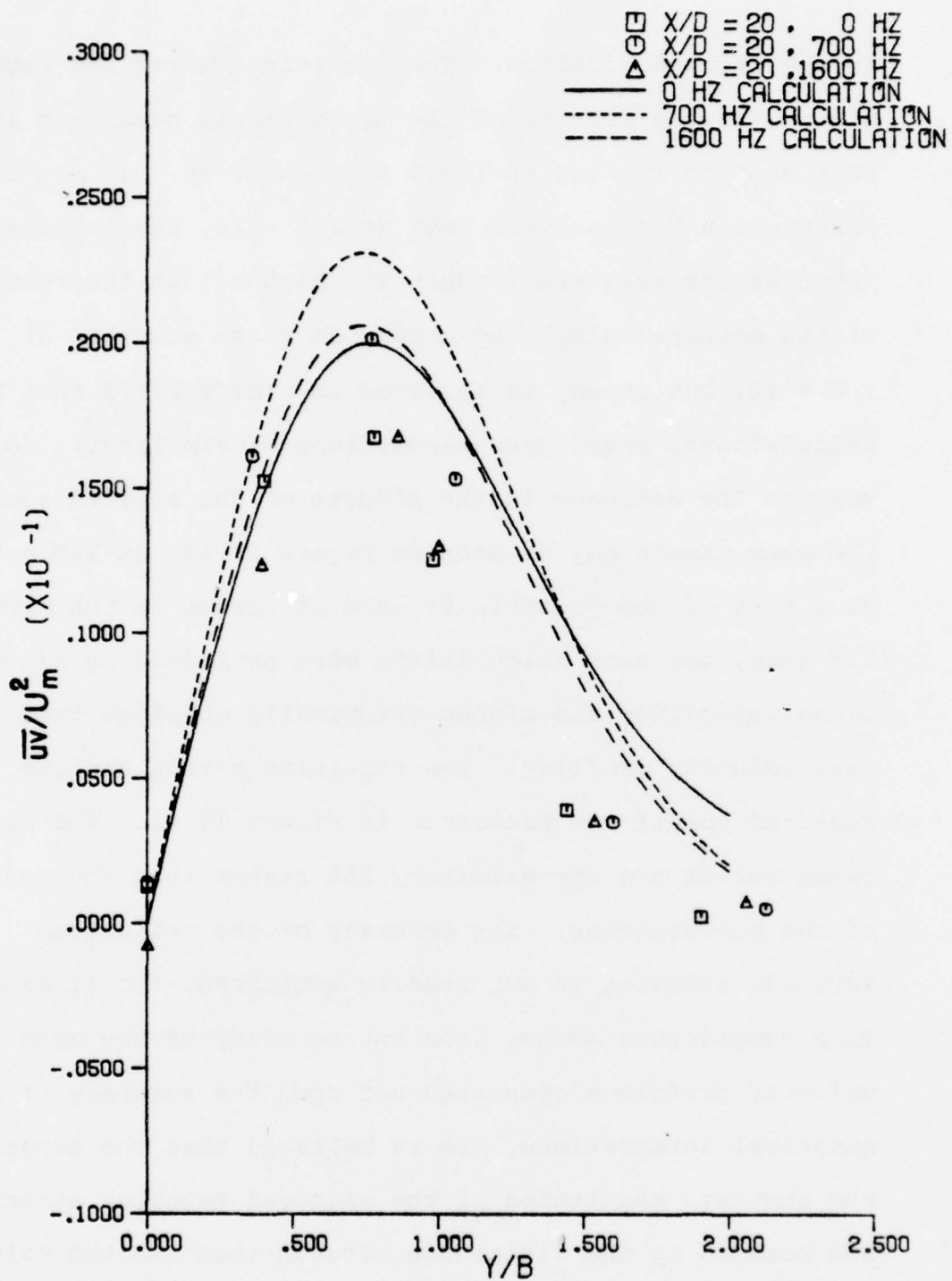


Figure IV-38 Calculated Reynolds Stresses at X/D = 20

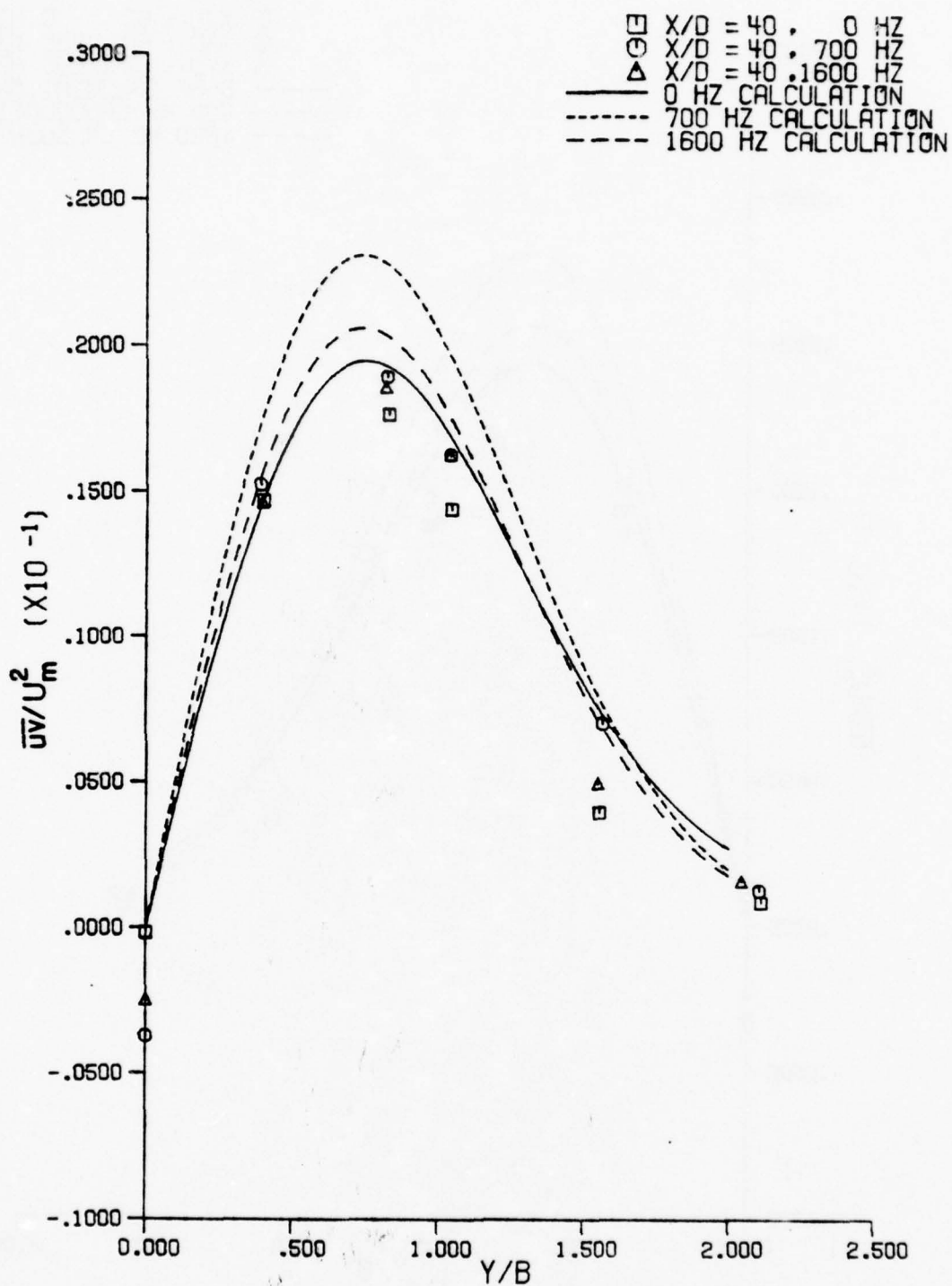


Figure IV-39 Calculated Reynolds Stresses at X/D = 40

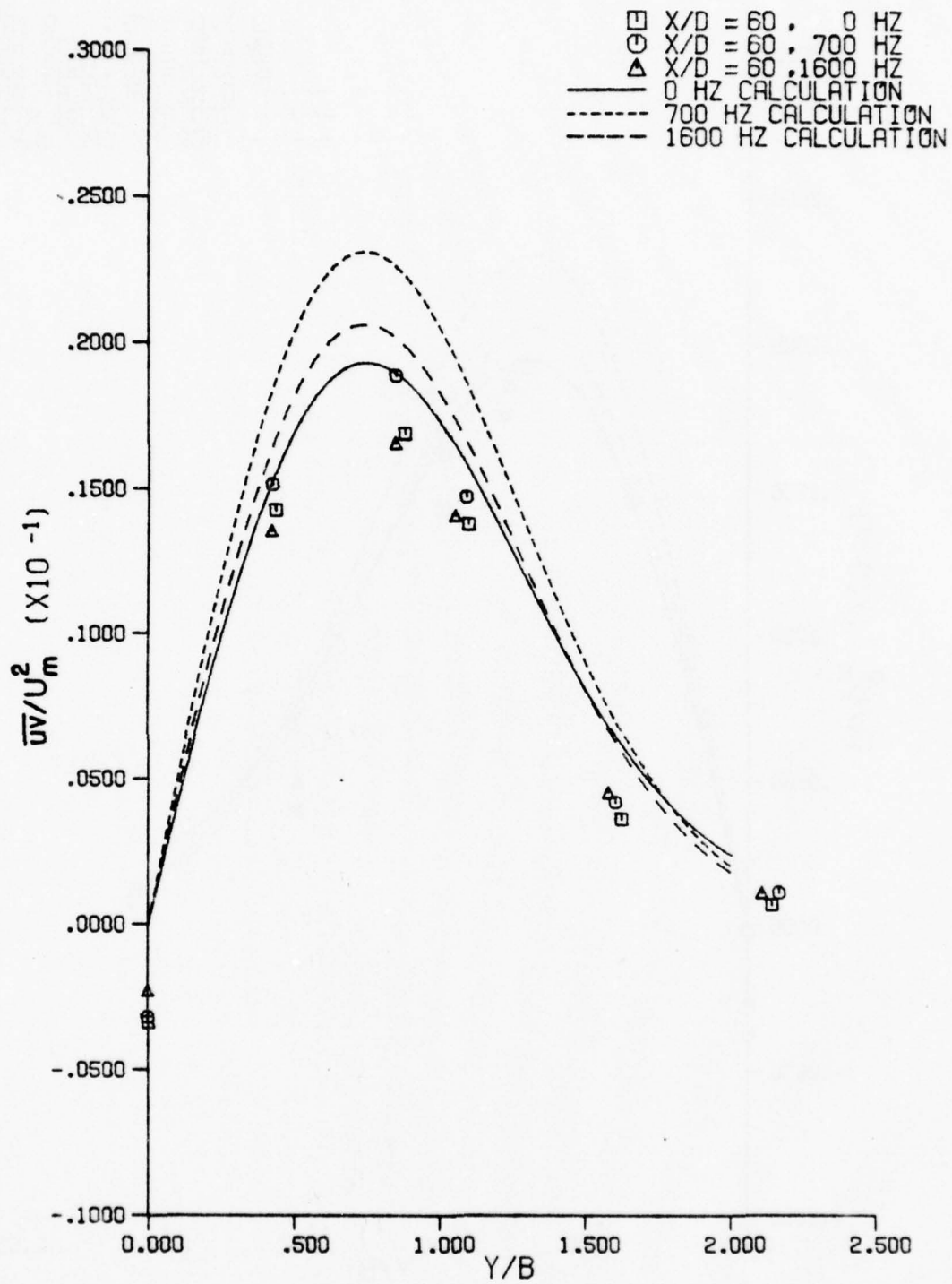


Figure IV-40 Calculated Reynolds Stresses at X/D = 60

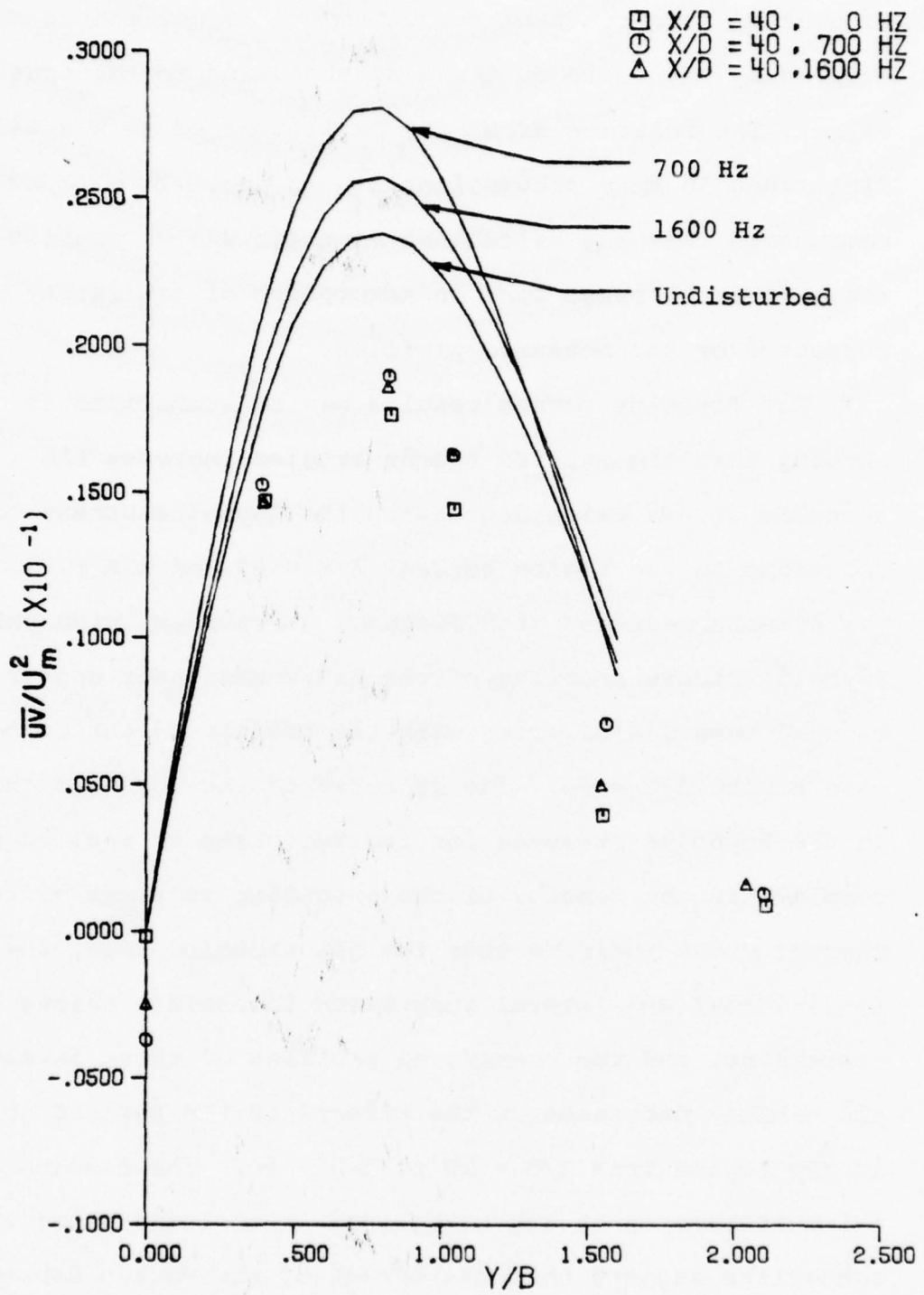


Figure IV-41 Reynolds Stresses Calculated with Graphical Mean Velocity Profile Slopes

thought of as a constant factor common to all points expressing the ratio of the measured value to the true value. The relative error may be thought of as a small difference in this proportionality factor. It must be remembered that the calculated Reynolds stress profiles are calculated based upon an assumption of similarity not supported by the measured profiles.

The Reynolds stress results may be summarized as showing that the applied sounds studied increase the Reynolds stress while decreasing the Reynolds stress correlations in the region between  $X/D = 20$  and  $X/D = 60$ . The effects decrease with distance downstream, with the Reynolds stress profiles of the disturbed cases appearing to tend toward similarity with the profile of the no sound case beyond  $X/D = 60$ . The decrease in the measured changes in the Reynolds stresses for the two cases of applied sound complements the results of the preceding sections of the chapter which indicate that the jet widening rate, the longitudinal and lateral turbulence intensities along the centerline, and the transverse profiles of these intensities all exhibit decreases in the effects of the applied sounds in the region from  $X/D = 20$  to  $X/D = 80$ . The results of the measurements of the turbulence intensities along the centerline suggest that the effect of the sounds develops in the initial region of the jet. Measurements of the turbulent energy spectra were performed in this region in

an effort to uncover the characteristics of the growth of the effects of the applied sounds. The results of these measurements are presented in the next section.

#### 5. Turbulent Energy Spectrum Measurements

The results presented so far in this chapter indicate that the effect of the applied sound upon the jet is dependent upon the frequency of the sound. It was observed that different frequencies produced different widening and decay rates in the main region of the jet. The detailed structural measurements using two frequencies revealed that sound-induced changes in the turbulent structure begin in the initial region of the jet and decay towards the no sound values at large downstream distances. The review of instability revealed that the turbulence in a free shear layer originates in the initial instabilities. The growth of these instabilities was seen to be dependent upon the disturbance frequency. Furthermore, it was learned that in the initial region the fluctuation energy distribution changes from a discrete spectrum to the broad spectrum characteristic of developed turbulent flow. It was believed that a better understanding of the interaction between the applied sound and the turbulent flow could be gained through a study of the changes in the turbulent energy spectrum development produced by the applied sound. Therefore, turbulence energy spectra were measured in the initial and main regions of the jet.

The energy spectra presented here are spectra of the longitudinal turbulence intensity obtained from non-linearized straight wire probes. The spectra are therefore not spectra of the total energy, but one-dimensional spectra of the energy in the longitudinal fluctuations.

It was believed that the relation between the frequency of the applied sound and the natural frequencies of the instabilities in the shear layers at the edges of the jet potential core could be important in determining the effects of sound upon the jet. To measure these instability frequencies, spectra of the longitudinal turbulence fluctuations were performed at  $X/D = 0.25$  and  $Y/B = 1.0$  for the three cases. The hot wire was placed in the vertical plane in order to allow more accurate positioning and space resolution at the  $Y/B = 1.0$  position, a position of extremely steep slope in the initial region velocity profile. The no sound case spectrum is presented in Figure IV-42. The spectrum reveals peaks at frequencies of roughly 155 Hz, 305 Hz and 545 Hz. The spectral components are described in terms of dimensional frequency rather than Strouhal number for ease of comparison with the applied sound frequencies. The 700 Hz case spectrum in Figure IV-43 displays very strong peaks at 700 Hz and 350 Hz along with weaker peaks at the same frequencies observed in the no sound spectrum. Figure IV-44 displays the 1600 Hz case spectrum, which exhibits a large number of relatively strong peaks.

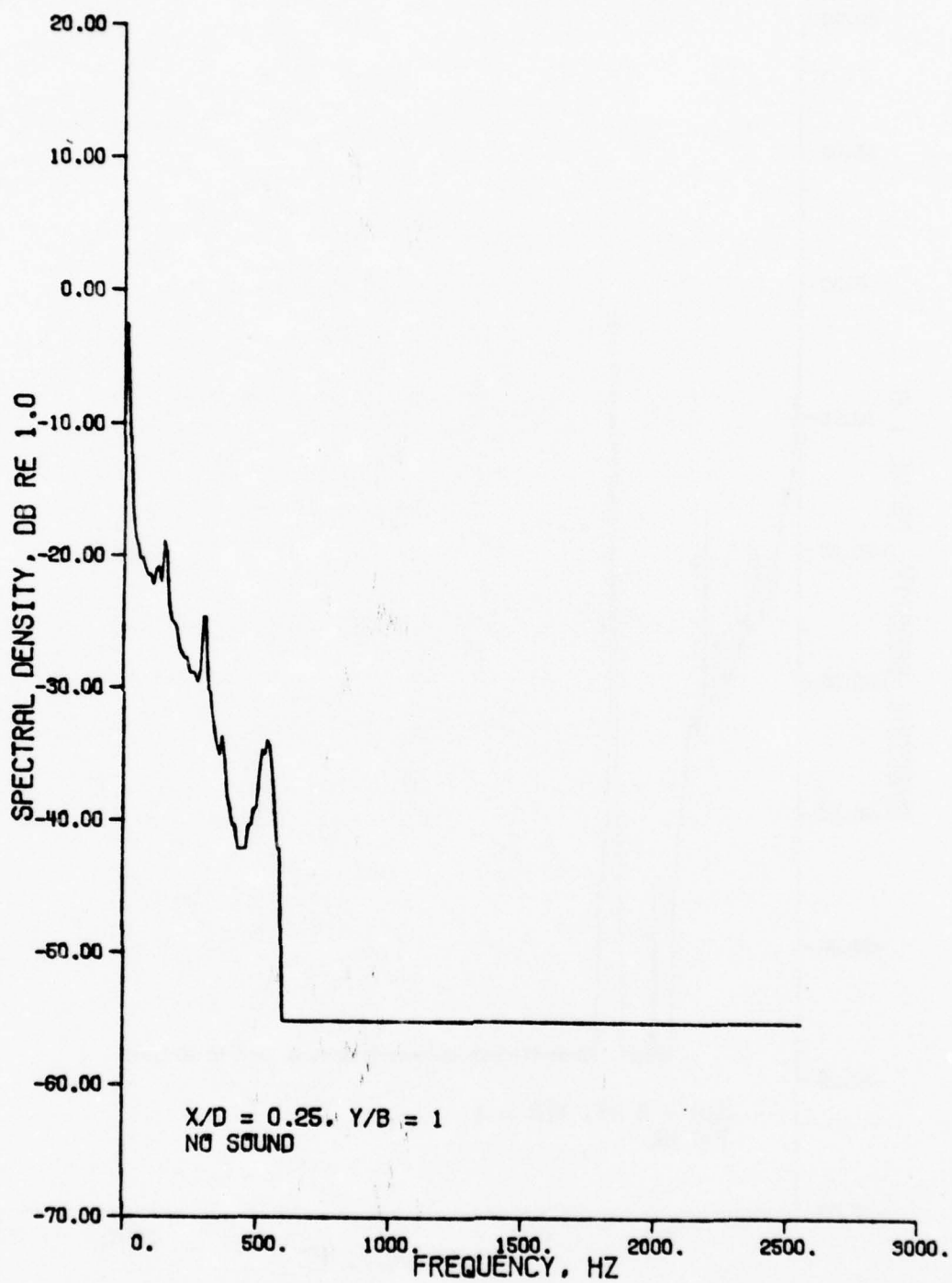


Figure IV-42 Undisturbed Case Shear Layer Spectrum

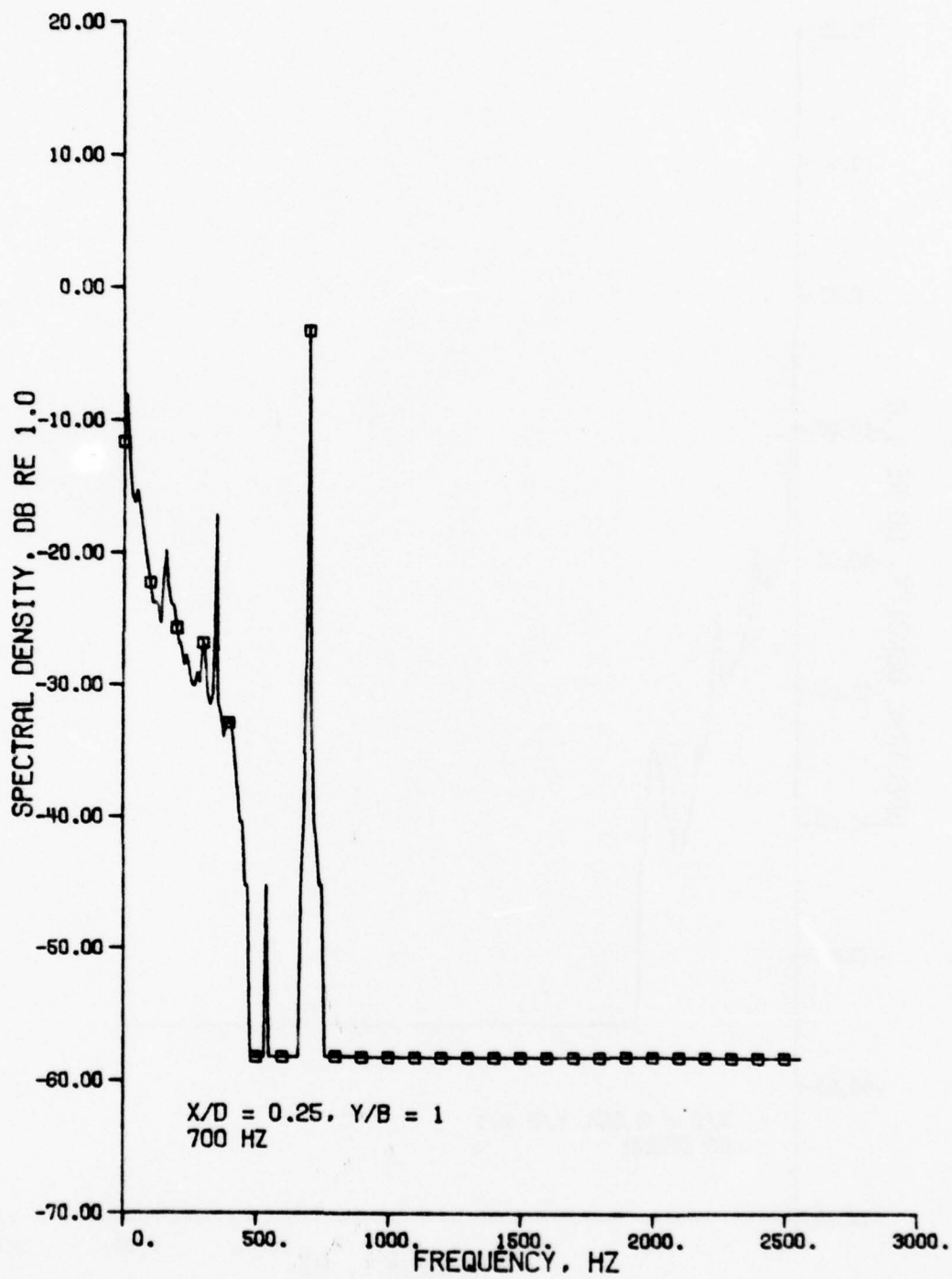


Figure IV-43 700 Hz Case Shear Layer Spectrum

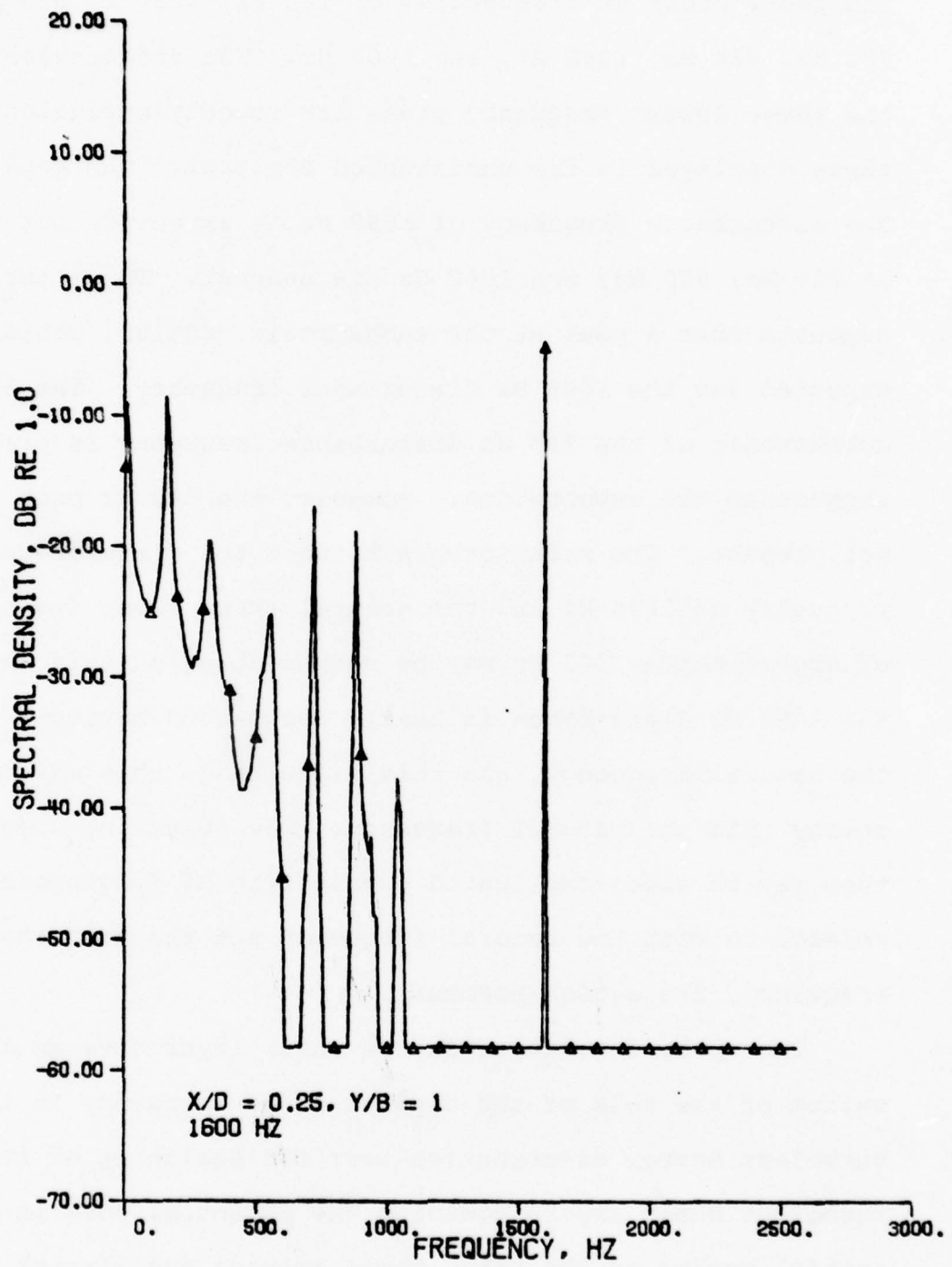


Figure IV-44 1600 Hz Case Shear Layer Spectrum

The peaks occur at frequencies of 160 Hz, 325 Hz, 555 Hz, 720 Hz, 880 Hz, 1040 Hz, and 1600 Hz. The frequencies of the three lowest frequency peaks are roughly equivalent to those displayed in the undisturbed spectrum. The peak at the disturbance frequency of 1600 Hz is expected, but those at 720 Hz, 880 Hz, and 1040 Hz are unusual. The literature suggests that a peak at the subharmonic, 800 Hz, could be expected for the 1600 Hz disturbance frequency. The 350 Hz subharmonic of the 700 Hz disturbance frequency is present, supporting the expectation. However, the 800 Hz peak is not present. The relationship between the disturbance frequency of 1600 Hz and the natural shear layer frequency of approximately 545 Hz may be responsible for this absence. The 1600 Hz disturbance is nearly the second harmonic of the natural frequency, and this disturbance thus may feed energy into the natural frequency. The resulting spectrum then may be some complicated combination of frequencies related to both the natural frequency and the disturbance frequency, its second harmonic.

The spectra measured in the shear layer give an indication of the role of the applied sound frequency in the turbulent energy distribution near the beginning of the turbulent shear layers bounding the potential core in the initial region of the jet. These spectra are also of use in interpretation of the spectra that were measured along the jet centerline.

The centerline spectra were measured for each of the three cases at integer values of  $X/D$  from 0 to 10, and at  $X/D = 15, 20, 30,$  and  $40$ . Not all the spectra are presented, for the spectra change relatively slowly moving downstream, and the trends are clearly represented by a representative sample. The first spectra presented are those for  $X/D = 1$ . The spectra of the no sound case, the 700 Hz case, and the 1600 Hz case are presented in Figures IV-45, IV-46, and IV-47 respectively. Note that these figures have different scales than the previous spectra of the shear layer. These spectra are scaled in terms of the dB relative to a signal of 100% turbulence intensity. Thus a signal of turbulence intensity 0.2 composed of a single spike would have a peak of magnitude  $10 \log_{10} \frac{(0.2)^2}{(1.0)^2}$ . With  $\phi$  as the spectral density, this means that

$$\int_0^{f_{\max}} \phi \, df = \left( \frac{u'}{U} \right)^2.$$

The no sound spectrum reveals sharp peaks at 60 Hz, 180 Hz, and 300 Hz. It is believed that at least the 60 Hz peak is attributable to the electronic noise of the instruments, which appears to be at the same level as the turbulent signal at this position of extremely low turbulence intensity. Following the sharp peaks are two broad peaks centered at approximately 630 Hz and 795 Hz. The spectrum of the 700 Hz case at  $X/D = 1$  exhibits small peaks at 60 Hz, 120 Hz, and 180 Hz, but is dominated by sharp peaks at the

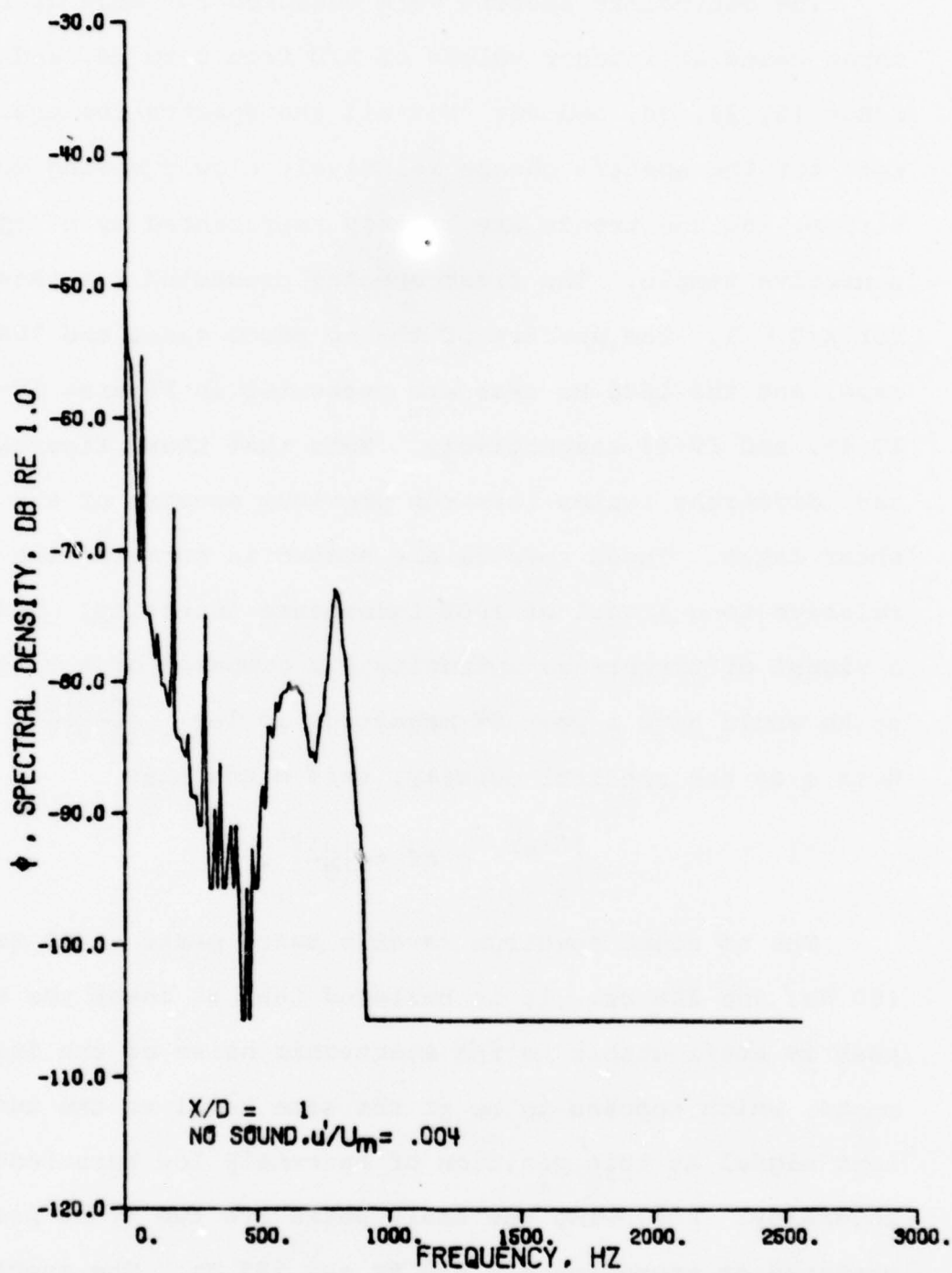


Figure IV-45 Undisturbed Case Spectrum at X/D = 1

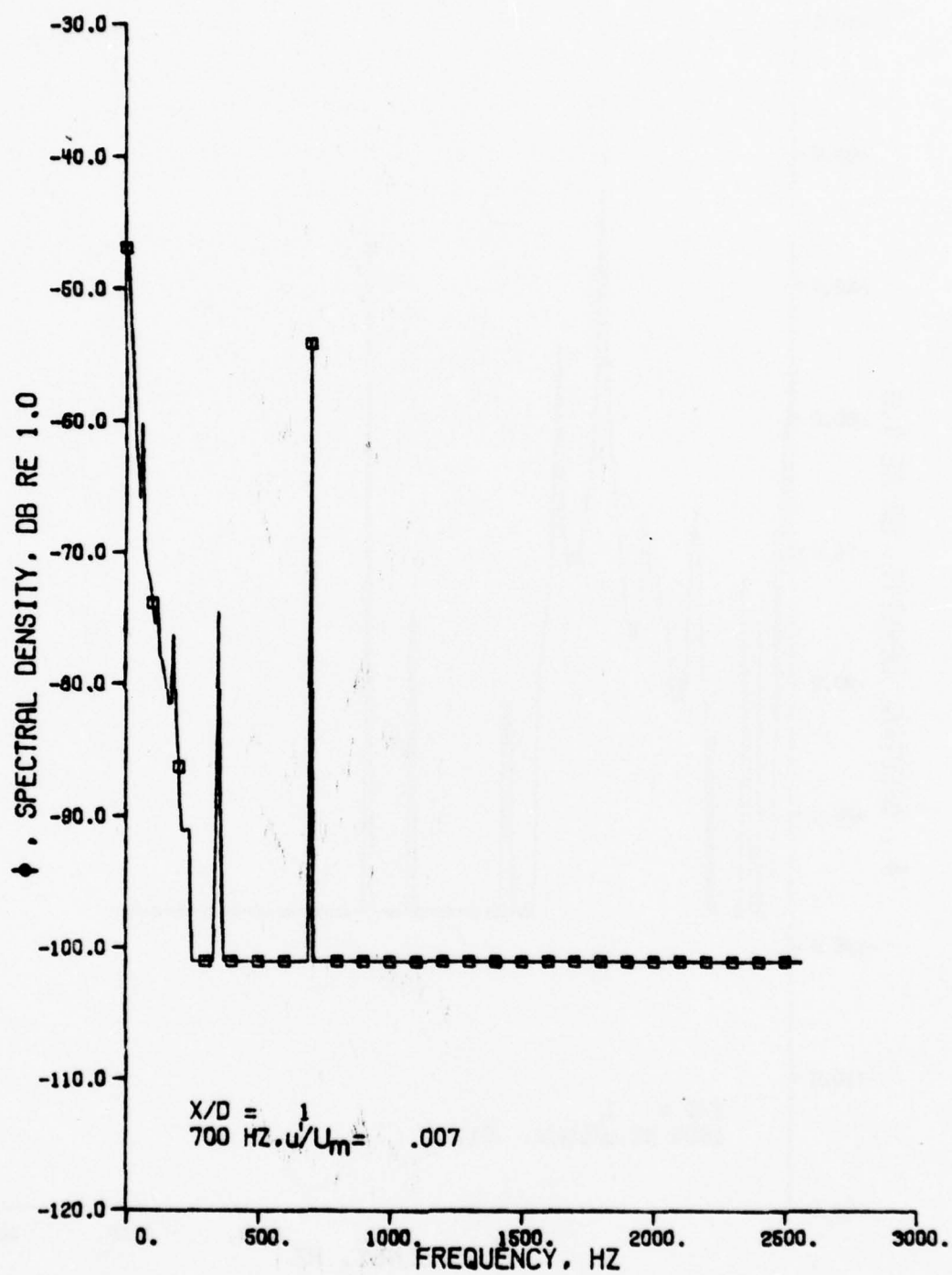


Figure IV-46 700 Hz Case Spectrum at X/D = 1

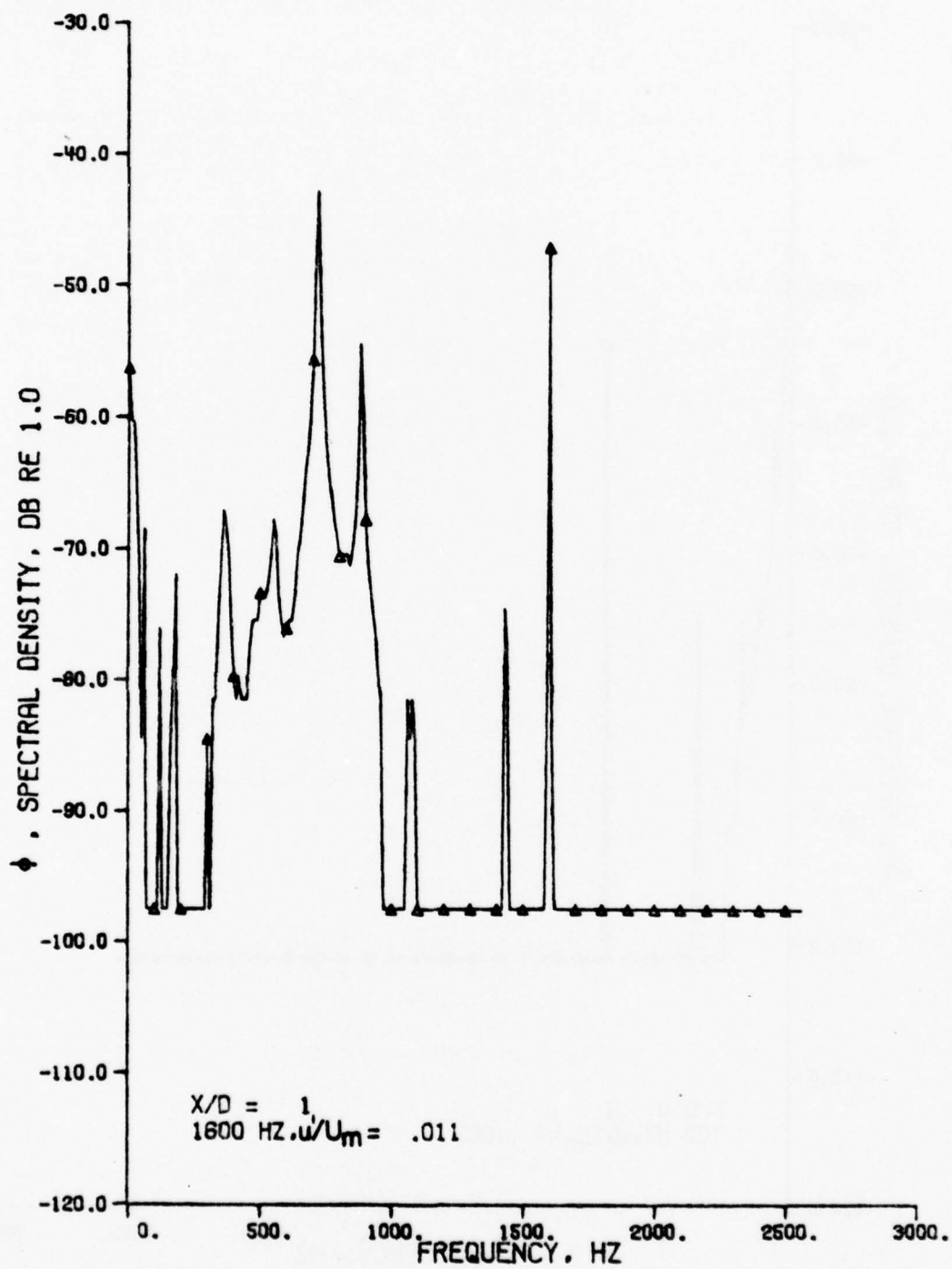
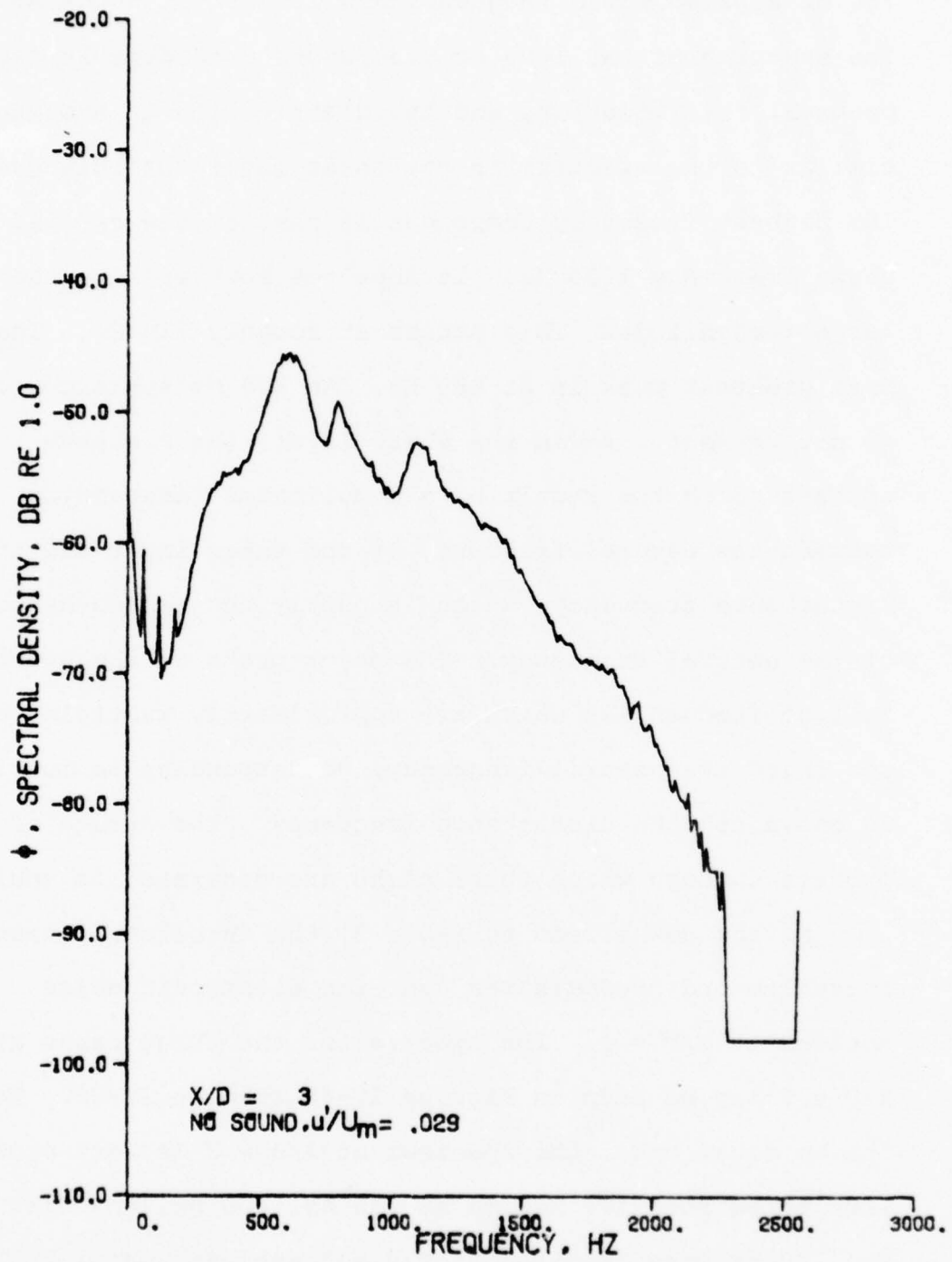


Figure IV-47 1600 Hz Case Spectrum at X/D = 1

700 Hz applied sound frequency and its 350 Hz subharmonic. The spectrum of the 1600 Hz case shows considerably more peaks at this location, and the distribution is somewhat similar to the spectrum in the shear layer for this case. The highest frequency component is that of the applied sound frequency 1600 Hz. It does not however have the largest magnitude. This occurs at roughly 720 Hz. The next greatest peak is at 880 Hz. An 800 Hz subharmonic is not present. As in the shear layer, the spectrum appears to be the result of a complicated interaction between the natural frequency of the shear layer and the disturbance frequency, which is nearly the second harmonic of the natural frequency. The major peaks of the spectrum fall at frequencies which are approximately multiples of one third the natural frequency, corresponding to multiples of one ninth the disturbance frequency. The nature of the process through which these peaks are generated is unclear.

Moving downstream to  $X/D = 3$ , the turbulence intensity increases and predominates over the electronic noise noticed at  $X/D = 1$ . The spectra for the three cases at  $X/D = 3$  may be seen in Figures IV-48 through IV-50. For the no sound case, the spectrum at  $X/D = 3$  is very broad with three relative maxima at 620 Hz, 800 Hz, and 1110 Hz. The 700 Hz case spectrum at  $X/D = 3$  exhibits major peaks at 700 Hz, 350 Hz, 1400 Hz, and 1050 Hz. These frequencies are all either harmonics, subharmonics, or at 1050 Hz, the

Figure IV-48 Undisturbed Case Spectrum at  $X/D = 3$

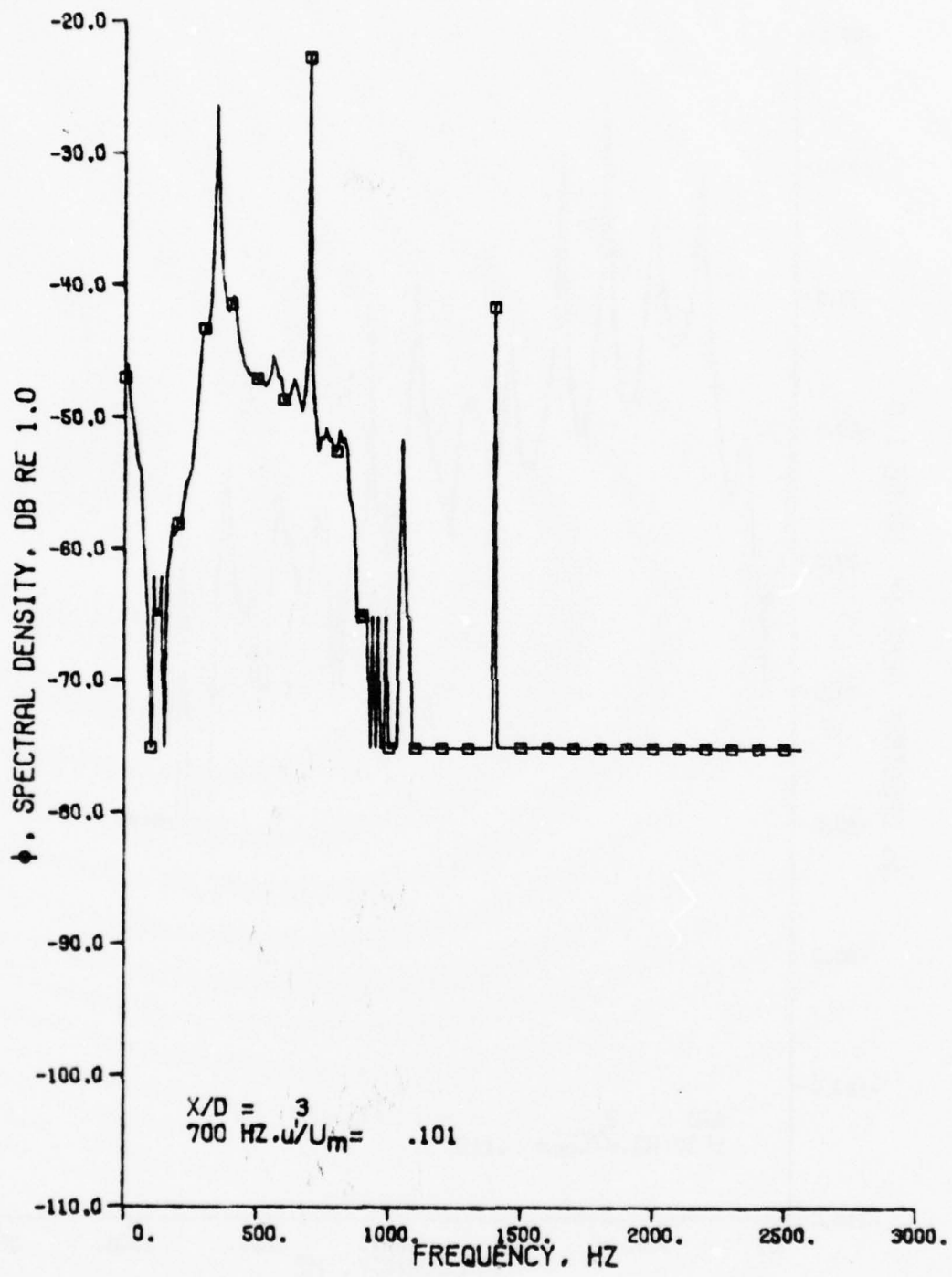


Figure IV-49 700 Hz Case Spectrum at X/D = 3

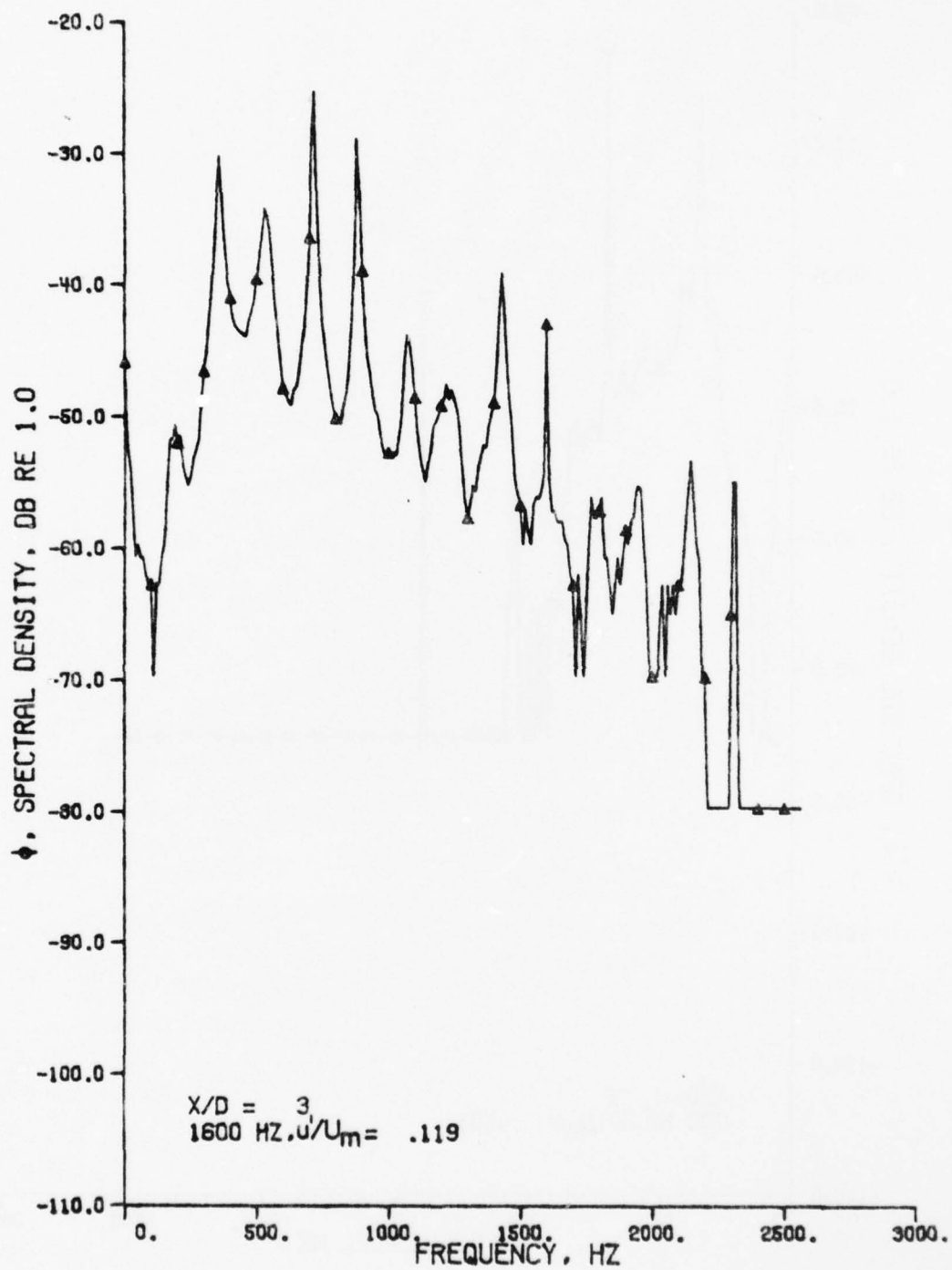


Figure IV-50 1600 Hz Case Spectrum at X/D = 3

harmonic of a subharmonic. The fundamental has the highest magnitude. The spectrum of the 1600 Hz case at  $X/D = 3$  is similar to that at  $X/D = 1$  except for the addition of a broad base and a number of higher frequency peaks. All of the peaks are spaced in the same way as at  $X/D = 1$ , including those at frequencies greater than the applied sound frequency.

The spectra at  $X/D = 5$  are presented in Figures IV-51 through IV-53. The spectra reveal small changes as compared to those at  $X/D = 3$ . The no sound spectrum is smoothed and broadened. The 700 Hz case spectrum also shows some broadening. Some of the peaks seen in the spectra at  $X/D = 3$  are buried in the broad-band component of the spectrum at  $X/D = 5$ , and the previously sharp peaks display spreading bases. The 1600 Hz spectrum exhibits similar changes. The regions between the peaks appear more "filled-in", and the magnitudes of the peaks relative to the broad band level are decreased. Beyond  $X/D = 5$ , the spectra continue to appear smoother.

The sharp peaks characteristic of the spectra at small  $X/D$ 's fade into broad band spectra as  $X/D$  increases. Figure IV-54 displays the three spectra at  $X/D = 9$ . Only a few of the original peaks are visible in the figure. The spectra at  $X/D = 15$  are shown in Figure IV-55, and the only apparent difference is in the levels of the spectra. This difference is a result of the difference in turbulence intensities of

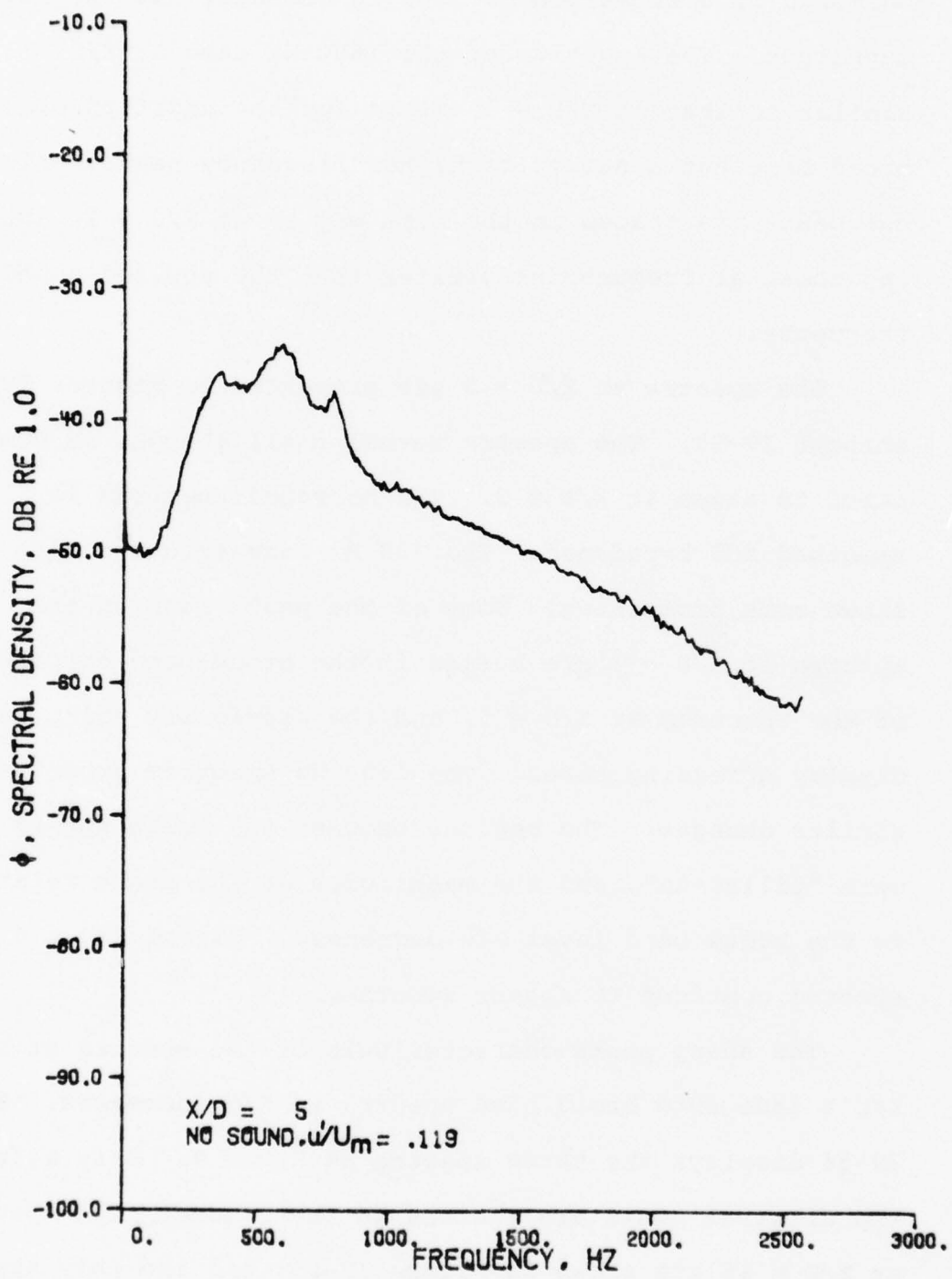
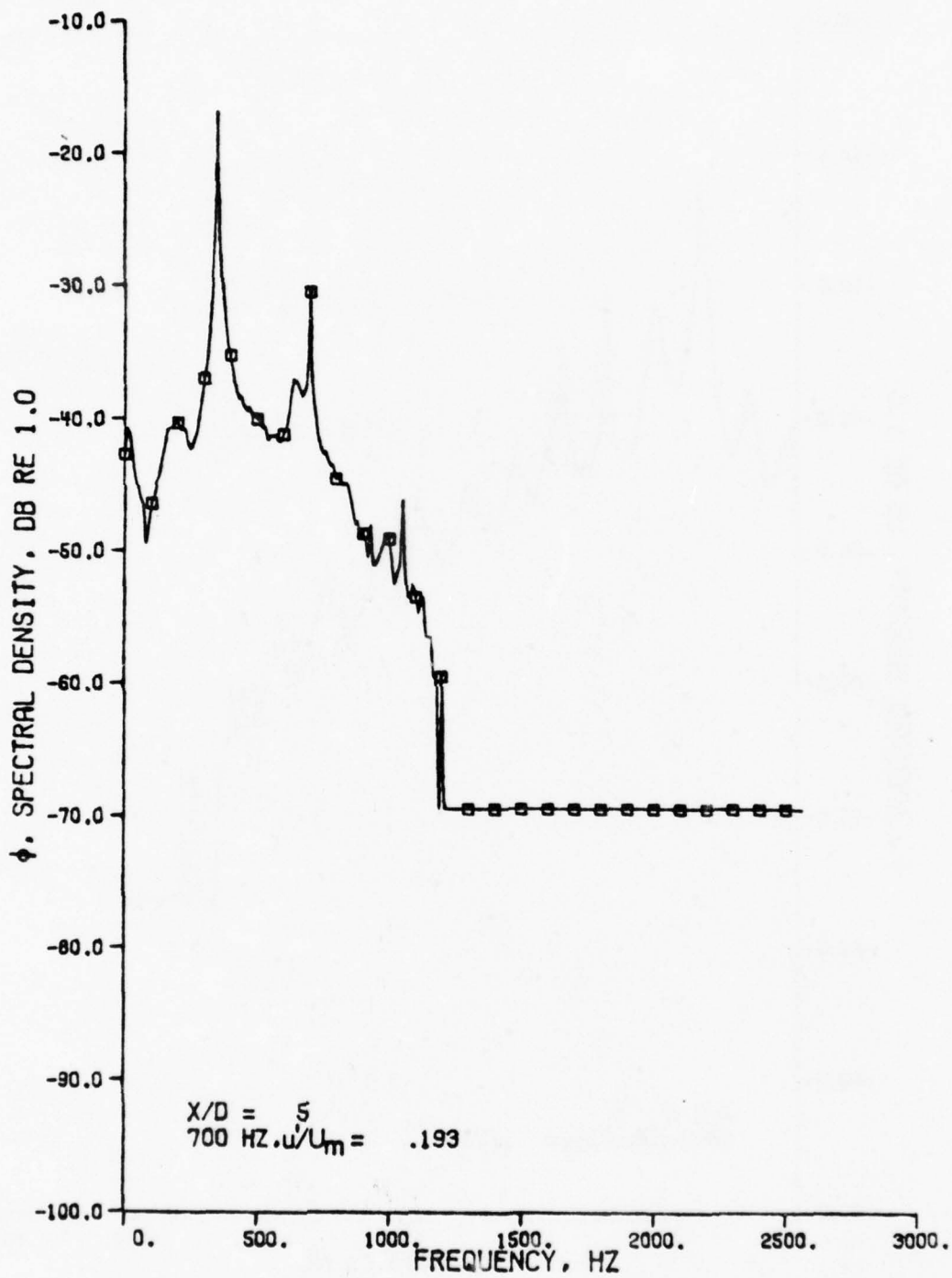


Figure IV-51 Undisturbed Case Spectrum at X/D = 5

Figure IV-52 700 Hz Case Spectrum at  $X/D = 5$

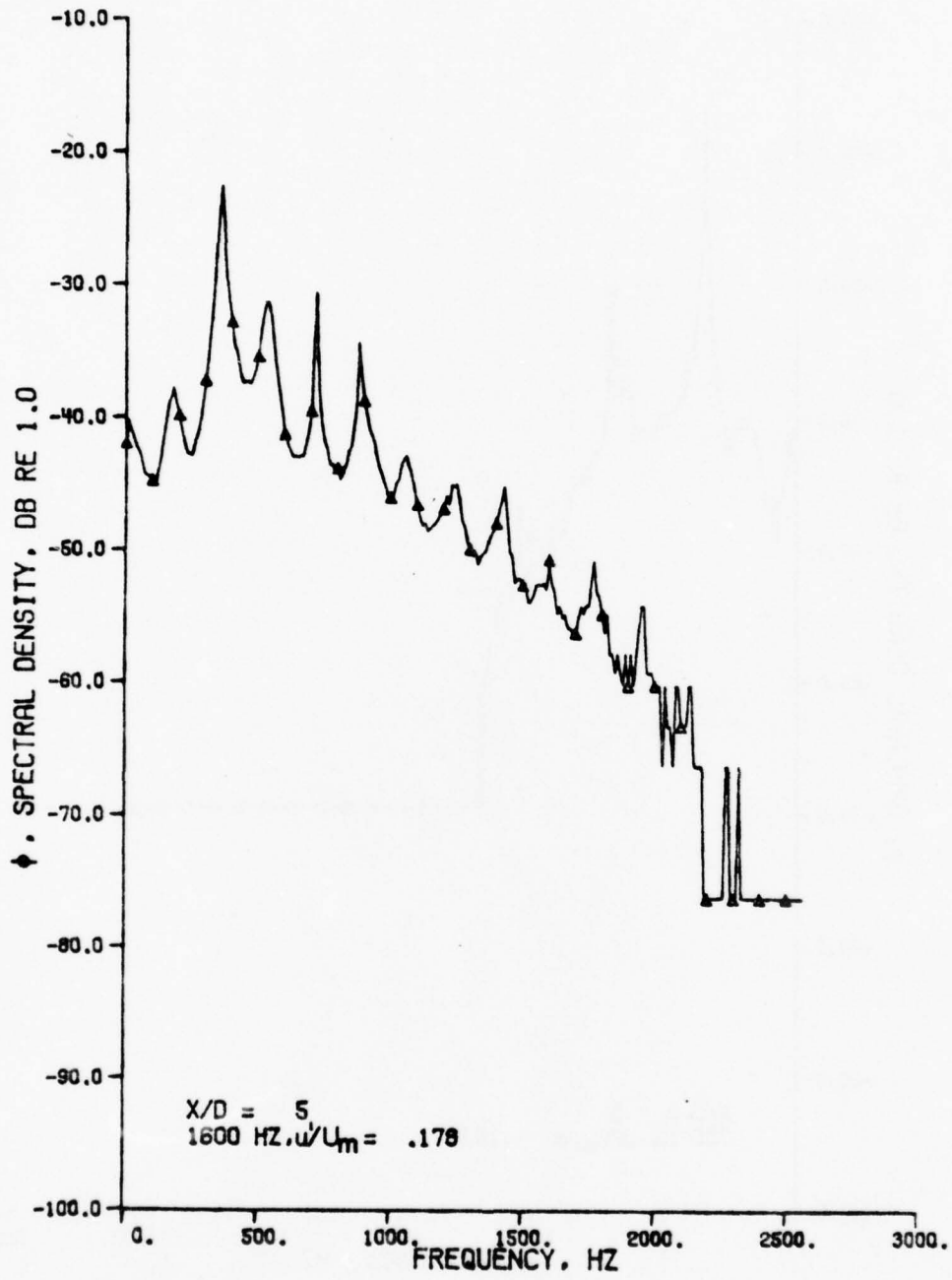
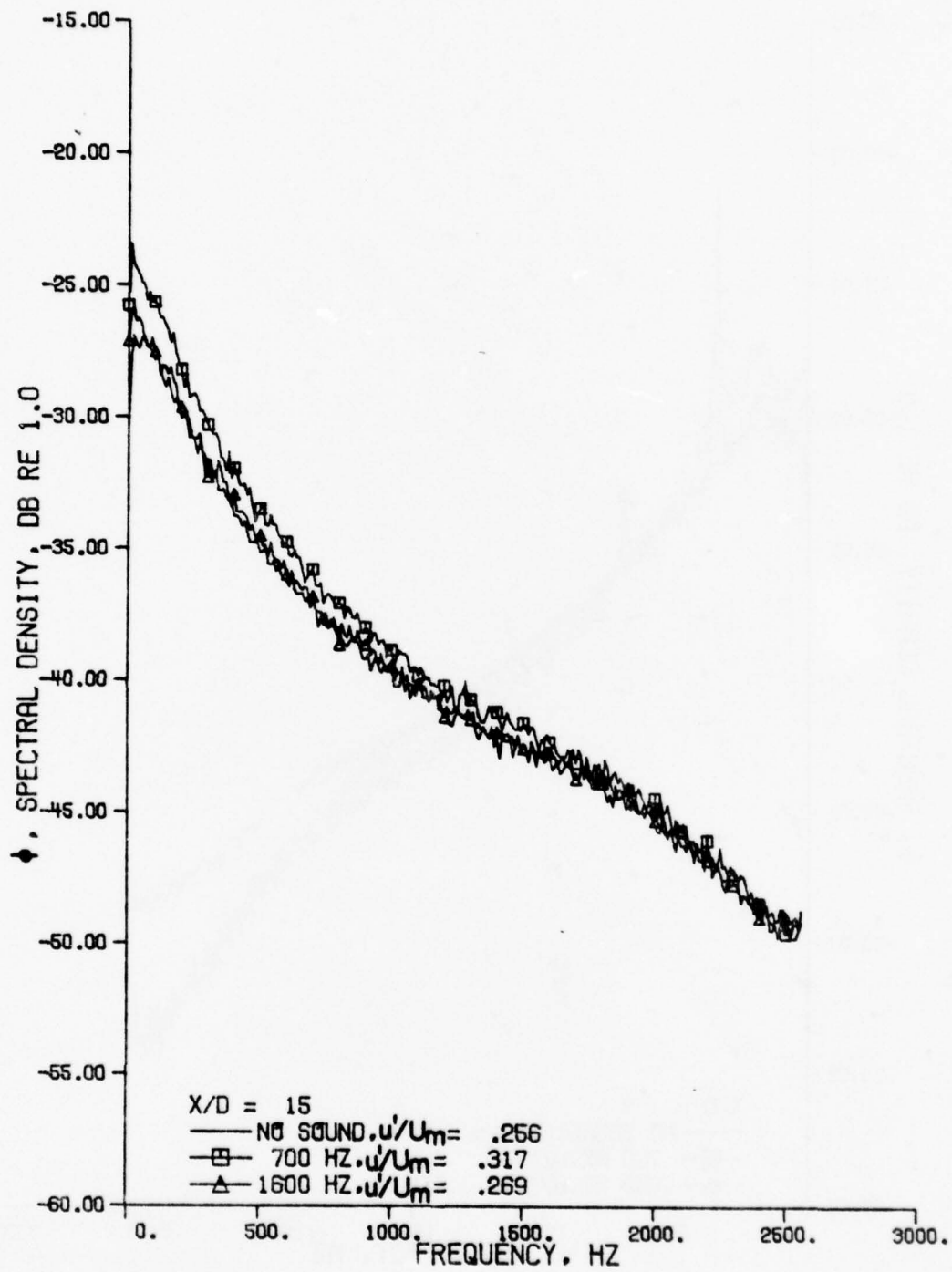


Figure IV-53 1600 Hz Case Spectrum at X/D = 5



Figure IV-55 Spectra at  $X/D = 15$

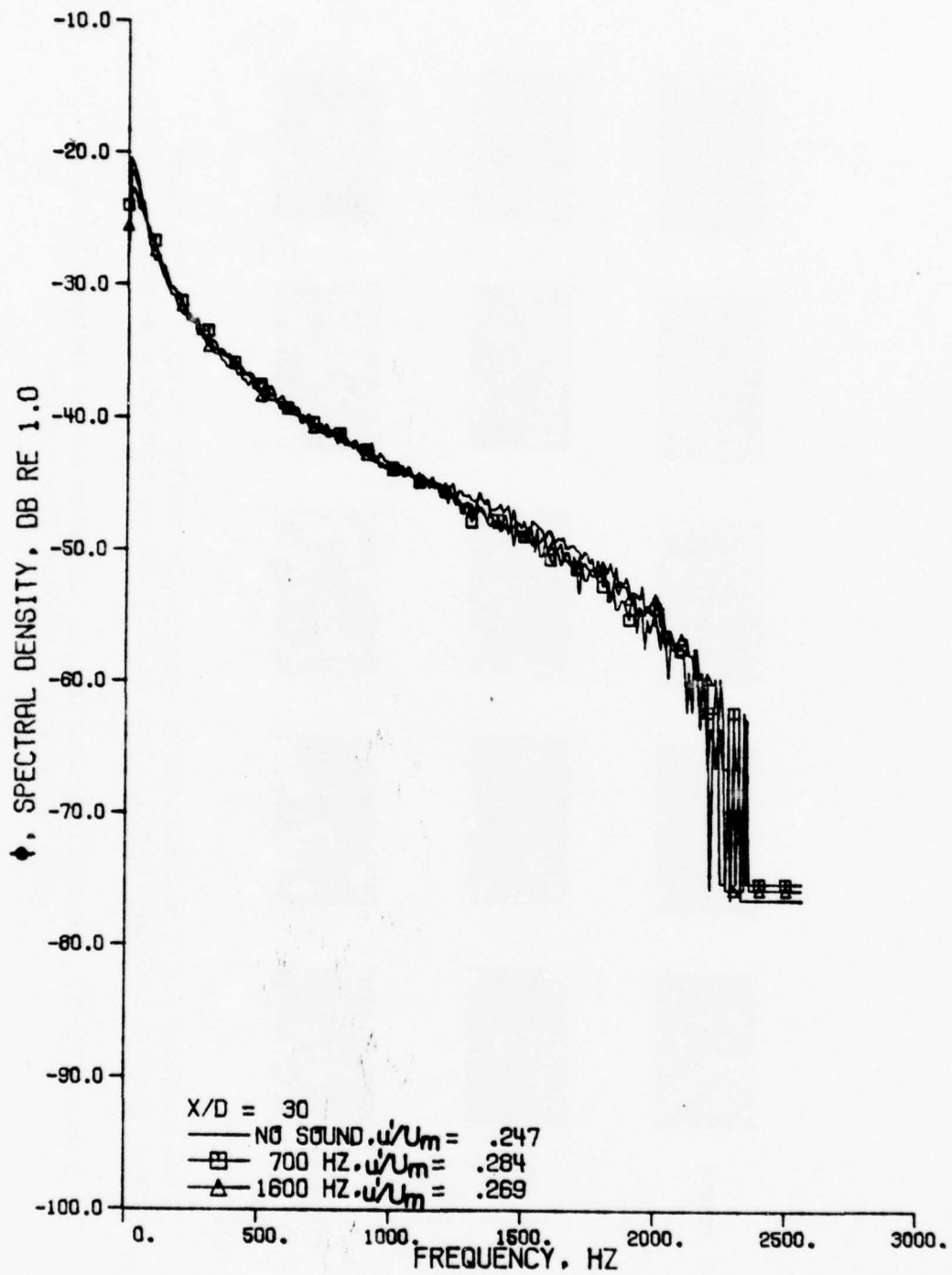
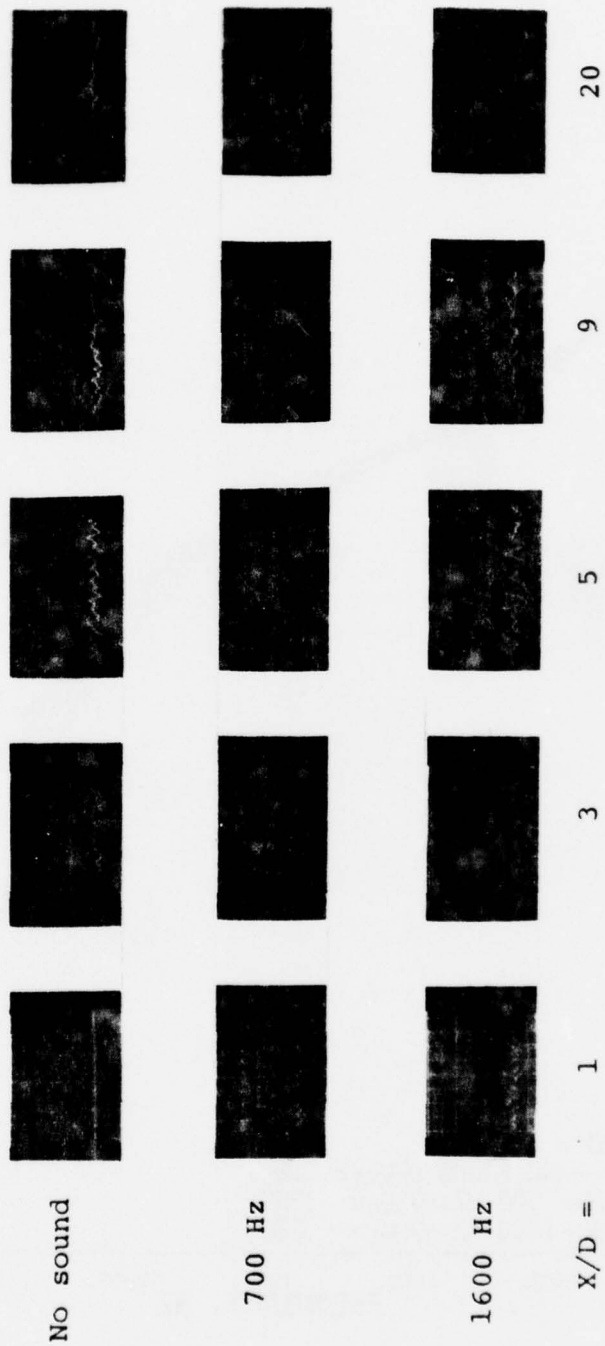


Figure IV-56 Spectra at X/D = 30



Time scales all 2 ms/division, amplitude scales vary. Disturbed case traces include oscillator signal above hot wire signal.

Figure IV-57 Oscilloscope Traces of Anemometer Output with Probe Positioned on Jet Centerline

the three cases and of the scaling chosen for the spectra. The spectra at larger  $X/D$ 's display even smaller differences and appear to tend toward similarity. The three spectra at  $X/D = 30$  are shown in Figure IV-56.

Thus the turbulence energy spectra indicate that the applied sounds produce large changes in the spectral distribution of turbulence energy in the initial region of the jet. These changes and the subsequent decay of the effect are visible in the oscilloscope traces of the turbulent velocity signals shown in Figure IV-57. The spectral changes decrease with increasing  $X/D$ , and the spectra appear to approach similarity beyond  $X/D = 30$ .

### C. Summary of Experimental Results

The results presented in this chapter describe large changes in the mean and turbulent flow structure of the jet under the influence of applied sounds. Changes in the jet widening rate, velocity decay rate, and virtual origins were observed to depend upon the frequency of the applied sounds. These effects are summarized in Table IV-18. Two frequencies which were found to produce large changes in these characteristics of the mean flow were also found to produce changes in the turbulent structure. Under the influence of these sounds, the turbulence intensities in the initial region of the jet were found to grow to higher levels than in the undisturbed jet. These higher intensities were found to be produced on the centerline and across

TABLE IV-18  
SUMMARY OF FREQUENCY DEPENDENT CHANGES IN MEAN FLOW

Strouhal Number $St_D = fd/U_0$	Widening Rate $K_1$	Geometric Origin $C_1$	Velocity Decay Rate $K_2$	Velocity Origin $C_2$
Below 0.4	Noticeable, fairly repeatable increases	Scattered with slight tendency towards downstream shifts	Tendency towards increases with some scatter	Scattered with tendency towards upstream shifts
0.4 to 0.6	Large scatter as a result of intermittent fluctuations	Very large scatter as a result of intermittent fluctuations	Large scatter with tendency towards substantial decrease near top of range	Very large scatter with tendency towards upstream shifts
0.6 to 0.87	Repeatable local maxima at harmonics of peaks below $St_D = 0.4$	Relatively repeatable with upstream and downstream shifts	Repeatable increases and decreases	Relatively repeatable large upstream and smaller downstream shifts
0.87 to 1.1	Local maxima	Local maxima	Local maxima	Local maxima
Above 1.1	Very small effects	Small effects	Very small effects	Small effects

the entire jet in the main region. They were observed to decay toward the lower levels characteristic of the undisturbed jet in the region from  $X/D = 20$  to  $X/D = 80$ . The Reynolds stress distribution behaved in a similar manner. Turbulence energy spectra revealed that the applied sound changed the spectral distribution and transfer of energy in the turbulent flow. These changes also were observed to decay, although at a faster rate.

The implications of these results are discussed in the following chapter, with emphasis placed upon comparison of these results with those in the literature, and upon formulation of a possible model of the interaction mechanism responsible for the changes.

## CHAPTER V DISCUSSION OF THE INTERACTION

The results of the measurements of the effects of sound on the plane turbulent jet were presented in the preceding chapter. In this chapter, the results are compared to measurements reported in the literature, and to the implications of the available theories of the interaction. Further characteristics of the interaction process are developed through discussion of calculations performed using assumptions of similarity, and the results of these comparisons and discussions are used to suggest a possible model of the interaction.

A. Comparison of Experimental Results to the Literature

The experimental results of the present study are compared to the results in the literature in three sections. The first considers frequency dependence results, the second mean flow effects, and the third turbulence structure effects.

1. Frequency Dependence Comparison

This section compares the measured frequency dependence of effects in the main region of the jet with various sensitive or natural frequencies reported in the literature.

The reported frequencies may be grouped into three categories. The first category includes frequencies determined through studies of disturbed jets and mixing layers. Generally, the frequencies in this category were determined through studies of gross changes in the mean flow resulting from acoustical or vibrational disturbance of the flow. The second category contains the frequencies found to exhibit maximum growth in experimental and theoretical studies of shear layer instability. Experimental instability studies often involve the use of applied sound to regulate the instability frequency and simplify measurements. Measurements over a range of frequencies reveal the disturbance frequency which exhibits a maximal growth rate in the initial region of the shear layer, where linearized equations are often applied. The third category contains frequencies determined from large scale structures. Large scale structures are relatively orderly vortex structures that occur well beyond the linear (exponential growth) region of the shear layer.

The comparison of the measured frequency dependence to frequencies reported in the literature is complicated by the different characteristic lengths used in the reported Strouhal and Reynolds numbers. The centerline mean velocity at the mouth of the jet,  $U_0$ , was used as the characteristic velocity in the present study. The nozzle slot width,  $D$ , was used as the characteristic length. A

different characteristic length is commonly used in studies of shear layer instability. This length is the shear layer momentum thickness, defined as,

$$\theta = \int_0^{\infty} \frac{\bar{U}}{U_m} \left( 1 - \frac{\bar{U}}{U_m} \right) dy \quad (V-1)$$

The instability literature suggests that the momentum thickness is most characteristic of the linear instability region in mixing layers and also in jets so long as the jet diameter is much greater than the momentum thickness. In the present study, measurements described in Appendix A indicate that  $D/\theta = 63.3$  for the undisturbed jet as well as for the jet disturbed at 700 Hz and 1600 Hz. It may be assumed that this same ratio holds for the other disturbance frequencies and hence that the nozzle width is much greater than the momentum thickness for all cases of the present study. This property implies that the momentum thickness-based Strouhal and Reynolds numbers would be most characteristic of the instability process in the present study. However, since all momentum thicknesses were not measured, the frequency dependence results were presented in Chapter IV as functions of nozzle width Strouhal number. With the apparently constant momentum thickness, these Strouhal numbers are directly proportional to the momentum thickness Strouhal numbers, being larger by the factor  $D/\theta$ . This proportionality allowed the following procedure to be used in compiling Table V-1, which

presents comparisons of the Strouhal and Reynolds number reported in the literature to the present results.

Results in the literature presented as Strouhal and Reynolds numbers based upon nozzle diameter or width are compared directly. In those cases in which the Strouhal number is presented as a function of Reynolds number, the Reynolds number of the present study, 6000, is used to obtain the corresponding Strouhal number. Results in the literature presented solely as Strouhal and Reynolds numbers based upon momentum thickness are converted to numbers based on the nozzle width of the present set-up by multiplying by 63.3. Comparison to the nozzle width Strouhal number results in Chapter IV is then equivalent to comparison to momentum thickness Strouhal numbers, for both are multiplied by the same constant. In the case of reported Strouhal numbers based on both momentum thickness and nozzle width, both numbers are presented in the table; the width-based number directly and the momentum thickness number converted by multiplication by 63.3. It is believed that the converted momentum thickness numbers are most appropriate for the comparisons due to the literature's suggestions of the nozzle width independence of the initial instability process.

Study of the tabulated Strouhal numbers reveals that they appear to fall into roughly four numerical groups. These groups are under 0.45, between 0.5 and 0.65, in the

TABLE V-1

NATURAL FREQUENCIES AND SENSITIVE FREQUENCIES REPORTED FOR FREE SHEAR FLOWS

Reference	Reynolds Number $\rho U_0 D$ $Re_D = \frac{\mu}{\rho U_0 D}$ unless otherwise indicated	Reported Strouhal Number $St_D = \frac{fD}{U_0}$ $St_\theta = \frac{f\theta}{U_0}$ or as indicated	Equivalent Strouhal Number of Present Study $St_D = \frac{fD}{U_0}$ (a)	Description
Present Study	6000 or $Re_\theta = 95$	$St_D = 0.24$ or $St_\theta = 0.0038$	0.24	Experimental shear layer natural frequency
	6000 or $Re_\theta = 95$	$St_D = 0.38$ or $St_\theta = 0.0060$	0.38	Most sensitive frequency experimentally determined
Winant and Browand (1974) and Browand and Weidman (1976)	$Re_h = \frac{\Delta U h}{\nu} = 300$ (See description)	$St_h = \frac{fh}{U} = 0.19$	3.04	Experimental mixing layer study of large scale structure. Results scaled on mean velocity difference across layer and velocity profile slope $h = \frac{\Delta U}{\left(\frac{dU}{dy}\right)_{max}}$

TABLE V-1 (continued)

Browand (1966)	$Re_{\theta} \approx 230$	$\frac{4\pi\theta f}{\bar{U}} = 0.227$	1.14	Experimental mixing layer instability study with information from Miksad (1971)
Freymuth (1966)	$42 < Re_{\theta} < 334$	$St_{\theta} = 0.017$	1.08	Experimental mixing layer instability study
Michalke (1965)	Inviscid theory	$St_{\theta} = 0.0167$	1.05	Inviscid instability theory calculation
Miksad (1972)	$Re_{\theta} = 150$	$\frac{4\pi\theta f}{\bar{U}} = 0.2175$	1.10	Experimental mixing layer instability study
	Inviscid theory	$\frac{4\pi\theta f}{\bar{U}} = 0.2216$	1.12	Spatial instability theory calculation
Becker and Massaro (1968)	$600 - 20,000$	$St_D = 0.012 Re_D^{\frac{1}{2}}$	0.93	Experimental study of disturbed round jet
Rockwell (1972) and Rockwell and Nicolis (1972)	$1860 - 10,800$	$St_D = 0.012 Re_D^{\frac{1}{2}}$	0.93	Flow visualization studies of a plane jet. Natural breakdown frequency

TABLE V-1 (continued)

Sato (1960)	1500 - 8000 or $100 < Re_{\theta} < 400$	$St_D = 0.23$ or $St_{\theta} = 0.015$	0.95	Symmetric mode of experimental plane jet instability study. Velocity profiles developed and undeveloped.
Beavers and Wilson (1970)	500 - 3000	$St_D = 0.63$	0.63	Experimental round jet vortex pattern study
Lau and Fisher (1975)	62,000	$St_D = 0.52$	0.52	Experimental round jet vortex structure study
Mattingley and Criminale (1971)	600	$St_D = 0.55$	0.55	Viscous non-linear instability theory calculation
Rockwell (1971)	6000	$St_D = 0.52 - 1.3$	0.52 - 1.3	Survey of reported round jet sensitive frequencies
Rockwell and Toda (1971)	700 - 5000	$St_D = 0.009 Re_D^{1/2}$	0.70	Experimental determination most sensitive frequencies for a disturbed attached plane jet
Sato (1960)	1500 0 8000 or $100 < Re_{\theta} < 400$	$St_D = 0.14$ or $St_{\theta} = 0.0092$	0.58	Anti-symmetric mode of experimental plane jet instability study

TABLE V-1 (continued)

Thompson (1975)	26,700	$St_D = 0.18$ or $St_\theta = 0.0093$	0.59	Experimental study of a disturbed plane jet. Disturbance frequency producing highest growth on jet centerline (Note that equivalent step was calculated using $St_\theta$ )
Wille (1963)	Inviscid theory	$\frac{f\delta^*}{U_0} = 0.0161$ (See description)	0.53	Inviscid instability theory for a plane jet using a broken line velocity profile. Frequency scaled on boundary layer displacement thickness, $\delta^*$
Beavers and Wilson (1970)	500 - 3000	$St_D = 0.43$	0.43	Experimental plane jet vortex pattern study
Crow and Champagne (1971)	> 10,000	$St_D = 0.3$	0.3	Experimental study of a disturbed round jet with a tripped boundary layer

TABLE V-1 (continued)

Hussain and Zaman (1975)	11,000 - 113,000	$St_D = 0.3$	0.3	Tripped boundary layer case of experimental study of a disturbed round jet
		$St_D = 0.4$	0.4	Untripped case of study
Kaiser (1971)	4500	$St_D = 0.38$	0.38	Experimental study of most sensitive frequency for an acoustically disturbed plane jet
	5150	$St_D = 0.37$	0.37	
	6000	$St_D = 0.42$	0.42	
Rockwell (1971)	6000	$St_D = 0.15 - 0.65$	0.15 - 0.65	Survey of reported plane jet sensitive frequencies
Roffman and Toda (1969)	200 - 4300	$St_D = 0.14$	0.14	Flow visualization study of a disturbed plane jet
Thompson (1975)	11,000	$St_D = 0.45$ or $St_\theta = 0.0061$	0.39	Experimental study of disturbed plane jet. Frequency producing highest disturbance growth in shear layer. (Note that equivalent $St_D$ calculated using $St_\theta$ )

TABLE V-1 (continued)

Vlasov and Ginevskii (1967)	30,000 - 260,000	$St_D = 0.33 - 0.54$	0.33 - 0.54	Experimental study of most sensitive frequencies of a disturbed round jet
Wille (1963)	> 15,000	$\frac{f\delta^*}{U_0} = 0.0161$	0.37	Experimental study of plane jet instability. Frequency scaled on boundary layer displacement thickness
Wooldridge, Wooten, and Amaro (1972)	26,000 - 60,000	$St_D = 0.4 - 0.5$	0.4 - 0.5	Experimental study of an undisturbed round jet with an untripped boundary layer

(a) See description of calculation procedure in text

vicinity of 0.93, and between 1.05 and 1.15. In Figure IV-2, the present study shows the greatest effects upon the widening rate at Strouhal numbers between 0.3 and 0.4, corresponding to frequencies higher than the natural frequency of  $St_D = 0.24$  determined from the measurement of the undisturbed shear layer energy spectrum. Appreciable widening rate effects are apparent for Strouhal numbers from roughly 0.1, the lowest frequencies studied, to approximately 1.0. Enhanced widening rates at 0.6 and 0.8 suggest a harmonic relationship to the Strouhal numbers producing the largest effects. A comparison of the present results with the groups apparent in the table is useful.

Mixing layer instability studies comprise the group around  $St_D = 1.1$ , where in Figure IV-2 the present study shows but one point of definitely increased widening rate. These studies by Michalke (1965), Freymuth (1966), Browand (1966), and Miksad (1971) were of laminar shear layers. The mean flow profiles of the nozzle boundary layer just upstream of the mouth of the jet in the present study reveal that the boundary layer was laminar. In addition, the initial shear layer mean velocity profile of the present study compares well to the hyperbolic tangent profile commonly found in the experimental and theoretical instability studies. These velocity profiles are described in Appendix A. Thus the findings of the instability studies

in the literature could be expected to apply to the present flow. However the present results reveal that the Strouhal numbers corresponding to the surveyed studies did not have appreciable effects upon the widening rates in the main region of the jet. These reported Strouhal numbers are considerably higher than either the most sensitive frequency or the natural frequency of the present study. The reason for the lack of agreement is discussed later in this chapter.

Three studies of jets make up the group around 0.93. Sato (1960) found a Strouhal number corresponding to 0.95 for symmetric modes of plane jet instability. Asymmetric modes, as observed in the present study, were found to occur near 0.58 by Sato. His study concentrated upon jets with fully developed (parabolic) initial velocity profiles, unlike the present study. Some of his results were for what he called "wide" jets which he indicated had less developed profiles. Rockwell and Niccolls (1972) and Rockwell (1972) reported natural breakdown Strouhal numbers corresponding to 0.93 in their experimental studies of the initial region of plane jets. This Strouhal number lies above the sensitive region indicated by Rockwell (1971) in a survey of earlier works. The present study revealed small effects upon the widening rate at this Strouhal number.

Several of the tabulated studies report sensitive frequencies in the Strouhal number range between 0.5 and 0.65. This group contains a number of studies of round jets as well as plane jets. The present study does not exhibit large effects in this range. The difference between the shear layer structure of a round jet and a plane jet may be of some significance in the effects of disturbances upon main region mean flow behavior. The shear layer sheathing the potential core of a round jet is symmetrical and tends to exhibit symmetric toroidal vortex modes. The plane jet in contrast is bounded by two separate plane shear layers. These layers do not appear to interact until they merge at the end of the potential core. Flow visualization photographs of asymmetric plane jet modes presented by Rockwell (1972) and Rockwell and Niccolls (1972) show that these asymmetric modes can produce severe distortions of the instantaneous jet velocity profiles. It appears that these distortions could produce different effects upon the mean flow behavior in the main region than could symmetric modes such as those observed in round jets. Thus it might be expected that round jets would exhibit different sensitive frequencies than plane jets. However, a number of plane jet studies also reported Strouhal numbers in the range between 0.5 and 0.65. Rockwell and Toda (1971) found a plane attached jet of the type found in fluidic devices was most sensitive

at  $St_D = 0.64$ . Sato's (1960) study of plane jet instability found asymmetric modes corresponding to  $St_D = 0.58$ . Recall that Sato's study was primarily concerned with jets with developed initial profiles. Wille (1963) used inviscid linear stability theory to predict the frequency of highest growth in a plane shear layer. This frequency corresponded to  $St_D = 0.53$  when converted for comparison to the present study. Thompson (1975) studied the growth of disturbances in the initial region of a plane jet and found that on the jet centerline, a frequency corresponding to  $St_D = 0.59$  showed the greatest growth.

However, in the same jet, Thompson found that in the shear layer, the frequency corresponding to  $St_D = 0.39$  for the present study displayed the highest growth. This frequency falls within the lowest group evident in Table IV-1, and is very close to the frequency producing the highest widening rate in the present study. The results of Wille's (1963) experimental study of plane jet instability also fall within this group. Wille's study yielded a frequency corresponding to a Strouhal number  $St_D = 0.37$ , which also compares well to the value of 0.38 found to produce the greatest widening rate in the present study. Beavers and Wilson's (1970) study of vortex growth in a plane jet also reports a frequency in this region, although their results for a round jet correspond to frequencies in the next higher frequency group in the table. The similar

Reynolds numbers and techniques employed in their study of plane and round jets does lend some support to the possibility that the frequency sensitivities of plane and round jets are different.

The study most comparable to the frequency dependence phase of the present study was that performed by Kaiser (1971) in a completely different set-up. The flow fields used in the two studies were very similar. The jets had the same width, aspect ratio, and contraction ratio, although differing in nozzle contraction shape. Sound was applied to both jets from the side of the flow field rather than upstream of the mouth, as in the case of a number of the surveyed studies. In addition, the studies were performed at the same Reynolds numbers, and the same parameter, the widening rate, was used to determine the most sensitive frequencies. Kaiser found this frequency to correspond to  $St_D = 0.38$  at  $Re_D = 4500$ ,  $St_D = 0.37$  at  $Re_D = 5150$ , and  $St_D = 0.42$  at  $Re_D = 6000$ . Recall that the present study found  $St_D = 0.38$  at the same Reynolds number of 6000. This relatively small difference in sensitive frequencies might be attributed to differences in the initial turbulent intensity and mean velocity profiles. The initial turbulent intensity at the centerline of Kaiser's jet was roughly 70% higher than that in the present study, although this still corresponded to a very low value. An initial mean velocity profile was not

measured by Kaiser, but it was indicated that the jet had a "top hat" profile similar to that of the present study. The initial shear layer thickness of the two jets likely was somewhat different as a result of the different nozzle contraction shapes. These factors could be responsible for the different behavior of the two jets. Both jets exhibited somewhat harmonic sensitivities, with the frequencies at twice the most sensitive frequency also exhibiting significantly increased widening rates. Kaiser's results displayed a more peaked nature than those of the present study shown in Figure IV-2.

Studies of large scale structure in round jets were performed by Crow and Champagne (1971) and by Hussain and Zaman (1975). In both of these very similar studies, a tripped nozzle boundary layer and acoustical disturbance upstream of the nozzle mouth were found to result in a frequency for the large scale structure corresponding to  $St_D = 0.3$ . Crow and Champagne note the inability of linear instability theory to predict this frequency. In addition, Hussain and Zaman showed that the upstream conditions play an important role in the sensitivity by finding that when the nozzle boundary layer was not tripped, the Strouhal number corresponding to the large scale structure increased to a value of 0.4.

This finding points out the important influence of the conditions upstream of the nozzle on the development of a

jet flow. A dependence upon the upstream conditions may be responsible for the wide range of reported sensitive frequencies. The results of Crow and Champagne and of Hussain and Zaman suggest another reason for the wide range of reported sensitive frequencies. The Strouhal number they found is roughly one-half the Strouhal number found for round jets by many other researchers. This relationship suggests that vortex coalescence phenomena, which lead to the formation of a one-half frequency subharmonic may be involved. Indeed, Crow and Champagne (1971) note that disturbing their jet at a frequency twice the natural frequency resulted in violent subharmonic formation. Recall that it was observed in the present study and that of Kaiser (1971) that disturbance at twice the most sensitive frequency did result in noticeably increased widening rates. It might be speculated that disturbance at such frequencies may result in the formation of strong subharmonics which are at the most sensitive frequency. These subharmonics could play a role in the observed widening rate increases. A violent subharmonic formation also is believed to be the cause of the intermittent fluctuation behavior described in Appendix C. This intermittent behavior was strongest when the flow was disturbed at a frequency of 1100 Hz, very close to twice the natural frequency of the shear layer. Harmonic relationships based upon a fundamental of  $St_D = 0.3$  also are crudely suggested by the groups in which the

AD-A071 261

PURDUE UNIV LAFAYETTE IND RAY W HERRICK LABS  
ACOUSTIC INTERACTION WITH A TURBULENT PLANE JET. (U)  
AUG 77 F W CHAMBERS, F WILLIAMS

F/G 20/4

UNCLASSIFIED

HL-77-31

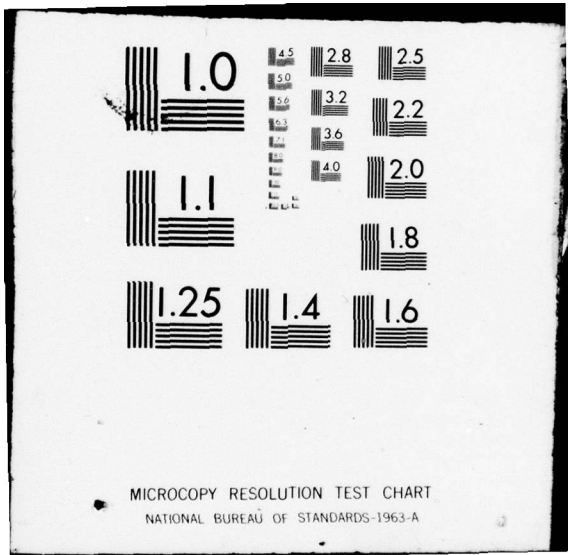
N00014-67-A-0226-0025

NL

4 of 5

AD  
A071261





tabulated Strouhal numbers fall. A further discussion of harmonic and subharmonic phenomena is presented later in this chapter in the analysis of the measured turbulent energy spectra.

The comparison of the sensitive frequencies reveals that the jet was most affected by frequencies which did not correspond to those predicted by instability theory. The dimensionless frequencies were found to correspond with some found in similar plane jet studies and round jet large scale structure studies.

## 2. Comparison of Mean Flow Results With the Literature

This section compares undisturbed and disturbed case mean flow behavior measured in the present study to that reported in the literature. The first comparison to be made is that of the undisturbed case results. The widening rates, velocity decay rates, geometric origins, and velocity origins reported for some of the major studies of turbulent plane jets are presented with those of the current study in Table V-2. It may be observed that the results for the present study are comparable to the results in the literature. The velocity origin is slightly lower than most, but is closer to the geometric origin than is the case in a number of studies in the table. It is shown in Appendix E that for a turbulent plane jet to be self-preserving, the two origins must coincide. This

TABLE V-2  
 MEAN FLOW PROPERTIES REPORTED FOR TURBULENT PLANE JETS

Reference and Comments	Reynolds Number $Re_D$	Widening Rate K1	Decay Rate K2	Geometric Origin C1	Velocity Origin C2
Present study (Ranges produced by acoustic disturbances in cases of six measured pressure profiles)	$6.0 \times 10^3$	0.094 to 0.130	0.136 to 0.236	-10.4 to -1.1	-13.4 to -0.3
Ajagu (1976)	$1.6 \times 10^4$	0.092	0.182	-0.7	3.30
Cervantes (1976)	$1.0 \times 10^4$	0.083	0.24	-6.62	4.53
Flora (1969) (Different nozzles and initial turbulent intensities)	2 to $3 \times 10^4$	0.109 to 0.130	0.158 to 0.227	-15.0	2.0
Gutmark and Wygnanski (1976)	$3 \times 10^4$	0.1	0.19	-2	4.7
van der Hegge Zijnen (1958)	$1.33 \times 10^4$	0.100	0.205	0	-1.70
Heskestad (1965)	$2.5 \times 10^4$	0.113	0.364	5.3	5.3

TABLE V-2 (continued)

Jenkins (1974) (Jet at different temperatures above ambient)	1.45 x 10 <sup>4</sup>	0.088 to 0.096	0.160	-4.5 to -2.5	4.0
Kaiser (1971) (Ranges produced by acoustic disturbance)	4.5 to 6.0 x 10 <sup>3</sup>	0.100 to 0.128	0.187 to 0.260	-4.6 to 1.2	0.0
Miller and Comings (1957)	1.78 x 10 <sup>4</sup>	0.0983	0.227	-1.572	-1.572
Mulej (1975)	1.6 x 10 <sup>4</sup>	0.095	0.185	-0.789	13.2
Ott (1972)	1 x 10 <sup>4</sup>	0.0968	0.228	-3.0	7.0
Young (1973)	1 x 10 <sup>4</sup>	0.0875	0.150	-8.75	-1.25

requirement suggests that the difference in the location of the two origins may be of greater significance than the individual locations. The differences between the undisturbed mean flow parameters of this study and those in the literature may be attributed to different flow conditions upstream of the mouth.

The belief that these conditions control the downstream development of the jet is widely held, although the mechanism of this control is not understood. Flora and Goldschmidt (1969) performed a study which showed that different turbulent intensities upstream of the mouth did result in different mean flow development. Gutmark and Wagnanski (1976) note that these upstream conditions appear to have an effect upon both mean flow parameters and turbulent intensity distributions. They also observe that there is a very small amount of evidence suggesting that these conditions may exert an influence upon the form of the self-preserving flow far downstream in the jet. This observation leads to the conclusion that all jets may not approach the same asymptotic universal self-preserving state, and the exact agreement of results from different jets cannot be expected. These differences between various jets are, however, sufficiently small that qualitative and quantitative comparisons are meaningful.

The undisturbed jet has been found to compare well to other undisturbed jets. The comparison of the mean flow

behavior of the disturbed jet to that reported for other disturbed jets may now be considered. Rockwell's (1971) survey of disturbed jets revealed that the most common effect of a disturbance near the most sensitive frequency is an increase in the jet mean velocity profile width and a decrease in the centerline mean velocity. Such changes can result from various combinations of changes in the virtual origins, the widening rate, and the decay rate.

In the present study, the tendencies were for the geometric and velocity origins to shift upstream; the widening rate to increase, and the velocity decay rate either to increase or decrease when the jet was disturbed at frequencies near the most sensitive frequency. These changes resulted in disturbed mean velocity profiles similar to those described in Rockwell's (1971) survey, and reported by Vlasov and Ginevskii (1967), Becker and Massaro (1968), Roffman and Toda (1969), Rockwell and Toda (1971), Kaiser (1971), Crow and Champagne (1971), Thompson (1975), and Hussain and Zaman (1975). A comparison of the results of the present study to those of Kaiser (1971) is of particular interest due to the similarity of the conditions of the studies. Kaiser found increases in widening rate, upstream and downstream shifts of the geometric origin, no change in the velocity origin, and both increases and decreases in the velocity decay rate in the region near the most sensitive frequency. The behavior of the

origins exhibits a difference between the two flows. Kaiser found no change in the velocity origin and downstream shifts of the geometric origin at the most sensitive frequency, while the present study did find appreciable shifts of the velocity origin and upstream shifts of the geometric origin at the most sensitive frequency. The comparison improves when it is noted that Kaiser did find upstream shifts of the geometric origin at frequencies close to the most sensitive frequency. The magnitudes of the effects are also comparable. Kaiser found maximum widening rates approximately twenty per cent greater than the undisturbed case, and the present study found maximum increases of roughly twenty-five per cent. The errors involved in these measurements are approximately five per cent, so the comparison is quite good. Kaiser found no cases of decreases in the widening rate, while some were observed in the present study. The present study involved measurements at a considerably larger number of frequencies than that of Kaiser and thus may have found effects missed in the wider unmeasured frequency gaps in his measurements. In addition, some of the widening rate decreases in the present study occurred in the region of intermittent fluctuations described in Appendix C. The measurements in this region are characterized by greater errors than those in other frequency regions. A more important difference between the two studies involved the effects produced

by disturbance at relatively high frequencies.

Rockwell (1972) characterized the disturbance of jets by five frequency regimes. He found that disturbance at frequencies higher than three to four times the natural frequency of the jet produced no appreciable effect. He termed this the "upper zone regime." The results of the present study show no effects at frequencies beyond three times the most sensitive frequency, and thus are in agreement with Rockwell's findings. Kaiser (1971) on the other hand, found increased widening at frequencies up to five times the most sensitive frequency. The widening was of course frequency dependent, and Kaiser's results have a harmonic appearance. The present results do not exhibit such a clearly harmonic nature. Harmonics of the frequencies of the relative maxima of the widening rate in the region near the most sensitive frequency ( $St_D = 0.3 - 0.4$ ) do appear to produce increased widening rates. This behavior is suggested by Figures IV-2 and IV-6. The second figure suggests multiple harmonics based upon a fundamental frequency corresponding to a Strouhal number of approximately 0.07. However, a comparison of the two figures and consideration of the scatter present in the data suggests great caution in applying such an interpretation.

Rockwell (1972) calls the regime between the frequency of maximum sensitivity and the upper zone regime the "preservation" regime, for he found that disturbance of the

jet at frequencies in this regime extended the length of the potential core. It would be expected that in this case the virtual origins would be shifted downstream. Figures IV-5 and IV-9 do suggest such a shift of the velocity origin in the vicinity of  $St_D = 0.8$ , while Figures IV-3 and IV-7 exhibit very small shifts of the geometric origins. Kaiser's geometric origins exhibit weak downstream shifts in this frequency region. Such shifts of the geometric origin would result in narrower mean velocity profiles at points downstream in the jet. Rockwell (1971, 1972) and Vlasov and Ginevskii (1967) report that narrowed profiles are found in jets disturbed in this frequency range. A narrowing of the profile could also be the result of a decrease in widening rate. Kaiser (1971) did not find any cases of decreased widening rate, but at some frequencies very small decreases were observed in this region in the present study. Thus the present study and Kaiser's similar study exhibit only very small indications of preservation regime behavior. A possible reason for this lack of agreement may lie in the vortex structure of the jets. Rockwell's (1972) jet exhibited symmetric vortex modes, while the jet used in the present study appeared to exhibit anti-symmetric modes. The modal behavior of the present study was not determined very adequately, but it is useful to consider the possible differences resulting from anti-symmetric behavior. Photographs of such behavior in

Rockwell's paper suggest that the anti-symmetric modes produce greater lateral distortion of the flow in the initial region than do the symmetric modes which for this reason appear more likely to preserve the potential core.

Disturbance frequencies less than approximately one-third the most sensitive frequency comprise what Rockwell (1972) terms the forced fusion regime. He observed that mean velocity profiles had been found to widen with disturbance in this frequency region. The present study included only a few frequencies which fall in this region, and the lowest of them do not exhibit appreciable changes in widening rate or geometric origin, the parameters controlling the profile width. Beginning at frequencies corresponding to about one-third the most sensitive frequency, appreciable increases in widening rate may be observed. The present results do not include a sufficient number of points to make a valid conclusion about agreement with hypotheses about the forced fusion regime. Kaiser's (1971) results did not extend to this range.

The differences between the observed results and those surveyed in the literature may be attributed to several sources. First, as discussed previously, the initial conditions of the flow play a role in the flow development which is not understood clearly at the present time. These conditions also appear to play an important role in the effects of disturbances upon the jet. In the study of the

intermittent fluctuation phenomenon described in Appendix C, various devices were placed upstream of the jet nozzle changing these conditions. It was found that the jet could be made more sensitive or apparently insensitive to disturbances through these changes. A second source of differences is the physical environment of the study. This environment may effect the sensitivity of the jet to disturbances. Low level background noise or vibrations might not in themselves disturb the flow, but perhaps could alter its sensitivity to other disturbances. The present study was conducted in an anechoic room isolated from building vibrations by a separate foundation, and hence may be considered to be very well isolated with low background noise and vibration levels. Kaiser's (1971) similar study also was performed in an anechoic room, although one not as well vibration isolated. Other studies did appear to take care to reduce background noise and vibration levels, although background conditions were not as well controlled. A third cause of differences may be the way in which the jets were disturbed. Some were disturbed by resonances induced in the plenum upstream of the nozzle, others by loudspeakers outside the nozzle; and others were water jets disturbed by pressure waves produced by an oscillating bar. The various methods may be assumed to result in appreciably different spatial distributions of the disturbance levels, and corresponding differences in symmetry. Morkovin and Paranjape's (1971)

study led them to conclude that the spatial pressure gradient at the nozzle lip is the parameter truly representative of the effective disturbance level. The role of the disturbance level is discussed by Rockwell (1971), Rockwell and Toda (1971) and Hussain and Zaman (1975). It has been reported, and confirmed in the present study of intermittent fluctuations, in Appendix C, that the effect of the disturbance level may indicate both a threshold and a saturation level. These levels may differ for different frequencies, and hence in a study such as the present one in which the disturbance level was held constant for all frequencies, various frequencies may have been disturbed at levels ranging from below their threshold level to above their saturation level. Thus comparisons of various studies, each with its own spatial disturbance distribution and disturbance level, would appear likely to be characterized by less than perfect agreement.

Substantial agreement with the literature was found. Similar gross changes in the flow field were observed in the region near the most sensitive frequency. Also in agreement, no appreciable effects were observed at relatively high frequencies. At intermediate frequencies, increased widening rates were observed at some frequencies. These frequencies corresponded to the first harmonics of frequencies which produced large effects in the region near the most sensitive frequency. This behavior differs from

some reports in the literature, but generally agrees with Kaiser's (1971) study. At the lowest frequencies studied, no appreciable effects were observed. Immediately above these frequencies, widening rates were found to increase as the literature suggests. Considering the numerous factors contributing to differences in the studies surveyed, it may be concluded that the mean flow results compare reasonably well to the literature, and particularly to Kaiser's (1971) very similar study.

### 3. Comparison of Turbulent Characteristics with the Literature

The results of measurements of parameters which describe the turbulent flow field were presented in Chapter IV. Distributions of the longitudinal turbulent intensity, the lateral turbulent intensity, the Reynolds shear stress, and the turbulent energy spectra were reported. In this section, these results are compared to the results of similar studies available in the literature. The available studies do not include reports of measurements of lateral intensities or Reynolds stresses in the main region of disturbed jets, and consequently these results of the present study are compared only to results for undisturbed jets.

Studies of undisturbed turbulent plane jets by Bradbury (1965), Heskestad (1965), and Gutmark and Wygnanski (1976) are used in the comparisons. These studies are among the most thorough recent studies, and contain much

information about the turbulent characteristics of plane jets. The distributions of the turbulent intensities along the jet centerline are among the most basic of these characteristics, and the three studies all report these distributions of the longitudinal intensity. These results are shown in Figure V-1 along with the disturbed and undisturbed case distributions reported in the present study and in that of Kaiser (1971). The distributions of the first three studies exhibit smooth growth to asymptotic levels characteristic of self-preserving states, while those of Kaiser and the present study show early peaks followed by continued slow development. A number of reasons for these differences may be considered.

Bradbury's measurements were performed in a jet exhausting into a low velocity co-flowing stream, and this somewhat different physical situation must limit conclusive comparisons with his results. The major portions of the studies of Heskestad and of Gutmark and Wygnanski were performed at Reynolds numbers somewhat higher than those of Kaiser and the present study. However, Heskestad did investigate the effects upon the intensity distribution of changes in Reynolds number, with his results extending to a lowest Reynolds number of 4700, lower than the value of 6000 used in the present study and that of Kaiser. Heskestad's results indicate that the shape of the intensity distribution is not changed but that the downstream

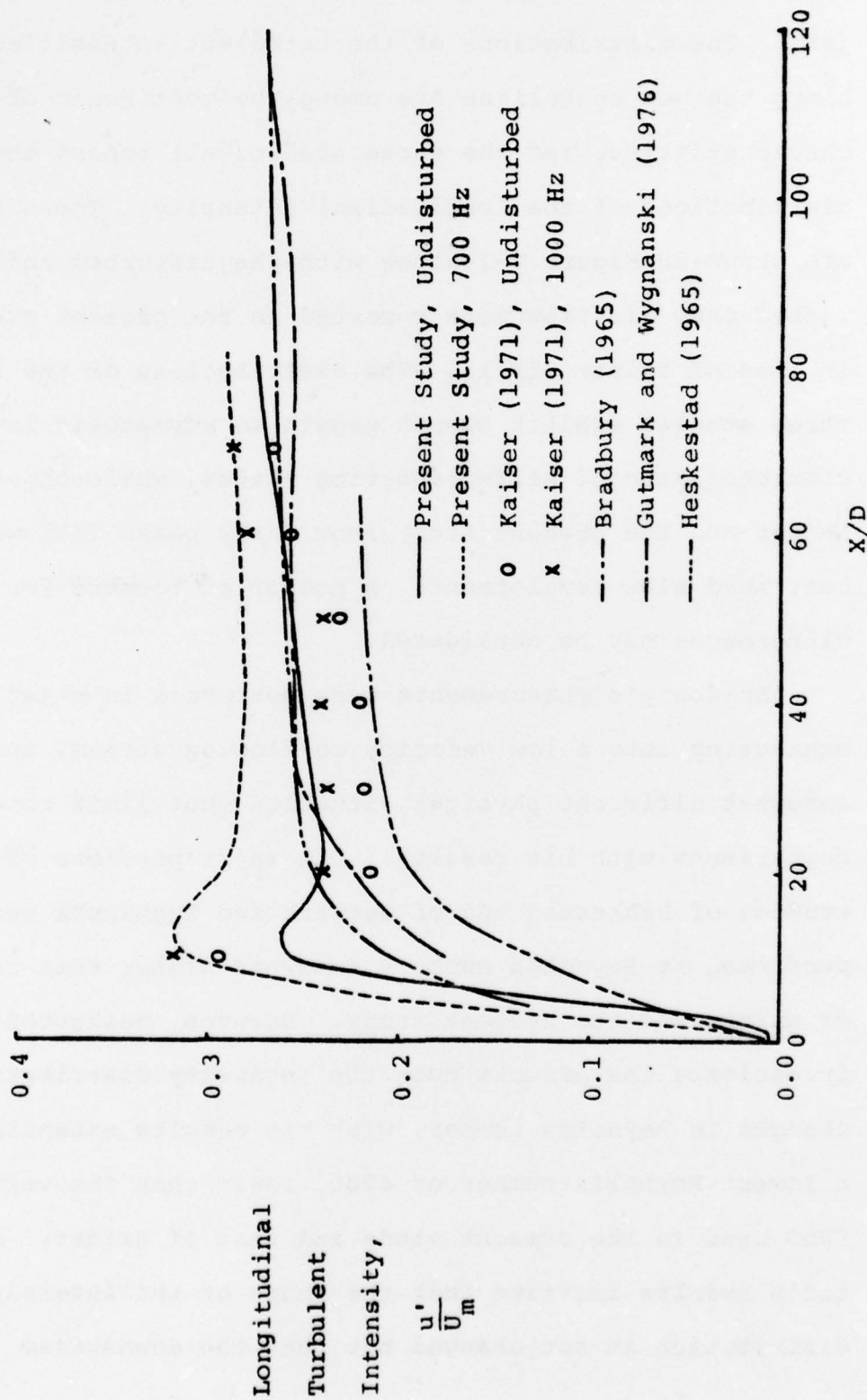


Figure V-1 Longitudinal Turbulent Intensities Along Jet Centerline

asymptotic level increases with decreases in the Reynolds number. Another factor which may explain the differences in the shapes of the intensity distributions is the velocity profile at the mouth of the jet. Heskestad's nozzle had a contraction ratio of only two, and resembled an orifice plate. It is believed that Heskestad's initial velocity profile was more developed than the top hat profiles of Kaiser and the present study. This difference might exert a significant influence upon the flow development in the initial region of the jet. The nozzle used by Kaiser had the same contraction ratio as that used in the present study, and inspection of Figure V-1 reveals that both the disturbed and undisturbed distributions of Kaiser display distributions similar to those of the present study. The disturbed case distribution of Kaiser in Figure V-1 resulted from a disturbance at 1000 Hz, the most sensitive frequency of his study. The 700 Hz disturbed case intensity distribution of the present study is shown in the figure. Another similarity between the two studies is that in both, the disturbance was found not to increase the initial turbulent intensity at the mouth of the jet.

Thus the present study and that of Kaiser, performed in very similar jets, do display very similar longitudinal intensity distributions along the jet centerline. These distributions differ from those of Bradbury (1965),

Heskestad (1965), and Gutmark and Wygnanski (1976) primarily in exhibiting early peaks followed by very slow approaches to an asymptotic self-preserving level. The intensity distributions of the present study do appear to be accurate indications of the behavior of the flow. The measurements were studied in an attempt to uncover possible errors. The effect of using the slope of the non-linearized hot wire calibration curve at the mean velocity point to calculate the turbulent intensity was investigated and found to be small. The calculated intensities were compared to intensities obtained graphically, and found to differ by less than two per cent. The distributions of the intensity non-dimensionalized by the mean velocity at the mouth rather than the local centerline mean velocity were also studied and found not to exhibit any irregularities or unusual behavior. It is believed that the difference between the peaked intensity distributions of Kaiser and the present study and the smoother distributions of other reviewed plane jet studies lies solely in the relationship between the turbulent growth and the centerline mean velocity decay. In Kaiser's and the present study, the relationship was such that the ratio of the root mean square of the longitudinal velocity fluctuations to the local centerline mean velocity reached a peak near  $X/D = 12$ , while in the other studies the relationship was such that no peak was formed.

The 700 Hz case longitudinal intensity distribution may be observed in Figure V-1 to compare well to Kaiser's most sensitive frequency case. Comparisons to other disturbed jet results may also be made. Vlasov and Ginevskii (1967) found that when disturbed at  $St_D = 0.38$ , the intensity distribution of their round jet grew faster and reached higher magnitudes than when undisturbed. Crow and Champagne (1971), Binder and Favre-Marinet (1973), Thompson (1975), and Hussain and Zaman (1975) reported similar effects in the initial region of their jets. Thompson did not report an undisturbed case, but comparison with lower Strouhal number cases having smaller effects suggests that the behavior was similar. Thus the reviewed studies and the present study agree in reporting two effects of disturbances near the most sensitive frequency on the longitudinal intensity distribution on the centerline. The first effect is a faster growth of the intensity near the mouth, and the second is that a higher magnitude is reached. Only Kaiser and the present study presented results in the main region of the jet, and these results indicate that the higher magnitudes continue at least to  $X/D = 60$ .

The axial distributions of the lateral component of turbulent intensity measured in the present study exhibit distributions similar to those of the longitudinal intensity. The undisturbed and the 700 Hz disturbed case lateral intensity distributions of the present study are

compared to the results of Gutmark and Wygnanski's (1976) study of an undisturbed jet in Figure V-2. It may be observed that the shapes of the distributions differ in the same ways that the longitudinal intensity distributions differ. The reason for the differences would appear to be the same; a different relation between the growth of turbulence and the mean velocity decay.

The centerline distribution of the intensities is not necessarily indicative of the growth of the entire turbulent flow, and for this reason, the present study included measurements of the transverse distributions of the lateral and longitudinal intensities at three  $X/D$  locations in the main region of the jet. The results of these measurements may be compared to those of the three previously reviewed studies of undisturbed jets. The transverse profiles reported in these studies were measured in the self-preserving region of the flow. The measurements of the present study were performed before the flow had reached a self-preserving state, but at  $X/D = 60$  the flow was close to self-preservation and the profiles at this location are assumed to be comparable.

The transverse profiles of the longitudinal intensities measured in undisturbed jets by Bradbury (1965), Heskestad (1965), and Gutmark and Wygnanski (1976), are compared in Figure V-3 to a fourth order polynomial fit to the undisturbed longitudinal intensities measured at

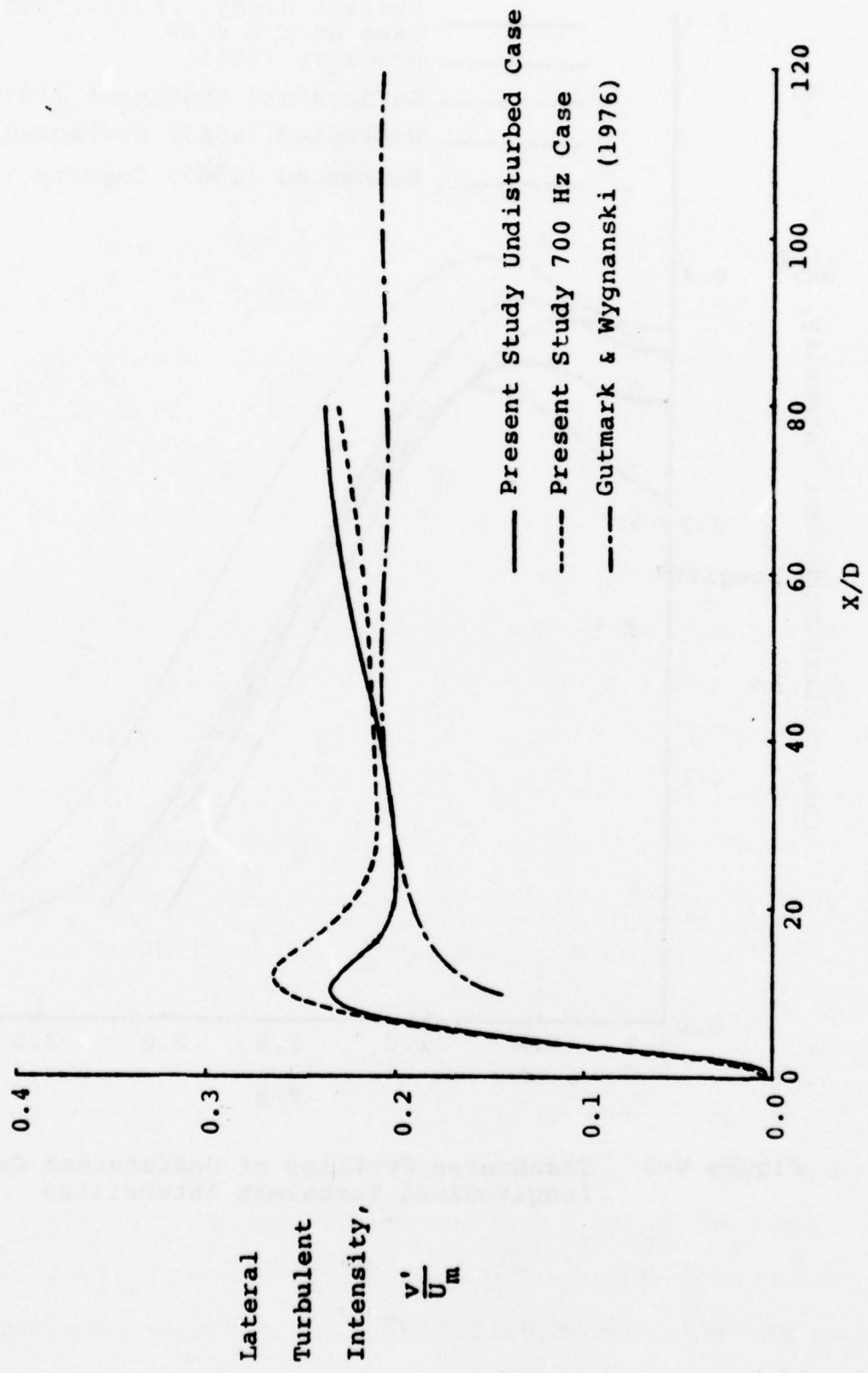


Figure V-2 Lateral Turbulent Intensities Along Jet Centerline

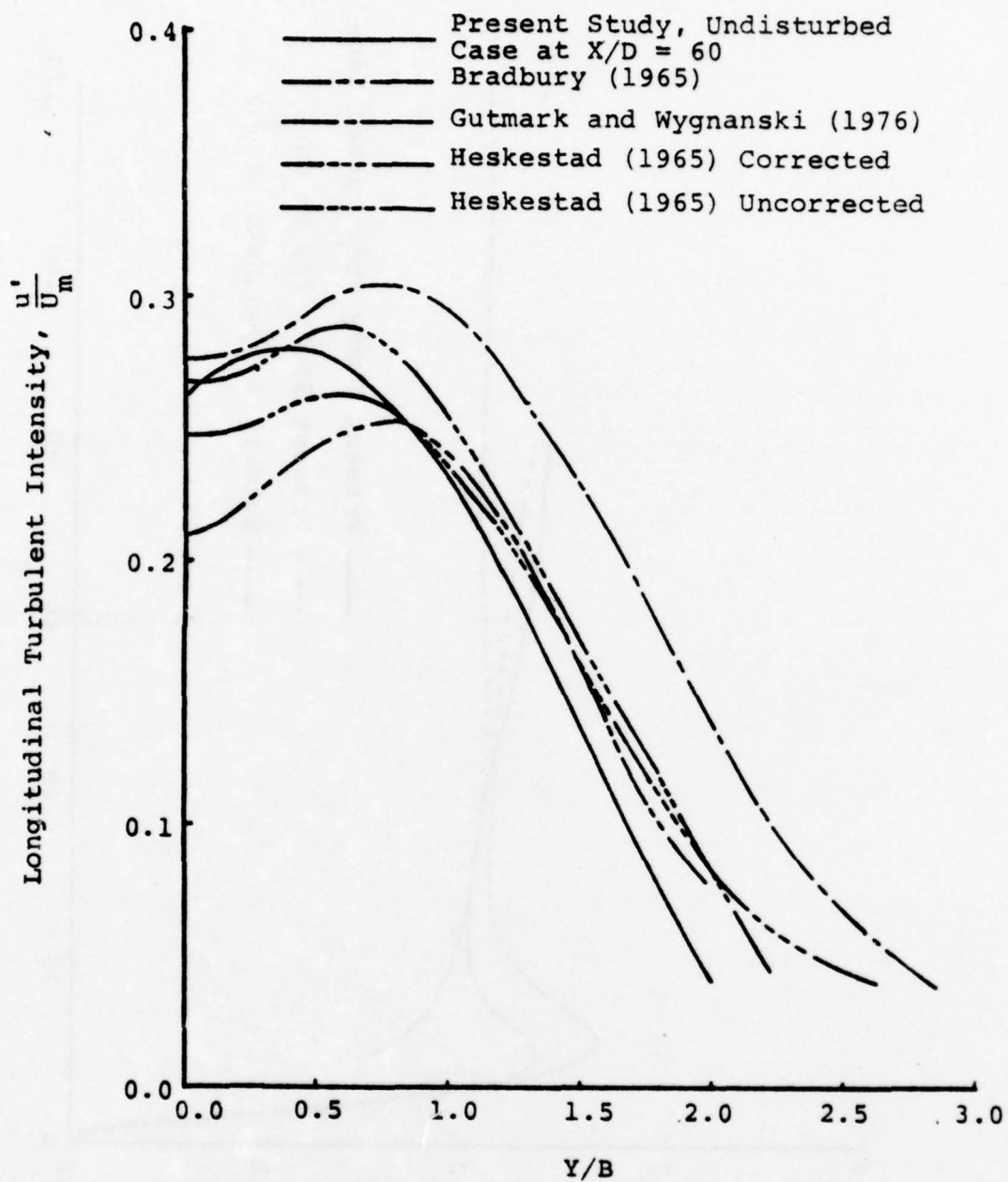


Figure V-3 Transverse Profiles of Undisturbed Case Longitudinal Turbulent Intensities

$X/D = 60$  in the present study. Note that as a result of the small number of points used to generate this curve, it lacks the inflection point near the centerline displayed by the other curves in the figure. Aside from the inflection point, the shapes of the profiles may be observed to be in general agreement, with the largest differences being in the magnitudes at large values of  $Y/B$ . A number of factors may account for the differences. One factor is the different initial conditions of the flows in the various studies, and another is the lack of self-preservation in the present study. The results of the present study were not corrected for finite three-dimensional levels of turbulence, and these levels do contribute to errors in the uncorrected intensity. The importance of these corrections may be seen in the corrected and uncorrected profiles of Heskestad shown in the figure. In addition, the measurements in the present study were performed with non-linearized hot wires, and this non-linearized operation also contributes to errors in the measured turbulent intensity. This non-linearized error is largest near the edges of the jet, where the turbulent intensity non-dimensionalized by the local mean velocity is high. Note again that Bradbury's measurements were performed in a jet exhausting into a co-flowing stream, and are not completely comparable. Despite these factors contributing to the variations between the longitudinal

intensity profiles of the reviewed studies and the present study, the profiles may be considered to be in general agreement.

The agreement of the lateral intensity profiles of the reviewed studies and a curve fit to the undisturbed lateral intensity points measured at  $X/D = 60$  in the present study may be examined in Figure V-4. The profile of the present study may be observed to compare well to that of Gutmark and Wagnanski in the central region of the jet, and have a shape similar to the profile of Bradbury (1965), although at a lower level. The influence of the co-flowing stream in Bradbury's measurements likely is responsible for the higher levels. Heskestad's (1965) profile exhibits a considerably different shape, which Gutmark and Wagnanski speculate to be an effect of drafts in the room surrounding his experimental apparatus. Their experimental set up was surrounded by wire mesh screens in order to reduce the effects of such drafts upon the edges of the flow. The present study's experimental set up was confined within a closed anechoic room, and also would seem to have been protected from drafts. The good agreement with the profile of Gutmark and Wagnanski supports this contention. It may then be concluded that the present study's transverse profiles of the longitudinal and the lateral intensity do, in the undisturbed case at  $X/D = 60$ , display general agreement with the results in the literature.

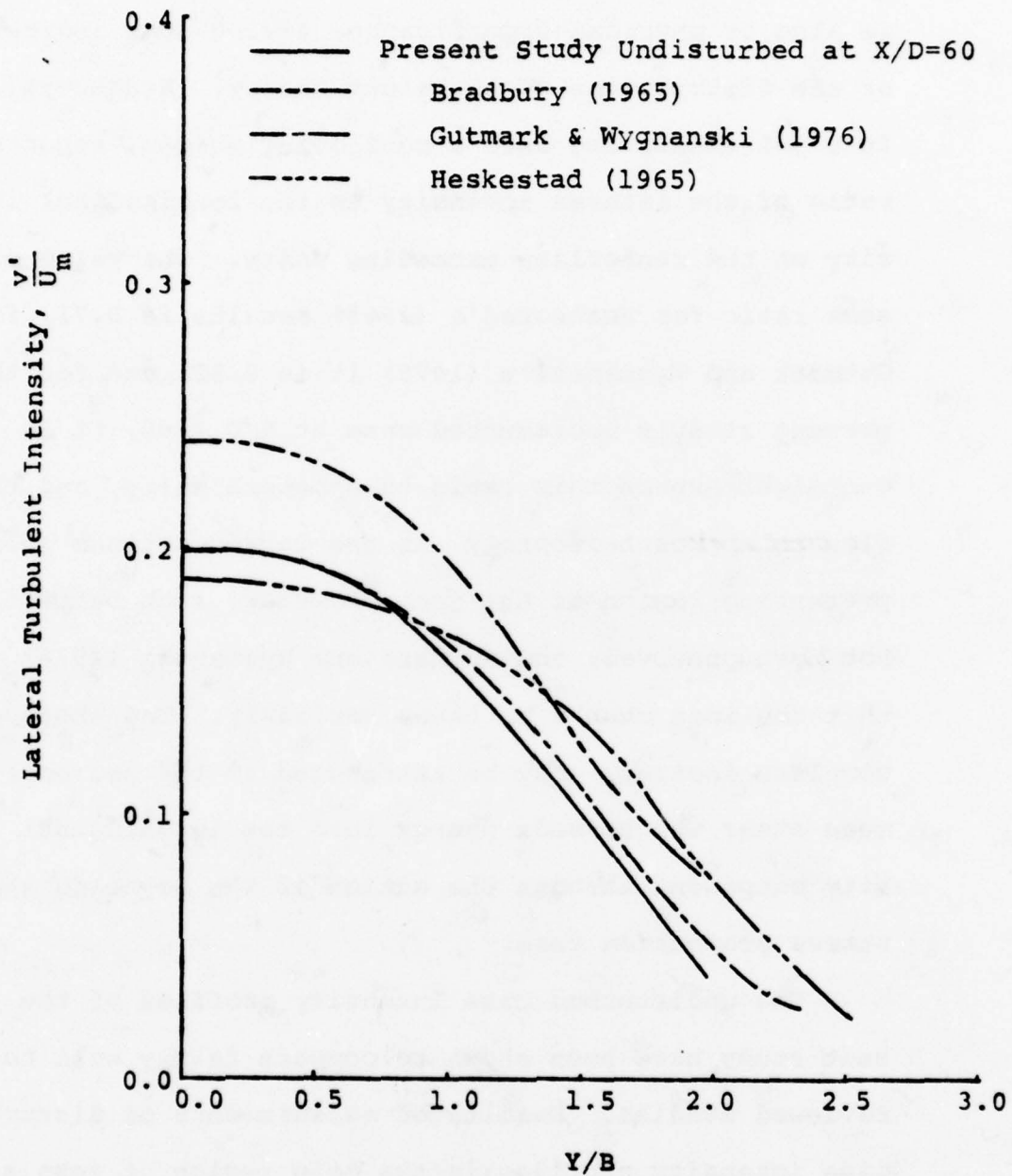


Figure V-4 Undisturbed Transverse Profiles of Lateral Turbulent Intensities

The two intensities have thus far been treated separately. The ratio of the two intensities on the centerline is also of physical significance, giving some indication of the distribution of turbulent energy. Bradbury (1965), in a jet exhausting into a co-flowing stream, reports a ratio of the lateral intensity to the longitudinal intensity on the centerline exceeding unity. The value of the same ratio for Heskestad's (1965) results is 0.71, for Gutmark and Wygnanski's (1976) it is 0.82, and for the present study's undisturbed case at  $X/D = 60$ , it is 0.75. One might expect this ratio to approach unity, and the flow to approach isotropy in the far downstream self-preserving region of the jet. However, such behavior has not been observed, and Gutmark and Wygnanski (1976) comment that the idea cannot be taken seriously. The absence of complete isotropy may be attributed to the presence of a mean shear which feeds energy into the longitudinal intensity component through the action of the Reynolds shear stress production term.

The undisturbed case intensity profiles of the present study have been shown to compare fairly well to the reviewed studies. Results of measurements of disturbed case intensity profiles in the main region of jets are not available for comparison with the results of the present study. Consequently comparisons are made only to the undisturbed profiles previously discussed, and to reported

intensity profile measurements in the initial region of disturbed jets.

Fourth order polynomial curves were fit to the longitudinal intensities measured at  $X/D = 20$  and  $X/D = 60$  in the 700 Hz disturbance case of the present study. These curves are compared to the undisturbed longitudinal intensity profiles of Bradbury (1965), Heskestad (1965), and Gutmark and Wygnanski (1976) in Figure V-5. It may be observed that these disturbed case profiles are greatly increased in the central region of the jet, while exhibiting smaller changes in the outer region. These profiles are based upon the disturbed case velocity half-widths. Note that in going from  $X/D = 20$  to  $X/D = 60$ , the shapes of the disturbed profiles inside  $Y/B = 0.5$  undergo large changes.

The saddle-shaped profiles of the longitudinal intensity are characteristic of plane jets. Gutmark and Wygnanski suggest that this profile is a result of the flow in the initial region. Within the first five jet widths, the longitudinal intensity profile is composed of a central region of low turbulence, the potential core, bounded by two highly turbulent mixing layers. At the end of the potential core, the mixing layers merge, and further development continues into the main region of the jet. Gutmark and Wygnanski hypothesize that the limited ability of turbulence to adjust to local conditions allows this

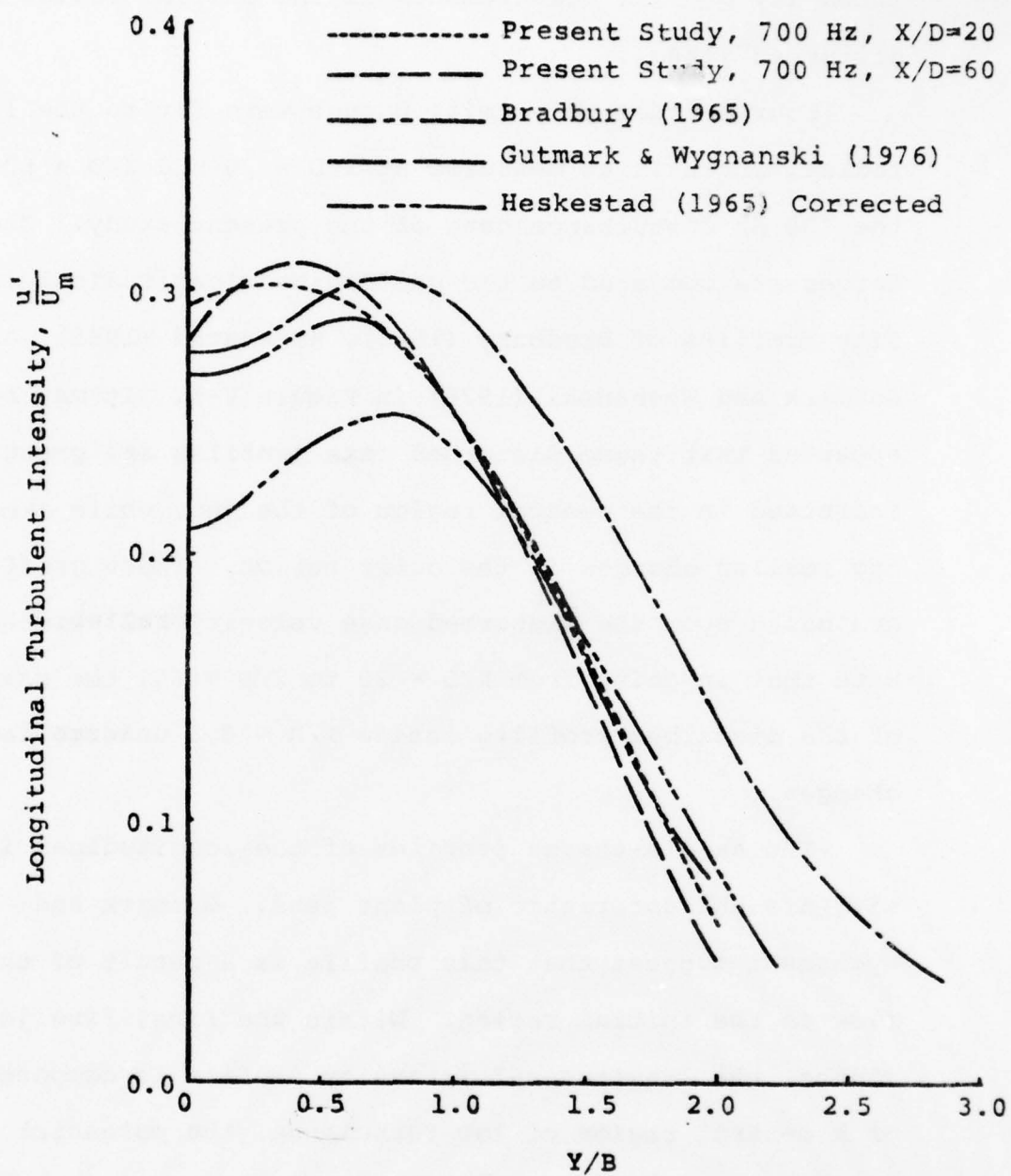


Figure V-5 Transverse Profiles of Disturbed and Undisturbed Longitudinal Turbulence Intensities

initial intensity profile to have a strong influence on the profile far downstream. They note that in a round jet Wygnanski and Fiedler (1969) found such profiles only inside  $X/D = 30$ , and conclude that at sufficiently large distances downstream in a plane jet the saddle should disappear. The 700 Hz case profiles of the present study, shown in Figures IV-16 and V-5, appear to contradict these hypotheses. The profile at  $X/D = 20$  displays almost no saddle, the saddle at  $X/D = 40$  is somewhat more pronounced, and that at  $X/D = 60$  is the most severe. Thus the saddle increases rather than decreases with increasing distance downstream. This flow does not have an appreciable initial saddle-shaped profile to remember.

This behavior might be explained by consideration of the turbulent energy equation. At the center of the jet the turbulent shear stress production term of the equation is zero, and the normal stress production is very small. Gutmark and Wygnanski note that at the center of the jet most of the turbulent energy is gained through the mean flow's convection of turbulent energy produced farther out in the jet. In the self-preserving region, this convected energy is roughly balanced by the energy dissipated at the centerline. It thus would follow that if this balance were upset an increase or decrease in the intensity on the centerline would occur while the surrounding intensities might or might not change. It may be hypothesized that

a decrease in turbulent energy convected to the centerline could result in the observed behavior of the 700 Hz case longitudinal intensity profiles. It is believed that the saddle shape of the longitudinal intensity profiles results not only from the "memory" of the conditions of the initial region but also from the relation of the turbulent energy balance terms in the main region.

The 700 Hz disturbed case lateral intensity profiles at  $X/D = 20$  and  $X/D = 60$  are shown in Figure V-6 with the undisturbed profile of Gutmark and Wygnanski (1976). These disturbed intensity profiles do not exhibit the fascinating changes in shape of the disturbed longitudinal intensity profiles. As may be observed, the major effect appears to be increased magnitudes in the central region of the jet. At the larger distances from the nozzle, the effect is less apparent, and the profile compares well to the undisturbed profile of Gutmark and Wygnanski.

Disturbed intensity profiles have not been reported in the literature for the main region of jets. For this reason, reported measurements in the initial region are considered although they may not be directly comparable to the measurements of the present study. Thompson (1975) measured longitudinal intensity profiles in the initial region of a disturbed plane jet and found that for profiles at  $X/D = 8$  or less the difference between disturbed and undisturbed profiles was small. The difference was most

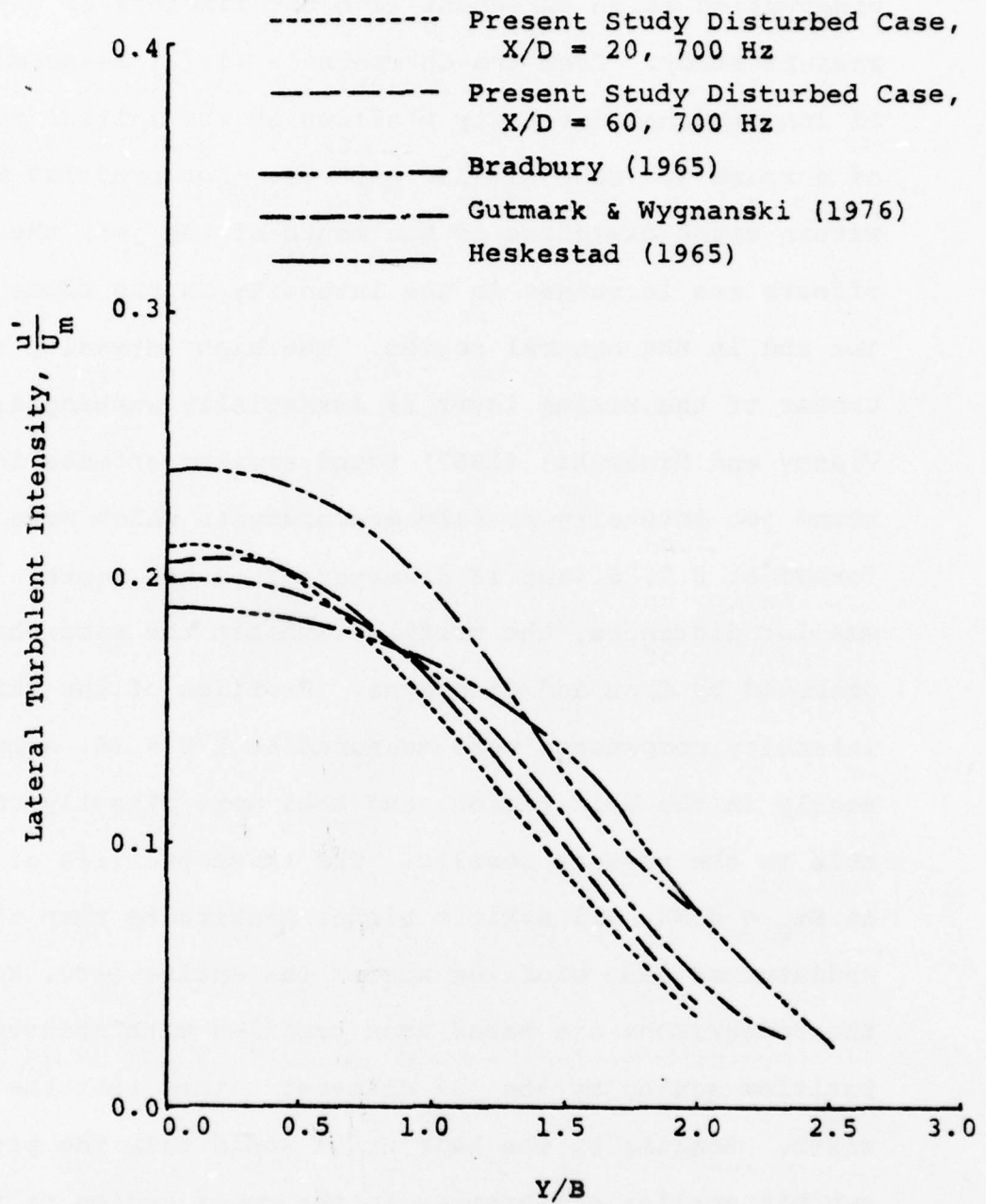


Figure V-6 Transverse Profiles of Disturbed and Undisturbed Lateral Turbulent Intensities

readily apparent in the central region of the flow. This observation is in agreement with the findings of the present study. Crow and Champagne's (1971) measurements of longitudinal intensity profiles in the initial region of a round jet show similar effects. For profiles measured within eight diameters of the mouth of the jet, the major effects are increases in the intensity on the edges of the jet and in the central region. The high intensity at the center of the mixing layer is essentially unchanged. Vlasov and Ginevskii (1967) found similar effects in their round jet intensity profile measurements which were performed at 0.2, 6, and 16 diameters from the mouth. At the smaller distances, the profiles exhibit the same changes observed by Crow and Champagne. Profiles of the three intensity components were measured at  $X/D = 16$ , a position nearly in the main region, and thus more directly comparable to the present results. The three profiles disturbed at  $St_D = 0.38$ , all exhibit higher magnitudes than the undisturbed case profiles across the entire jet. However, the comparisons are based upon profiles with transverse position scaled by the jet diameter rather than the half width. Scaling by the half width would make the profiles exhibit smaller differences in the outer region of the jet, but it appears that the magnitudes of the effect would still be greater than those of the present study. This behavior is, however, in agreement with the round jet

study of Crow and Champagne.

It appears that round jets in general exhibit greater increases in intensity in the outer regions of the profile than are apparent in the results of the present study. The central region effects appear to be comparable. The present study seems to display greater effects than would be expected from Thompson's (1975) plane jet measurements in the initial region. However, there are a number of differences between the studies which may account for the different results. The present study was performed at a lower Reynolds number, the flow was constrained to two-dimensional behavior by horizontal planes not employed by Thompson, and different disturbing sound fields were employed. Thompson's jet was forced by a loudspeaker located in the plenum upstream of the nozzle while the disturbance in the present study was applied transverse to the flow field outside the nozzle. Thompson's forcing method produced symmetric disturbance modes, while the transverse disturbance of the present study did not appear to produce purely symmetric modes. These differences might result in the considerably different behavior reported in the two studies.

Reynolds shear stress measurements results for undisturbed and disturbed cases of the present study were presented in the preceding chapter. The stresses were presented in two non-dimensional forms. One form is the

Reynolds stress divided by the square of the mean velocity on the centerline,  $\overline{uv}/U_m^2$ . In the present study, this form is called the non-dimensional Reynolds stress. The results for this stress were obtained in two ways; by direct measurement, and by calculations from mean flow parameters. It is shown in Appendix E that with assumptions of similarity, the Reynolds stress may be calculated from the mean velocity profile, the widening and decay rates, and the virtual origins. The other form of the Reynolds stress is the stress divided by the product of the longitudinal and lateral intensities,  $\overline{uv}/(u'v')$ . This form is commonly termed the Reynolds stress correlation, and was obtained only from direct measurements. The results of Bradbury (1965), Heskestad (1965), and Gutmark and Wagnanski (1976) for both forms of the Reynolds stress are compared to the undisturbed and disturbed case results of the present study in this section.

The measured and calculated at  $X/D = 60$  undisturbed case non-dimensional Reynolds stress results of the present study are compared to the results of the three plane jet studies in Figure V-7. A fifth order polynomial fit to the measured points of the present study is used in the comparison. It may be observed that all profiles have generally similar shapes with maxima between  $Y/B = 0.7$  and  $Y/B = 0.8$ . The magnitudes of the present results are lower than those of the reviewed studies, and several explanations

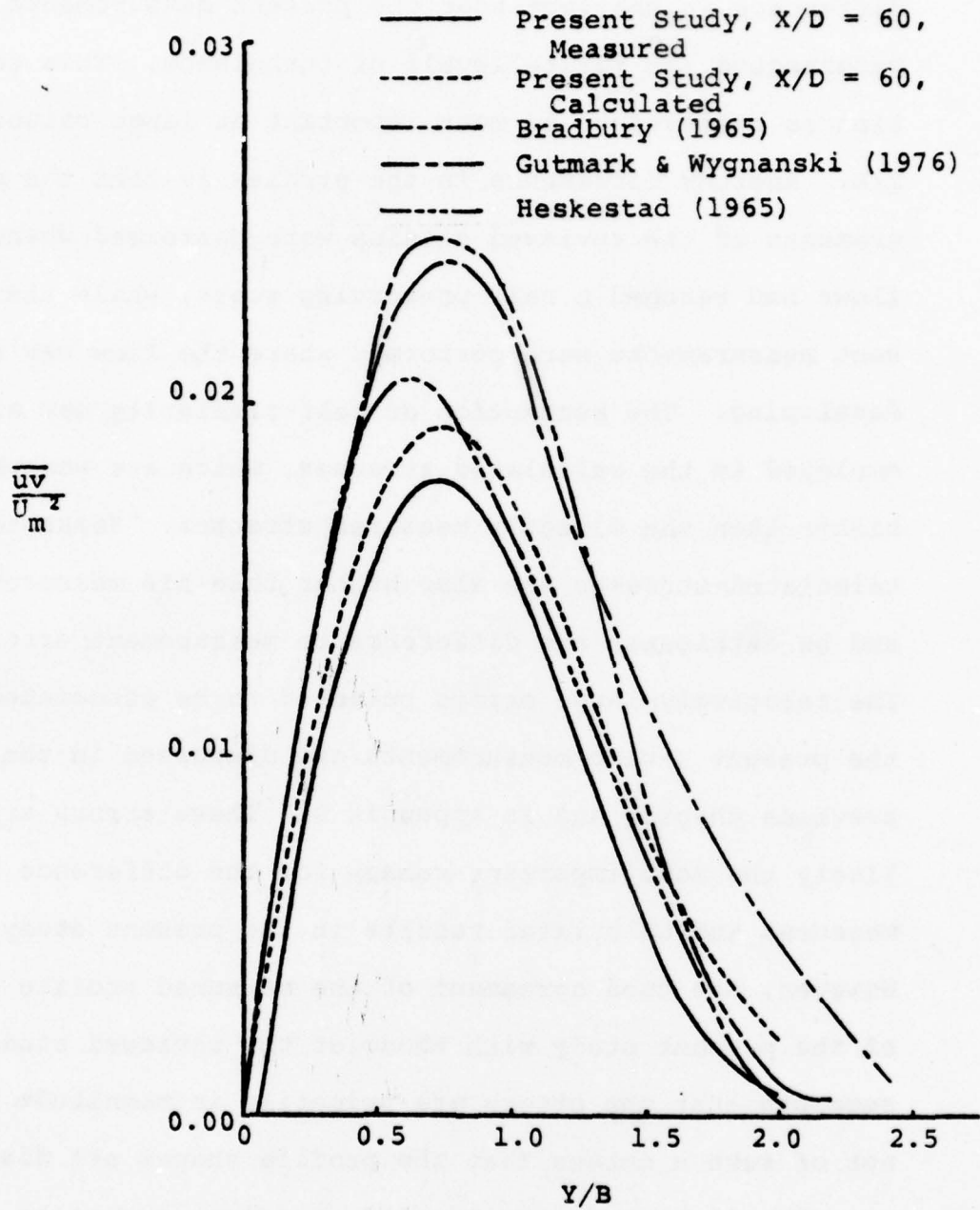


Figure V-7 Undisturbed Case Profiles of Non-Dimensional Reynolds Stress

are available for this difference. One contributor to the difference is the fact that the present measurements were uncorrected for finite levels of turbulence. This correction is believed to be most important at large values of  $Y/B$ . Another difference in the studies is that the measurements of the reviewed studies were performed where the flows had reached a self-preserving state, while the present measurements were performed where the flow was still developing. The assumption of self-similarity was also employed in the calculated stresses, which are somewhat higher than the directly measured stresses. Heskestad's calculated stresses are also higher than his measurements, and he attributes the difference to measurement errors. The relatively large errors believed to be associated with the present X-wire measurements are discussed in the previous chapter and in Appendix D. These errors are likely the most important reason for the difference between measured and calculated results in the present study. However, the good agreement of the measured profile shapes of the present study with those of the reviewed studies suggests that the errors are primarily in magnitude and not of such a nature that the profile shapes are distorted.

The disturbed case Reynolds stresses cannot be compared to similar disturbed plane jet results in the literature, for it is believed that the present measurements are unique. The measured and calculated non-dimensional

Reynolds stresses at  $X/D = 20$  and  $X/D = 60$  of the 700 Hz disturbed case of the present study are compared to the undisturbed jet results of Bradbury (1965), Heskestad (1965), and Gutmark and Wagnanski (1976) in Figure V-8. It may be observed that the disturbance appears to produce increases in the magnitudes of the profiles primarily in the vicinity of the peak. As a result, the disturbed profiles of the present study are less similar to the profiles in the literature than are the undisturbed profiles. The factors previously discussed as possible reasons for differences between the undisturbed Reynolds stress results and those in the literature also apply to the disturbed case results. The effect of non-self-preserving flow may be of greater significance, for the increased widening rates of the disturbed cases appear to approach that of the undisturbed case at  $X/D$ 's greater than sixty. This behavior certainly weakens the validity of the assumption of self-similarity employed in the calculation of the Reynolds stresses of the disturbed cases, particularly at the largest downstream distances. However, the extent of the agreement between the measured and calculated profiles does suggest that the changes in the disturbed case profiles agree with the tendencies of those calculated from the changes in the mean flow parameters. This agreement implies that additional momentum equation terms for the direct interaction of the acoustic

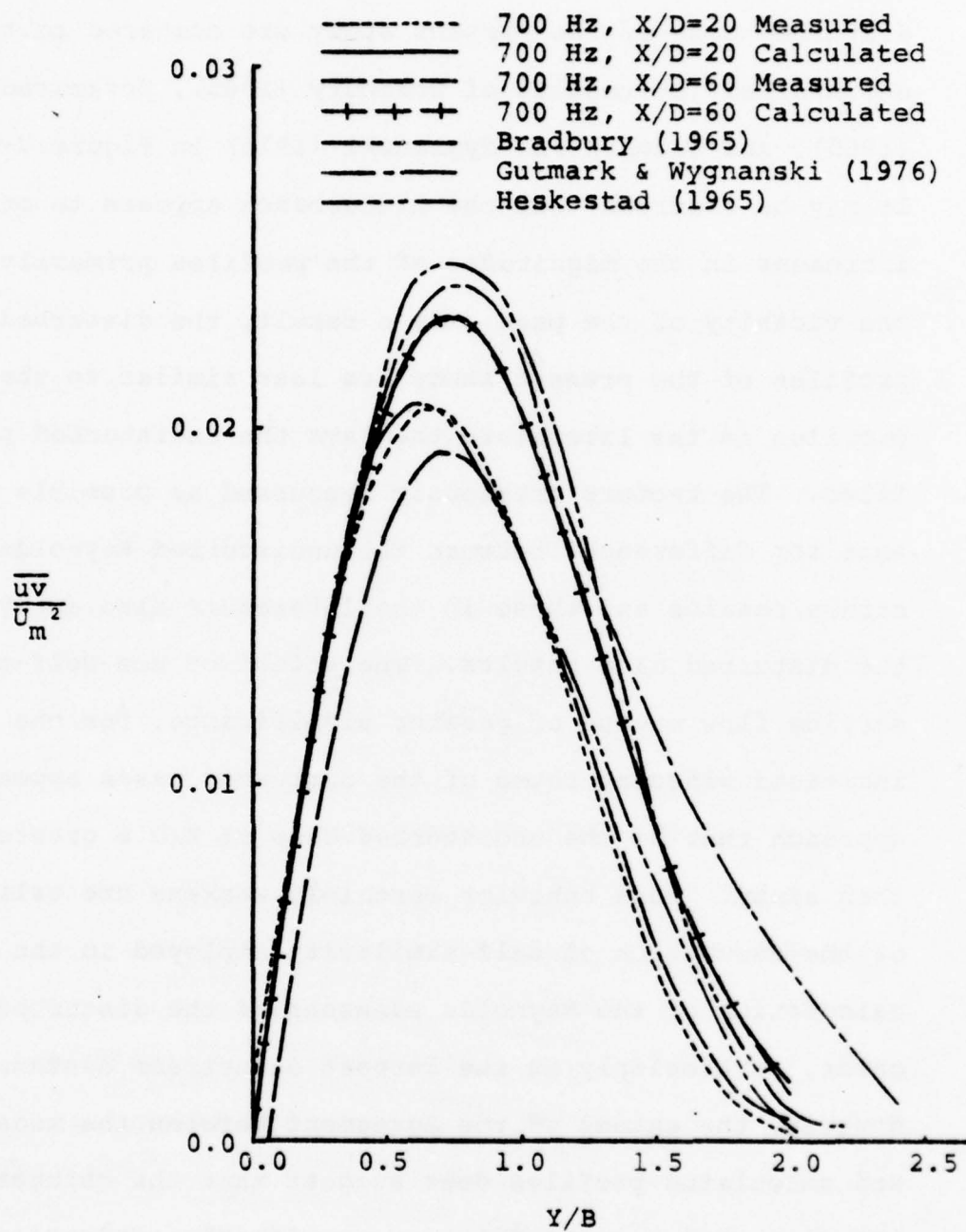


Figure V-8 700 Hz Case Profiles of Non-Dimensional Reynolds Stress

field with the turbulent field are of little importance, for the changes produced by the disturbance can be predicted without the addition of such terms.

The only reported measurements of Reynolds stresses in a disturbed jet that have been uncovered are those of Vlasov and Ginevskii (1967) in a round jet. Their measurements were performed at sixteen diameters downstream from the nozzle, and hence cannot be considered to be in the self-similar main region of the jet. The influences of changes in the virtual origins of the flow may be strong in this region, and hence comparisons of the various cases may be rather complicated. In their results, the non-dimensional Reynolds stress profile of the jet disturbed at a Strouhal number,  $St_D = 0.38$ , exhibits a peak at a larger distance from the centerline and a lower magnitude than that of the undisturbed case. Similar behavior was also observed in preliminary Reynolds stress measurements performed at  $X/D = 10$  and  $X/D = 6$  in the present study. However, the transition from the initial region to the main region occurs over a relatively short distance, and further measurements are required to interpret the Reynolds stress behavior in this region. It may be hypothesized that the shear layer structure, and particularly the merging of the layers at the end of the potential core may play an important role in the downstream development of the flow. The merging behavior might be related to the longitudinal

intensity distributions of the 700 Hz case, which displayed a profile at  $X/D = 20$  which nearly lacked the characteristic humped shape of the undisturbed case. The shear layer behavior also may be related to the increased magnitudes of the non-dimensional Reynolds stresses observed near the peaks of the profiles of the disturbed cases. The Reynolds stress correlation results also suggest the important influence of the initial region.

The present study's undisturbed case Reynolds stress correlation results at  $X/D = 60$ , and the 700 Hz disturbed case results at  $X/D = 20$  and  $X/D = 60$  are compared to the results of Bradbury (1965), Heskestad (1965), and Gutmark and Wygnanski (1976) in Figure V-9. Fourth order polynomial fits to the measured points are used to represent the results of the present study. Study of the figure reveals that with the exception of Bradbury's measurements in a jet exhausting into a co-flowing stream, the correlation profiles have similar shapes inside  $Y/B = 1$ . Major differences in behavior are apparent at larger values of  $Y/B$ . Gutmark and Wygnanski note this difference in behavior at the edges of the jet and pronounce it interesting without offering an explanation. Their conditional measurements in the turbulent zone display even higher correlation magnitudes at the edges of the jet. The major difference between their study, the others surveyed, and the present study is that they employed wire mesh screens

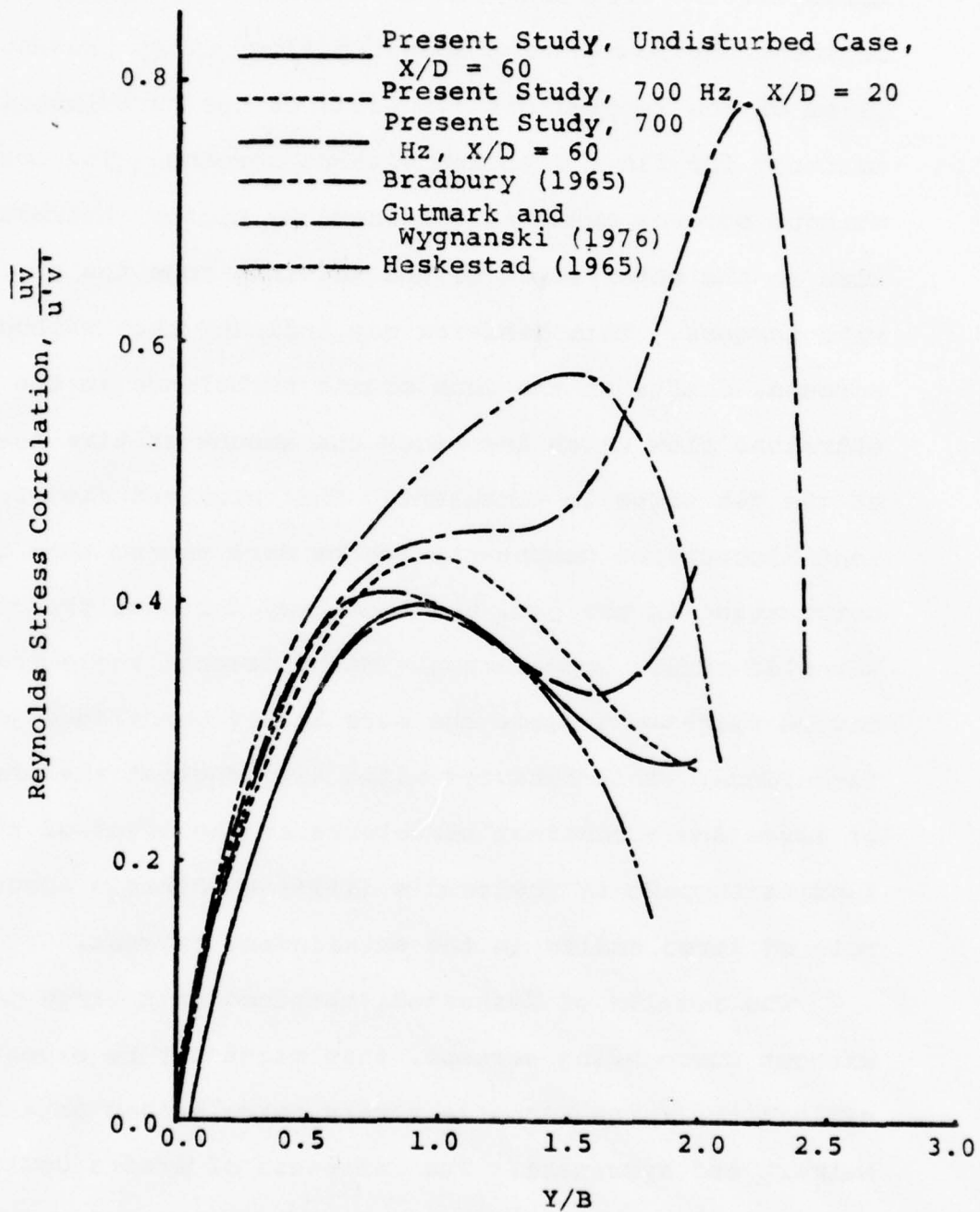


Figure V-9 Transverse Profiles of Reynolds Stress Correlation

bordering the flow field in an attempt to decrease the influence of room drafts upon the flow. They present profiles of the lateral distributions of the turbulent intermittency for flows with and without screens. The profile without screens exhibits considerably higher intermittencies at the outer edges of the jet than does the profile with screens. This behavior may indicate that without screens, drafts in the room create turbulence in the entrained flow which increases the amount of time the flow at the jet edges is turbulent. The entrained flow turbulent fluctuation components may be more random than those originating in the jet, and hence may decrease the overall Reynolds stress correlation. With screens, the correlation may be weighted towards the more highly correlated jet turbulence. This behavior might also suggest the presence of large scale coherent structures at the edges of the jet, lending support to Townsend's (1956) hypothesis about the role of large eddies in the entrainment process.

The results of Heskestad, obtained in a large jet without surrounding screens, thus might not be expected to exhibit the large Reynolds stress correlations obtained by Gutmark and Wygnanski. The influence of drafts could be expected to be high. Bradbury's jet surrounded by a low velocity co-flowing stream suggests alternative explanations. First, it might be argued that free stream flow fluctuations originating in the wind tunnel or jet nozzle

outside wall boundary layers might play a role similar to that of drafts in a room surrounding a jet exhausting into "still" air, thus, by the present hypothesis, decreasing the outer region Reynolds stress correlation. On the contrary, it might be argued that the co-flowing stream and the corresponding finite velocity at the edge of the jet could decrease the influence of outside fluctuations.

The present study's Reynolds stress correlation results display some outer region values comparable to those of Heskestad and Bradbury, while most are considerably higher, although lower than those of Gutmark and Wagnanski. This is the case for both the disturbed and undisturbed case profiles, and in all cases the  $X/D = 20$  profile displays the lowest outer region correlation. The flow field of the present study was located inside a closed anechoic room, and hence despite the absence of surrounding screens, it may be imagined that the influence of drafts upon the jet was very small. Thus, if the preceding hypothesis about the high Reynolds stress correlations is correct, agreement with Gutmark and Wagnanski's results would be expected. Other hypotheses may also be made based upon comparisons of the present results with those of the reviewed undisturbed jet studies.

The magnitudes of the correlations near  $Y/B = 1$  for all three cases of the present study agree well with the reviewed studies. This agreement suggests that the

Reynolds stress measurements were in error by a constant which cancels in the non-dimensionalizing of the correlations. The agreement also suggests that the effect of the disturbing sound field is not an ordering or regularizing of the turbulent structure of the flow in this region of the profile. In such a case, higher magnitude correlations would be expected for the disturbed cases. In fact, in the vicinity of  $Y/B = 0.5$ , the disturbed case correlations are slightly lower than those of the undisturbed case. Only in the outer region of the profile are the disturbed case correlations generally higher. The highest of these correlations occur at the largest distances from the nozzle.

A possible explanation may be that these high correlations are the results of large scale orderly structures originating in the initial region of the jet. Closer to the mouth of the jet, these large scale structures may be accompanied by smaller scale turbulence which contributes to the high turbulence intensities and the lower Reynolds stress correlations of the disturbed cases. As the flow moves downstream, this smaller scale turbulence decays faster in the outer region of the jet than does the large scale structure. In the central region of the jet, the smaller scale turbulence is replenished through the Reynolds shear stress production from the mean flow, while in the outer region of low production, the low intensity large scale structure comes to dominate the flow and the

Reynolds stress correlation. This explanation is but hypothesis, and makes a number of assumptions about the structure of the flow in the initial region of the jet.

The structure of the flow is partially described by the one-dimensional turbulent energy spectra that were measured. These spectra provide information about the frequency distribution of the turbulent energy of the flow. In this section, the spectra measured in the jet shear layer and on the jet centerline are compared to similar spectral measurements reported in the literature.

The measured shear layer spectra may be qualitatively compared to the measurements reported by Browand (1966) and by Miksad (1971) for shear layer instability studies. The present shear layer measurements were performed at one location within one-half wavelength of the nozzle, assuming a wavelength calculated with the local mean velocity and natural or disturbed frequency. This location is comparable to those of the measurements of Miksad, and slightly upstream of Browand's, although suitable for qualitative comparison. The results of the studies are similar in displaying relatively broadly peaked spectra in the undisturbed cases and much more sharply peaked spectra in the forced case. The three studies all display subharmonic components in both undisturbed and disturbed spectra. The present study differs by displaying subharmonics without the presence of harmonics. The present

measurements were performed at only one location in the shear layer, while the reviewed studies include measurements at a number of locations. They indicate that harmonic components generally appear before the subharmonics. The 1600 Hz case spectra also differs from the two shear layer studies in the large number of lower frequency peaks displayed. As previously discussed, these peaks appear to result from the relation between the disturbing frequency and the natural shear layer frequency.

The spectra measured along the jet centerline in the present study exhibit behavior similar to that of the shear layer spectra. The undisturbed spectra have very broad peaks, and the 700 Hz case spectra are very peaked with an exact subharmonic, harmonic and  $3/2$  subharmonic. The 1600 Hz spectra, like the 1600 Hz shear layer spectra, display large numbers of peaks occurring at the multiples of approximately one-ninth the fundamental. These peaked distributions broaden as the distance downstream is increased, and the spectra of the three cases are similar at distances greater than fifteen nozzle widths downstream. The characteristics of these spectra may be compared to those of other jet spectra measurements in the reviewed studies.

Most of the jet spectral measurements are for round jets, and were obtained in studies concerned with the problem of aircraft jet noise. Such studies are concerned with the initial region, the source of jet noise. One such

study is that of Ko and Davies (1971). They raise the question of what a hot wire anemometer probe measures in the low turbulence potential core of a jet. This question must be considered before analyzing the results of the measurements. Ko and Davies conclude that a probe in the potential core is more sensitive to density fluctuations resulting from pressure fluctuations in the shear layer than to local velocity fluctuations. Planchon (1974) offers partial support for this contention with his fluctuating pressure measurements, but Lau, Fisher, and Fuchs (1972) present a proof that a probe is much more sensitive to the velocity fluctuations in the potential core. The present results appear to support Lau et al., for the disturbed case turbulent intensities measured on the centerline near and at the mouth of the jet are not appreciably changed from those of the undisturbed case, suggesting an insensitivity of the probe directly to the applied sound field density fluctuations or indirectly to pressure fluctuations produced in the shear layers by the sound field. It should be pointed out that the experiment of Ko and Davies was performed in a "noisy" jet at a Mach number of 0.22, and the pressure fluctuations were considerably stronger than those of the present study. It may be concluded that the probe in the present study did respond primarily to velocity fluctuations, and that the resulting spectra are turbulent energy spectra.

Ko and Davies (1971) also present results indicating a difference in frequency between the peak of the spectrum in the shear layer and the peak in the potential core, and along the centerline. The results of the present study also indicate such a difference. In the undisturbed case of the present study, the spectral peak on the centerline in the potential core is at a slightly higher frequency than the peak in the shear layer. The peak on the centerline also decreases with distance downstream in agreement with their findings. Ko and Davies also report a relation between the broad spectral hump at downstream positions on the centerline and the spectra of the shear layer at the same downstream position. The spectra in the shear layer have similar magnitudes at the frequencies of the centerline hump, but appear flat because the greater turbulence of the shear layer raises the spectral magnitudes at frequencies below the hump to the same level as the hump. Similar spectra are presented by Bradshaw, Ferriss, and Johnson (1964), by Wooldridge, Wooten, and Amaro (1972), by Lau, Fisher, and Fuchs (1972), and by Planchon (1974). This "burying" of the hump in turbulence appears similar to the rapid smoothing of the centerline spectra observed in the present study. Similar peak-broadening is observable in the shear layer spectra of Browand (1966) and Miksad (1971).

Spectra measured in shear layers or the initial regions of jets are the only spectra in the reviewed studies which display subharmonics. Kaiser (1971) presents relatively broad band spectra measured in the outer region of the shear layer, and some of the disturbed case spectra exhibit subharmonics. Crow and Champagne (1971) and Vlasov and Ginevskii (1967) present centerline spectra in round jets that display harmonics of the disturbing frequency without subharmonics. The subharmonics in these cases may have been absent because the nozzle boundary layers were tripped, destroying the initial linear instability process. However, Crow and Champagne note, as do Hussain and Zaman (1975), that when their round jet was disturbed at twice the natural frequency, strong subharmonics were formed. Strong subharmonic formation appears to be the reason for the intermittent fluctuation behavior of the present study. This behavior, which is described in Appendix C, involved intermittent subharmonic formation and appeared to be strongest when the jet was forced at frequencies near 1100 Hz, roughly twice the natural frequency revealed in the undisturbed shear layer spectrum.

None of the reviewed studies display spectra similar to those found in the case of the 1600 Hz disturbances. Kelly (1967) in a paper which provides an analytical description of the process of subharmonic formation, does consider the case of a flow interacting with two waves of

different frequencies, concluding that wave amplification does not result. The interaction of the 1600 Hz disturbance with the shear layer natural frequency of approximately 545 Hz may be considered such a case. Borisov and Rozenfeld (1971) describe a study which found that two frequencies above the instability region of a boundary layer but with a difference within the region resulted in instabilities at the difference frequency. Davies and Yule (1975) report that M. V. Morkovin and R. S. Norman found a similar effect in a study of the shear layer formed behind a rectangular object in a laminar boundary layer. They note that vorticity waves with various algebraic sums of the two forcing frequencies were found, but that only the difference frequency resulted in transition to turbulence. In addition, forcing by a single frequency equal to the difference frequency did not produce the effect. It might be speculated that in the present study, forcing at 1600 Hz results in disturbance at the frequency difference between 1600 Hz and the shear layer natural frequency, 545 Hz. This difference frequency, 1055 Hz, is very close to that producing the strongest intermittent fluctuations, and these fluctuations may involve subharmonic formation at the shear layer natural frequency. Peaks in the spectra are present at these frequencies. An explanation for the appearance of the other peaks is not apparent, and the phenomenon suggests the need for further study of disturbed shear layers.

The comparison of the spectra of the present study to those in the literature also suggests the need for further study of the spectral behavior of the turbulent energy in the initial region of turbulent plane jets. Few studies are available for comparison, and the disturbance of the jet reveals interesting and seemingly complicated phenomena. In general, the comparison of the experimental results to those in the literature reveals substantial agreement. The most important disagreement appears to involve the difference between the shear layer instability frequencies predicted by theory and the natural frequency determined from the measured shear layer spectrum. An explanation for this difference is not available.

The experimental results discussed to this point in the chapter provide much insight into the effects of acoustic disturbances upon the jet. Further insight into the dynamics of the flow may be gained by performing some simple analyses.

B. Analysis of the Behavior of the Flow Based upon Assumptions of Self-Similarity

Chapter IV contains a comparison of measured Reynolds stresses to calculated Reynolds stresses. The calculated stresses were computed using measured characteristics of the mean flow in equations derived from the equations of motion under assumptions of flow field self-similarity. Other characteristics of the flow may be calculated in a

like manner. In this section, a number of these characteristics are considered with particular emphasis placed upon their dependence on the distance from the nozzle. Those to be considered include: the existence time, the local mass flow rate, the entrainment rate, and the turbulent energy production rate.

The basic assumptions used to calculate these characteristics are as follows. First, it is assumed that the jet widening rate, velocity decay rate, and virtual origins remain constant in the main flow region. That is, they do not change with position in the jet. The values used in the calculations were obtained from the widening rate measurements which used pressure profiles at  $X/D = 20, 25, 30, 40, 45,$  and  $50$ . The second assumption employed is that the mean velocity profiles are all similar, as indicated in Figure IV-1. The equation of the curve in the figure was used in the calculations. The equation is

$$\frac{\bar{U}}{\bar{U}_m} = 1 - \tanh \left( A \cdot \frac{Y}{B} \left( 1 + G \left( \frac{Y}{B} \right)^2 \right) \right) \quad (V-2)$$

where A and G are empirical constants with  
 values       $A = 0.793$   
                   $G = 0.111$

Other assumptions will be described in the discussion of the calculation in which they were employed.

### 1. Existence Time

One of the characteristic parameters which was calculated is the existence time, a parameter defined by Bradbury (1965). It represents the time required for a particle moving at the local centerline mean velocity to travel from the mouth of the jet along the centerline to a given downstream distance. Bradbury used the parameter to estimate the distance required for the flow to reach a self-preserving state, assuming that the existence time required to reach the state should be the same as that required to reach self-preservation in a plane wake. He used Townsend's (1956) results for a wake and found that this method predicted a distance of 90 to 160 nozzle widths for the flow to reach self-preservation. This distance was somewhat longer than the distance indicated directly by measurements, but appeared to be a reasonable approximation.

The calculation was performed using the present data in order to determine the changes in existence time resulting from the changes in velocity decay rate and origin produced by the acoustic disturbance. In the calculation, the velocity on the axis was assumed equal to  $U_0$  for  $X/D = 0$  to  $X/D = 5$ , and assumed to follow the velocity decay equation for  $X/D > 5$ . The discontinuity and jump in velocity at  $X/D = 5$  using these assumptions was assumed to be of little importance in this simple calculation. The

equation for the existence time is given in Appendix E. The following values were calculated for the existence times at  $X/D = 80$ .

TABLE V-3

## CALCULATED EXISTENCE TIMES

Frequency (Hz)	Existence Time $U_0 t_e / D$
0	217
700	229
1600	223

The experimental half width measurements presented in Figure IV-10 indicate that the disturbed cases reached a self-preserving state later than the undisturbed case, contradicting the implications of the calculated existence times. Consequently, the existence time calculations appear to be of little help in gaining additional understanding of the phenomenon.

## 2. Local Mass Flow Rate

The local mass flow rate was calculated by integrating the mean velocity profile and non-dimensionalizing by the mass flow rate at the nozzle, which was assumed to equal  $U_0 D$  per unit height. The mean velocity profile integration was performed using Equation V-2 from  $Y/B = 0$  to 1.5, and a tangent straight line from  $Y/B = 1.5$  to an intercept of approximately  $Y/B = 1.8$ . The final equation for the mass

flow rate is given in Appendix E. The results of calculations for the two disturbed cases and the undisturbed case are shown in Figure V-10. It may be observed that the disturbed case mass flow rates at a given distance from the nozzle are always higher than that of the undisturbed case. This increase is not simply explained by an inward shift of the origin, as observed by Crow and Champagne (1971). It must be noted however, that in the derivation of the mass flow rate equation, it was assumed that the widening and decay rates remained constant for each case, and hence the behavior of the disturbed curves beyond  $X/D = 60$  is not the same as that actually observed. This is attributed to the fact that these disturbed cases exhibit decreases in widening rate in this region. It may be noted that in a practical mixing problem, the 700 Hz case would produce a mass flow rate at  $X/D = 50$  which is roughly twelve per cent higher than that of the undisturbed case. The slopes of the mass flow rate curves are not constant.

### 3. Entrainment

The slope of the mass flow rate curve is the entrainment, or rate of increase in the mass flow rate per unit distance. The entrainment rate was calculated by taking the derivative of the mass flow rate equation with respect to  $X/D$  in order to obtain a non-dimensional entrainment rate,  $\frac{d(Q/Q_0)}{d(X/D)}$ . The results of the calculation are shown

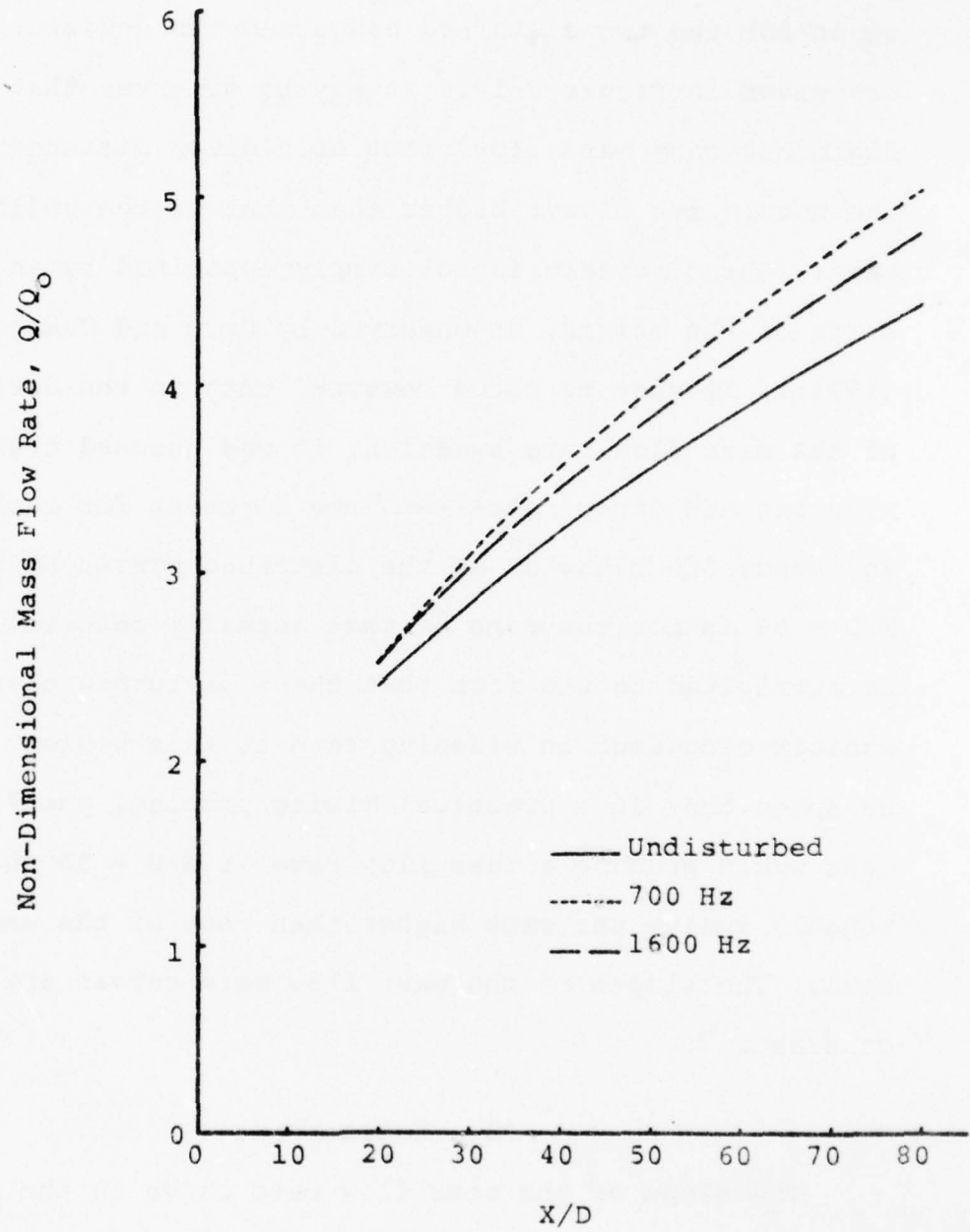


Figure V-10 Calculated Mass Flow Rate Behavior

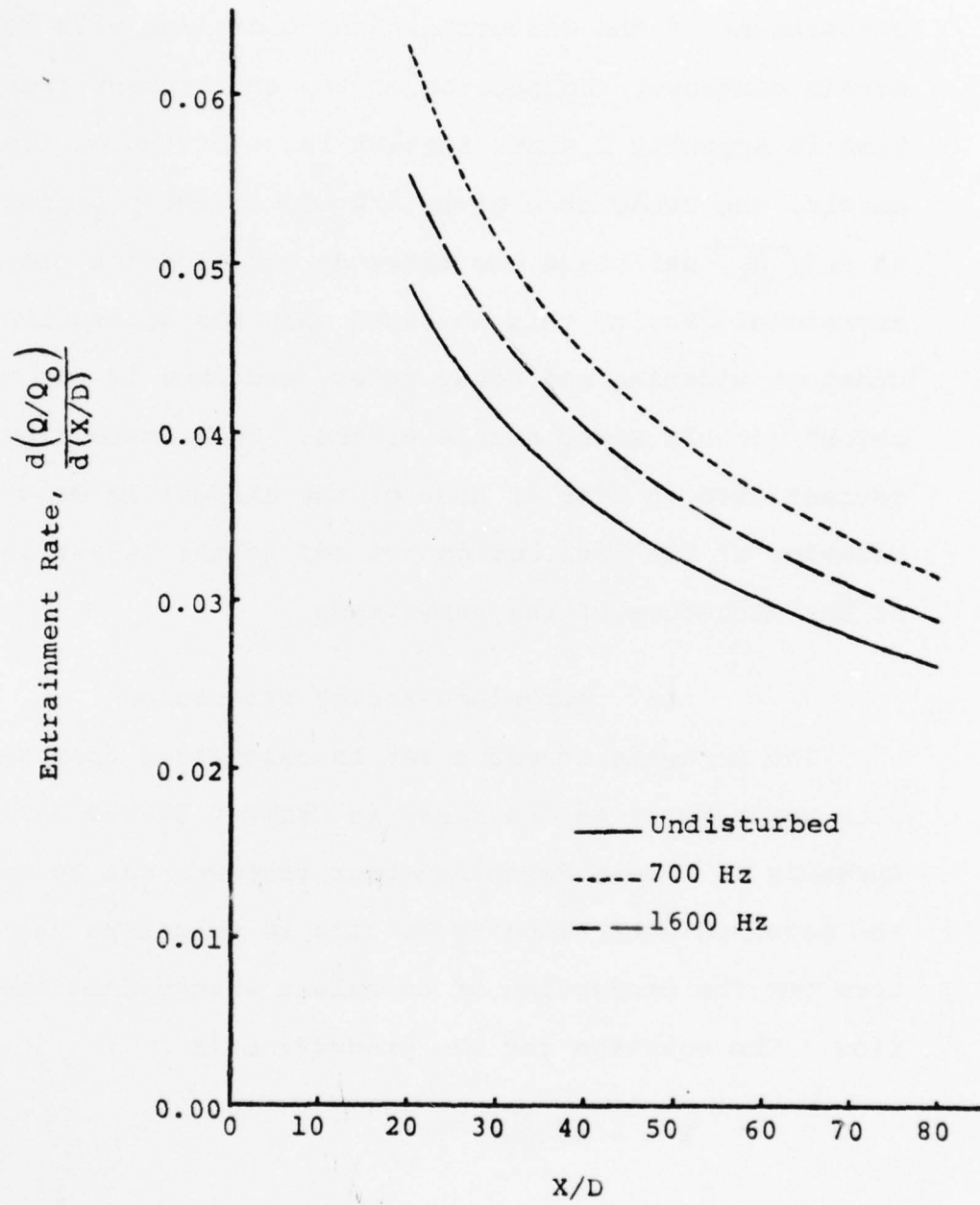


Figure V-11 Calculated Entrainment Rate Behavior

in Figure V-11. The curves indicate that the increased entrainment of the disturbed cases decreases with downstream distance. Inspection of the entrainment rate equation in Appendix E shows that at large distances from the nozzle, the rates at a given  $X/D$  are directly proportional to  $K_1/\sqrt{K_2}$ , and hence the rates do not approach the same asymptote. Again, this is based upon the assumption of constant widening and decay rates, and thus is not valid beyond roughly sixty nozzle widths. These mass flow calculations give an idea of some of the changes in mean flow behavior of the jet, but do not add to the understanding of the structure of the turbulence.

#### 4. Turbulent Energy Production

The Reynolds stresses can be calculated from the mean flow parameters, as described in Chapter IV and derived in Appendix E. These Reynolds shear stresses can be used with the measured mean velocity profile to calculate the major term for the production of turbulent energy from the mean flow. The equation for the production is

$$P = - \overline{uv} \frac{\partial \bar{U}}{\partial Y} \quad (V-3)$$

This production rate may be calculated at points across the jet to obtain the distribution of the production rate and this production rate distribution then may be integrated across the jet to obtain the total production rate per unit height in a plane at a given distance from the

nozzle. The equations used in these calculations are derived in Appendix E.

The production rate distributions and total production rates were calculated for the Reynolds shear stresses measured at  $X/D = 40$  and  $X/D = 60$  by first fitting curves to the measured points and then performing the calculations. The curves were fit by iteratively adjusting parameters in the mean flow similarity Reynolds stress calculation until a good fit was obtained near the peak of the Reynolds stress profile. These curves are shown in Figures V-12 and V-13. The production distributions calculated from these curves are shown with points corresponding to the production calculated using the measured stresses in Figures V-14 and V-15. It may be observed that the distributions peak at roughly the same locations and are not greatly skewed. Thus the disturbing sound field does not appear to have a large direct effect upon the turbulent energy production rate distribution. The sound field does not, for example, shift the peak production to the outer region of the jet, and so suggest a strong interaction with the eddies responsible for the entrainment. The difference in the magnitudes of the distributions does, however, play a role in the total turbulent energy production rate.

A technique described in Appendix E was used to calculate the total turbulent energy production rate of each

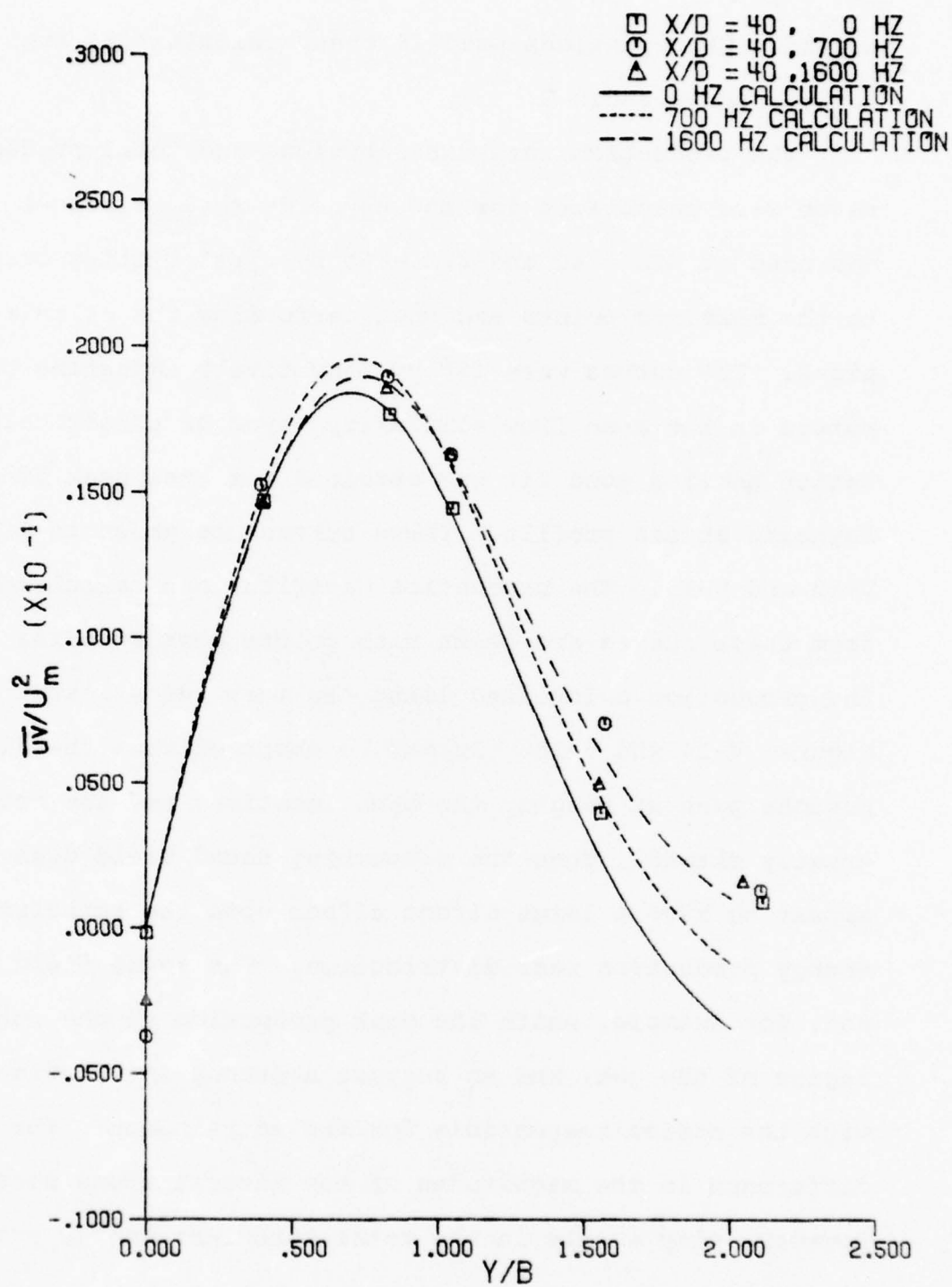


Figure V-12 Reynolds Stress Profiles Fit to Data at X/D = 40

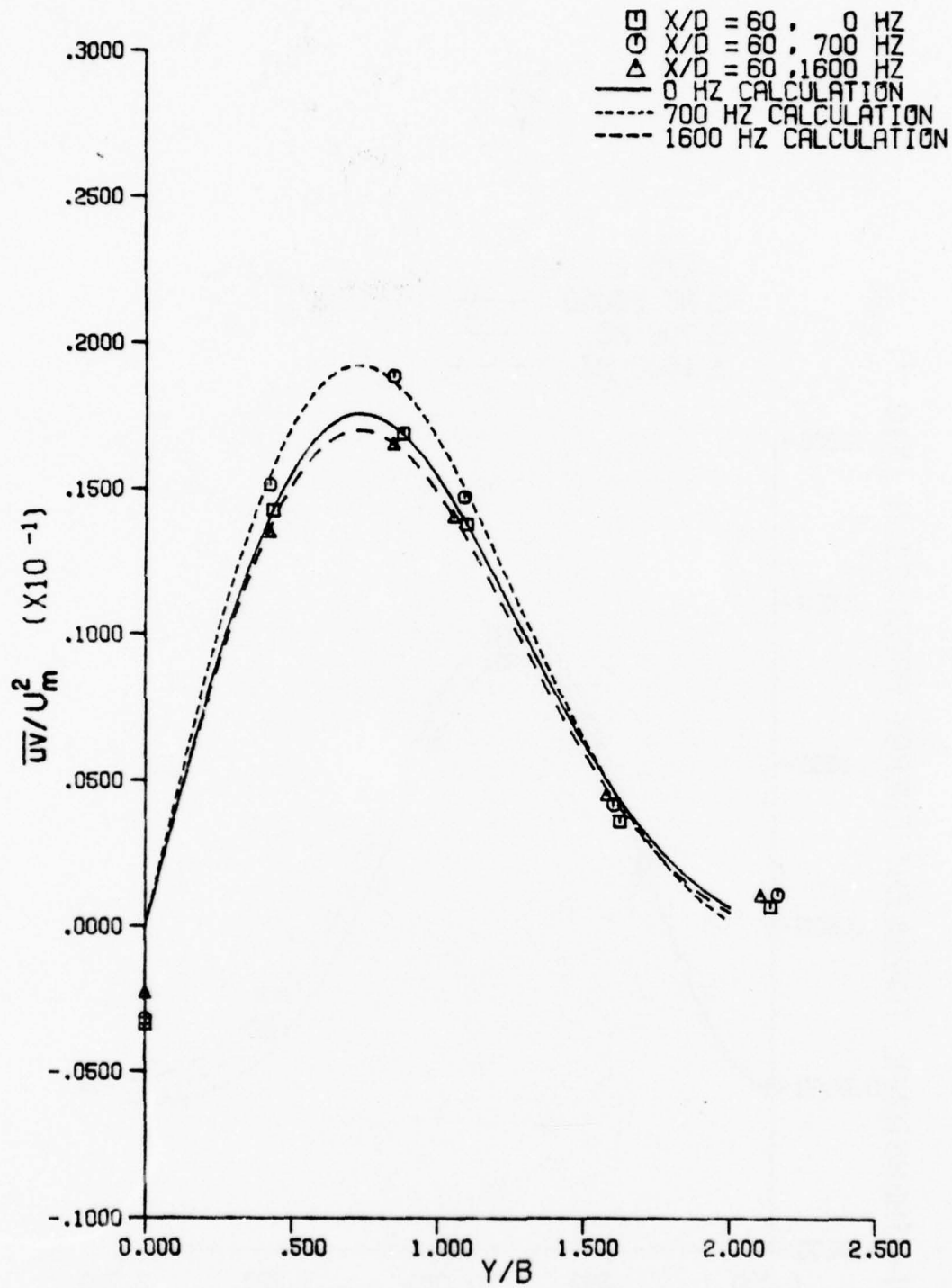


Figure V-13 Reynolds Stress Profiles Fit to Data at X/D = 60

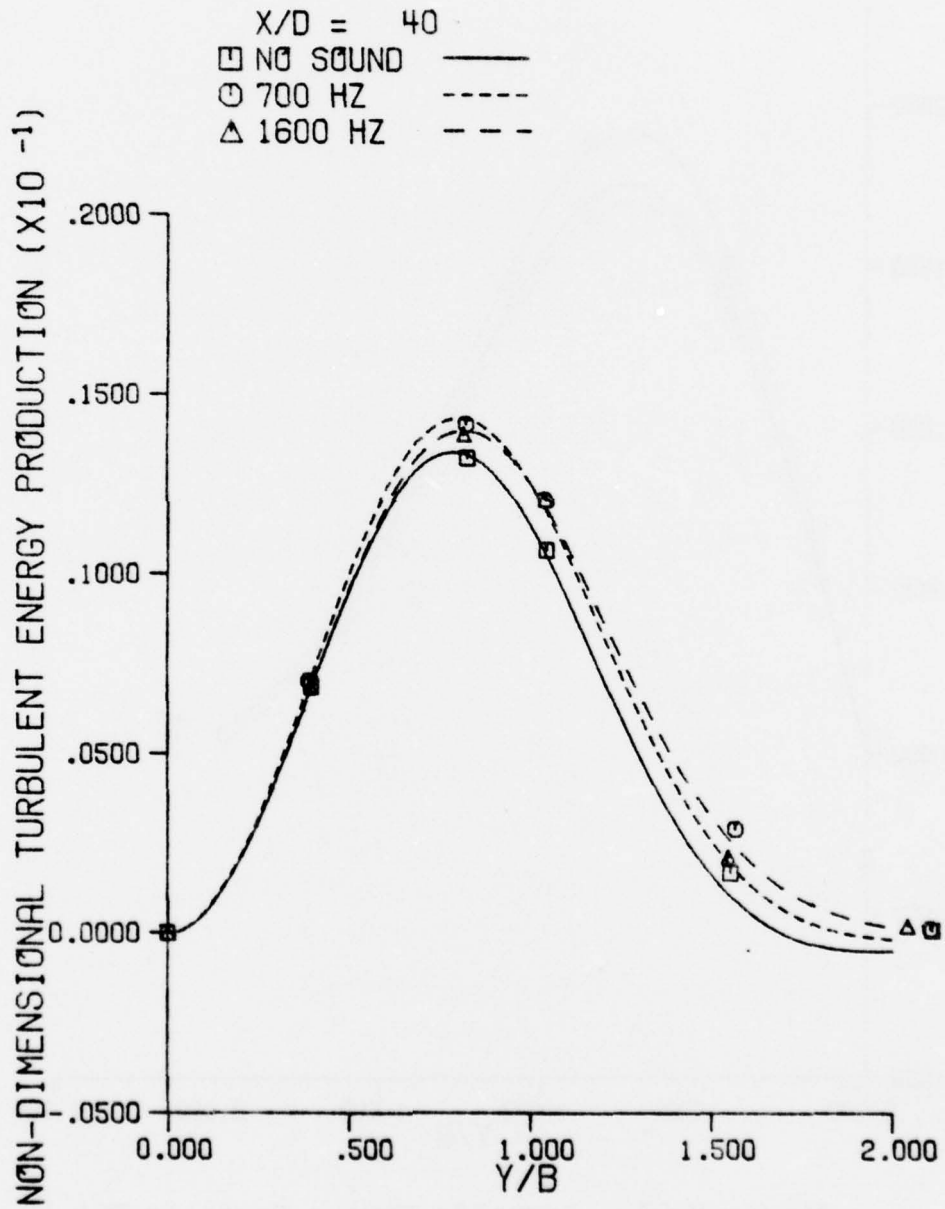


Figure V-14      Calculated Turbulent Energy  
Production Profiles at  $X/D = 40$

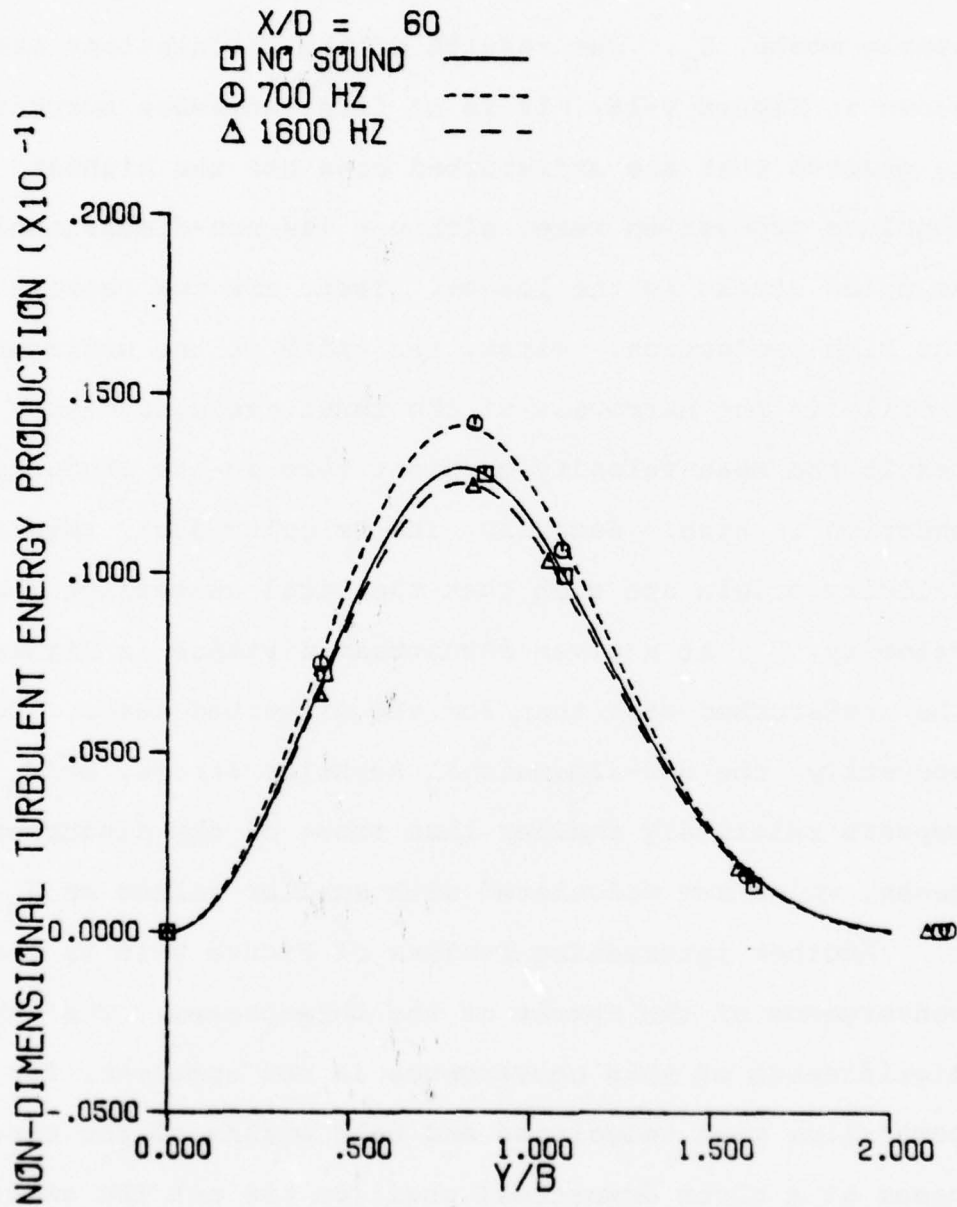


Figure V-15    Calculated Turbulent Energy  
Production Profiles at  $X/D = 60$

case as a function of the distance from the nozzle. Mean flow parameters rather than measured Reynolds stresses were employed in the calculations. To enable absolute comparisons of the production rates, they were all non-dimensionalized by a single value, the mean flow velocity of the nozzle mouth,  $U_0$ . The results of the calculations are shown in Figure V-16. It is at first somewhat surprising to observe that the undisturbed case has the highest absolute production rate, although its non-dimensionalized Reynolds stress is the lowest. There are two reasons for the high production. First, the width of the undisturbed profile is the narrowest of the three cases, and as a result the mean velocity gradient term in the production equation is high. Secondly, the velocity decay rate and velocity origin are such that the local centerline mean velocity,  $U_m$ , at a given downstream distance is higher for the undisturbed case than for the disturbed cases. Consequently, the non-dimensional Reynolds stress,  $\overline{uv}/U_m^2$ , appears relatively smaller than those of the disturbed cases, which are calculated with smaller values of  $U_m$ .

Another interesting feature of Figure V-16 is the convergence of the curves of the three cases. The physical significance of this convergence is not apparent, for the centerline mean velocities and half widths of the three cases at a given downstream position are not the same. Plotting the curves as functions of the mass flow rate or

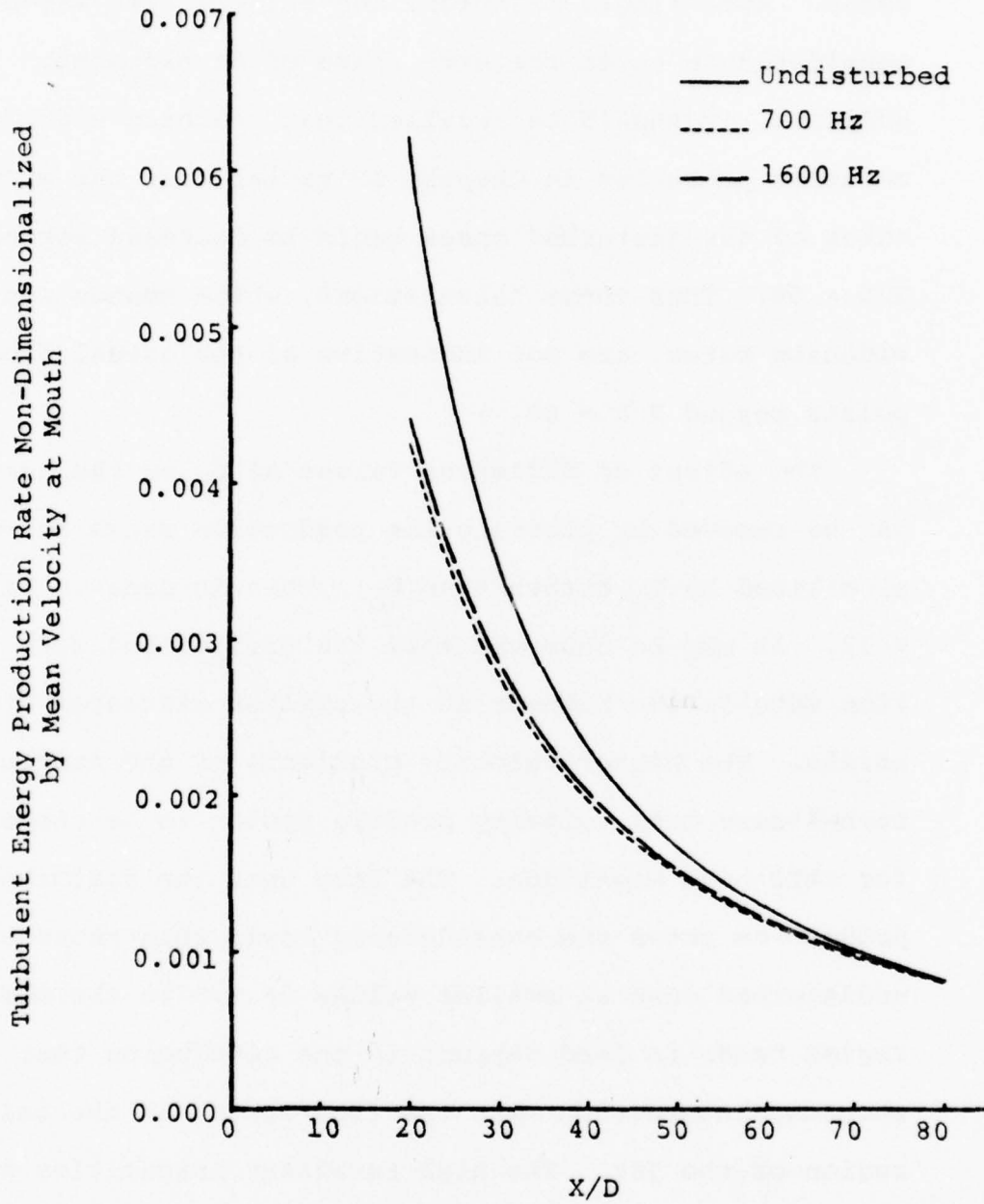


Figure V-16 Calculated Turbulent Energy Production Rate Non-Dimensionalized by Mean Velocity at Mouth

entrainment rather than  $X/D$  does not result in a convergence. At a single position, the three curves may not be considered to be in the same stage of development. In addition, it should be recalled that the half width measurements presented in Chapter IV reveal that the widening rates of the disturbed cases begin to decrease beyond  $X/D = 60$ . Thus these calculations, which assume constant widening rates, are not indicative of the actual flow at points beyond  $X/D = 60$ .

The effect of different values of  $U_m$  on the curves may be removed by plotting the production rates non-dimensionalized by  $U_m$  rather than  $U_o$ . This is done in Figure V-17. It may be observed that the undisturbed case production rate is the highest at the smaller distances from the nozzle. The higher velocity gradients of the narrow undisturbed case mean velocity profile appear to be responsible for this high magnitude. The fact that the disturbed case production rates are considerably lower than those of the undisturbed case at smaller values of  $X/D$  in the main region tends to lend support to the conclusion that the acoustic interaction with the flow occurs in the initial region of the jet. The high turbulent intensities of the disturbed cases reported in Chapter IV do not appear to result from high turbulent energy production in the main region. These high intensities seem to be after effects of high production in the initial region.

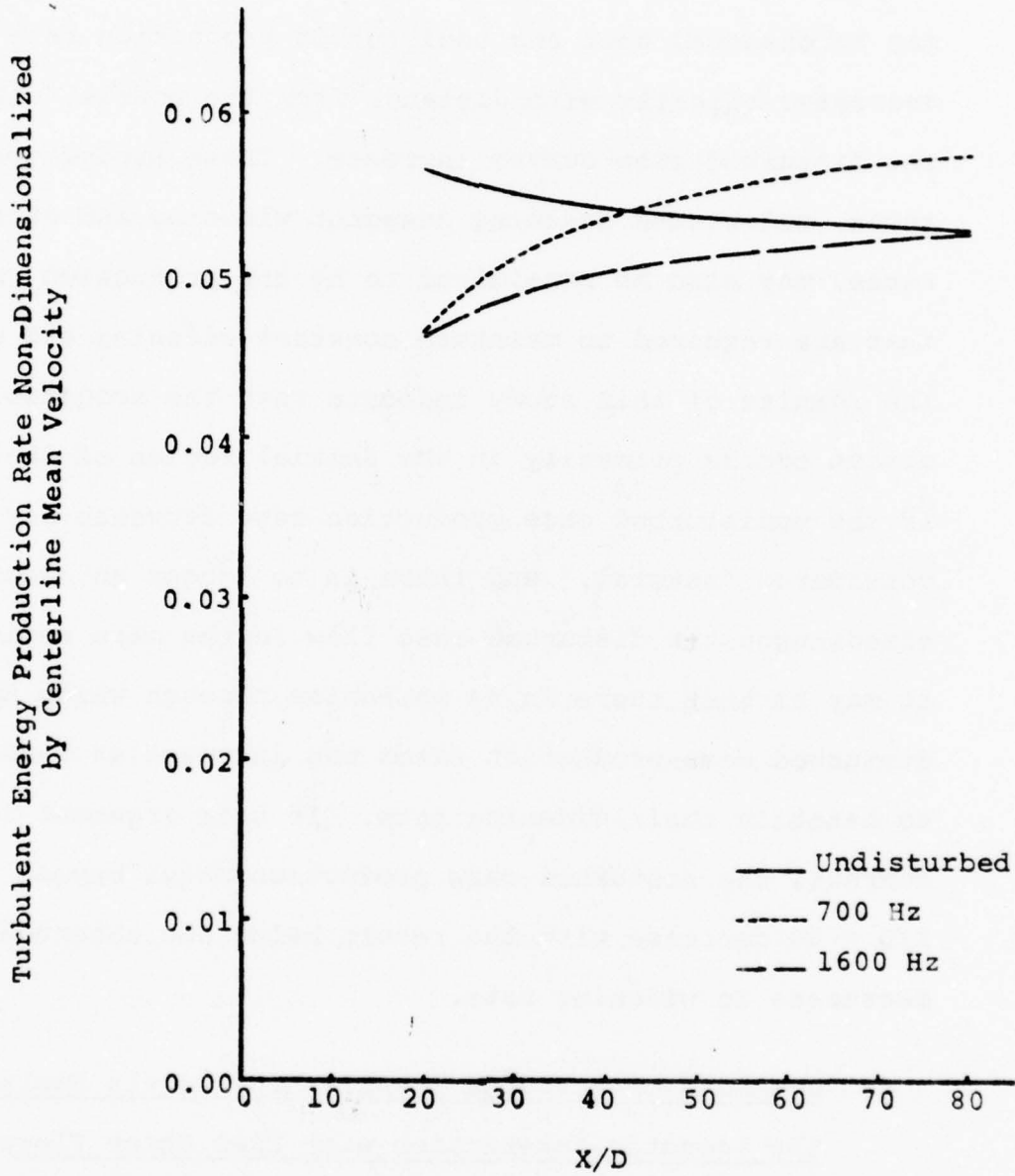


Figure V-17 Calculated Turbulent Energy Production Rate Non-Dimensionalized by Centerline Mean Velocity

The shapes of the curves in Figure V-17 also may be interpreted as giving some insight to the previously discussed widening rate changes of the disturbed cases. It may be observed that the undisturbed production rate decreases slightly with distance from the nozzle, while the disturbed case curves increase. These production rates, calculated assuming constant widening and decay rates, may also be considered to be the production rates that are required to maintain constant widening and decay. The results of this study indicate that the acoustic interaction occurs primarily in the initial region of the jet. If the undisturbed case production rate decrease may be considered "natural," and there is no longer an acoustic effect upon the disturbed case flow in the main region, it may be that there is no mechanism through which the disturbed case production rates can increase as required to maintain their widening rate. If this argument is correct, the disturbed case production rates beyond  $X/D = 60$  decrease with the result being the observed decreases in widening rate.

C. Comments on Proposed Theories and Models Explaining the Acoustic Interaction with Free Shear Flows

Possible mechanisms of interaction between turbulent shear flows and acoustic disturbances have been proposed by Simcox (1969), Morkovin and Paranjape (1971), Crow and Champagne (1971), Rockwell (1972), Winant and Browand (1974),

and others. These are discussed in the sections that follow.

#### 1. Simcox and Hoglund

The direct interaction theory of Simcox (1969) states that the effects of sound upon free shear flows are produced through a stretching of the vorticity field by the acoustic field. The theory implies that the acoustic field interacts directly with vortices having the same wave number, and that the effect upon the mean flow is the result of a disruption of the turbulent energy cascade process. A further implication drawn by Simcox and Hoglund (1971) is that the Reynolds stresses of the flow will be changed only in such a way as to agree with the changed mean flow. The behavior of the Reynolds shear stresses measured in the present study appears to agree with this prediction. However, in the main flow region, the spectra of the disturbed and undisturbed cases of the present study do not appear appreciably different, as may be seen in Figure IV-56. There is no apparent modification of the spectra and hence the cascade by a direct interaction. The spectra from the initial region of the jet, Figure IV-46 for example, display additional energy at frequencies equal to the applied sound frequency rather than at frequencies corresponding to equal wave numbers. Hence the direct interaction theory does not appear to predict the measured changes in the flow produced by the applied sound field.

## 2. Morkovin and Paranjape

Morkovin and Paranjape (1971) suggest that sound affects the flow through a pressure field induced oscillation of the stagnation point of the flow leaving the nozzle lip. They further propose that the magnitude of the effect is proportional to the gradient of the pressure field across the lip. The measurements of the present study are not sufficiently detailed to evaluate the pressure gradient effect, but do indicate that the flow very near the nozzle is affected by the sound field. The shear layer spectra were measured at a position within 1.6 mm (0.063 in) of the nozzle lip and display high magnitudes at the applied sound frequencies. Thus the results of the present study do tend to support the hypothesis that the sound affects the flow through an oscillation of the stagnation point on the nozzle. This hypothesis about the mechanism through which the sound field adds a disturbance to the flow may serve as a starting point for other theories which describe the manner in which such an initial disturbance modifies the structure of the flow.

## 3. Crow and Champagne

Linear stability theory offers predictions of the frequency dependence of the growth rate for disturbances in the initial region of the laminar shear layer. The frequency of maximum growth rate predicted by such theory is roughly three times higher than the disturbance

frequency experimentally determined to produce the maximum widening rate in the main region of the jet. Thus, for the present study, the disturbance of maximum growth rate does not produce the greatest effect, and stability theory is not very useful. Crow and Champagne (1971) also found that linear stability theory failed to predict the frequency of the large scale structure that they found in a round jet. They hypothesize that the frequency responsible for such structure must be the one which is least capable of generating a harmonic. They explain that such a wave should grow to the highest amplitude before saturation, for waves generating harmonics lose energy to the harmonic. The large scale structure resulting from the wave reaching the highest amplitude might be expected to increase entrainment in the main region of the flow and hence increase the widening rate. Crow and Champagne's results did not extend to the main region, but did show greatly increased entrainment in the initial region and an upstream shift in the virtual origins of the flow. The results of the present experiment do appear to exhibit some agreement with this theory. The frequency producing the greatest widening rate is roughly 800 Hz, and hence its first harmonic is 1600 Hz. The 800 Hz case was not studied in detail, but the case of disturbance at 1600 Hz was. It was found that the 1600 Hz disturbance produced unusual spectra that lacked the expected subharmonic at 800 Hz. It might be

speculated that the converse might also be true; that disturbance at 800 Hz thus might not produce a 1600 Hz harmonic. There is limited reason to believe that a frequency which does not readily generate a harmonic is the frequency which does produce the greatest widening rate. If this speculation is correct, the results of the present study agree with some aspects of the large scale structure theory proposed by Crow and Champagne.

#### 4. Rockwell

The influence of the large scale structure in the initial region of a plane jet upon the properties of the flow in the main region has been considered by Rockwell (1972). He states that the changes in the vortex structure which were observed in the initial region appear to be of such a nature that they could result in the observed main region changes. As previously discussed, the frequency dependence results of the present study show some agreement with the characteristics of the disturbance frequency regimes described by Rockwell (1972). Thus, the results of the present study appear to exhibit some agreement with Crow and Champagne's (1971) theory about the frequency of the large scale structure, and with Rockwell's (1972) observations of the large scale structure and hypotheses about the effects of this structure upon the main region flow.

### 5. Winant and Browand

A hypothesis proposed by Winant and Browand (1974) appears to contradict the results of the present study. They suggest that disturbing a mixing layer with a pure tone signal should decrease the mixing layer growth. They claim that such a disturbance will reduce the randomness which is responsible for the vortex coalescence phenomenon and the resulting mixing layer growth. This hypothesis is contrary to the results of the present study and of the reviewed studies. It appears that this hypothesis may be based upon a rather idealized view of the capabilities of a disturbance signal to regularize the flow. The logic of the hypothesis appears correct, but it seems that the forcing disturbance may increase the growth of instabilities in the initial linear region of the layer, bringing them to saturation. It may be speculated that the saturation process introduces sufficient randomness to produce coalescences, and that since the instabilities were initially driven to high amplitudes, the coalescence of these stronger vortices leads to increased mixing layer growth. Thus Winant and Browand's hypothesis may be logically correct but inapplicable to a real flow.

### 6. Other Theories or Mechanisms

The theories of Crow and Champagne, Rockwell, and Winant and Browand are concerned primarily with the structure of the flow in the initial region. Another theory of

the mechanism through which a disturbing sound field affects the flow is based on an effect upon the interface of the jet. The entrainment which is necessary for the growth of the jet is simply fluid which crosses the turbulent-non-turbulent interface of the jet. A direct effect upon the interface could thus result in direct changes in the growth of the jet. An attraction of a theory concerning a direct effect upon the interface is the fact that at the interface, the velocity of the jet is at a minimum and hence appears most susceptible to the influence of disturbances. Ajagu (1976) performed a limited study of the effect of applied sound on the characteristics of the interface. It was found that for a frequency which increased the widening rate, the per cent of fold-over events in the interface increased proportionate to the increase in widening. Fold-overs are engulfments of the non-turbulent fluid by contortions of the interface, and are believed to be primarily responsible for entrainment. Thus Ajagu's measurements show that when the flow is disturbed, the interface behavior changes, but the mechanism of the change is uncertain. The change may result from a direct effect of sound upon the interface or an indirect effect resulting from changes upstream near the mouth of the jet. The results of the present study do not thoroughly clarify the problem. The mean velocity profiles exhibit no significant changes at the flow edges.

The turbulence intensity and non-dimensional Reynolds stress distributions exhibit small changes at the edge of the jet which appear to be part of overall changes in the profiles. The Reynolds stress correlation profiles appear to exhibit somewhat more significant changes. The increased correlations at the edges of the jet were discussed previously, and it was speculated that they resulted from increases in the large scale structure responsible for entrainment. The fact that the other properties of the flow show changes which appear to originate in the initial region of the flow suggests that these effects observable in the Reynolds stress correlations also originate in the initial region. However, at this point, there is insufficient evidence to prove this hypothesis. Thus further study is required to understand the effects upon the interface.

Other theories concerning effects of the disturbance upon the flow in the main region may be proposed, but such theories tend to involve the same question of the origin of the effect. Cervantes (1976) studied the lateral flapping of a plane jet. This flapping is observable through correlations across the jet, and it was found to be present from the initial region of the jet outwards. This flapping might be thought to increase the apparent widening of the jet, but limited tests with acoustic disturbances revealed no changes in the flapping. The flapping is another

characteristic of the plane jet that appears to originate in the initial region.

The available theories for the interaction of disturbances with free shear flows tend to concentrate upon effects within the initial region of the jet. The results of the present study also suggest that the interaction occurs primarily, if not solely, in the initial region. Thus a theory to predict the effects of acoustic disturbances upon the main region flow behavior would have to be able to predict the development of the flow in the main region from initial conditions obtained from non-linear viscous instability theory. Such capabilities are considerably beyond those presently available in theories of turbulent flows.

#### D. Possible Mechanism of the Interaction

The results of the present study and their comparison to the literature do suggest a possible mechanism for the interaction of a disturbing acoustic field and the turbulent plane jet. The mechanism to be described is speculative, and further study is required to confirm its accuracy.

It is believed that the interaction originates in the shear layer in the vicinity of the nozzle mouth. The Morkovin-Paranjape model of an acoustic pressure field oscillation of the stagnation point of the flow leaving the nozzle appears to be a good explanation of the way the disturbance is introduced to the shear layer. In the shear

layer the disturbance is amplified at a rate dependent upon its frequency, and undergoes various non-linear processes resulting in harmonic and subharmonic components. The energy in the shear layer is highly organized in these components. The shear layer then breaks down to fully turbulent flow while maintaining greater organization than in the undisturbed case. The turbulence intensities produced in the potential core have grown faster than in the undisturbed case and have reached higher magnitudes. The two shear layers merge, ending the potential core. The organized components of the merging shear layers may interact, with changes in phase, magnitude, or spectral distribution. The broadband turbulence intensity grows, obscuring the spectral components of the orderly structure. The mean velocity profiles attain similarity, and the jet widens at a faster rate than the undisturbed case. The greater widening may be attributed to higher turbulence intensities and Reynolds stresses and to greater entrainment by the large scale structure. As the flow proceeds, the intensities and Reynolds stresses decrease towards the undisturbed case values, and the greater widening and decay rates can no longer be sustained. Beyond  $X/D = 60$ , the widening rates and centerline intensities indicate that the flow properties asymptotically approach the properties of the undisturbed flow. It may be speculated that at sufficiently large distances downstream, the flow appears to be

identical to the undisturbed flow except for apparent virtual origins situated farther upstream.

CHAPTER VI    CONCLUSIONS AND RECOMMENDATIONS  
FOR FURTHER STUDY

The purpose of this study was to examine the interaction between an acoustic field and a turbulent plane jet. Particular emphasis was placed upon study of the changes in the turbulent structure of the flow and the mechanism through which these changes are produced.

The following conclusions have resulted from this study:

- 1) Acoustic fields of a wide frequency range produce changes in the mean flow of a jet.
- 2) Certain frequencies produce changes in the mean and turbulent flow characteristics in the main region of the jet. The differences between the disturbed flows and the undisturbed flow decrease at larger distances from the nozzle.
- 3) The turbulent intensities and Reynolds shear stresses in the main region of the flow are generally increased by the disturbance. The shapes of the transverse profiles of these properties are not greatly altered.
- 4) The interaction of the acoustic field and the turbulent plane jet appears to originate in the shear

layers in the initial region of the jet.

The following recommendations for extensions of this research are made:

1) A wider jet should be used in a detailed study of the behavior of the individual shear layers and their merging. The study should be performed using local sound sources which allow the excitation of either symmetric or asymmetric modes.

2) The turbulent energy balance terms should be measured in the main region for undisturbed and disturbed flows.

3) The behavior of the undisturbed and disturbed flows in the transition region from  $X/D = 5$  to  $X/D = 20$  should be studied.

4) A carefully controlled study of the effects upon the main region of different initial turbulent intensity magnitudes and spectral distributions should be performed.

5) A study of the effects of acoustic disturbances upon the interface and entrainment processes should be made.

6) The effect of entrainment region drafts on the jet behavior should be investigated.

LIST OF REFERENCES

## LIST OF REFERENCES

1. Acton, E., "The Modelling of Large Eddies in a Two-Dimensional Shear Layer," *J. Fluid Mech.*, 76, 3, pp. 561-592, 1976.
2. Ajagu, C. O., "Foldover, Intermittency, and Crossing Frequency of a Plane Jet Interface with and without an Acoustic Disturbance," MSME Thesis, Purdue University, 1976.
3. Bashir, J., and Uberoi, M. S., "Experiments on Turbulent Structure and Heat Transfer in a Two-Dimensional Jet," *The Physics of Fluids*, 18, 4, pp. 405-410, 1975.
4. Batchelor, G. K., The Theory of Homogenous Turbulence, Cambridge University Press, Cambridge, 1970.
5. Beavers, G. S., and Wilson, T. A., "Vortex Growth in Jets," *J. Fluid Mech.*, 44, 1, pp. 97-112, 1970.
6. Becker, H. A., and Massaro, T. A., "Vortex Evolution in a Round Jet," *J. Fluid Mech.*, 31, 3, pp. 435-448, 1968.
7. Bendat, J. S., and Piersol, A. G., Random Data: Analysis and Measurement Procedures, Wiley-Interscience, New York, 1971.
8. Betchov, R., and Criminale, W. O., Stability of Parallel Flows, Academic Press, New York, 1967.
9. Binder, G., and Favre-Marinet, M., "Mixing Improvement in Pulsating Turbulent Jets," *Proc. ASME Symp. Fluid Mech. of Mixing*, Atlanta, Georgia, pp. 167-172, 1973.
10. Borisov, Y. V., and Rosenfeld, E. I., "Action of Acoustic Oscillations on Flow Stability and Structure," *Soviet Physics-Acoustics*, 17, 2, pp. 154-168, 1971.
11. Bradbury, L. J. S., "The Structure of a Self-Preserving Turbulent Plane Jet," *J. Fluid Mech.*, 23, 1, pp. 31-64, 1965.
12. Bradshaw, P., "The Effects of Initial Conditions on the Development of a Free Shear Layer," *J. Fluid Mech.*, 26, pp. 225-236, 1966.

13. Bradshaw, P., An Introduction to Turbulence and its Measurement, Pergamon Press, Oxford, 1971.
14. Bradshaw, P., Ferriss, D. H., and Johnson, R. F., "Turbulence in the Noise-Producing Region of a Circular Jet," *J. Fluid Mech.*, 19, 4, pp. 591-624, 1964.
15. Browand, F. K., "An Experimental Investigation of the Instability of an Incompressible, Separated Shear Layer," *J. Fluid Mech.*, 26, 2, pp. 281-307, 1966.
16. Browand, F. K., and Weidman, P. D., "Large Scales in the Developing Mixing Layer," *J. Fluid Mech.*, 76, 1, pp. 127-144, 1976.
17. Brown, G. B., "On Sensitive Flames," *Phil. Mag.*, 13, 82, pp. 161-195, 1932.
18. Brown, G. B., "On Vortex Motion in Gaseous Jets and the Origin of their Sensitivity to Sound," *Phys. Soc. of London Proc.*, 47, pp. 703-732, 1935.
19. Brown, G. L., and Roshko, A., "On Density Effects and Large Structure in Turbulent Mixing Layers," *J. Fluid Mech.*, 64, 4, pp. 775-816, 1974.
20. Cervantes de Gortari, J. G., "An Experimental Study of a Turbulent Plane Jet," Ph.D. Thesis, Purdue University, 1976.
21. Champagne, F. H., "Turbulence Measurements with Inclined Hot Wires," Ph.D. Thesis, University of Washington, 1966.
22. Champagne, F. H., Pao, Y. H., and Wygnanski, I. J., "On the Two-Dimensional Mixing Region," *J. Fluid Mech.*, 74, 2, pp. 209-250, 1976.
23. Chanaud, R. C., and Powell, A., "Experiments Concerning the Sound-Sensitive Jet," *J. Acoustical Soc. of Am.*, 34, 7, pp. 907-915, 1962.
24. Collis, D. C., and Williams, N. J., "Two-Dimensional Convection from Heated Wires at Low Reynolds Number," *J. Fluid Mech.*, 6, pp. 357-384, 1959.
25. Crow, S. C., and Champagne, F. H., "Orderly Structure in Jet Turbulence," *J. Fluid Mech.*, 48, 3, pp. 547-591, 1971.

26. Curtet, R. M., and Girard, J. P., "Visualization of a Pulsating Jet," Proc. ASME Symp. Fluid Mech. of Mixing, Atlanta, Georgia, pp. 173-180, 1973.
27. Davies, P. O. A. L., "Structure of Turbulence," J. Sound and Vib., 28, 3, pp. 513-526, 1973.
28. Davies, P. O. A. L., and Yule, A. J., "Coherent Structures in Turbulence," J. Fluid Mech., 69, pp. 513-537, 1975.
29. Flora, J. J. Jr., and Goldschmidt, V. W., "Virtual Origins of a Free Plane Turbulent Jet," AIAA Journal, 7, 12, pp. 2344-2346, 1969.
30. Freymuth, P., "On Transition in a Separated Laminar Boundary Layer," J. Fluid Mech., 25, 4, pp. 683-704, 1966.
31. Friehe, C. A., and Schwarz, W. H., "Deviations From the Cosine Law for Yawed Cylindrical Anemometer Sensors," Trans. of ASME, J. of Applied Mech. E., 35, 4, pp. 655-662, 1968.
32. Fuchs, H. V., "Space Correlations of the Fluctuating Pressure on Subsonic Turbulent Jets," J. Sound and Vib., 23, 1, pp. 77-99, 1972.
33. Gaster, M., "The Role of Spatially Growing Waves in the Theory of Hydrodynamic Stability," Progress in Aeronautical Sciences, ed. by D. Küchemann and L. H. G. Steme, pp. 251-270, 1965.
34. Glass, D. R., "Effects of Acoustic Feedback on the Spread and Decay of Supersonic Jets," AIAA Jrnl., 6, 10, pp. 1890-1897, 1968.
35. Görtler, H., "Berechnung von Aufgaben der freien Turbulenz auf Grund eines neuen Näherungsansatzes," Z. angew. Math. Mech., 22, 5, pp. 244-254, 1942.
36. Goldschmidt, V. W., and Kaiser, K. F., "Interaction of an Acoustic Field and a Turbulent Plane Jet: Mean Flow Measurements," AICHE Chem. Eng. Prog. Symp. Series, 67, 109, pp. 91-98, 1971.
37. Grant, A. J., "A Numerical Model of Instability in Axisymmetric Jets," J. Fluid Mech., 56, 4, pp. 707-724, 1974.
38. Grant, H. L., "The Large Eddies of Turbulent Motion," J. Fluid Mech., 4, pp. 149-190, 1958.

39. Gutmark, E., and Wagnanski, I., "The Planar Turbulent Jet," *J. Fluid Mech.*, 73, 3, pp. 465-495, 1976.
40. Hegge Zijnen, B. G. van der, "Measurements of Velocity Distribution in a Plane Turbulent Jet," *Appl. Sci. Res.*, 7, A, pp. 256-276, 1958.
41. Heskestad, G., "Hot Wire Measurements in a Plane Turbulent Jet," *Trans. of ASME J. App. Mech.*, pp. 721-734, 1965.
42. Hinze, J. O. Turbulence: An Introduction to Its Mechanism and Theory, McGraw-Hill, New York, 1975.
43. Hussain, A. K. M. F., and Zaman, K. B. M. Q., "Effect of Acoustic Excitation on the Turbulent Structure of a Circular Jet," *Third Interagency Symposium on University Research in Transportation Noise*, University of Utah, Salt Lake City, Utah, pp. 314-326, Nov. 12-14, 1975.
44. Ivanov, N. N. "Acoustic Effect on the Root Part of a Turbulent Jet," *Izv. AN SSSR, Mekhanika Zhidkosti i Gaza*, 4, pp. 182-186, 1970.
45. Jenkins, P. E., "A Study of the Intermittent Region of a Heated Two-Dimensional Plane Jet," Ph.D. Thesis, Purdue University, 1974.
46. Jenkins, P. E., and Goldschmidt, V. W., "Mean Temperature and Velocity in a Plane Turbulent Jet," *Trans. of ASME, J. Fluids Eng.*, 95, 1, 4, pp. 581-584, 1973.
47. Kaiser, K. F., "An Experimental Investigation of the Interaction of an Acoustic Field and a Plane Turbulent Jet," M.S. Thesis, Purdue University, 1971.
48. Kelly, R. E., "On the Stability of an Inviscid Boundary Layer which is Periodic in Space and Time," *J. Fluid Mech.*, 27, 4, pp. 657-689, 1967.
49. Ko, N. W. M., and Davies, P. O. A. L., "The Noise Spectrum within the Potential Cone of Subsonic Cold Jets," *J. Fluid Mech.*, 50, 1, pp. 49-78, 1971.
50. Lau, J. C., and Fisher, M. J. "The Vortex-Street Structure of 'Turbulent' Jets. Part 1," *J. Fluid Mech.*, 67, 2, pp. 299-337, 1975.
51. Lau, J. C., Fisher, M. J., and Fuchs, H. V., "The Intrinsic Structure of Turbulent Jets," *J. Sound and Vib.*, 22, 4, pp. 379-406, 1972.

52. Laufer, J., "New Trends in Experimental Turbulence Research," *Ann. Rev. Fluid Mech.*, 7, pp. 307-326, 1975.
53. Lebedev, N. G., and Telenin, G. F., "Interaction between a Supersonic Jet and an Acoustic Field," *Izv. AN SSSR, Mekhanika Zhidkosti i Gaza*, 4, pp. 82-94, 1970.
54. Leconte, John, "On the Influence of Musical Sounds on the Flame of a Jet of Coal-Gas," *Phil Mag.*, 15, pp. 235-239, 1858.
55. Lin, C. C., The Theory of Hydrodynamic Stability, Cambridge University Press, Cambridge, U. K., 1955.
56. Mattingly, G. E., and Criminale, W. O., Jr., "Disturbance Characteristics in a Plane Jet," *Physics of Fluids*, 14, 11, pp. 2258-2264, 1971.
57. Michalke, A., "On Spatially Growing Disturbances in an Inviscid Shear Layer," *J. Fluid Mech.*, 23, 3, pp. 521-544, 1965.
58. Miksad, R. W., "Experiments on the Nonlinear Stages of Free-Shear-Layer Transition," *J. Fluid Mech.*, 56, 4, pp. 695-719, 1972.
59. Miller, D. R., and Comings, E. W., "Static Pressure Distribution in the Free Turbulent Jet," *J. Fluid Mech.*, 3, 1, pp. 1-6, 1957.
60. Mollo-Christensen, Erik, "Jet Noise and Shear Flow Instability Seen From an Experimenter's Viewpoint," *ASME Transactions, J. Applied Mech.*, 89, 1, pp. 1-7, 1967.
61. Monin, A. S., and Yaglom, A. M., Statistical Fluid Mechanics: Mechanics of Turbulence, 1, MIT Press, Cambridge, Mass., 1971.
62. Morkovin, M. V., and Paranjape, S. V., "On Acoustic Excitation of Shear Layers," *Z. Flugwiss*, 19, 8/9, pp. 328-335, 1971.
63. Mulej, D. J., "Velocity and Foldover of the Turbulent Non-Turbulent Interface in a Plane Jet," MSME Thesis, Purdue University, 1975.
64. Murthy, S. N. B., ed., Turbulent Mixing in Nonreactive and Reactive Flows, Plenum Press, New York, 1975.

65. Ott, E. S., "Convective Velocities in a Turbulent Plane Jet," MSME Thesis, Purdue University, 1972.
66. Planchon, Harry P., "The Fluctuating Static Pressure Field in a Round Jet Turbulent Mixing Region," Ph.D. Dissertation, University of Illinois at Urbana-Champaign, 1974.
67. Reichardt, H., "Gesetzmässigkeiten der freien Turbulenz," VDI-Forschungsheft 414, 1942.
68. Rockwell, D. O., "The Macroscopic Nature of Jet Flows Subjected to Small Amplitude Periodic Disturbances," AICHE Chem. Engr. Progress Symposium Series, 67, 109, pp. 99-107, 1971.
69. Rockwell, D. O., "External Excitation of Planar Jets," Trans. of ASME, J. App. Mech., 39, 4, pp. 883-890, 1972.
70. Rockwell, D. O., and Niccolls, W. O., "Natural Break-down of Planar Jets," Trans. of ASME, J. of Basic Eng., 94, 4, pp. 720-730, 1972.
71. Rockwell, D. O., and Toda, K., "Effects of Applied Acoustic Fields on Attached Jet Flows," Trans. of ASME, J. of Basic Eng., 93, 1, pp. 63-73, 1971.
72. Roffman, G. L., and Toda, K., "A Discussion of the Effects of Sound on Jets and Fluoric Devices," Trans. of ASME, J. of Eng. for Ind., 91, pp. 1161-1167, 1969.
73. Roshko, A., "Progress and Problems in Understanding Turbulent Shear Flows," Turbulent Mixing in Non-Reactive and Reactive Flows, a Project SQUID Workshop, edited by S. N. B. Murthy, Plenum Press, New York and London, pp. 295-316, 1975.
74. Roshko, A., "Structure of Turbulent Shear Flows: A New Look," AIAA Journal, 14, 10, pp. 1349-1357, 1976.
75. Sandborn, V. A., Resistance Temperature Transducers, Metrology Press, Fort Collins, Colorado, 1972.
76. Sato, H., "The Stability and Transition of a Two-Dimensional Jet," J. Fluid Mech., 7, 1, pp. 53-80, 1960.
77. Sato, H., and Sakao, F., "An Experimental Investigation of the Instability of a Two-Dimensional Jet at Low Reynolds Numbers," J. Fluid Mech., 20, 2, pp. 337-352, 1964.

78. Schlichting, H., Boundary Layer Theory, 6th ed., McGraw Hill, New York, 1968.
79. Simcox, D. D., "A Theoretical Investigation of Acoustic-Turbulence Interactions with Application to Free-Jet Spreading," Ph.D. Thesis, Purdue University, 1969.
80. Simcox, C. D., and Hoglund, R. F., "Acoustic Interactions with Turbulent Jets," Trans. of ASME, J. Basic Eng., 93, pp. 42-46, 1971.
81. Tennekes, H., and Lumley, J. L., A First Course in Turbulence, The MIT Press, Cambridge, Mass., 1972.
82. Thompson, C. A., "Organized Motions in a Plane Turbulent Jet under Controlled Excitation," Ph.D. Thesis, University of Houston, 1975.
83. Townsend, A. A., "The Mechanism of Entrainment in Free Turbulent Flows," J. Fluid Mech., 26, 4, pp. 689-715, 1966.
84. Townsend, A. A., The Structure of Turbulent Shear Flow, Cambridge University Press, Cambridge, U. K., 1956.
85. Vlasov, E. V., and Ginevskii, A. S., "Acoustic Modification of the Aerodynamic Characteristics of a Turbulent Jet," Izv. AN SSSR, Mekhanika Zhidkosti i Gaza, 2, 4, pp. 133-138, 1967.
86. Wille, Rudolf, "Growth of Velocity Fluctuations Leading to Turbulence in Free Shear Flow," Defense Documentation Center AD 418294, 1963 or Air Force Office of Scientific Research Technical Report AF 61(052)-412 TR, 1963.
87. Winant, C. D., and Browand, F. K., "Vortex Pairing: the Mechanism of Turbulent Mixing Layer Growth at Moderate Reynolds Number," J. Fluid Mech., 63, 2, pp. 237-255, 1974.
88. Witze, P. O., and Dwyer, H. A., "The Turbulent Radial Jet," J. Fluid Mech., 75, 3, pp. 401-417, 1976.
89. Wooldridge, C. E., and Wooten, D. C., "A Study of the Large-Scale Eddies of Jet Turbulence Producing Jet Noise," AIAA Paper No. 71-154, 1971.
90. Wooldridge, C. E., Wooten, D. C., and Amaro, A. J., "The Structure of Jet Turbulence Producing Jet Noise," AIAA Paper No. 72-158, 1972.

91. Wygnanski, I., and Fiedler, H., "Some Measurements in the Self Preserving Jet," J. Fluid Mech., 38, 3, pp. 577-612, 1969.
92. Wygnanski, I., and Fiedler, H. E., "The Two-Dimensional Mixing Region," J. Fluid Mech., 41, 2, pp. 327-361, 1970.
93. Young, M. F., "A Turbulence Study: Convective Velocities, Energy Spectra, and Turbulent Scales in a Plane Air Jet," MSME Thesis, Purdue University, 1973.

APPENDICES

## APPENDIX A BASIC MEAN FLOW PROPERTIES

A number of measurements were performed to evaluate the two-dimensionality of the flow field and determine some properties of the mean flow. The similarity of the mean velocity profiles in the main region of the flow is observable in Figure IV-1. The measured half widths and centerline mean velocities indicate that the jet widening and centerline velocity decay did follow the form of Equations II-1 and II-2, as expected of a two-dimensional plane free jet.

1. Vertical Uniformity of Centerline Mean Velocity

A further evaluation of the two-dimensionality of the flow field was obtained through measurements of the vertical distributions of the centerline mean velocity. The measured profiles are shown in Figure A-1. Within the central two-thirds of the flow field, the measured points display deviations from uniformity that are at most less than seven per cent. Most points are well within this range. The uniformity is sufficient to consider the central region of the jet representative of a two-dimensional jet. All other reported flow field measurements were performed in the centerplane of the jet. It is particularly

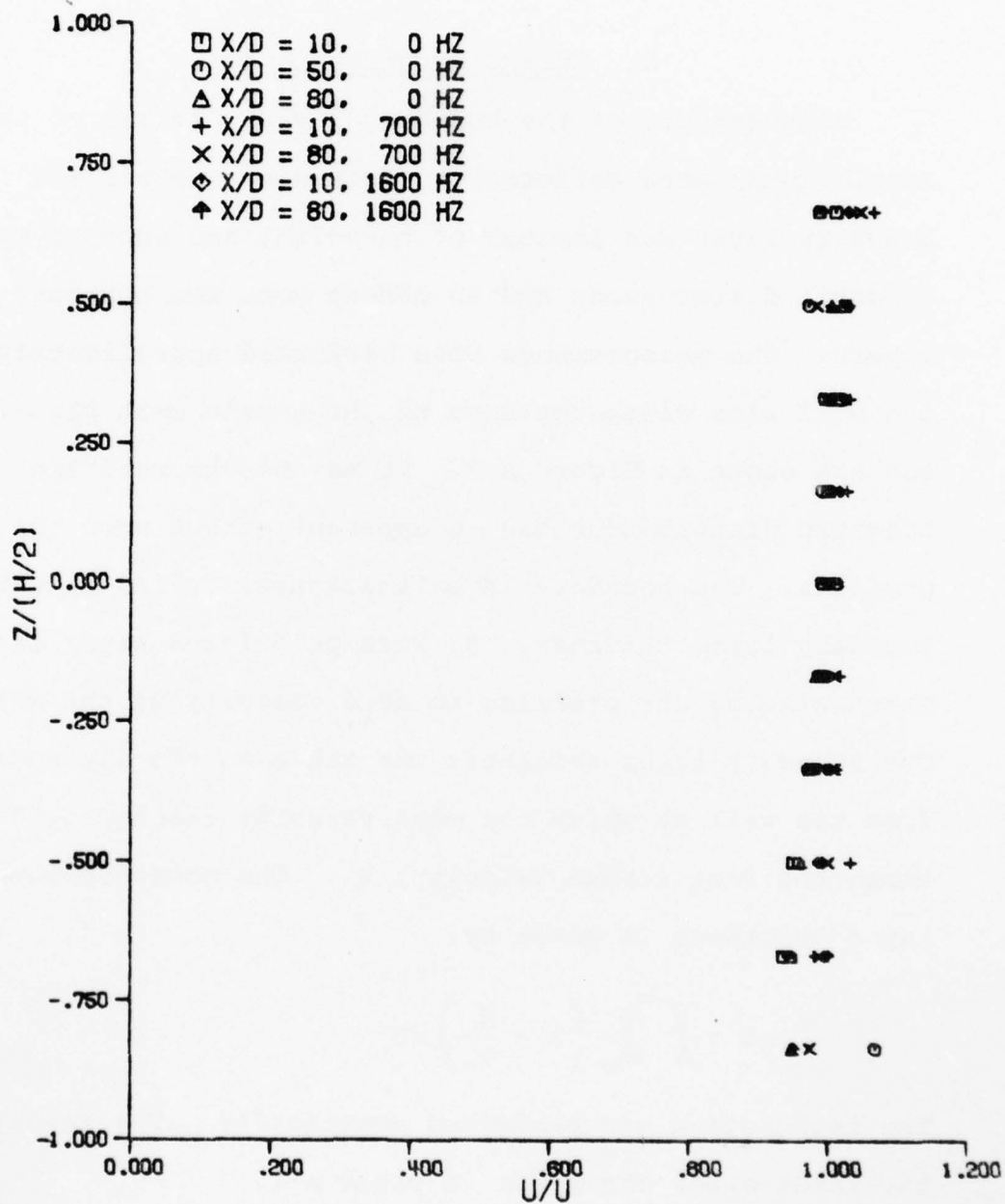


Figure A-1 Vertical Profiles of Mean Velocity

noteworthy that the acoustically disturbed case profiles display the same uniformity. The disturbance does not destroy the two-dimensionality of the flow field.

## 2. Nozzle Boundary Layers

Measurements of the boundary layer upstream of the nozzle mouth were performed to determine whether the boundary layer was laminar or turbulent and whether the acoustic disturbances had an effect upon the boundary layers. The measurements were performed approximately one half slot width upstream of the nozzle exit plane, and are shown in Figure A-2. It may be observed that the acoustic disturbances had no apparent effect upon the profiles. The boundary layer thickness,  $\delta$ , and momentum boundary layer thickness,  $\theta$ , were calculated after linearly extrapolating the profiles to zero velocity at the wall. The boundary layer thickness was taken as the distance from the wall at which the mean velocity reached 0.99 times the free stream velocity,  $U_\infty$ . The momentum boundary layer thickness is given by:

$$\theta = \int_0^\infty \frac{\bar{U}}{U_\infty} \left( 1 - \frac{\bar{U}}{U_\infty} \right) dy \quad (\text{A-1})$$

The integration was performed numerically. The results for the three cases are given in Table A-1.

Schlichting (1968) presents the results of numerical calculations for a laminar flat plate boundary layer, and

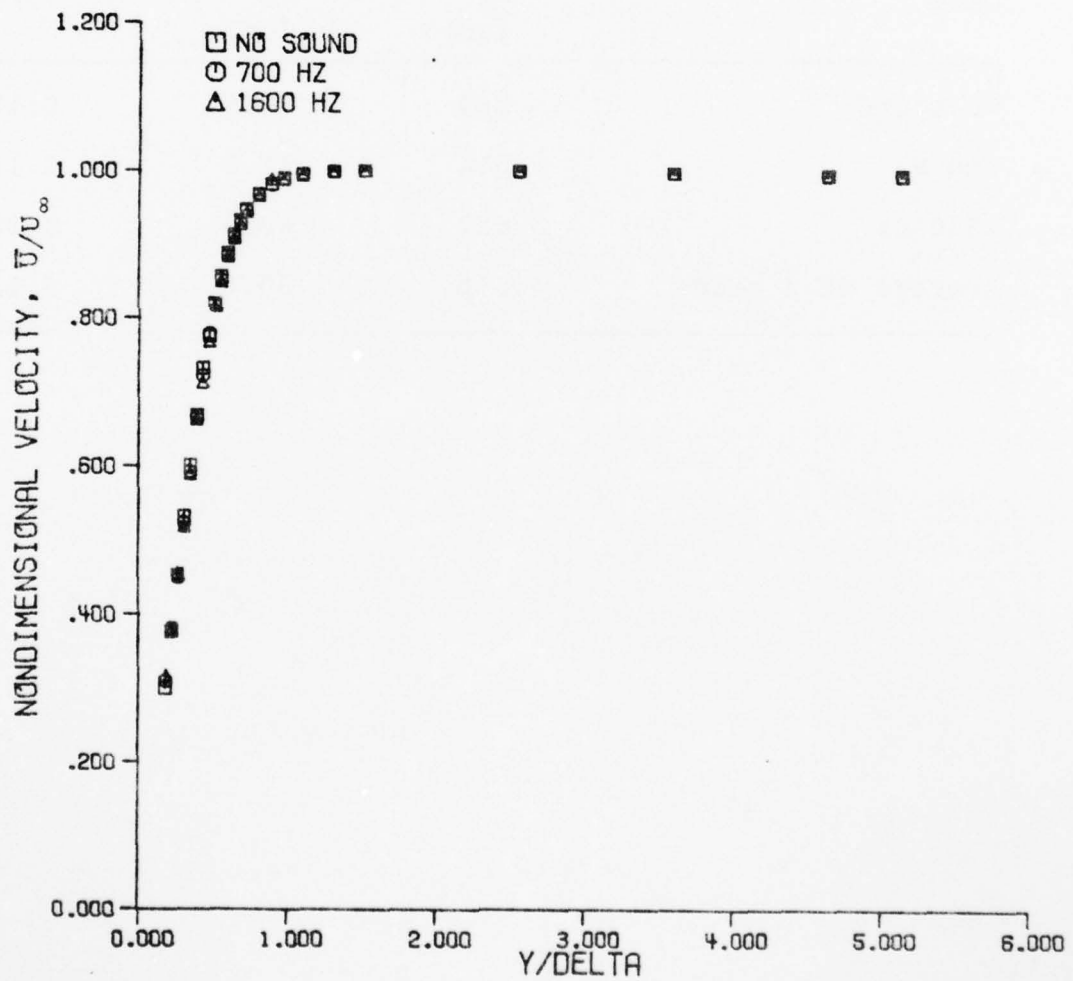


Figure A-2 Nozzle Boundary Layer Mean Velocity Profiles

TABLE A-1  
NOZZLE BOUNDARY LAYER PROPERTIES

Case	$\delta$ ( $\mu\text{m}$ )	$\theta$ ( $\mu\text{m}$ )	$\theta/\delta$
No sound	599	78.9	0.132
700 Hz	614	81.5	0.133
1600 Hz	617	80.9	0.131
Average of 3 cases	610	80.4	0.132

the resulting ratio of the momentum boundary layer thickness to the boundary layer thickness is 0.133. The results of the measurements in the nozzle are in very good agreement with this number. They are considerably higher than the value of 0.097 reported by Schlichting (1968) for a turbulent one seventh power law boundary layer over a flat plate. These results indicate that the nozzle boundary layers were laminar and little affected by the disturbance sound field.

### 3. Jet Initial Velocity Profiles

The mean velocity profiles of the jet were measured at  $X/D \approx 0.25$  for the three cases. The resulting non-dimensional profiles are shown in Figure A-3. It may be observed that the disturbed case profiles are negligibly different from that of the undisturbed case. The momentum thicknesses of the profiles were calculated using the following equation.

$$\theta_+ + \theta_- = - \int_{\infty}^{-\infty} \frac{\bar{U}}{\bar{U}_m} \left( 1 - \frac{\bar{U}}{\bar{U}_m} \right) dY \quad (A-2)$$

The thicknesses on the positive and negative "Y" sides of the profile were separated by splitting the numerically integrated integral at the centerline. The results are given in Table A-2. Note that  $\theta_+$  corresponds to the side farthest from the disturbing sound source. The average of the three cases was used in calculating Strouhal numbers for Table V-1.

TABLE A-2  
SHEAR LAYER MOMENTUM THICKNESSES

Case	$\theta_-$ ( $\mu\text{m}$ )	$\theta_+$ ( $\mu\text{m}$ )	$\theta_{\text{avg}} = \frac{\theta_+ + \theta_-}{2}$ ( $\mu\text{m}$ )
No sound	101	95.3	97.9
700 Hz	97.0	102	99.7
1600 Hz	106	100	103
Average of three cases	101	99.3	100

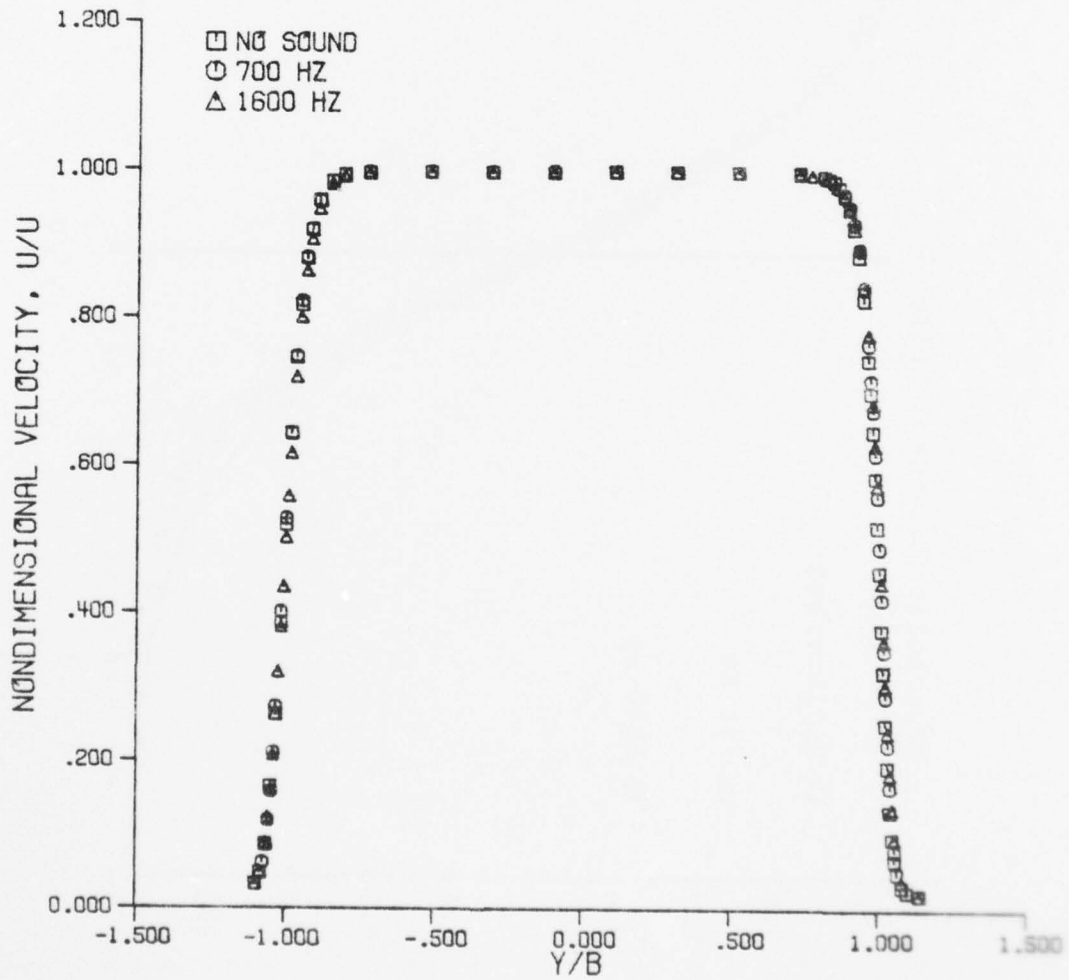


Figure A-3 Mean Velocity Profiles at Jet Mouth

AD-A071 261

PURDUE UNIV LAFAYETTE IND RAY W HERRICK LABS  
ACOUSTIC INTERACTION WITH A TURBULENT PLANE JET. (U)  
AUG 77 F W CHAMBERS, F WILLIAMS  
HL-77-31

F/6 20/4

N00014-67-A-0226-0025  
NL

UNCLASSIFIED

5 of 5  
AD  
A071261



END  
DATE  
FILMED  
8-79  
DDC



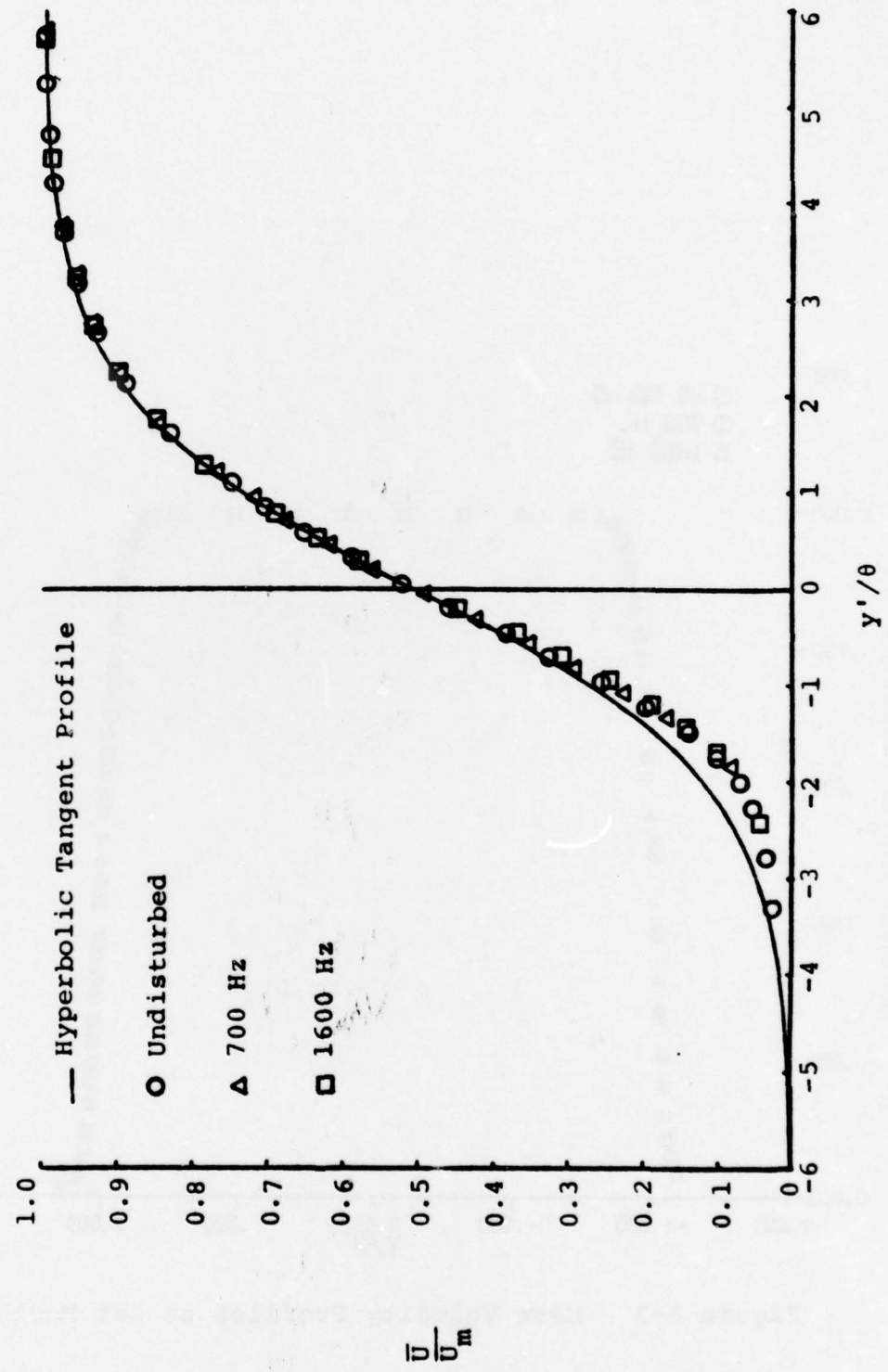


Figure A-4 Comparison of Measured Mean Velocity Profile at Mouth to Hyperbolic Tangent Profile

The shear layer mean velocity profile is an important factor in instability calculations. The shear layer portions of the profiles in Figure A-3 are plotted on different coordinates in Figure A-4 along with the hyperbolic tangent profile commonly used in instability calculations. The hyperbolic tangent profile equation is given by the following equation:

$$\frac{\bar{U}}{U_m} = 0.5 \left[ 1 + \tanh (0.5y'/\theta) \right] \quad (A-3)$$

In Equation A-3,  $y'$  is the distance from the point at which  $\frac{\bar{U}}{U_m} = 0.5$ , with the positive direction being towards the center of the jet. It may be observed that at positive values of  $y'$ , the measured profiles coincide with the theoretical profile, while at negative values the measured profiles are lower. The profiles were measured with a linearized straight wire with the wire axis positioned vertically. This wire may have been subject to effects of lateral entrainment velocities at the outer edges of the profiles with a resulting decrease in accuracy.

## APPENDIX B SOUND FIELD MEASUREMENTS

A series of measurements of the disturbing sound fields applied to the jet flow field were performed. The motivation for these measurements was the belief that although the disturbance sound pressure level was held constant at a single measuring position, non-uniformities in the sound field could result in effectively different disturbing amplitudes.

1. Frequency Dependence of Sound Pressure Levels Near the Nozzle Mouth

It was believed that the sound pressure level in the region near the nozzle mouth might be of some significance in the interaction mechanism between the sound field and the flow. For this reason, the sound pressure levels at  $X/D = 4$  and  $Y/D = 4$  in the vertical center plane of the jet were measured during the course of some of the widening rate measurements. The results are presented in Figure B-1. Note that these measurements were performed with flow, and hence the undisturbed case results plotted at zero frequency reflect the sound pressure level produced by the jet in its near field. The major conclusion that may be reached upon examination of the results is

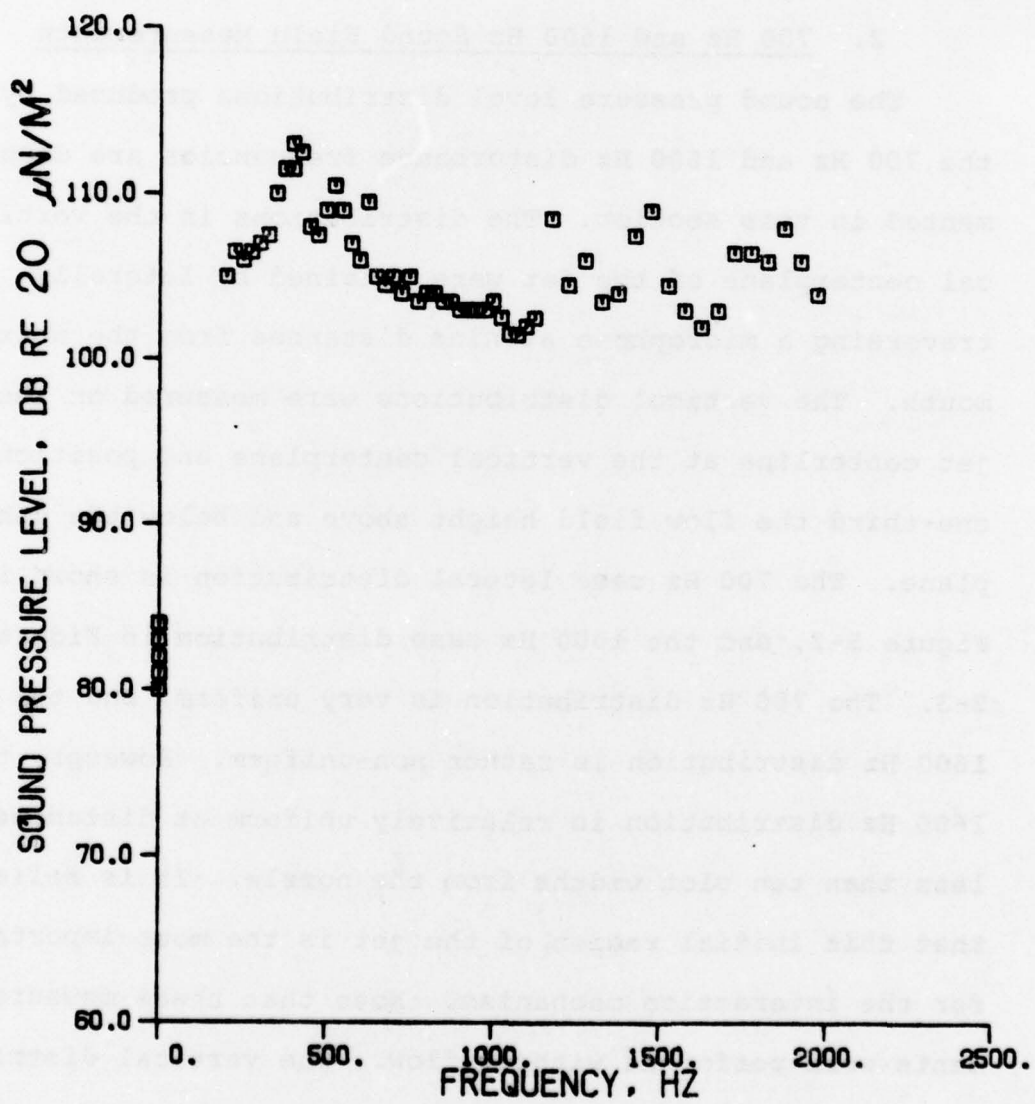


Figure B-1 Frequency Dependence of Sound Pressure Levels Measured Near Mouth of Jet

that while the levels were dependent upon frequency, the peaks in the distribution do not correspond to the peaks of the widening rate distribution in Figure IV-2. Therefore the interaction mechanism does not appear to be strongly dependent upon the sound pressure level near the nozzle mouth.

## 2. 700 Hz and 1600 Hz Sound Field Measurements

The sound pressure level distributions produced by the 700 Hz and 1600 Hz disturbance frequencies are documented in this section. The distributions in the vertical centerplane of the jet were obtained by laterally traversing a microphone at nine distances from the nozzle mouth. The vertical distributions were measured on the jet centerline at the vertical centerplane and positions one-third the flow field height above and below the centerplane. The 700 Hz case lateral distribution is shown in Figure B-2, and the 1600 Hz case distribution in Figure B-3. The 700 Hz distribution is very uniform, and the 1600 Hz distribution is rather non-uniform. However, the 1600 Hz distribution is relatively uniform at distances less than ten slot widths from the nozzle. It is believed that this initial region of the jet is the most important for the interaction mechanism. Note that these measurements were performed without flow. The vertical distributions for both cases are presented in Figure B-4. It may be seen that these distributions are relatively

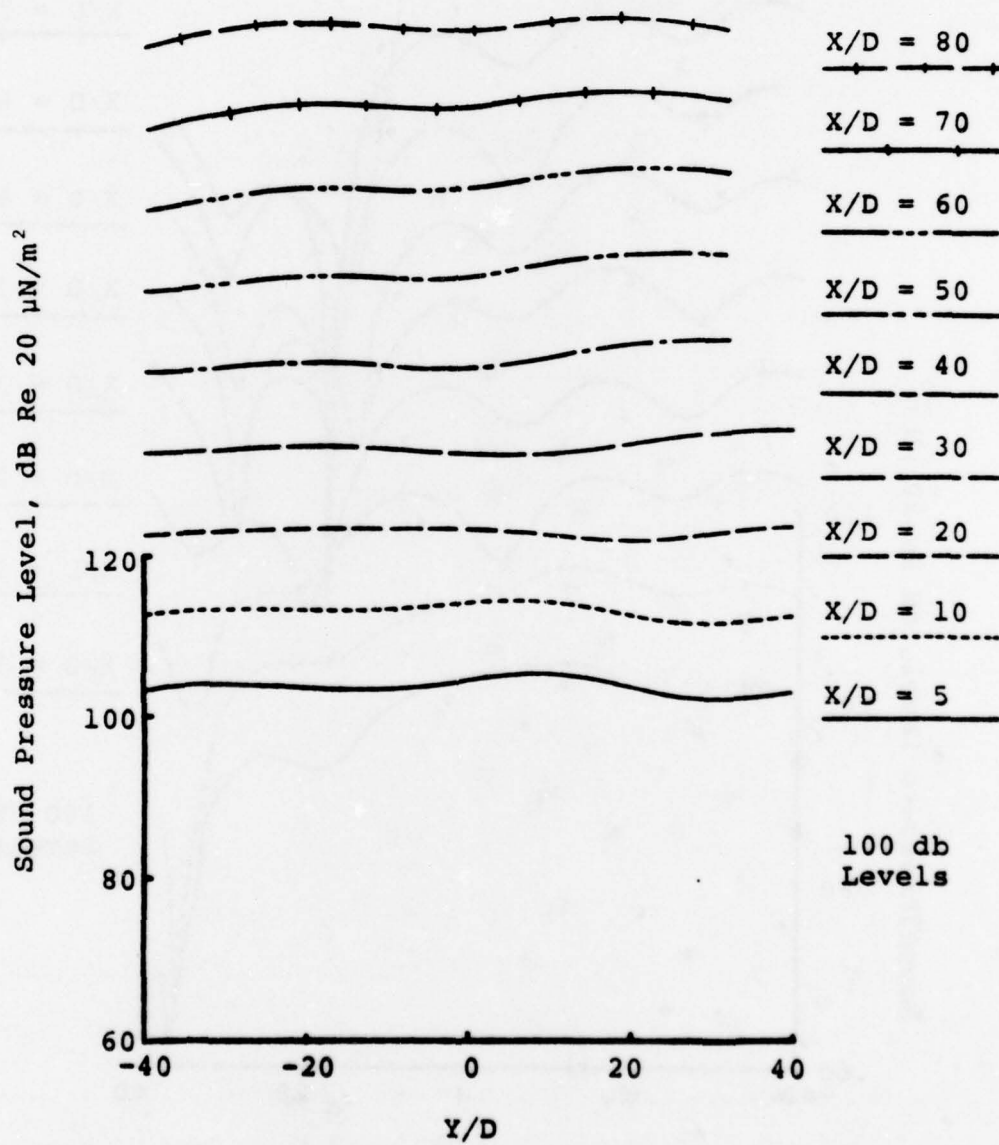


Figure B-2 700 Hz Case Transverse Sound Pressure Level Profiles

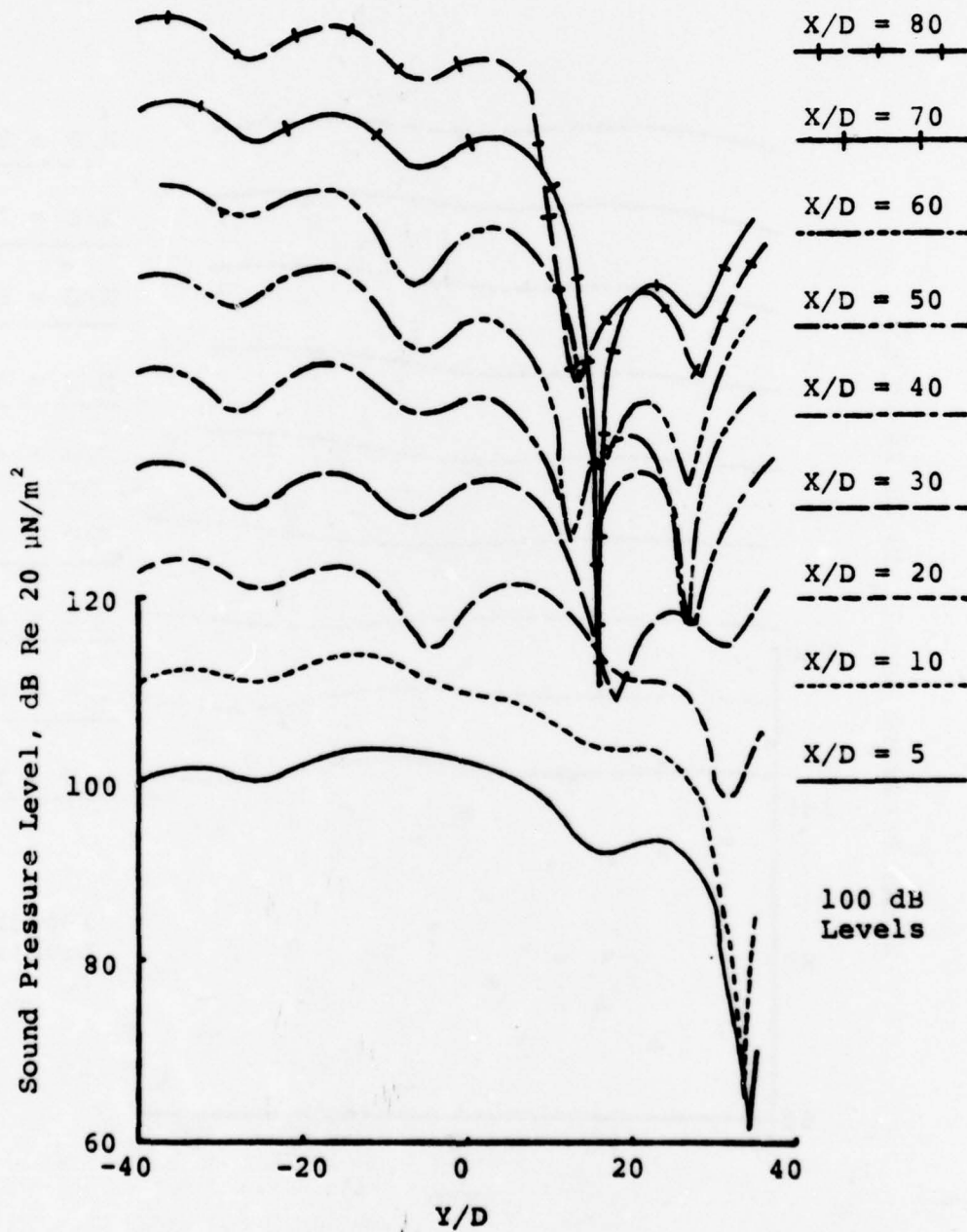


Figure B-3 1600 Hz Case Transverse Sound Pressure Level Profiles

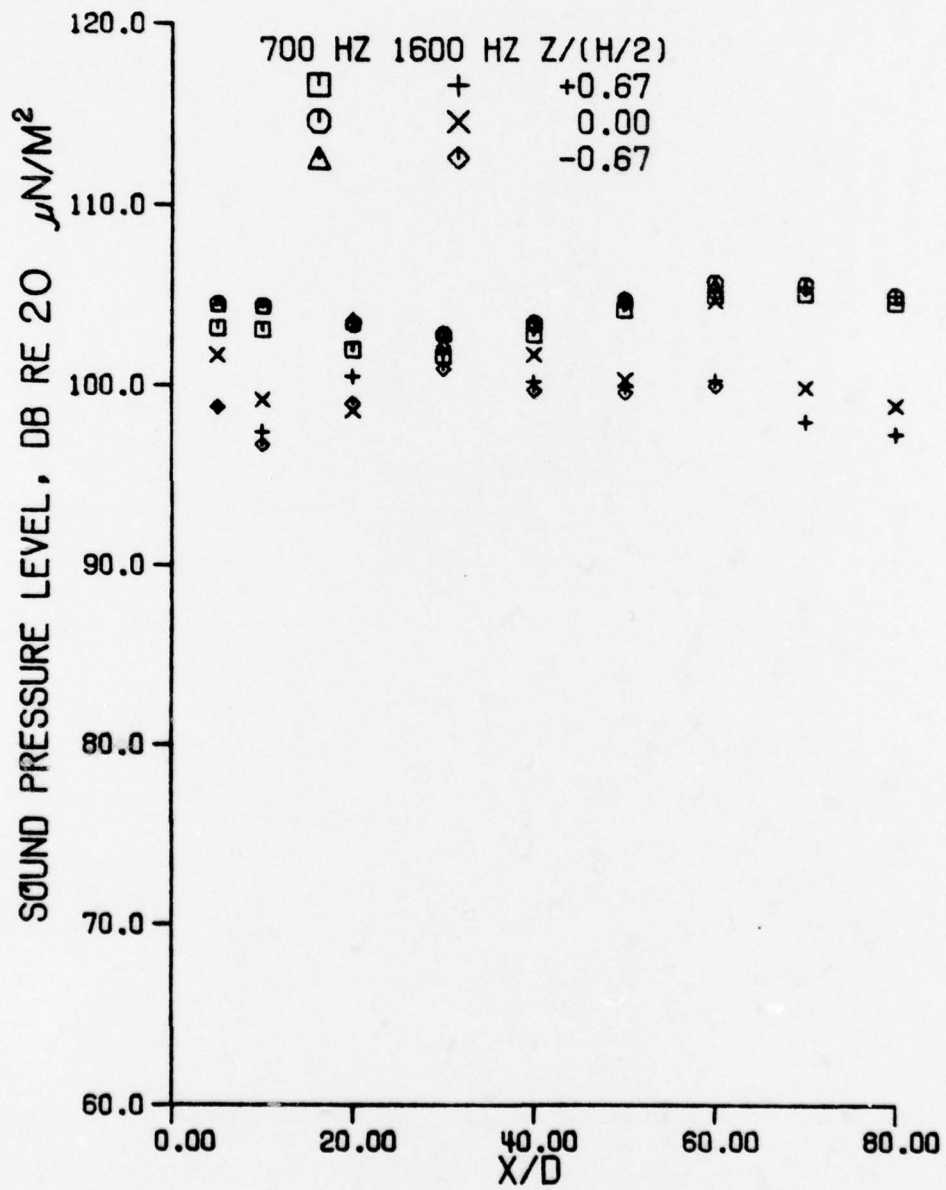


Figure B-4 Sound Pressure Levels at Various Vertical Positions along Jet Centerline

uniform for both cases, particularly close to the nozzle. The non-uniformities of the sound fields do not appear to be sufficiently severe to be important factors in the measured flow field effects of the interaction.

## APPENDIX C FLUCTUATION PHENOMENON STUDY

The jet was found to exhibit peculiar behavior when disturbed at frequencies between roughly 800 Hz and 1400 Hz. The pressure profiles used to determine the jet widening and decay rates display greatly increased fluctuations for disturbance frequencies within this range. Figure C-1 is a pair of pressure profiles plotted for a disturbance frequency of 1100 Hz, at which the phenomenon appeared to be the most severe. It may be observed that these profiles display much greater levels of fluctuation than do the typical profiles of Figure III-7. While the profiles were being plotted, it was observed that the fluctuations seemed to indicate a tendency for the mean pressure profile to make intermittent, short excursions to a lower mean level. A study of this phenomenon was performed, with initial attempts made to determine whether the phenomenon resulted from the behavior of the experimental equipment.

Quickly eliminated as causes of the phenomenon were vibrations of the traversing mechanism and problems in the plotter or signal processing instrumentation. Nor were there fluctuations occurring in the applied sound field.

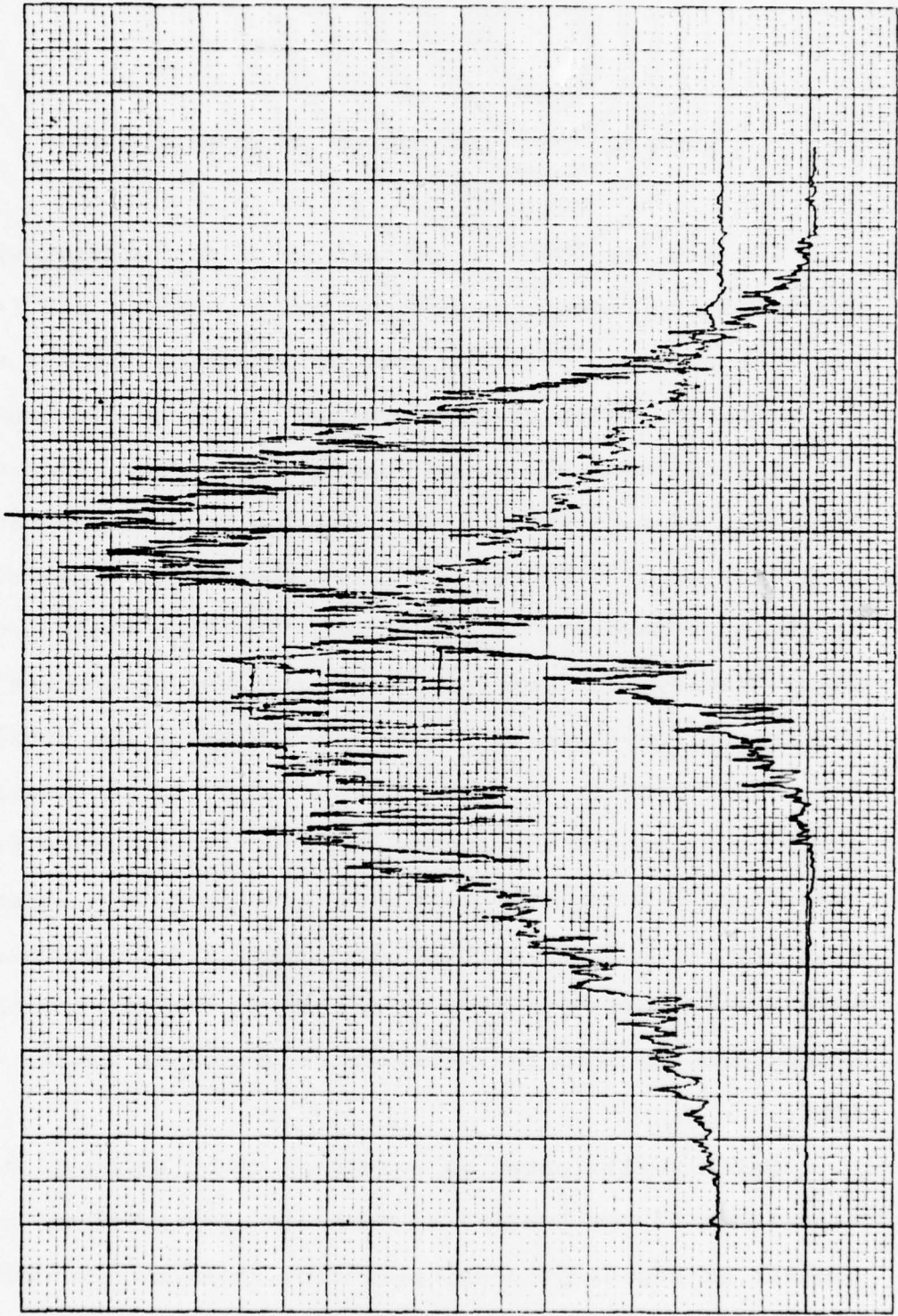
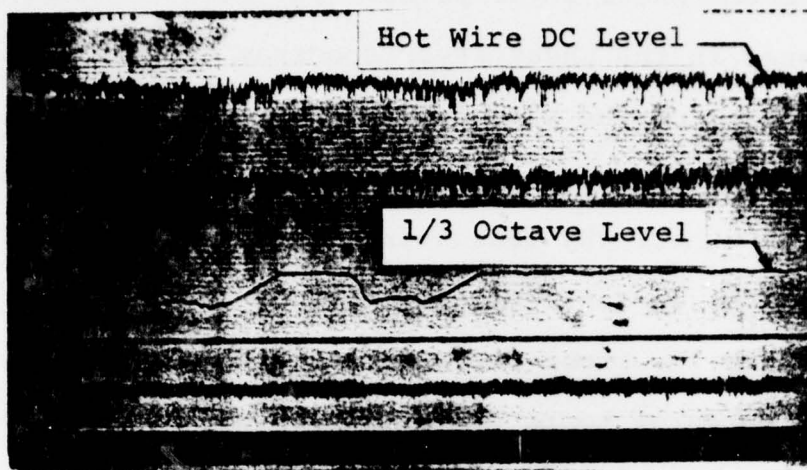


Figure C-1 Pressure Profiles Displaying Intermittent Fluctuations  
for an 1100 Hz Disturbance Frequency

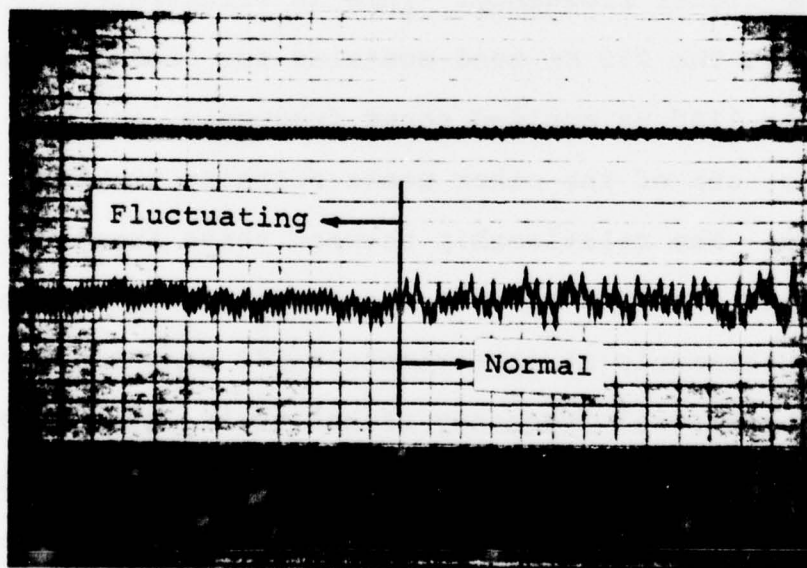
Other possible causes considered were resonances or vibrations in the jet confining plates or in the duct leading to the nozzle. Attempts were made to add damping and stiffness to these, but the phenomenon persisted. Efforts were also made to eliminate any other parasitic sources of noise or disturbance such as small leaks in the plenum.

In order to study the flow in more detail, a hot wire anemometer was used. The fluctuations were most noticeable within the center part of the jet and at axial positions of  $X/D = 40$  and  $50$ . The phenomenon was strongest at an applied sound frequency of  $1100$  Hz, so this frequency was used to disturb the jet. The hot wire probe was positioned on the jet centerline at  $X/D = 40$ , and the autocorrelation of the turbulent signal was measured using a SAICOR SAI-42 Correlation and Probability Analyzer. The autocorrelation did not reveal any regular, periodic component. A second hot wire anemometer and probe were added and attempts were made to crosscorrelate between the probe on the centerline at  $X/D = 40$  and the second probe positioned in the mouth of the jet. The results were inconclusive. A Hewlett Packard 8054A Real Time Audio Spectrum Analyzer was then used to look at the real time one third octave spectra of the signal from the hot wire at  $X/D = 40$ . Nothing unusual was observed. The probe at the mouth of the jet was repositioned at  $X/D = 1$  in the shear layer on one side of the jet. The signal from this probe was then fed to the

real time analyzer, and it was observed that the spectrum had an intermittent fluctuation in the 250 Hz one third octave band. The amplitude of this band occasionally dropped more than 10 dB for a moment while the other peaks in the spectrum changed by no more than 2 dB. The sudden drop of the spectrum at 250 Hz was compared with the fluctuations of the mean pressure profile by simultaneously recording the two signals. The microphone output from the B&K 2107 Frequency Analyzer (proportional to the applied sound pressure level), the dc and ac signals from the hot wire in the shear layer at  $X/D = 1$ , the output of the 250 Hz band of the real time analyzer (a dc level proportional to amplitude), and the dc and ac signals from the hot wire probe on the jet centerline at  $X/D = 40$  were all fed to a Honeywell Accudata 117 DC Amplifier which was connected to a Honeywell 1508 Visicorder. Long visicorder recordings revealed that the two phenomena occurred at approximately the same time. This is illustrated in Figure C-2a, however the limited length shown does not make it very clear. The drop in the 250 Hz band of the spectrum of the probe in the shear layer was accompanied by a drop in the dc level of the probe at  $X/D = 40$ . It was unclear whether the phenomenon began in the shear layer and carried on to larger  $X/D$ 's or was simultaneous. The damping in the real time analyzer obscured this. The real time analyzer was replaced by bandpassing the 250 Hz



a. Comparison of Mean Velocity at  $X/D = 40$  and 250 Hz 1/3 Octave Band Component of Signal from Hot Wire in Shear Layer



b. Changes in Signal from Hot Wire in Shear Layer

Figure C-2 Recordings of the Intermittent Fluctuations

signal from the shear layer probe. The relative timing of the change in the shear layer spectrum and the change in the dc level of the signal from the probe at  $X/D = 40$  was still uncertain. It could not be seen whether one preceded the other. By increasing the recording speed, it was possible to see the change in the shape of the ac signal from the probe in the shear layer. Normally the signal appeared to be composed of a superposition of a low frequency signal (in the 250 Hz band) and another signal of approximately twice this frequency. During changes in the spectrum, the lower frequency component disappeared and the signal assumed a more purely sinusoidal form at the higher frequency. This is illustrated in Figure C-2b. The 250 Hz band contains the second subharmonic of the 1100 Hz applied sound frequency, and the 500 Hz band, one of the other peaks contains the first subharmonic. The relationship between these frequencies suggests that the 1100 Hz disturbance frequency may form a strong subharmonic at approximately 540 Hz which corresponds to the natural frequency of the shear layer reported in Chapter IV. The natural shear layer frequency then forms its first subharmonic, which is a frequency within the 250 Hz one third octave band. The intermittent disappearance of this subharmonic then appears to result in very large changes in the character of the flow in the main region of the jet. These changes, and their

dependence upon the initial conditions of the flow were investigated using the following technique.

A hot wire probe was positioned on the jet centerline at  $X/D = 50$ . The probe was connected to a Thermo Systems Model 1050 Anemometer. The anemometer bridge voltage was input to a Hewlett Packard 5450A Fourier Analyzer System using dc coupling. The desired conditions of sound and turbulence generation were applied to the jet, and the Fourier analyzer was used to take a histogram of the anemometer bridge voltage. The analyzer was then used to normalize the histogram, forming a probability density function for the anemometer bridge voltage. This probability density function was then punched on paper tape for input to the digital computer. On the digital computer, a previous calibration curve for the hot wire probe was used to convert the probability density function for the anemometer voltage to a probability density function for absolute velocity.

It should be noted that the hot wire calibration curve used was not taken on the same day as the histograms, and is probably slightly in error. However, the same calibration was used for all of the histograms, and the velocities are all correct in a relative sense. In addition, a different total time was used to obtain each of the histograms. This was a result of the method the Fourier analyzer used to obtain the histogram. The input

attenuator was set so that the 1024 load addresses of the analyzer were divided over a range of eight volts. That corresponded to 128 addresses per volt. The sampling rate was set at 200  $\mu$ s per sample. The analyzer then obtained the histogram by sampling at this rate and putting a count in the load address corresponding to each sample voltage. The counts were accumulated until the number of counts in one of the load addresses reached 32,767. The histogram was then complete. A rough calculation was done to find the total sample time used to compile a histogram, and it was found to be greater than about 140 seconds. This corresponds to a long averaging time.

The first set of histograms was taken without adding any turbulence generators to the jet. The probability density functions for this case with no applied sound, 500 Hz at 105 dB SPL re 20  $\mu$ N/m<sup>2</sup>, 800 Hz at 105 dB, and 1100 Hz at 105 dB are shown in Figure C-3. The peak probability density for each curve corresponds roughly to the mean velocity. It may be observed that as the sound is applied and the frequency is increased, the magnitude of the peak probability is lowered and the mean velocity corresponding to this peak probability also is lowered. These changes imply that the velocity decay rate is increasing (or the velocity origin is moving upstream) and the turbulence intensity is increasing. These are also the trends that were seen in widening and decay rate and

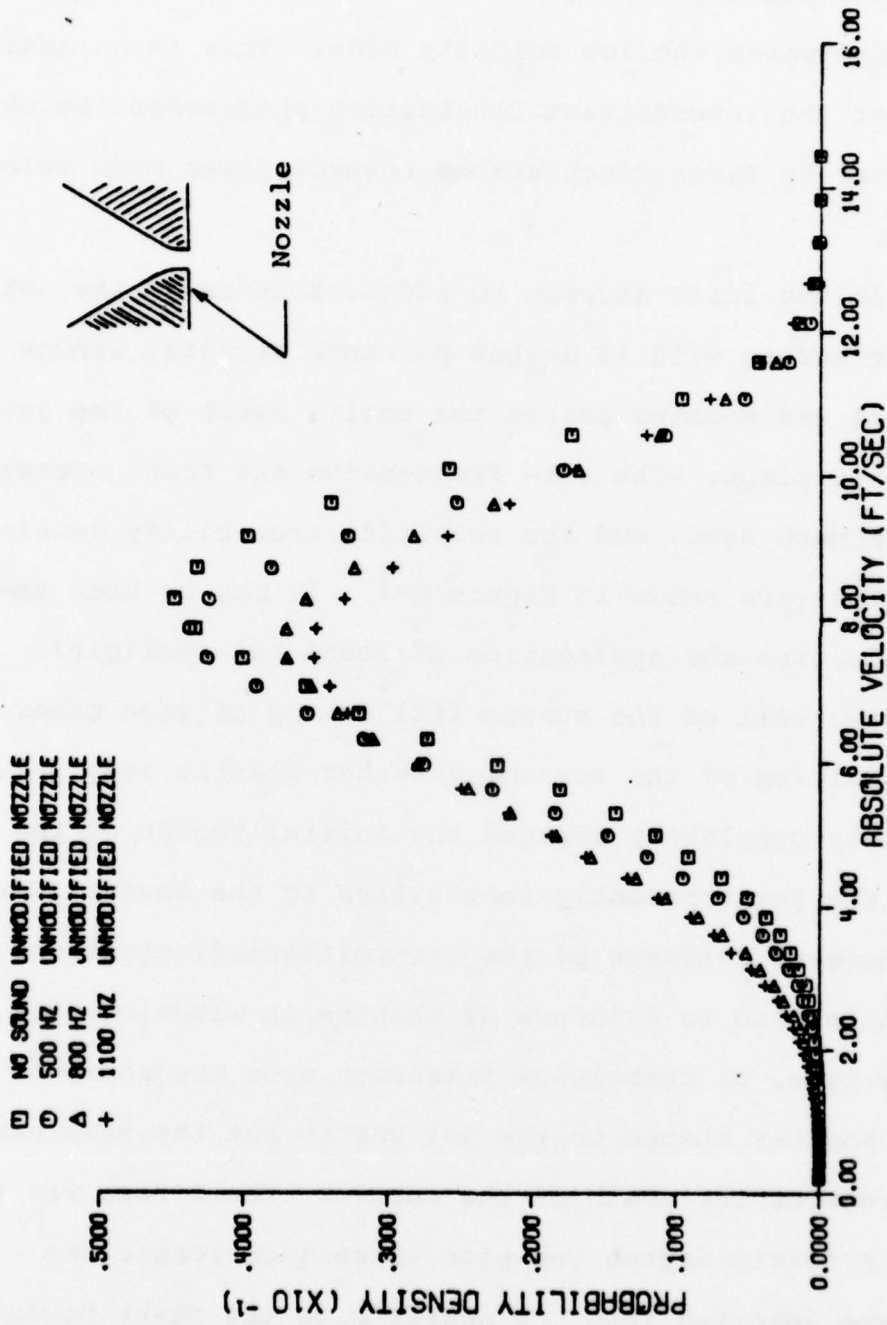


Figure C-3 Probability Density of Velocity on Jet Centerline at X/D = 50 for Unmodified Nozzle

turbulence intensity data. With careful observation (it is more apparent with an expanded scale), it may be seen that the density function for the 1100 Hz case is more skewed towards the low velocity side. This is an indication of the intermittent fluctuation phenomenon, which was observed to favor fluctuations towards lower mean velocities.

In the first attempt to add turbulence to the jet, a copper screen with 18 meshes per inch (typical window screen) was mounted across the entire mouth of the jet in the exit plane. The same frequencies and sound pressure levels were used, and the resulting probability density functions are shown in Figure C-4. It may be seen that in this case the application of sound had negligible effects. All of the curves fall on top of each other. The addition of the screen, a rather drastic step which probably completely changed the initial region of the jet, made the jet apparently insensitive to the sound. Not only is there no evidence of the intermittent fluctuations, there is also no evidence of changes in widening rate, decay rate, or turbulence intensity over the no sound case.

Another change to the jet was to put the same screen upstream of the mouth of the nozzle. The screen was folded into a thirty degree vee with three inch long sides. The vee was inserted into the nozzle with the point downstream and the sides extending upstream in contact with the

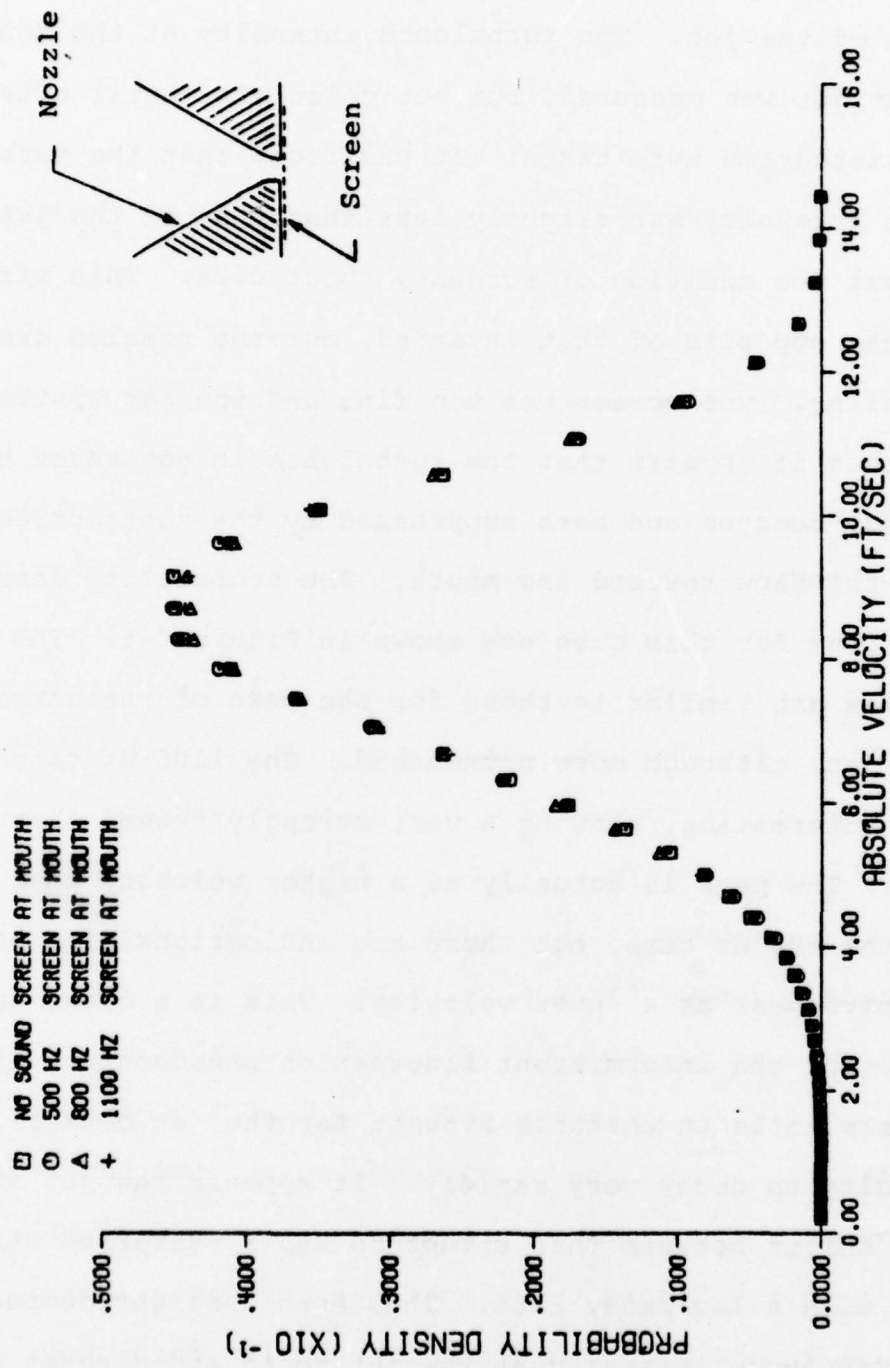


Figure C-4 Probability Density of Velocity on Jet Centerline at X/D = 50 for Nozzle with Screen at Mouth

converging section of the nozzle. The vertex of the vee was approximately two and one half inches upstream of the mouth of the jet. The turbulence intensity at the mouth of the jet was measured, but not calculated until after the histograms were taken. It was found that the turbulence intensity was slightly less than that of the jet without the addition of screens, about 0.2%. This effect was the opposite of that intended, but the results are revealing. The screen was too fine and too far upstream, and thus it appears that the turbulence it generated had already decayed and been suppressed by the contraction when the flow reached the mouth. The probability density functions for this case are shown in Figure C-5. The results are similar to those for the case of the unmodified jet, although more pronounced. The 1100 Hz case is very interesting, showing a very strongly skewed distribution. The peak is actually at a higher velocity than that for the 800 Hz case, but there are indications of a second relative peak at a lower velocity. This is a clear indication of the intermittent fluctuation phenomenon. There appears to be an unstable attempt for the jet centerline velocity to decay very rapidly. It appears the jet structure shifts between this structure and a preferred structure with a low decay rate. Thus even a slight decrease in turbulence intensity at the jet mouth and perhaps in the nozzle boundary layers apparently makes the jet more

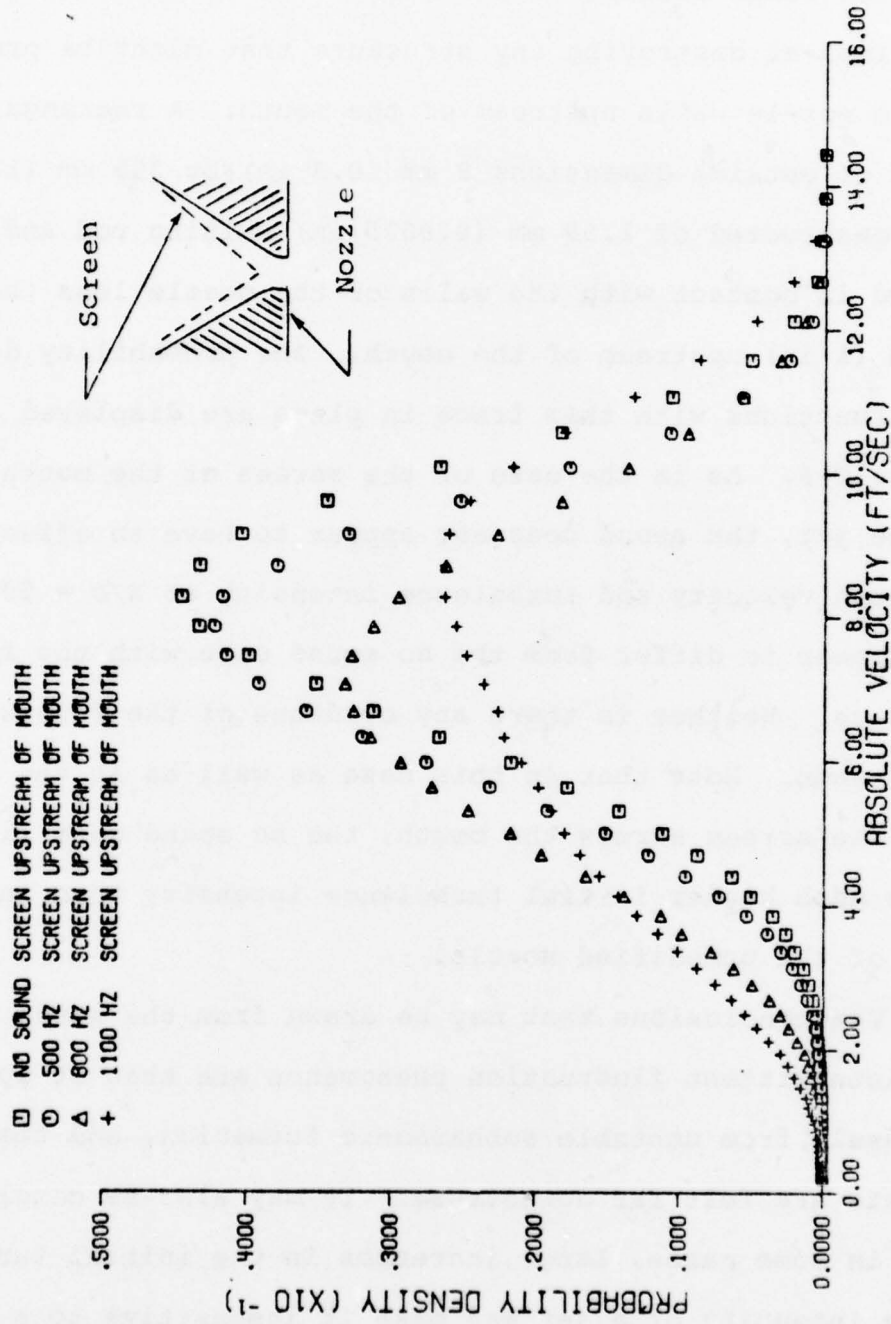


Figure C-5 Probability Density of Velocity on Jet Centerline at X/D = 50 for Nozzle with Screen Upstream

sensitive to applied sound and more susceptible to the fluctuation phenomenon.

The final attempt to add turbulence to the nozzle was aimed at destroying any structure that might be present on the nozzle walls upstream of the mouth. A rectangular frame of outside dimensions 8 mm (0.3 in) by 305 mm (12 in) was constructed of 1.59 mm (0.0625 in) welding rod and placed in contact with the walls of the nozzle less than 25 mm (1 in) upstream of the mouth. The probability density functions with this frame in place are displayed in Figure C-6. As in the case of the screen at the mouth of the jet, the sound does not appear to have an effect. The mean velocity and turbulence intensity at  $X/D = 50$  do not appear to differ from the no sound case with the frame in place. Neither is there any evidence of the fluctuation phenomenon. Note that in this case as well as in the case with the screen across the mouth, the no sound case likely has a much higher initial turbulence intensity than in the case of the unmodified nozzle.

The conclusions that may be drawn from the study of the intermittent fluctuation phenomenon are that it appears to result from unstable subharmonic formation, and that its effects are felt far downstream. It may also be concluded that in some cases, large increases in the initial turbulence intensity of a jet may make it insensitive to a disturbing sound field. This last conclusion may be of some

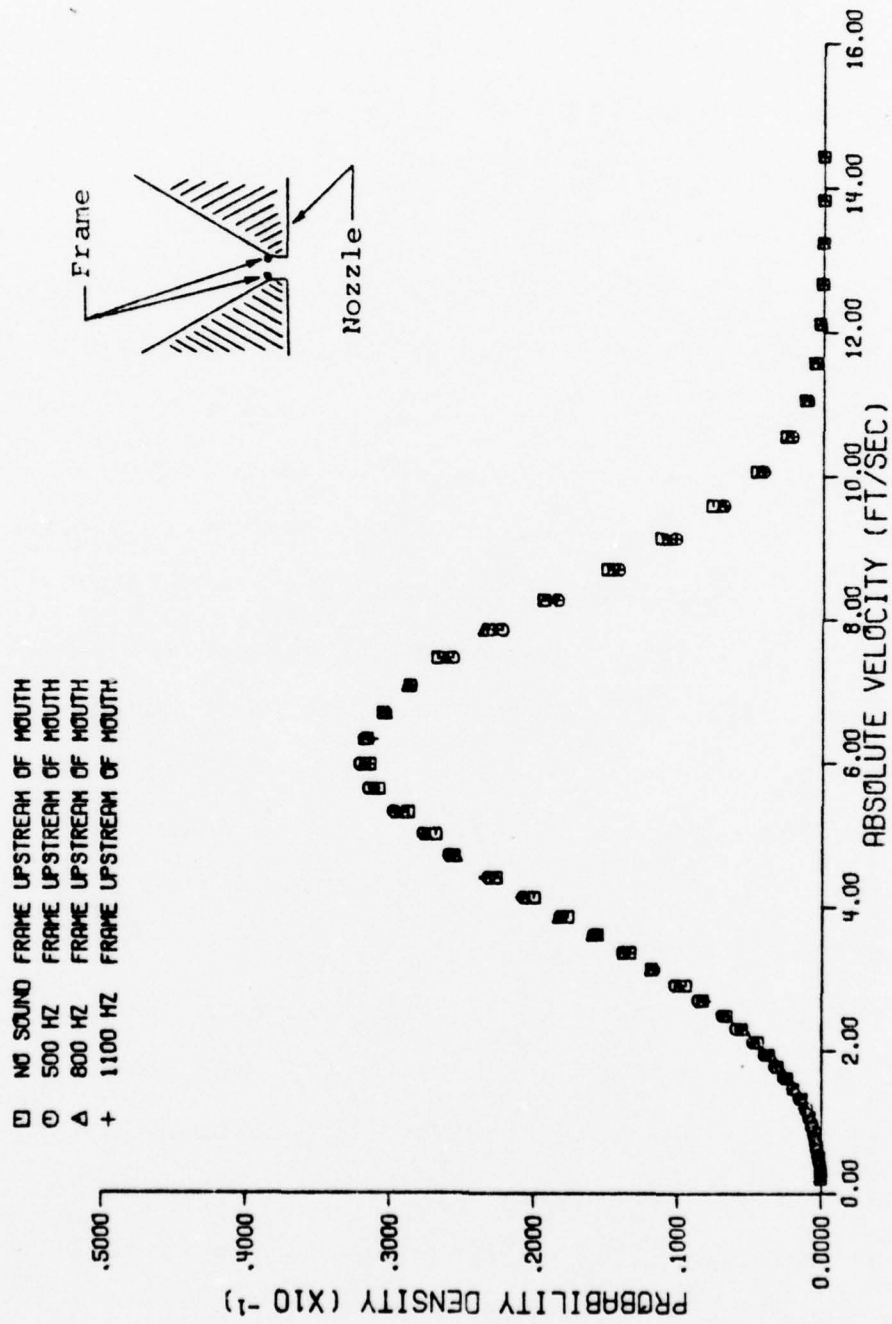


Figure C-6 Probability Density of Velocity on Jet Centerline at X/D = 50 for Nozzle with Frame Upstream

practical significance in connection with the use of fluidic devices in environments with high noise levels.

APPENDIX D X-WIRE MEASUREMENT DERIVATION,  
PROGRAM, AND DISCUSSION

The sensitivity relations used to convert the X-wire probe voltages to velocity components are derived in this appendix. In addition, the program used for digital processing of the X-wire signals on the Hewlett Packard 5450A Fourier Analyzer System is presented, and the accuracy of the results of the analog and digitally processed results are discussed.

1. Sensitivity Relation Derivation

The sensitivity relations for the X-wire probe serve to relate the measured output voltage fluctuations of the two wires to the X- and Y-component fluctuations of the instantaneous velocity,  $u$  and  $v$ . Consider Figure D-1.

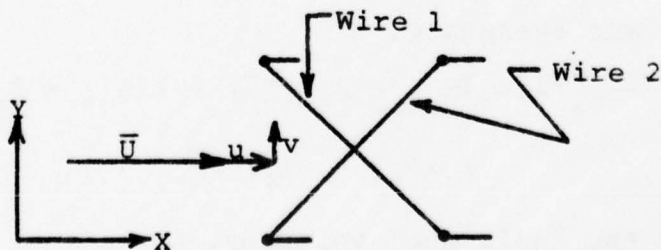


Figure D-1 X-Wire Terminology

The fluctuating output voltages of the two wires may be assumed to be related to the two components of the velocity fluctuations in the following way.

$$\text{Let } e_1 = S_{u_1} u + S_{v_1} v \quad (\text{D-1})$$

where  $e_1$  = output voltage of wire 1

$S_{u_1}$  = sensitivity of wire 1 to X-component  
velocity fluctuations

$S_{v_1}$  = sensitivity of wire 1 to Y-component  
velocity fluctuations

Similarly, for wire 2,

$$e_2 = S_{u_2} u + S_{v_2} v \quad (\text{D-2})$$

The sum of the two voltages is then,

$$e_1 + e_2 = (S_{u_1} + S_{u_2})u + (S_{v_1} + S_{v_2})v$$

Squaring and averaging,

$$\begin{aligned} \overline{(e_1 + e_2)^2} &= (S_{u_1} + S_{u_2})^2 \overline{u^2} + 2(S_{u_1} + S_{u_2})(S_{v_1} + S_{v_2}) \overline{uv} \\ &\quad + (S_{v_1} + S_{v_2})^2 \overline{v^2} \end{aligned} \quad (\text{D-3})$$

The difference of the two voltages is,

$$e_1 - e_2 = (S_{u_1} - S_{u_2})u + (S_{v_1} - S_{v_2})v$$

Squaring and averaging,

$$\begin{aligned} \overline{(e_1 - e_2)^2} &= (S_{u_1} - S_{u_2})^2 \overline{u^2} + 2(S_{u_1} - S_{u_2})(S_{v_1} - S_{v_2}) \overline{uv} \\ &\quad + (S_{v_1} - S_{v_2})^2 \overline{v^2} \end{aligned} \quad (\text{D-4})$$

Squaring the individual voltages,

$$e_1^2 = S_{u_1}^2 u^2 + 2S_{u_1} S_{v_1} uv + S_{v_1}^2 v^2$$

$$e_2^2 = S_{u_2}^2 u^2 + 2 S_{u_2} S_{v_2} uv + S_{v_2}^2 v^2$$

Taking the average of the instantaneous difference of the squares,

$$\begin{aligned} \overline{(e_1^2 - e_2^2)} &= (S_{u_1}^2 - S_{u_2}^2) \overline{u^2} + 2(S_{u_1} S_{v_1} - S_{u_2} S_{v_2}) \overline{uv} \\ &+ (S_{v_1}^2 - S_{v_2}^2) \overline{v^2} \end{aligned} \quad (D-5)$$

Thus Equations D-3, D-4, and D-5 provide relations between the variance of the X-component velocity,  $\overline{u^2}$ , the variance of the Y-component velocity,  $\overline{v^2}$ , the Reynolds shear stress  $\overline{uv}$ , and the voltages obtained in the experiments and the sensitivities obtained from calibrations. The equations then may be solved for the velocities in terms of the voltages and sensitivities.

First solving for  $\overline{v^2}$  in Equation D-4,

$$\begin{aligned} (S_{v_1} - S_{v_2})^2 \overline{v^2} &= \overline{(e_1 - e_2)^2} - (S_{u_1} - S_{u_2})^2 \overline{u^2} \\ &- 2(S_{u_1} - S_{u_2})(S_{v_1} - S_{v_2}) \overline{uv} \end{aligned}$$

Dividing,

$$\begin{aligned} \overline{v^2} &= \frac{\overline{(e_1 - e_2)^2}}{(S_{v_1} - S_{v_2})^2} - \frac{(S_{u_1} - S_{u_2})^2 \overline{u^2}}{(S_{v_1} - S_{v_2})^2} \\ &- \frac{2(S_{u_1} - S_{u_2}) \overline{uv}}{(S_{v_1} - S_{v_2})} \end{aligned} \quad (D-6)$$

Substituting Equation D-6 into Equation D-3,

$$\begin{aligned} \overline{(e_1 + e_2)^2} &= (S_{u_1} + S_{u_2})^2 \overline{u^2} \\ &+ 2(S_{u_1} + S_{u_2})(S_{v_1} + S_{v_2})\overline{uv} \\ &+ (S_{v_1} + S_{v_2})^2 \left[ \frac{(e_1 - e_2)^2}{(S_{v_1} - S_{v_2})^2} \right. \\ &\quad \left. - \frac{(S_{u_1} - S_{u_2})^2 \overline{u^2}}{(S_{v_1} - S_{v_2})^2} - \frac{2(S_{u_1} - S_{u_2})\overline{uv}}{(S_{v_1} - S_{v_2})} \right] \end{aligned}$$

Grouping terms,

$$\begin{aligned} \overline{(e_1 + e_2)^2} &= \left[ (S_{u_1} + S_{u_2})^2 \right. \\ &\quad \left. - \frac{(S_{v_1} + S_{v_2})^2 (S_{u_1} - S_{u_2})^2}{(S_{v_1} - S_{v_2})^2} \right] \overline{u^2} \\ &+ \left[ 2(S_{u_1} + S_{u_2})(S_{v_1} + S_{v_2}) \right. \\ &\quad \left. - \frac{2(S_{v_1} + S_{v_2})^2 (S_{u_1} - S_{u_2})}{(S_{v_1} - S_{v_2})} \right] \overline{uv} \\ &+ \left[ \frac{(S_{v_1} + S_{v_2})^2}{(S_{v_1} - S_{v_2})^2} \right] \overline{(e_1 - e_2)^2} \end{aligned} \quad (D-7)$$

Now,

$$\begin{aligned} \text{let } A_1 &= \left[ (S_{u_1} + S_{u_2})^2 \right. \\ &\quad \left. - \frac{(S_{v_1} + S_{v_2})^2 (S_{u_1} - S_{u_2})^2}{(S_{v_1} - S_{v_2})^2} \right] \end{aligned} \quad (D-8)$$

$$\text{and let } A_2 = \left[ 2 (S_{u1} + S_{u2}) (S_{v1} + S_{v2}) - \frac{2(S_{v1} + S_{v2})^2 (S_{u1} - S_{u2})}{(S_{v1} - S_{v2})} \right] \quad (\text{D-9})$$

Solving for  $\overline{u^2}$  in Equation D-7,

$$A_1 \overline{u^2} = \overline{(e_1 + e_2)^2} - A_2 \overline{uv} - \left[ \frac{(S_{v1} + S_{v2})^2}{(S_{v1} - S_{v2})^2} \right] \overline{(e_1 - e_2)^2}$$

Or,

$$\overline{u^2} = \frac{\overline{(e_1 + e_2)^2}}{A_1} - \left[ \frac{(S_{v1} + S_{v2})^2}{A_1 (S_{v1} - S_{v2})^2} \right] \overline{(e_1 - e_2)^2} - \frac{A_2}{A_1} \overline{uv} \quad (\text{D-10})$$

Substituting Equation D-6 for  $\overline{v^2}$  into Equation D-5,

$$\begin{aligned} \overline{(e_1^2 - e_2^2)} &= (S_{u1}^2 - S_{u2}^2) \overline{u^2} + 2(S_{u1} S_{v1} - S_{u2} S_{v2}) \overline{uv} \\ &+ (S_{v1}^2 - S_{v2}^2) \left[ \frac{\overline{(e_1 - e_2)^2}}{(S_{v1} - S_{v2})^2} \right. \\ &\left. - \frac{(S_{u1} - S_{u2})^2 \overline{u^2}}{(S_{v1} - S_{v2})^2} - \frac{2(S_{u1} - S_{u2}) \overline{uv}}{(S_{v1} - S_{v2})} \right] \end{aligned}$$

Grouping terms,

$$\begin{aligned} \overline{(e_1^2 - e_2^2)} &= \left[ \frac{(S_{V1} + S_{V2})}{(S_{V1} - S_{V2})} \right] \overline{(e_1 - e_2)^2} \\ &+ \left\{ (S_{U1} - S_{U2}) \left[ (S_{U1} + S_{U2}) \right. \right. \\ &\quad \left. \left. - \frac{(S_{V1} + S_{V2})(S_{U1} - S_{U2})}{(S_{V1} - S_{V2})} \right] \right\} \overline{u^2} \\ &+ 2(S_{U2}S_{V1} - S_{U1}S_{V2})\overline{uv} \end{aligned} \quad (D-11)$$

Now,

$$\text{let } A_3 = \left\{ (S_{U1} - S_{U2}) \left[ (S_{U1} + S_{U2}) \right. \right. \\ \left. \left. - \frac{(S_{V1} + S_{V2})(S_{U1} - S_{U2})}{(S_{V1} - S_{V2})} \right] \right\}$$

Substituting Equation D-10 for  $\overline{u^2}$  into Equation D-11,

$$\begin{aligned} \overline{(e_1^2 - e_2^2)} &= \left[ \frac{S_{V1} + S_{V2}}{S_{V1} - S_{V2}} \right] \overline{(e_1 - e_2)^2} \\ &+ A_3 \left\{ \frac{\overline{(e_1 + e_2)^2}}{A_1} \right. \\ &\quad \left. - \left[ \frac{(S_{V1} + S_{V2})^2}{A_1(S_{V1} - S_{V2})^2} \right] \overline{(e_1 - e_2)^2} \right. \\ &\quad \left. - \frac{A_2}{A_1} \overline{uv} \right\} + 2(S_{U2}S_{V1} - S_{U1}S_{V2})\overline{uv} \end{aligned}$$

Rearranging terms,

$$\begin{aligned} \left[ 2(S_{u_2} S_{v_1} - S_{u_1} S_{v_2}) - \frac{A_3 A_2}{A_1} \right] \overline{uv} &= \overline{(e_1^2 - e_2^2)} \\ &+ \left[ \frac{A_3}{A_1} \frac{(S_{v_1} + S_{v_2})^2}{(S_{v_1} - S_{v_2})^2} - \frac{(S_{v_1} + S_{v_2})}{(S_{v_1} - S_{v_2})} \right] \overline{(e_1 - e_2)^2} \\ &- \frac{A_3}{A_1} \overline{(e_1 + e_2)^2} \end{aligned} \quad (D-12)$$

Letting,

$$A_4 = 2(S_{u_2} S_{v_1} - S_{u_1} S_{v_2}) - \frac{A_3 A_2}{A_1}$$

and,

$$A_5 = \frac{A_3 (S_{v_1} + S_{v_2})^2}{A_1 (S_{v_1} - S_{v_2})^2} - \frac{(S_{v_1} + S_{v_2})}{(S_{v_1} - S_{v_2})}$$

Solving Equation D-12 for  $\overline{uv}$

$$\overline{uv} = \frac{\overline{(e_1^2 - e_2^2)}}{A_4} + \frac{A_5 \overline{(e_1 - e_2)^2}}{A_4} - \frac{A_3 \overline{(e_1 + e_2)^2}}{A_1 A_4} \quad (D-13)$$

Note that in Equation D-13, the first term is of the greatest importance. If  $S_{u_1} = S_{u_2}$  and  $S_{v_1} = -S_{v_2}$ , as often is assumed, the coefficients  $A_5$  and  $A_3$  would both equal zero, leaving only the first term. Thus the last two terms may be considered correction factors for the small differences in sensitivities of the two wires.

The value of  $\overline{uv}$  can then be substituted into Equation D-10 for  $\overline{u^2}$ . It may be observed that if the sensitivities

are matched, as described in the previous paragraph, only the first term would remain. The last two terms again may be considered correction terms for the small differences in sensitivities. Similarly, the values of  $\overline{u^2}$  and  $\overline{uv}$  may then be substituted into Equation D-6 to obtain  $\overline{v^2}$ . If the sensitivities are matched, only the first term remains; thus the terms containing  $\overline{u^2}$  and  $\overline{uv}$  appear only as corrections for unmatched sensitivities.

Equations D-13, D-10, and D-6 were used to calculate  $\overline{uv}$ ,  $\overline{u^2}$ , and  $\overline{v^2}$  respectively as described, and thus the effects of the small differences in the sensitivities of the two wires were always accounted for in the reported results. The same equations were used in evaluating data obtained using analog and digital techniques.

## 2. Digital Processing Program

The measurements performed with the X-wire probes were obtained in two ways. As described in Chapter III, analog signal processing was performed using a Thermo Systems Model 1015C Correlator which yielded the sum and difference of the voltages from the two wires directly. The mean squares of the sum and difference were formed with rms voltmeters. In the case of digital signal processing, a Hewlett Packard 5450A Fourier analyzer system was used to form and average the square of the sum, the square of the difference, and the difference of the squares of the two wire voltages. The sampling parameters employed are

described in Chapter III. The following program was used in the signal processing.

<u>Program Statement</u>		<u>Description</u>
Label	1	Label beginning of program
Clear	0	Empty block 0
Clear	1	Empty block 1
Clear	2	Empty block 2
Clear	3	Empty block 3
Clear	4	Empty block 4
Clear	5	Empty block 5
Label	2	Label beginning of loop
Analog in	0 1 0	Take samples of voltage $e_1$ into block 0 and $e_2$ into block 1
Add	1	$(e_1 + e_2)$ formed in block 0, $e_2$ left in block 1
Store	2	$(e_1 + e_2)$ also placed in block 2
Multiply	1 2	$2e_2$ formed in block 1
Subtract	1	Block 1 subtracted from block 0 to leave $(e_1 - e_2)$ in block 0, $2e_2$ in block 1
Store	1	$(e_1 - e_2)$ also placed in block 1
Multiply	2	Block 0 multiplied by block 2 to form $(e_1 - e_2)^2$ in block 0
Add	5	Sum of previous $(e_1 - e_2)^2$ 's in block 5 added to present $(e_1 - e_2)^2$ in block 0
Store	5	New $\Sigma(e_1 - e_2)^2$ placed in block 5
Load	1	Present $(e_1 - e_2)$ stored in block 0
Multiply		$(e_1 - e_2)^2$ formed in block 0
Add	4	Sum of previous $(e_1 - e_2)^2$ 's in block 4 added to present $(e_1 - e_2)^2$ in block 0
Store	4	New $\Sigma(e_1 - e_2)^2$ placed in block 4
Load	2	Present $(e_1 + e_2)$ stored in block 2 placed in block 0
Multiply		$(e_1 + e_2)^2$ formed in block 0
Add	3	Sum of previous $(e_1 + e_2)^2$ 's in block 3 added to present $(e_1 + e_2)^2$ in block 0
Store	3	New $\Sigma(e_1 + e_2)^2$ placed in block 3
Count	2 300	Loop from label 2 to this point to be performed 300 times

Integrate 3			$\Sigma(e_1 + e_2)^2$ at each of 512 positions in block 3 added to form total in position 511
Integrate 4			Total $\Sigma(e_1 - e_2)^2$ formed and placed in position 511 of block 4
Integrate 5			Total $\Sigma(e_1^2 - e_2^2)$ formed and placed in position 511 of block 5
Write	3	511	Total $\Sigma(e_1 + e_2)^2$ printed on teletype
Write	4	511	Total $\Sigma(e_1 - e_2)^2$ printed
Write	5	511	Total $\Sigma(e_1^2 - e_2^2)$ printed
Display	5		Block 5 displayed on system oscilloscope
End			

### 3. X-Wire Measurement Accuracy

The results of the X-wire measurements performed in the present study reveal magnitudes somewhat lower than those that might be expected. The measured non-dimensional Reynolds shear stresses are lower than those calculated from mean flow parameters using assumptions of similarity. They also are lower than values reported in the literature, although the differences in mean flow parameters eliminate the possibility of universal similarity. In this section, the accuracy of the X-wire measurements and various factors which determine the accuracy are discussed.

The measured Reynolds shear stresses are, as discussed previously, somewhat lower than expected. In addition, longitudinal turbulence intensities obtained from X-wire measurements are lower than those obtained using straight wires. Figure D-2 displays longitudinal intensities along the jet centerline measured simultaneously with a

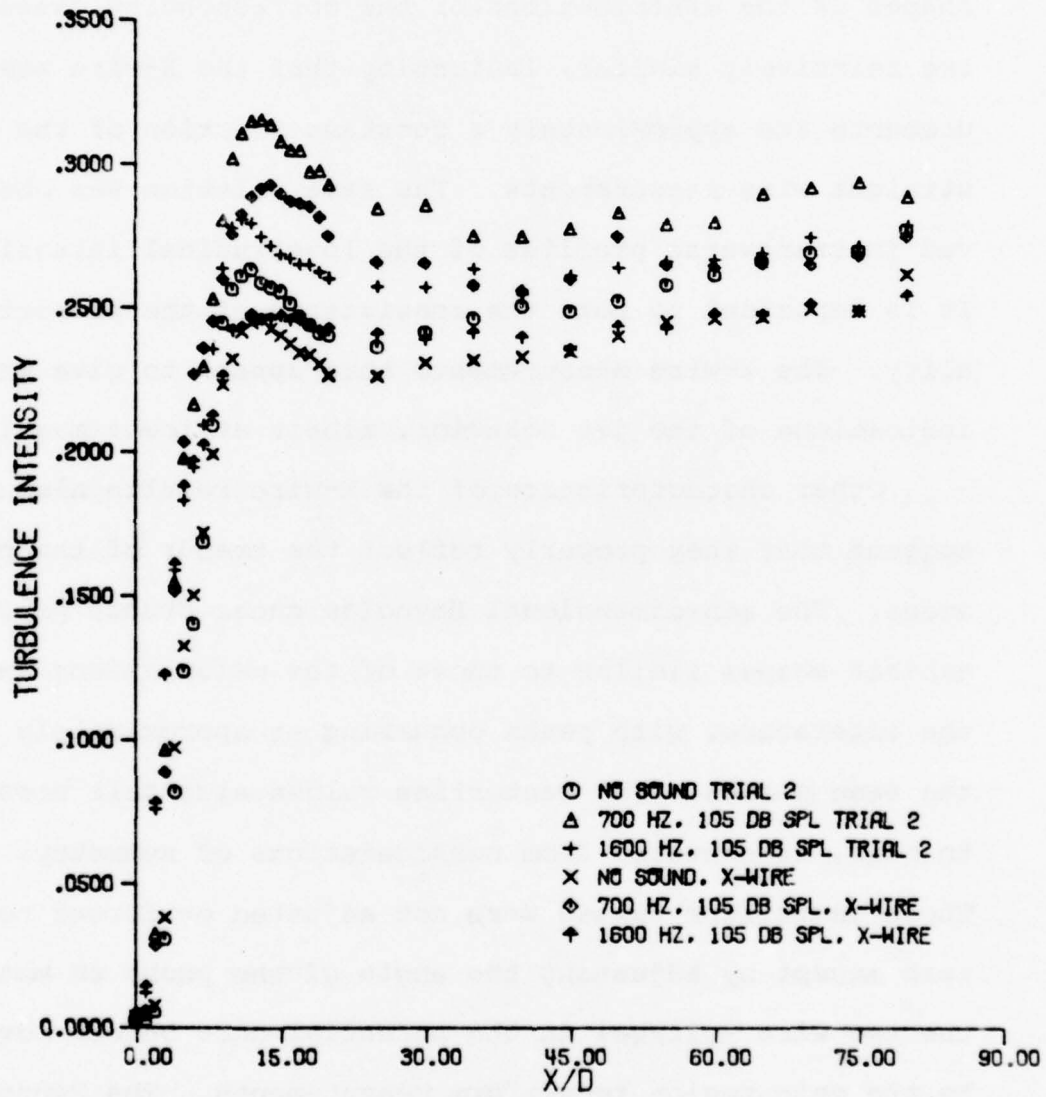


Figure D-2 Comparison of Longitudinal Intensities Measured with a Straight Wire Probe and an X-Wire Probe

non-linearized straight wire and an X-wire. The X-wire signal was processed using analog methods. It may be observed that the straight wire measurements are consistently higher in magnitude than those of the X-wire. The shapes of the distributions of the corresponding cases are relatively similar, indicating that the X-wire measurements are approximately a constant fraction of the straight wire measurements. The same relation was observed in transverse profiles of the longitudinal intensity. It is important to note the consistency of the proportionality. The X-wire measurements thus appear to give good indications of the jet behavior, albeit at lower magnitudes.

Other characteristics of the X-wire results also suggest that they properly reflect the trends of the phenomena. The non-dimensional Reynolds shear stress profiles exhibit shapes similar to those of the calculations and the literature, with peaks occurring at approximately the same places. The centerline values also fall close to zero, as expected from considerations of symmetry. These centerline values were not adjusted or forced toward zero except by adjusting the angle of the probe to match the two wire voltages in the potential core before moving to the main region to perform measurements. The Reynolds stress correlations exhibit very good agreement with those in the literature. This agreement suggests further that errors in the measurements are in the form of constants

of proportionality, for in the correlations, these constants would cancel. The fact that repeated measurements resulted in similar trends and relationships between the two cases of acoustic disturbance and the undisturbed case also provides support for this form of error.

It must, however, be pointed out that the constant of proportionality between the results and the expected values appeared to vary from measurement session to measurement session. Numerous factors may be responsible for this variability. Recall that the X-wire probe was calibrated outside the set-up using a low turbulence compressed air calibration jet and then moved to the set-up and aligned with the jet axes in the potential core. This procedure immediately suggests the possibility of differences in alignment with the mean flow direction of the calibration jet and the actual disturbed jet flow field. Misalignment in all three planes was possible. Small changes in alignment might also be expected to result in some differences in the interference effects between the two wires. Such changes in interference could be very sensitive to small angular misalignments. The behavior of the wire in the actual jet might also differ from that in the calibration jet as a result of the effects of the finite levels of turbulence present in the actual jet but not the calibration jet. No corrections were made to the measurements for the effects of the finite level of the

vertical component of the turbulence intensity which was present.

The instrumentation following the anemometers might also be responsible for some of the errors. Slight differences in the linearization of the two wires would result in errors. Such errors would seem to be particularly likely for measurements in the outer regions of the jet where the mean velocities are lower than those used in adjusting the linearizer. In this outer region, the linearization is essentially an extrapolation of the linearization performed at higher velocities. The correlator used in the analog measurements to produce the instantaneous sum and difference of the wire voltages also may have contributed to errors. The correlator did have variable gains which were calibrated at the beginning of each measurement session. The analog to digital converter section of the Fourier analyzer used in the digital processing is another probable source of errors. It had a somewhat limited low frequency response in the ac coupling mode and did at times produce random errors which eventually caused a shift to analog processing for the final results.

These errors resulting from the various sources discussed are not readily quantifiable. However, the measurement results do suggest strongly that the errors were of a proportional nature and thus the measurements are of use

for comparisons of trends in distributions and relative magnitudes.

APPENDIX E    DERIVATIONS BASED UPON ASSUMPTIONS  
OF SIMILARITY

This appendix presents derivations of expressions for the Reynolds shear stress, the local turbulent energy production by the Reynolds shear stress, and the total turbulent energy production by the Reynolds shear stresses for a cross section of the jet. Also presented are derivations of the existence time, the mass flow rate, and the entrainment rate as functions of non-dimensional distance from the nozzle.

1.    Reynolds Shear Stress

The Reynolds shear stress may be derived from the two-dimensional streamwise momentum equation using the continuity equation, assumptions of similarity, and other assumptions about the orders of the terms in the equation. The two-dimensional velocity components are assumed to be of the following form:

$$U = \bar{U} + u \qquad (E-1)$$

$$V = \bar{V} + v \qquad (E-2)$$

where

U = instantaneous longitudinal velocity

V = instantaneous lateral velocity

$\bar{U}$  = mean longitudinal velocity

$\bar{V}$  = mean lateral velocity

$u$  = turbulent longitudinal velocity

$v$  = turbulent lateral velocity

The streamwise momentum equation may be written in the following form assuming that the downstream pressure gradient is zero.

$$\bar{U} \frac{\partial \bar{U}}{\partial X} + \bar{V} \frac{\partial \bar{U}}{\partial Y} + \frac{\partial}{\partial X} (\overline{u^2} - \overline{v^2}) + \frac{\partial}{\partial Y} (\overline{uv}) = \nu \left( \frac{\partial^2 \bar{U}}{\partial X^2} + \frac{\partial^2 \bar{U}}{\partial Y^2} \right) \quad (\text{E-3})$$

Assuming that the normal stress term,  $(\overline{u^2} - \overline{v^2})$ , and the viscous term are negligible compared to the other terms, the equation becomes,

$$\bar{U} \frac{\partial \bar{U}}{\partial X} + \bar{V} \frac{\partial \bar{U}}{\partial Y} + \frac{\partial}{\partial Y} (\overline{uv}) = 0 \quad (\text{E-4})$$

The mean continuity equation is,

$$\frac{\partial \bar{U}}{\partial X} + \frac{\partial \bar{V}}{\partial Y} = 0 \quad (\text{E-5})$$

This may be solved for  $\bar{V}$ ,

$$\bar{V} = -\int_0^Y \frac{\partial \bar{U}}{\partial X} dy \quad (\text{E-6})$$

Substituting Equation E-6 into Equation E-4 and rearranging terms,

$$-\frac{\partial \overline{uv}}{\partial Y} = \bar{U} \frac{\partial \bar{U}}{\partial X} - \left[ \int_0^Y \frac{\partial \bar{U}}{\partial X} dy \right] \frac{\partial \bar{U}}{\partial Y} \quad (\text{E-7})$$

Now an assumption of similarity is made for the longitudinal mean velocity profile. Assume that the

longitudinal mean velocity is given by,

$$\bar{U} = U_m f(\eta) \quad (\text{E-8})$$

where,

$U_m$  = local centerline mean velocity

$$\eta = Y/B$$

Substituting Equation E-8 into Equation E-7 and simplifying,

$$\begin{aligned} -\frac{\partial \bar{uv}}{\partial Y} &= U_m f \left[ \frac{f \partial U_m}{\partial X} + U_m f' \frac{\partial \eta}{\partial X} \right] \\ &- \left\{ \int_0^Y \left[ \frac{f \partial U_m}{\partial X} + U_m f' \frac{\partial \eta}{\partial X} \right] dY \right\} U_m f' \frac{\partial \eta}{\partial Y} \end{aligned} \quad (\text{E-9})$$

Noting that,

$$\frac{\partial \eta}{\partial X} = -\frac{\eta}{B} \frac{\partial B}{\partial X} \quad (\text{E-10})$$

and,

$$\frac{\partial \eta}{\partial Y} = \frac{1}{B} \quad (\text{E-11})$$

Substituting Equations E-10 and E-11 into Equation E-9,

$$\begin{aligned} -\frac{\partial \bar{uv}}{\partial Y} &= U_m f \left[ \frac{f \partial U_m}{\partial X} - \frac{U_m f' \eta}{B} \frac{\partial B}{\partial X} \right] \\ &- \left\{ \int_0^Y \left[ \frac{f \partial U_m}{\partial X} - \frac{U_m f' \eta}{B} \frac{\partial B}{\partial X} \right] dY \right\} \frac{U_m f'}{B} \end{aligned} \quad (\text{E-12})$$

Recalling that the half width and centerline mean velocity obey the following equations,

$$\frac{B}{D} = K_1 \left( \frac{X}{D} - C_1 \right) \quad (\text{II-1})$$

$$\left( \frac{U_m}{U_0} \right)^{-2} = K_2 \left( \frac{X}{D} - C_2 \right) \quad (\text{II-2})$$

It may be shown that,

$$\frac{\partial B}{\partial X} = K_1 \quad (\text{E-13})$$

and,

$$\frac{\partial U_m}{\partial X} = - \frac{U_0}{2DK_2^{1/2}} \left[ \frac{X}{D} - C_2 \right]^{-3/2} \quad (\text{E-14})$$

Substituting Equations E-13 and E-14 into Equation E-12 and simplifying,

$$\begin{aligned} - \frac{\partial \overline{uv}}{\partial Y} &= U_m f \left[ - \frac{fU_0}{2DK_2^{1/2} \left( \frac{X}{D} - C_2 \right)^{3/2}} - \frac{U_m f' \eta}{B} \frac{\partial B}{\partial X} \right] \\ &- \left\{ \int_0^Y \left[ - \frac{fU_0}{2DK_2^{1/2} \left( \frac{X}{D} - C_2 \right)^{3/2}} \right. \right. \\ &\quad \left. \left. - \frac{U_m f' \eta}{B} \frac{\partial B}{\partial X} \right] dY \right\} \frac{U_m f'}{B} \end{aligned} \quad (\text{E-15})$$

Multiplying by B, dividing by  $U_m^2$ , utilizing the relation of Equation II-2, and simplifying,

$$\begin{aligned} - \frac{\partial}{\partial \eta} \left[ \frac{\overline{uv}}{U_m^2} \right] &= - \frac{Bf^2}{2D \left( \frac{X}{D} - C_2 \right)} - f' f \eta \frac{\partial B}{\partial X} \\ &+ \frac{Bf'}{2D \left( \frac{X}{D} - C_2 \right)} \int_0^\eta f d\eta \\ &+ f' \frac{\partial B}{\partial X} \int_0^\eta \eta f' d\eta \end{aligned} \quad (\text{E-16})$$

Recalling the identity,  $\int r ds = rs - \int s dr$ , and employing it in the last term of Equation E-16,

$$\begin{aligned}
-\frac{\partial}{\partial \eta} \left[ \frac{\overline{uv}}{U_m^2} \right] &= -\frac{Bf^2}{2D\left(\frac{X}{D} - C_2\right)} - f'f\eta \frac{\partial B}{\partial X} \\
&+ \frac{Bf'}{2D\left(\frac{X}{D} - C_2\right)} \int_0^\eta f d\eta \\
&+ f' \frac{\partial B}{\partial X} \left[ \eta f - \int_0^\eta f d\eta \right]
\end{aligned} \tag{E-17}$$

Regrouping the terms in Equation E-17,

$$\begin{aligned}
\frac{\partial}{\partial \eta} \left[ \frac{\overline{uv}}{U_m^2} \right] &= \frac{Bf^2}{2D\left(\frac{X}{D} - C_2\right)} \\
&+ \left[ \frac{\partial B}{\partial X} - \frac{B}{2D\left(\frac{X}{D} - C_2\right)} \right] f' \int_0^\eta f d\eta
\end{aligned} \tag{E-18}$$

Substituting Equation II-1 for  $B/D$ , and  $\frac{\partial B}{\partial X} = K_1$ , into Equation E-18,

$$\begin{aligned}
\frac{\partial}{\partial \eta} \left[ \frac{\overline{uv}}{U_m^2} \right] &= K_1 \left\{ \frac{f^2 \left( \frac{X}{D} - C_1 \right)}{2 \left( \frac{X}{D} - C_2 \right)} \right. \\
&+ \left. \left[ 1 - \frac{\left( \frac{X}{D} - C_1 \right)}{2 \left( \frac{X}{D} - C_2 \right)} \right] f' \int_0^\eta f d\eta \right\}
\end{aligned} \tag{E-19}$$

Finally, the non-dimensional Reynolds stress is found by integrating the expression of Equation E-19 from zero to  $\eta$ ,

$$\begin{aligned}
 \frac{\overline{uv}}{U_m^2} = K_1 & \left\{ \left[ \frac{\left(\frac{x}{D} - c_1\right)}{2\left(\frac{x}{D} - c_2\right)} \right] \int_0^\eta f^2 d\eta \right. \\
 & + \left[ 1 - \frac{\left(\frac{x}{D} - c_1\right)}{2\left(\frac{x}{D} - c_2\right)} \right] \\
 & \left. \int_0^\eta \left[ f' \int_0^\eta f d\eta \right] d\eta \right\} \quad (E-20)
 \end{aligned}$$

This equation was employed in the calculated Reynolds shear stresses presented in Chapters IV and V. The integrations were performed numerically in a digital computer program.

## 2. Reynolds Shear Stress Turbulent Energy Production

The production of turbulent energy from the mean flow energy is dominated by the Reynolds shear stress production term, the negative product of the Reynolds shear stress and the local mean velocity lateral gradient. A non-dimensional local production term is formed by multiplying Equation E-20 by  $-\frac{\partial \bar{U}}{\partial \eta} \frac{\bar{U}}{U_m}$ . The resulting expression for the local production is,

$$\begin{aligned}
 -\frac{\overline{uv}}{U_m^2} \frac{\partial}{\partial \eta} \left[ \frac{\overline{U}}{U_m} \right] &= K_1 f' \left\{ \left[ \frac{\left( \frac{x}{D} - c_1 \right)}{2 \left( \frac{x}{D} - c_2 \right)} \right] \int_0^\eta f^2 d\eta \right. \\
 &\quad \left. + \left[ 1 - \frac{\left( \frac{x}{D} - c_1 \right)}{2 \left( \frac{x}{D} - c_2 \right)} \right] \right. \\
 &\quad \left. \int_0^\eta \left[ f' \int_0^\eta f d\eta \right] d\eta \right\} \quad (E-21)
 \end{aligned}$$

This expression was used to calculate the shear stress turbulent energy production distributions presented in Chapter V.

The net production of turbulent energy by the shear stresses in a given cross section of the jet may be calculated by integrating Equation E-21 from minus infinity to positive infinity. The result is an energy production non-dimensionalized by the cube of the local centerline mean velocity. In order to obtain a comparison of the net productions based upon a single absolute non-dimensionalizing velocity, Equation E-21 was multiplied by  $2 \left( \frac{U_m}{U_0} \right)^3$  obtained from Equation II-2, and integrated from  $\eta = 0$  to  $\eta = 1.75$ , a point at which the production is negligible. The resulting expression for the net turbulent energy production at a given cross section by the shear stress is,

$$\frac{1}{U_0^3} \int_{-1.75B}^{1.75B} - \overline{uv} \frac{\partial \bar{U}}{\partial Y} dY =$$

$$\left\{ \frac{2K_1}{\left[ K_2 \left( \frac{X}{D} - C_2 \right) \right]^{1.5}} \left[ \frac{\left( \frac{X}{D} - C_1 \right)}{2 \left( \frac{X}{D} - C_2 \right)} \right] P_1 \right.$$

$$\left. + \left[ 1 - \frac{\left( \frac{X}{D} - C_1 \right)}{2 \left( \frac{X}{D} - C_2 \right)} \right] P_2 \right\} \quad (E-22)$$

where

$$P_1 = \int_0^{1.75} f' \left[ \int_0^\eta f^2 d\eta_1 \right] d\eta \quad (E-23)$$

and,

$$P_2 = \int_0^{1.75} f' \left\{ \int_0^\eta f' \left[ \int_0^{\eta_2} f d\eta_1 \right] d\eta_2 \right\} d\eta \quad (E-24)$$

Numerical integrations were performed to evaluate  $P_1$  and

$P_2$ . With  $f(\eta)$  given by,

$$f(\eta) = 1 - \tanh^2 \left[ 0.793\eta (1 + 0.111\eta^2) \right] \quad (E-25)$$

the values of  $P_1$  and  $P_2$  are,

$$P_1 = 0.888 \quad (E-26)$$

and,

$$P_2 = -0.397 \quad (E-27)$$

These values were substituted into Equation E-22 to calculate the net turbulent energy production by the shear stresses. The results are presented in Chapter V.

### 3. Existence Time

Bradbury (1965) defined the existence time as the time required for a particle moving at the local centerline mean velocity to travel along the centerline from the mouth to a given point. In the present case of a jet issuing into still air, the equation for the existence time reduces to the following:

$$t_e = \int_0^X \frac{dX}{U_m} \quad (\text{E-28})$$

Assuming that  $U_m = U_0$  inside  $X = 5D$ , and follows Equation II-2 for  $X > 5D$ ,

$$t_e = \frac{5D}{U_0} + \int_{5D}^X \frac{K_2^{1/2} \left(\frac{X}{D} - C_2\right)^{1/2}}{U_0} dX \quad (\text{E-29})$$

$$= \frac{5D}{U_0} + \frac{K_2^{1/2}}{U_0} \left[ \frac{2D}{3} \left(\frac{X}{D} - C_2\right)^{3/2} \right]_{5D}^X \quad (\text{E-30})$$

$$t_e = \frac{5D}{U_0} + \frac{2K_2^{1/2}D}{3U_0} \left[ \left(\frac{X}{D} - C_2\right)^{3/2} - (5 - C_2)^{3/2} \right] \quad (\text{E-31})$$

Non-dimensionalizing Equation E-31,

$$\frac{U_0 t_e}{D} = 5 + \frac{2K_2^{1/2}}{3} \left[ \left(\frac{X}{D} - C_2\right)^{3/2} - (5 - C_2)^{3/2} \right] \quad (\text{E-32})$$

This equation was used to calculate the non-dimensional existence times presented in Chapter V.

#### 4. Mass Flow and Entrainment Rates

The mass flow rate through a given cross section of the jet is given by:

$$Q = \int_{-\infty}^{\infty} \rho \bar{U} dy \quad (\text{E-33})$$

Substituting Equation E-8 into E-33, and moving constant terms outside,

$$Q = \rho U_m B \int_{-\infty}^{\infty} f d\eta \quad (\text{E-34})$$

Assuming that the initial mass flow rate is given by,

$$Q_0 = \rho U_0 D \quad (\text{E-35})$$

and using  $Q_0$  to non-dimensionalize Equation E-34,

$$\frac{Q}{Q_0} = \frac{U_m B}{U_0 D} \int_{-\infty}^{\infty} f d\eta \quad (\text{E-36})$$

Substituting Equations II-1 and II-2 into Equation E-36, the following equation for the non-dimensional mass flow rate is obtained,

$$\frac{Q}{Q_0} = \frac{K_1 \left( \frac{X}{D} - C_1 \right)}{K_2^{1/2} \left( \frac{X}{D} - C_2 \right)^{1/2}} \int_{-\infty}^{\infty} f d\eta \quad (\text{E-37})$$

The entrainment is simply the derivative of the mass flow rate with respect to longitudinal distance from the nozzle, and may be shown to equal the following equation in non-dimensional form:

$$\frac{\partial \left( \frac{Q}{Q_0} \right)}{\partial \left( \frac{X}{D} \right)} = \frac{K_1}{K_2^{1/2}} \left[ \frac{1}{\left( \frac{X}{D} - C_2 \right)^{1/2}} - \frac{\left( \frac{X}{D} - C_1 \right)}{2 \left( \frac{X}{D} - C_2 \right)^{3/2}} \right] \int_{-\infty}^{\infty} f d\eta \quad (\text{E-38})$$

Equations E-37 and E-38 were used to calculate the mass flow rates and entrainment rates presented in Chapter V. The integral in the equations was integrated numerically from  $\eta = 0$  to  $\eta = 1.5$  using  $f(\eta)$  given by Equation E-25. The tails of the profile at  $\eta > 1.5$  were integrated graphically using Figure IV-1. The sum of these integrations resulted in,

$$\int_{-\infty}^{\infty} f d\eta = 2.022 \quad (\text{E-39})$$

This value of the integral was used in the calculations.

##### 5. Requirements for Complete Self-Preservation

The ideal plane jet is completely self-preserving, and the total momentum flux at a cross section of the jet is a constant. It may be shown that for the momentum flux to be constant, the geometric and the velocity origin must coincide. In the case of a jet issuing into still air, the momentum flux is given by the following equation:

$$J = \int_{-\infty}^{\infty} \rho \bar{U}^2 dy \quad (\text{E-40})$$

Substituting Equation E-8 and changing variables,

$$J = \rho U_m^2 B \int_{-\infty}^{\infty} f^2 d\eta \quad (\text{E-41})$$

Assuming that the initial momentum flux is given by

$$J_0 = \rho U_0^2 D \quad (\text{E-42})$$

Forming a non-dimensional momentum flux from Equations E-41 and E-42,

$$\frac{J}{J_0} = \frac{U_m^2 B}{U_0^2 D} \int_{-\infty}^{\infty} f^2 d\eta \quad (\text{E-43})$$

Substituting Equations II-1 and II-2 into Equation E-43,

$$\frac{J}{J_0} = \frac{K_1 \left( \frac{X}{D} - C_1 \right)}{K_2 \left( \frac{X}{D} - C_2 \right)} \int_{-\infty}^{\infty} f^2 d\eta \quad (\text{E-44})$$

It may be observed that in the ideal jet, the only terms in the equation which may vary with distance from the nozzle are those within the parentheses. It is clear that the only way for the ratio of the terms to remain constant is for the origins to coincide;

$$C_1 = C_2 \quad (\text{E-45})$$

The integral was evaluated numerically using the Equation E-25 for  $f(\eta)$ . The integral was found to be:

$$\int_{-\infty}^{\infty} f^2 d\eta \approx 1.509 \quad (\text{E-46})$$

## APPENDIX F ENERGY SPECTRUM MEASUREMENT PROGRAM

The turbulent energy spectra were measured using a Hewlett Packard 5450A Fourier Analyzer System. The sampling parameters generally employed were a block size,  $N$ , of 512 points, and a frequency resolution,  $\Delta f$ , of 10 Hz. These parameters result in a maximum frequency,  $F_{\max}$ , of 2560 Hz, and an individual sample length,  $T$ , of 0.1 seconds. For spectra with these parameters, the spectra of 300 sample lengths were averaged, resulting in an average spectra for a total record length of 30 seconds. In a few cases, other sampling parameters were employed, but the number of averages was adjusted to maintain the 30 second record length. The following program was employed:

<u>Program Statement</u>	<u>Description</u>
Label 1	Label beginning of program
Clear 0	Empty block 0
Clear 1	Empty block 1
Label 2	Label beginning of loop
Analog In	Take sample of signal into block 0
Fourier Transform	Perform Fourier transform of signal in block 0 and leave result in block 0
Multiply Complex Conjugate	Multiply Fourier transform in block 0 by its complex conjugate to form energy spectrum, leaving result in block 0
Add 1	Add sum of previous spectra in block 1 to current spectrum, leaving new sum in block 0

Store	1		Store new sum in block 1
Count	2	300	Perform loop beginning at Label 2 and ending here 300 times
Divide	1	300	Divide sum of spectra in block 1 by 300 to form average spectrum
Load	1		Place average spectrum in block 0, also
Integrate	1		Integrate average spectrum in block 1, and perform manipulations which leave integral at all points in block 1
Rotate	1	255	
Clear	1	1 255	
Integrate	1		Divide all components of averaged spectrum in block 0 by integral of spectrum to form normalized average spectrum, leaving result in block 0
Divide	1		Display normalized spectrum in block 0 on oscilloscope and continue
Display	0	0	
Punch	0		Punch entire normalized spectrum of block 0 onto paper tape
End			End of program

